Synthesis, Properties and Application of Polyphenylene Phosphonium Salts

Dissertation

zur Erlangung des Grades

Doktor der Naturwissenschaften im Promotionsfach

Makromolekulare Chemie

Am Fachbereich Chemie, Pharmazie und Geowissenschaften

der Johannes Gutenberg-Universität in Mainz

vorgelegt von

Ralf Moritz

geboren in Hutthurm

Mainz, 2015

Dekan:

1. Berichterstatter:

2. Berichterstatter:

Tag der Mündlichen Prüfung: 13. April 2015

Die vorliegende Arbeit wurde am Max Planck Institut für Polymerforschung in Mainz im Zeitraum vom Februar 2011 bis Februar 2015 angefertigt.

Danksagung

Ich danke Herrn [redacted] herzlich für das spannende Thema meiner Arbeit, welches volle Begeisterung für die Chemie der Polyphenylen-Elektrolyte bei mir entfacht hat durch sein stetes Interesse und Motivation. Ich möchte mich besonders für seine hervorragende wissenschaftliche Betreuung und für seine unterstützenden Ratschläge hinsichtlich jeglicher persönlicher Anliegen bedanken.

Eine Vielzahl weiterer Personen haben das Entstehen dieser Arbeit unterstützt in einer freundlichen und kommunikativen Atmosphäre:
Ich danke meinen Laborkollegen [redacted] und [redacted] für die vielen interessanten Gespräche fachlicher und privater Natur. Die zahlreichen Gelegenheiten zum Ideenaustausch haben die Forschungsprojekte maßgeblich vorangetrieben und die lockeren Plaudereien gestalteten die Zeit im Labor stets kurzweilig.
Besonders herzlicher Dank gebührt [redacted] und [redacted] dafür, dass sie mich bei der Synthese und Aufarbeitung oft unterstützt und als guter Geist die vorbildliche Ordnung in unserem Labor gewahrt haben. Meinem Vorgänger [redacted] danke ich besonders für seine engagierte und gute Unterstützung bei meinem Start ins MPIP-Leben.
[redacted] danke ich für die vielen interessanten Gespräche und Lektionen über die Möglichkeiten der NMR sowie unvergesslichen Momenten des Triumphes auf dem Fußballplatz. Meinem Projektleiter [redacted] danke ich für die gute Betreuung und das gründliche Lesen dieses Manuskripts.
[redacted] danke ich für die vielen Analysen meiner Proben mittels MALDI-TOF und seinen schier unglaublich scheinenden Anekdoten über Modell-Eisenbahnbau und Minigolf.
Ich danke [redacted] und [redacted] für die wunderbare Stimmung in unserem Büro. Herzlich danke ich auch allen Mitgliedern dieses Arbeitskreises für die wunderbare gemeinsame Zeit, den guten Zusammenhalt und den vielen schönen gemeinsamen Erlebnissen.

Ganz herzlich danke ich meinen Eltern [redacted] und [redacted], die stets an mich geglaubt und mich immer mit allen Kräften unterstützt haben.
Schließlich danke ich von ganzem Herzen [redacted] dafür, dass sie immer für mich da ist.

Table of Contents

List of Abbreviations

AMSA	associative mean spherical approximation
CCDC	Cambridge Crystallographic Data Centre
CuAAC	copper(I)-catalyzed alkyne-azide cycloaddition
d	day
DCM	dichloromethane (or: methylene chloride)
DFT	density functional theory
diglyme	diglycol methyl ether (or: bis(2-methoxyethyl) ether)
DMSO	dimethylsulfoxide
DOSY	diffusion ordered spectroscopy
DSC	differential scanning calorimetry
EtO	ethoxy
GPC	gel permeation chromatography
h	hour
HOMO	highest occupied molecular orbital
HSQC	heteronuclear single quantum coherence
LUMO	lowest unoccupied molecular orbital
MALDI-TOF	matrix assisted laser desorption ionization – time of flight
Me	methyl
MeCN	acetonitrile
MHz	megahertz
min	minute
MO	molecular orbital
MSA	mean spherical approximation
NMR	nuclear magnetic resonance
PE	polyelectrolyte
PP	polyphenylene
PPD	polyphenylene Dendron
PPP	poly-(para-phenylene)
ppm	parts per million
s	second
SPC	Suzuki polycondensation

TBA^+	tetrabutylammonium
TBAF	tetrabutylammonium fluoride
TBTA	*tris*-(benzyltriazolylmethyl)amine
*t*Bu	*tert*-butyl
*t*BuONO	*tert*-butyl nitrite
TCNQ	tetracyanoquinodimethane
THF	tetrahydrofurane
T*i*PS	tri-isopropylsilyl
TMS	trimethylsilyl
TGA	thermogravimetric analysis
WCA	weakly coordinating anion
WCC	weakly coordinating cation
XRD	X-ray diffraction

Chapter 1 – Introduction

1.1 The Classiness of Monodisperse Materials

In William Shakespeare's tragedy "Antony and Cleopatra", the soothsayer responds upon being asked if he was the man who knows things: "In nature's book of secrecy. A little I can read." Still in nowadays thinkers, savants and scientists are greatly fascinated by the unique precision and astonishing complexity of the principles that count for the world we are living in. The bursting curiosity how to accumulate knowledge about nature's materials was subject of chemists' research and discussion longing back to the ancient empires lasting still up to people in modern society. The successful handling and utilization of various materials has great influence on the development of human life. A desire to analyze and synthesize new compounds can be reckoned as the forge of civilization, which continues constantly. The increasing number of methods and tools to fine-tune the properties of molecular structures yields a mere incredible amount of new compounds day by day. Among these numerous approaches, dendrimers provide a versatile platform due to the possibility to combine site-specific different functionalities within a single molecule.

Since the specific properties of a material are determined by their complexity regarding both chemical constitution and supramolecular assembly, a thorough study of structure-property relation is required. Dendrimers provide an excellent basis to combine the concepts of classical organic or inorganic molecules and macromolecular chemistry. They exhibit an architectural structure inspired from nature in many different kind of ways (**Figure 1-1**).

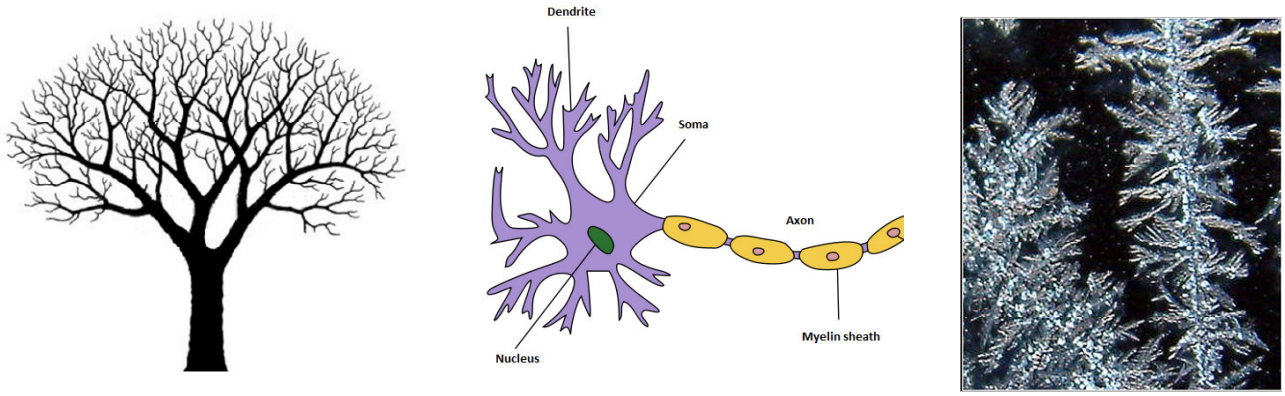

Figure 1-1: Dendritic structures inspired by nature. left: branched tree; middle: structure of a typical neuron; right: snow crystal under microscope view.

1.2 Dendrimers

An expedient division of polymers into linear, cross-linked and branched structures according to H. Staudinger serves as systematic description of macromolecule architectures. Dendrimers, derived from the greek words δενδρον (dendron, meaning "tree") and μεροσ (meros, meaning "part"), can be regarded as a special case of branched polymers with tree-like structure (other polymer architectures see **Figure 1-2**).[1], [2]

For the first time such highly symmetric, regularly branched poly-(propylenamine) POPAM molecules were described by F. Vögtle and termed "cascade-molecules" in 1978.[3] This term exactly encounters the increase in numbers of functional groups within the cascade-like growth stages, called generations. This is entitled as dendritic effect.[4]

.

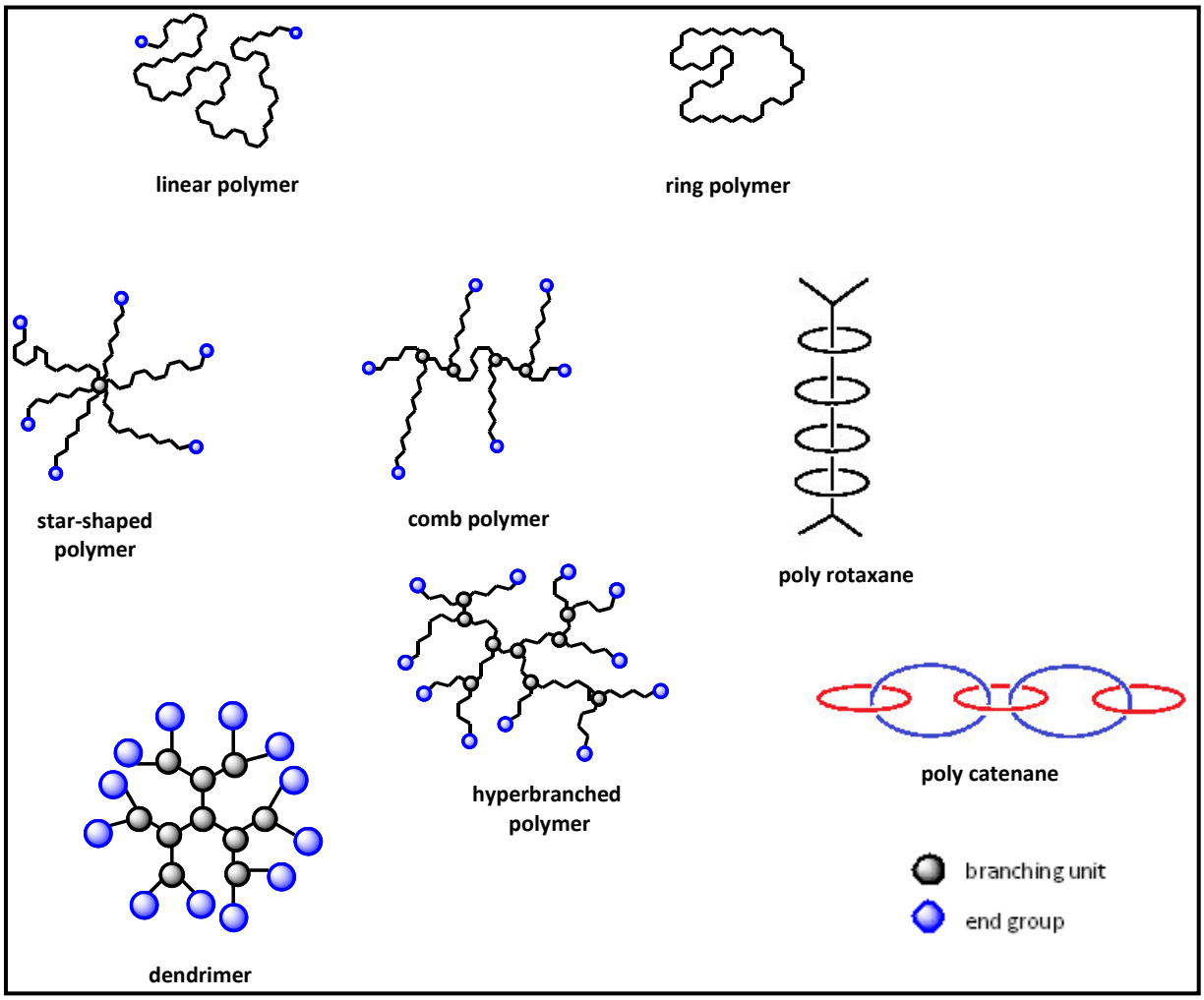

Figure 1-2: Two-dimensional illustration of different polymer architectures.

After some neologisms like “arborols”,[5] the term “dendrimer” most commonly used for such molecules was coined by D. A. Tomalia in his review 1990[1] and was employed also earlier for the denotation of branched poly-(amidoamines) PAMAM.[6]

Two general synthetic routes regarding the “direction” of growth can be distinguished for the preparation of dendrimers. The synthesis of a dendrimer starting from a functionalized central point (core) and subsequently propagating outwards in a step-wise manner is called “**divergent**”, whereas a “**convergent**” synthesis approach begins with the construction of peripheral dendrons, which are afterwards attached to the core in a final step.

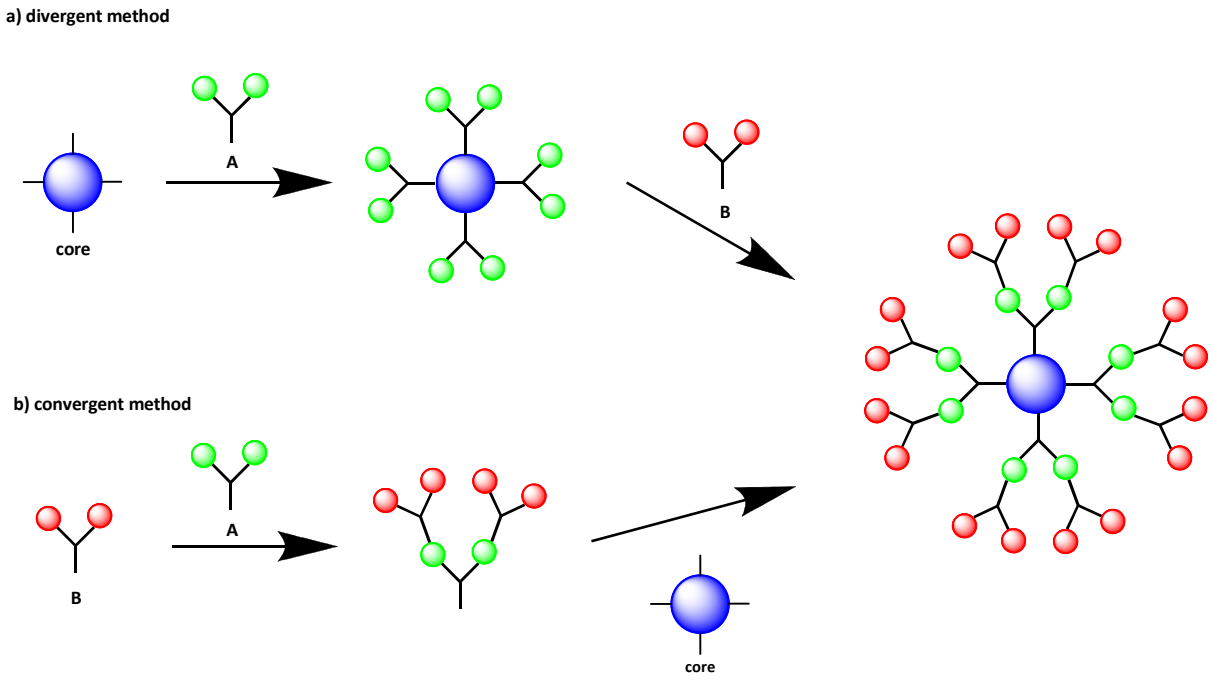

Figure 1-3: Schematic representation of dendrimer synthesis: a) divergent method starting from the core and successively reacting with building blocks A and B; b) convergent method starting from surface building block B, reacting with A and with the core in the final step.

The above mentioned POPAM dendrimers of *F. Vögtle*[3] as well as the PAMAM molecules described by *D. A. Tomalia*[6] are classic examples of dendrimers synthesized via the divergent route. The general principles of divergent dendrimer synthesis can be exemplarily illustrated by the reaction scheme of POPAM:

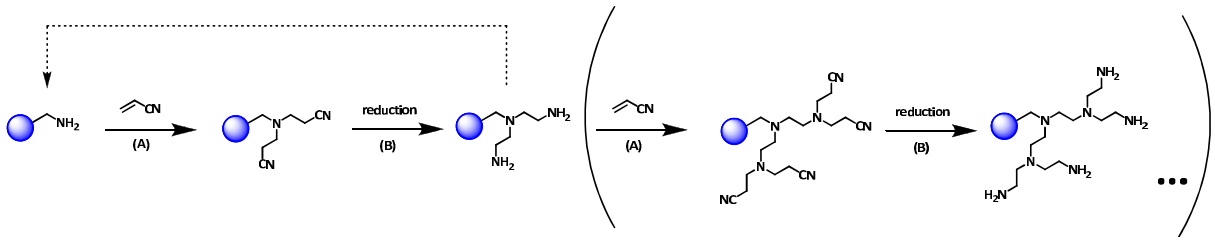

Figure 1-4: Synthesis of a POPAM dendrimer as described by *F. Vögtle*

Initially, the amine is functionalized via twofold Michael addition of acrylonitrile ("branching" step A). In a second step ("activation" step B), the reduction of the nitrile functionalities to primary amines allows for a repetition of the branching step. Thus, the continuous iteration of these synthesis cycles provides a growth in subsequent stages (called generations) and results in a structurally perfect branched dendrimer-architecture. The number of reactive functions is multiplied for each generation by the branching step (A), which is mathematically described by the following equation:

$$n_G = F_c\,(F_{br} - 1)^G \qquad \textbf{(Equation 1-1)}$$

where n_G is the number of functional groups on the surface; G denotes the number of generations and F_c and F_{br} corresponds to the number of functional groups in the core- and the branching building blocks respectively. Due to the exponentially growing number of reactive groups, the danger of incomplete conversion comprises the probability of structural defects in dendrimers synthesized by the divergent method.

In contrast to that, the convergent dendrimer synthesis reduces the number of growth-reactive functions to constantly low numbers independent of the dendrimer generation. Thus, the formation of structural defects due to incomplete conversion is reduced. Nevertheless, a major drawback for the convergent route arises from the steric congestion between the large pre-grown dendrons, so that a complete ligation with the core moiety is eventually impeded. Thereby, the applicability of the convergent method is often limited to

lower generations. Examples in the literature for successfully applied syntheses based on the convergent route are presented by poly-(aryl ether) dendrimers by *J. M. J. Fréchet* and *C. Hawker*,[7] polyphenylene dendrimers described by *T. M. Millller* and *T. X. Neenan*[8], [9] and poly-(phenylacetylene) dendrimers introduced by *J. S. Moore et al*.[10], [11]

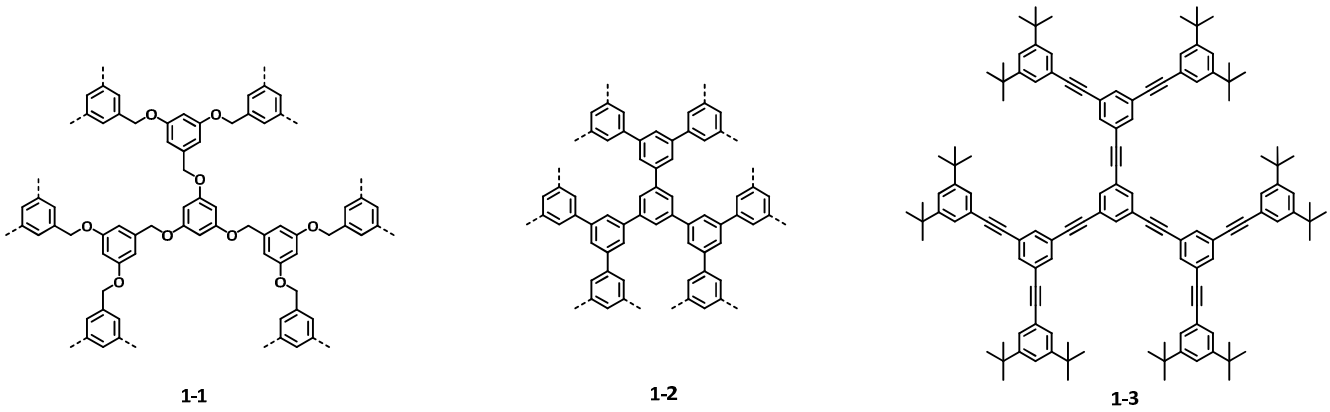

Figure 1-5: Polyaromatic dendritic structures accessed via convergent method: poly-(aryl ether) *Fréchet*-dendrimers **1-1**, polyphenylene dendrimers **1-2** according to *Miller et al.* and poly-(phenylenevinyl)-dendrimer **1-3** by *Moore et al.*

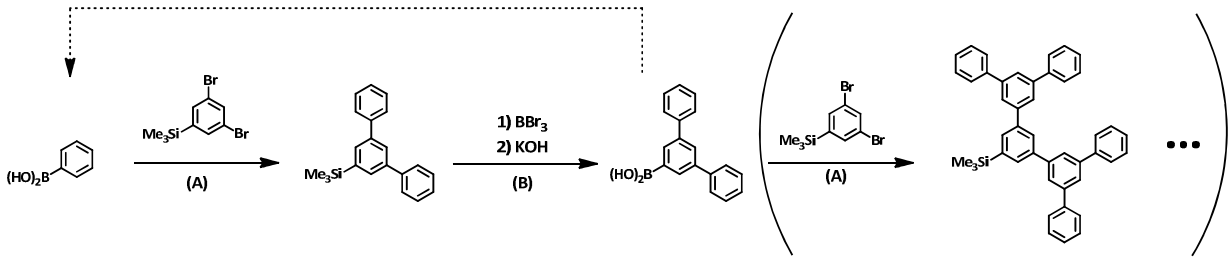

Figure 1-6: Synthesis of polyphenylene dendrimers as described by *Miller et al.*

The synthesis of polyphenylene dendrimers with a 1,3,5-branching pattern as described by *Miller et al.* [8], [9] is achieved via a palladium catalyzed coupling of phenylboronic acids to arylbromides followed by functional group conversion in order to generate relatively rigid dendrons consisting solely of benzene moieties.

1.3 Polyphenylene Dendrimers

In 1997, *K. Müllen* presented a novel approach for the synthesis of polyphenylene dendrimers (PPDs). Therefore, instead of utilizing transition metal catalyzed coupling reactions, the Diels-Alder cycloaddition of functionalized cyclopentadienones (CPs) to ethynyl groups was employed to construct new phenyl rings as branching units.[12] This concept for generating PPDs was initially purposed for the preparation of large, polycyclic aromatic hydrocarbons (PAHs),[13] since three-dimensional dendrimers provide highly symmetric precursors for PAHs that can be processed from solution without the attachment of additional alkyl chains. An example for this strategy is the successful synthesis of C222.[14] Furthermore, PAHs can be regarded as a defined section of graphene, due to which description *A. Gaim* and *K. Novoselov* were awarded with the Nobel prize in physics in 2011.[15]

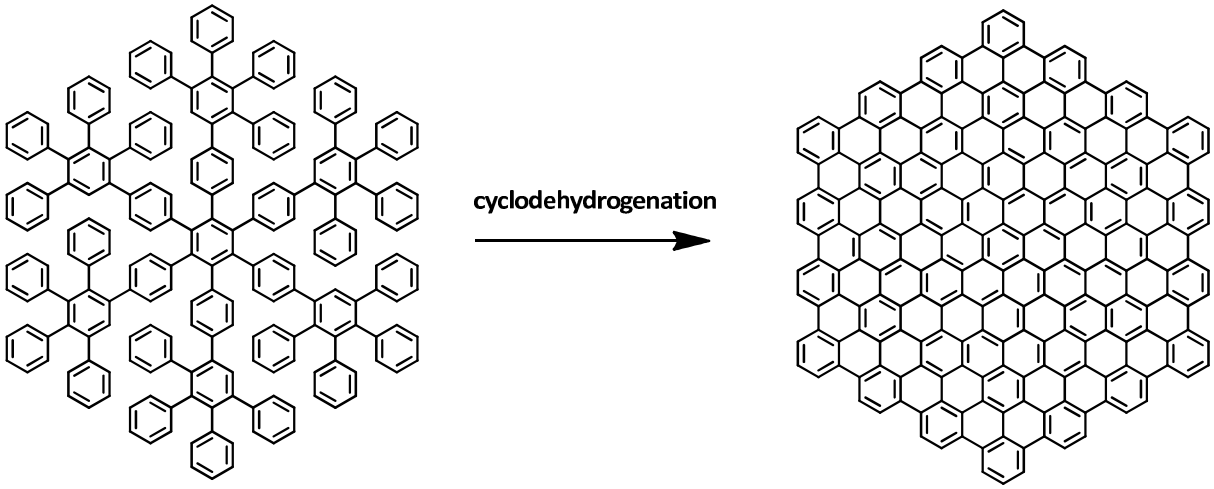

Figure 1-7: Synthesis of PAH C222 (**1-5**) via cyclodehydrogenation from HPB-G1 dendrimer (**1-4**).

Aside from serving as starting compounds for PAHs, polyphenylene dendrimers themself present an interesting class of regularly branched, monodisperse macromolecules, which form a rigid and shape-persistent structure due to branching chains of *para* connected phenyl units. The maintenance of the structural perfection as well as the inherent rigidity of PPDs result in unique characteristics making them attractive target molecules for a variety of functional materials and applications, which will be briefly overviewed after description of their synthesis.

1.4 Synthesis of Polyphenylene Dendrimers

The synthesis of polyphenylene dendrimers according to *Müllen* is based on two crucial reaction steps taking course in quantitative yields nearly lacking any side reactions: the "growing" step consists of a reversible *Diels-Alder* [4+2] cycloaddition of substituted acetylene moieties (dienophile) **1-6** with functionalized cyclopentadienones (diene) **1**-7, as first described by *W. Dilthey* in 1933.[16] This type of electrocyclic reaction with inverse electron-demand is carried out at elevated temperatures (> 140°C) resulting in the irreversible extrusion of carbon monoxide from the intermediary norbornadien-7-one derivative **1-8**, hence yielding a new, highly substituted aromatic target **1-9**. The second step, the "reactivation", involves the generation of free ethynyl groups obtained via desilylation, which are capable of continuous Diels-Alder cycloaddition steps.

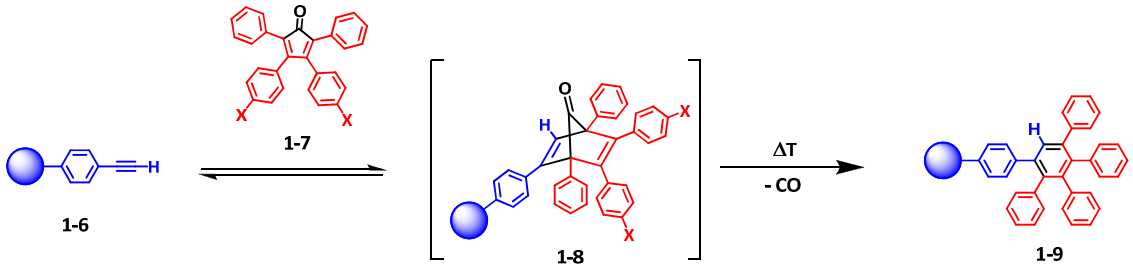

Figure 1-8: Diels-Alder cycloaddition of a phenylacetylene **1-7** with a tetracyclone building block **1-7** via norbornadien-7-one intermediate **1-8** yielding a pentaphenyl-benzene derivative **1-9**.

To enable a continuous cascade growth after the first completed cycloaddition, further reactive ethynyl groups must be generated afterwards from the resulting product. This requirement was facilitated by the synthesis of tetracyclone **1-10**,[12] which comprises both a diene and two protected ethynyl groups serving as dienophiles after deprotection. Thus, the reaction protocol becomes recursive and enables the repetitive synthesis of dendritic polyphenylene structures. Tetracyclone **1-10** serves as AB_2 building block, since a twofold branching point is introduced therewith and the number of available ethynyl groups is multiplied by the number of two. As indicated in **Figure 1-9**, the AB_2 building block is commonly synthesized by a *Knoevenagel* condensation of a TIPS-acetylene functionalized benzyl to diphenylacetone.[12]

In analogy to that, an AB_4 building block[17] **1-11** can be synthesized if a silyl-protected ethynyldiphenylacetone is used for the condensation respectively. By employing this unit, much higher degrees of branching in the resulting polyphenylene structures can be achieved.[18]

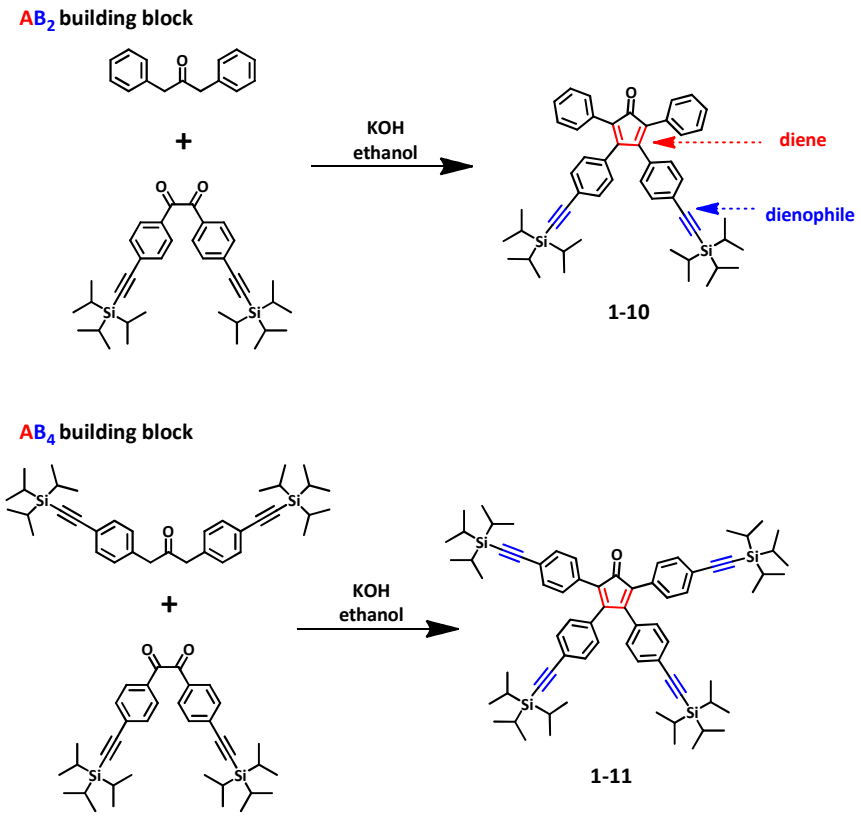

Figure 1-9: Synthesis of AB_2 building block **1-10** and AB_4 building block **1-11** via *Knoevenagel* condensation.

1.5 General Properties of Polyphenylene Dendrimers

Shortly after *Müllen*-type polyphenylene dendrimers were introduced as graphene precursors,[15] it was also realized that the unique properties of PPDs legitimates them as being regarded as new stand-alone material research area. Besides their outstanding thermal and chemical stability, PPDs exhibit an inherently rigid and shape-persistent architecture as a result of their structural main motif, *para*-connected benzene rings. Thus, there is no backfolding along the radial dendrimer phenylene-axis observable, which is in accordance with the experimentally determined persistence lengths of poly-para-phenylenes with values ranging from 13 to 28 nm.[19-22] Hence, in contrast to other types of dendrimers constituted from flexible moieties, PPDs cannot collapse into more compact forms, but instead possess a stiff scaffold structure with a globally defined shape. Small angle neutron scattering (SANS) experiments[23] confirmed the shape persistence and AFM studies revealed PPDs as discrete nano-sized objects matching also molecular modeling predictions.[24] From that main structural concept the most important and unique characteristics for polyphenylene dendrimers result:

i) bulky and sterically demanding
ii) shape persistence
iii) chemical and thermal stability
iv) spatially defined scaffold
v) defined geometry and periphery
vi) inherent hydrophobic voids

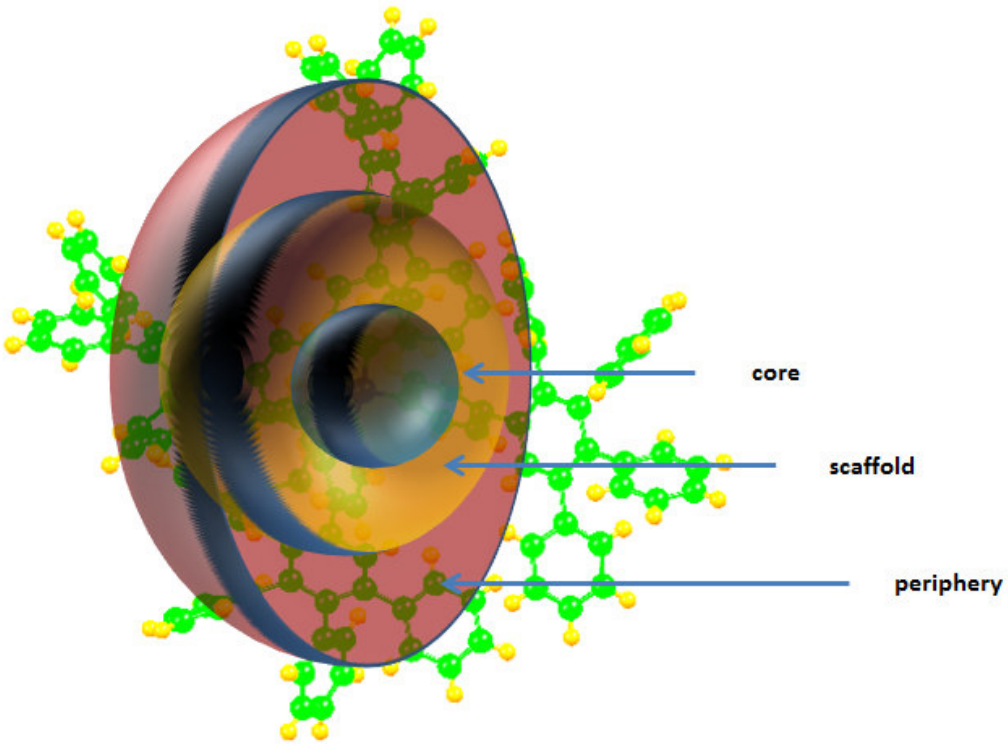

Figure 1-10: Schematic illustration of a polyphenylene dendrimer composed of core, scaffold and periphery.

Thus, PPDs can be targeted at the core, scaffold and periphery while their site specificity provides a spatially defined placement of functions maintaining their location due to the inherent stiffness. The above mentioned characteristics of PPDs have been exploited for a variety of functional materials and applications.[25]

1.5.1 Bulkiness: Steric Screening and Isolation of Functionality

The bulkiness of rigid PPDs enables an efficient screen of different kinds of functionalities from direct interactions by way of steric shielding. Thus, undesired effects including aggregation, association and emission quenching can be suppressed and in many cases solubility is remarkably increased thereby in comparison to non-dendronized analogues.

1.5.2 Site Specificity: Spatially Defined Placement of Functionalities

The modular design principle of dendritic systems enables the implantation of various functional groups of different kinds into a single macromolecule. The synergistic combination of their effects results in advanced material properties given that the placement of the functions is achieved in spatially defined positions and unregulated interaction among these groups is ruled out. In this regard, PPDs offer a great advantage over more flexible dendrimers due to their rigid scaffold structure.

1.5.3 Persistent Voids: Host-Guest Chemistry and Sensing Applications

From the rigidity and shape persistence of the dendritic polyphenylene framework follows the occurrence of permanent intramolecular vacant spaces or voids. These hydrophobic cavities were confirmed by positron lifetime spectroscopy[26] and evidenced by crystal structures of different PPDs.[27], [28] The persisting voids are prerequisites for these PPDs to act as versatile host material via hydrophobic interaction.[29], [30] Whereas the typical PPDs are assumed to have nonpolar cavities, synthetic modifications have resulted in the implementation of various functionalities inside the scaffold with respect to the specific structural objective. For instance, carboxylic acids could be placed throughout the scaffold that provided a polar environment for guest molecules.[31]

1.5.4. Surface Functionalization

The surfaces of PPDs play crucial roles in their solubility and polarity. Utilization of appropriate building blocks enable the tailor-made tuning of a dendrimers chemical and physical characteristics. It is possible to mount a variety of functionalities onto the surface of a dendrimer ranging from polar groups,[32], [33] sugars,[34], [35] amino acids[36] to nonpolar alkyl-chains and fluorine-rich units.[37], [38]

A breakthrough in modifying the surface of polyphenylene dendrimers was achieved by placing polar (sulfonate) and nonpolar (propyl) groups around the PPD with nano-site perfection in an alternating pattern.[39], [40] Thus, a nonpolar dendrimer construct was synthesized with polar patches on the periphery, where the amount, order, location and distance of the functional groups can be tailored by the synthetic protocol applied.

1.6 Ions, Salts and Electrolytes

1.6.1 Definition

In the previous section the impact of polar or even charged functional groups attached onto the periphery of polyphenylene dendrimers has been truncated, resulting in altered chemical and physical properties. Since the main objective of this thesis covers the investigation of salts, chemically modified by encapsulation into a hydrophobic shell, the next pages provide a general overview of the properties of ions, salts and electrolytes.

Due to their ubiquitous appearance in nature, ionic compounds play key roles in metabolism processes and biological systems. For instance, electrostatic potentials generated by ion concentration gradients along nerve cell membranes facilitate the signal transduction in humans and animals.

But also the benefits of an engineered modern world are amongst others founded on the technical application of ions as electrolytes in batteries, fuel cells and accumulators. Furthermore, various organic reactions are based on the interaction of reactive ionic species, which underlines the essential importance for chemists to investigate and understand the properties from materials composed of electrically charged units.

1.6.2 Physical Properties

The reason for the outstandingly high melting points of salts is based on the electrostatic attraction of oppositely charged ions. This principle as one of the four fundamental forces in the universe was first described by *C. A. de Coulomb* in 1785 (**Equation 1-2**).[41] The magnitude of the electrostatic force between two point charges (e.g. two ions with charges q_a and q_b) is directly proportional to the product of their charges q and inversely proportional to the square of the distance (r_{ab}) between them. If the two charges have the same sign, the electrostatic force is repulsive and in the case of different signs, the force between the two charges is attractive:

$$F_c = \frac{1}{4\pi\varepsilon_0}\frac{q_a q_b}{r_{ab}^2} \qquad \textbf{(Equation 1-2)}$$

where F_c denotes the *Coulomb* force and ε_0 is the permittivity of the vacuum

1.6.3 Solvation of Ions and Behavior of Electrolytes

Solvation is a progress in which solute particles interact with the solvent molecules surrounding them. The free Gibbs solvation energy ΔG^0_{solv} is defined as the standard chemical potential of a solute in the solution referred to that in the gaseous state. Solvent shell formation effects the dissolution and chemical reactions of an electrolyte in a particular solvent. The dissolution process of a crystalline electrolyte MX is illustrated by the *Haber-Born* cycle[42] (**Figure 1-11**):

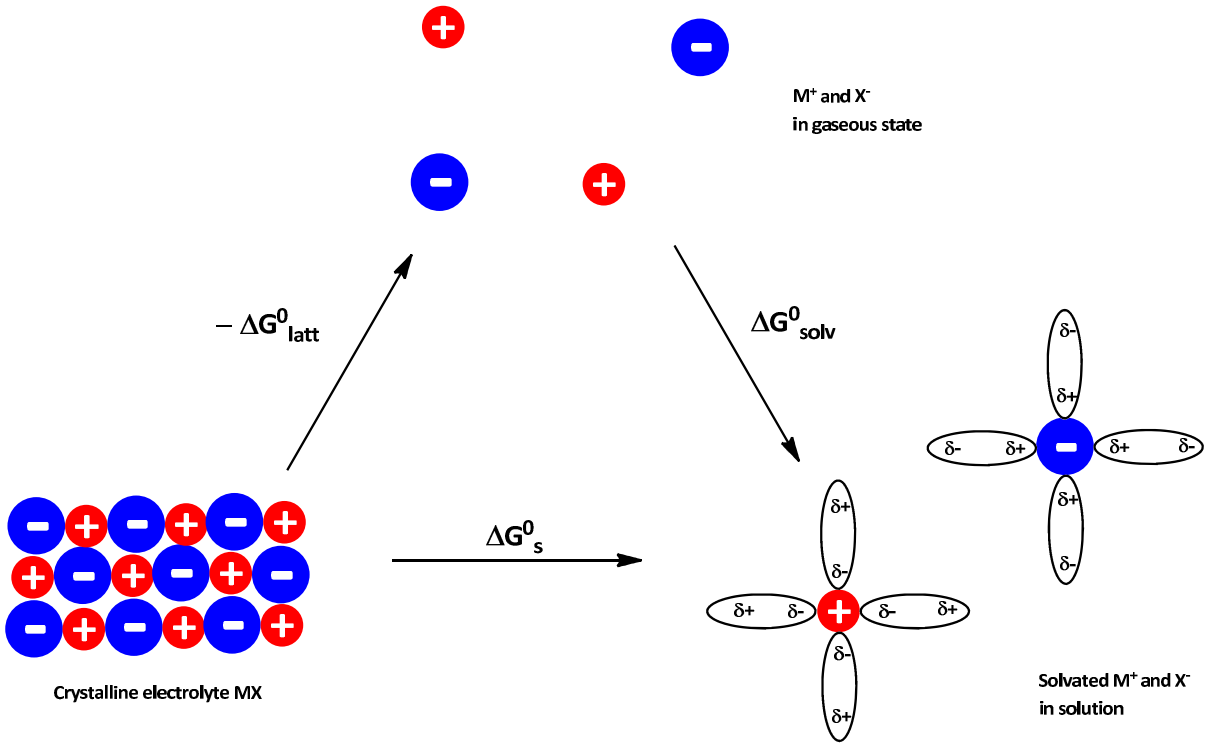

Figure 1-11: Dissolution process of crystalline electrolyte MX into a solvent

In summary the dissolution process can be regarded as the sum of energy input given by the negative free lattice energy $-\Delta G^0_{latt}$ to separate the electrostatically mutual attracted ions M^+ and X^-, and the gain in energy, which arises from the solvation of the free electrolytes expressed by the free solvation energy ΔG^0_{solv}:

$$\Delta G^0_s = -\Delta G^0_{latt} + \Delta G^0_{solv} \qquad \textbf{(Equation 1-3)}$$

It follows that an electrolyte is easily soluble if the sum of the solvation energies of the ions constituting the electrolyte is larger than the lattice Gibbs energy.

Most decisive for the solvation process is the difference between the electrostatic free energy of an ion *in vacuo* and that of the ion in a solution of a solvent with relative permittivity ε_R . A reasonable approximation to qualitatively describe this electrostatic ion – solvent interaction $\Delta G^0_{solv,i}$ of an ion with charge $q_i = z_i e$ and radius r_i in dependence of the relative permittivity ε_R of the solvent, was proposed by *M. Born* in 1920 (illustrated in **Figure 1-12**): [42], [43], [44]

$$\Delta G^0_{solv,i} = -\frac{1}{2}\frac{N_A z^2 e^2}{4\pi\varepsilon_0 r_i}\left(1-\frac{1}{\varepsilon_R}\right) \qquad \textbf{(Equation 1-4)}$$

where

	N_A	Avogadro constant ($6.02214 \cdot 10^{23} mol^{-1}$)
	ze	ionic charge
	r_i	radius of the ion i (nm)

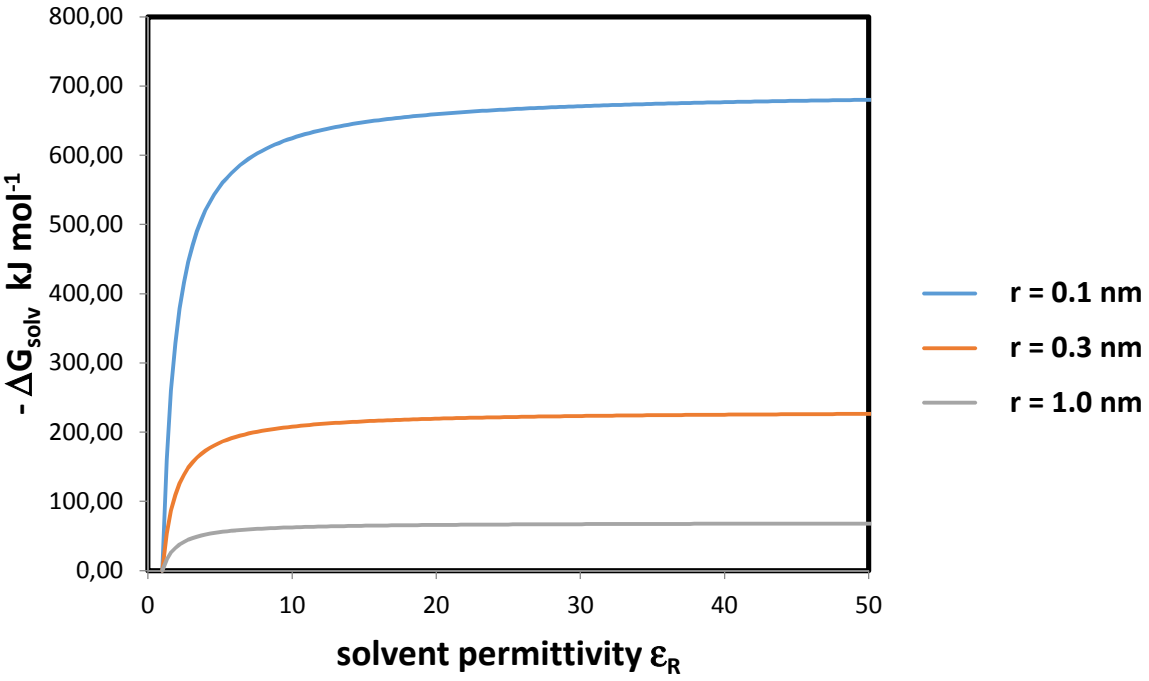

Figure 1-12: Illustration of the effect of solvent permittivity on the electrostatic solvation energy of an ion (with different radii of 0.1 nm, 0.3 nm and 1.0 nm) derived from the Born Equation (**Equation 1-4**).

The value of $-\Delta G^0_{solv}$ increases with ε_R, meaning there is a general avail in solvation energy for solvents in the high permittivity region ($\varepsilon_R > 20$). Furthermore it is obvious that for nonpolar solvents ($\varepsilon_R < 8$), the $-\Delta G^0_{solv}$ values rapidly drop, so that the polarity dependence is much more distinctive in the low permittivity region than between two high permittivity solvents.

1.6.4 Ion Association and Conductivity

The conductivity σ of an electrolyte solution depends on the number of available charge carriers n_i, their electrical charges q_i and their electric mobility μ_i.

$$\sigma = n^+q^+\mu^+ + n^-q^-\mu^- \qquad \textbf{(Equation 1-5)}$$

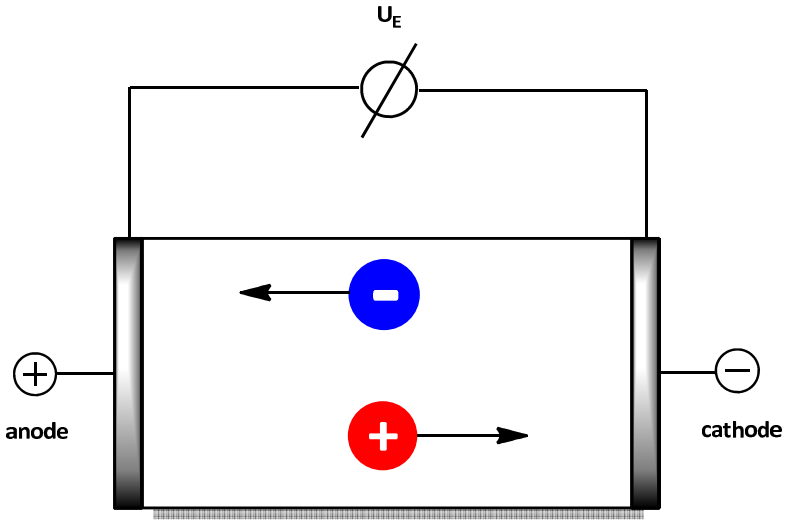

Figure 1-13: Illustration of the ionic conductivity in electrolyte solutions.

Upon applying a potential U_E to an electrolyte solution, an ion i gets accelerated due to the Coulomb force $\overrightarrow{F_C}$. The migration, however, is opposed according to Stokes by the friction with solvent molecules, so that in the equilibrium the ion mobility depends on the charge, size and shape of the ion as well as on the viscosity of the solution. It can be expressed from the laws of hydrodynamics:

$$\mu_i = \frac{z_i e}{6\pi\eta r_i} \qquad \textbf{(Equation 1-6)}$$

where

η	viscosity of the solvent
r_i	radius of the ion
$z_i e$	effective charge

In order to determine the absolute number of charge carriers in a certain volume it is necessary to take ion pair formation into account, since associated ion pairs M^+X^- are not contributing to electric conductivity of the solution. In low-permittivity solvents the electrostatic attractive force between two oppositely charged ions is longer in range

according to *Coulomb's* law, which means that in nonpolar solvents ion-pair formation is much more pronounced.

The concept of ion dissociation was described in detail for the first time by *N. J. Bjerrum*.[45] According to his theory, the energy of electrostatic interaction between two ions becomes equal to their mean kinetic energy $2k_BT$ at a critical distance l_B, defined as the **Bjerrum length**.[45] If two ions of opposite charges are at distance shorter than l_B ($r_{ab} < l_B$), they are associated. If $r_{ab} > l_B$, the ions remain unassociated in solution. The definition of the Bjerrum length leads to:

$$l_B = \frac{|z^+ z^-|\, e^2}{8\,\pi\,\varepsilon_0\,\varepsilon_R\,k_B\,T} \qquad \textbf{(Equation 1-7)}$$

where $k_B = R/N_A$ = Boltzmann constant ($k_B = 1.38065 \bullet 10^{-23}$ J K^{-1}).

In order to take general chemical balance considerations into account, the model of electrolyte solutions was put into a thermodynamic concept and a mixture of free ions and ion cluster were assumed to take part in chemical equilibria according to the corresponding mass action law.[46-48] So the original Bjerrum approach modified the *Debye-Hückel* (DH) theory[49] by using only the concentration of free ions and regarding the latter ones as point-like charges.

An extension of the DH theory to non-point ions was given in the framework of the mean spherical approximation (MSA),[50,51] which was corrected taking also the electrostatic contribution from ion clusters into account via the associative mean spherical approximation (AMSA)[52,53] on the basis of modern theories of associating fluids.[54-57]

1.7 Dielectric Spectroscopy

The versatile measuring method of choice within this work is dielectric spectroscopy (also called impedance spectroscopy) because of its inherent ability to provide both the degree of ion dissociation and transport through the measured dc-conductivity in the low frequency region. Thereby, the dielectric properties of a medium as a function of frequency (f or more common the radial frequency $\omega = 2\,\pi\,f$) and temperature are expressed as the complex permittivity function:

$$\varepsilon^*(\omega) = \varepsilon'(\omega) - i\,\varepsilon''(\omega) \qquad \textbf{(Equation 1-8)}$$

where $\varepsilon'(\omega)$ is the real and $\varepsilon''(\omega)$ is the imaginary part of the function.

The thus measured dielectric relaxation as a whole is the result of the movement of dipoles (dipole relaxation) and electric charges (ion conductivity) due to the applied alternating field. In order to obtain the pure electronic dc-conductivity-values, the sample measurements are operated at a critical low frequency (f = 1.7 * 10^3 Hz) for which the dipole relaxation contribution is negligible (after optimization of the experiment setup). By fitting the linear dielectric loss curves in the aforementioned low-frequency region, the mathematical correlation is given by:

$$\varepsilon''(\omega) = \frac{\sigma_{dc}}{\omega\varepsilon_0} \qquad \textbf{(Equation 1-9)}$$

Dielectric spectroscopy is applied in the following sections to investigate the unique solution properties of dendronized salts with very large, monodisperse charge carriers (chapter 4). Regarding these electrolytes as spherical entities encapsulated with a lipophilic polyphenylene shell, their size approaches the Bjerrum length (definition chapter 1.6) even in low polarity solvents (e.g. in THF, l_B = 7.4 nm). Thus, we herein were able to examine the effect of ion size upon ion association by the interpretation of impedance spectroscopy results in non-aqueous solution.

Literature

[1] Tomalia, D. A.; Naylor, A. M.; Goddard, W. A.; *Angewandte Chemie International Edition in English* **1990**, *29*, 138.
[2] Tomalia, D. A.; Naylor, A. M.; Goddard, W. A.; *Angewandte Chemie* **1990**, *102*, 119.
[3] Buhleier, E.; Wehner, W.; Vögtle, F.; *Synthesis* **1978**, 155.
[4] a) Newkome, G. R.; Moorefield, C. N.; Vögtle, F.; *VCH Weinheim* **2001**; b) Valerio, C.; Fillaut, J.-L.; Ruiz, J.; Guittard, J.; Blais, J.-C.; Astruc, D.; *J. Am. Chem. Soc.* **1997**, *119*, 2588-2589; c) Murer, P. K.; Lapierre, J.-M.; Greiveldinger, G.; Seebach D.; *Helv. Chim. Acta* **1997**, *80*, 1648-1681.
[5] Newkome, G. R.; Yao, Z.; Baker, G. R.; Gupta, V. K. *The Journal of Organic Chemistry* **1985**, *50*, 2003.
[6] Tomalia, D. A.; Baker, H.; Dewald, J.; Hall, M.; Kallos, G.; Martin, S.; Roeck, J.; Ryder, J.; Smith, P.; *Macromolecules* **1986**, *19*, 2466.
[7] Hawker, C.; Fréchet, J. M. J.; *Journal of the Chemical Society, Chemical Communications* **1990**, 1010.
[8] Miller, T. M.; Neenan, T. X.; *Chemistry of Materials* **1990**, 2, 346.
[9] Miller, T. M.; Neenan, T. X.; Zayas, R.; Bair, H. E.; *J. Am. Chem. Soc.* **1992**, 114, 1018.
[10] Xu, Z.; Moore, J. S.; *Angewandte Chemie International Edition in English* **1993**, 32, 246.
[11] Moore, J. S.; Xu, Z.; *Macromolecules* **1991**, 24, 5893.
[12] a) Morgenroth, F.; Reuther, E.; Müllen, K.; *Angewandte Chemie International Edition English* **1997**, 36, 631-634.
[13] Morgenroth, F.; Kubel, C.; Müllen, K.; *J. Mater. Chem.* **1997**, 7, 1207-1211.
[14] Müller, M.; Kubel, C.; Müllen, K.; *Chemistry- A European Journal* **1998**, 4, 2099-2109.
[15] a) Gerstner Ed, *Nat Phys* **2010**, 6, 836; b) Tomovi, Z.; Watson, M. D., Müllen, K.; *Angewandte Chemie* **2014**, 116, 773-777.
[16] a) Dilthey, W.; Schommer, W.; Trosken, O.; *Berichte der deutschen chemischen Gesellschaft (A and B Series)* **1933**, *66*, 1627; b) Dilthey, W.; Hurtig, G.; *Berichte der deutschen chemischen Gesellschaft (A and B Series)* **1934**, *67*, 2004; c) Dilthey, W.; Hurtig, G.; *Berichte der deutschen chemischen Gesellschaft (A and B Series)* **1934**, *67*, 495; d) Dilthey, W.; Schommer, W.; Hoschen, W.; Dietrichs, H.; *Berichte der deutschen chemischen Gesellschaft (A and B Series)* **1935**, *68*, 1159; e) Dilthey, W.; Henkels, S.; Schaefer, A.; *Berichte der deutschen chemischen Gesellschaft (A and B Series)* **1938**, *71*, 974; f) Hanack, M.; Massa, F.; *Tetrahedron Lett.* **1977**, 18, 661-664.
[17] Morgenroth, F.; *Chemical Communications* **1998**, 1139.
[18] Berresheim, A. J.; Müller, M.; Müllen, K.; *Chemical Reviews* **1999**, 99, 1747.
[19] Vanhee, S.; Rulkens, R.; Lehmann, U.; Rosenauer, C.; Schulze, M.; Kohler, W.; Wegner, G.; *Macromolecules* **1996**, *29*, 5136.
[20] Petekidis, G.; Vlassopoulos, D.; Galda, P.; Rehahn, M.; Ballauff, M.; *Macromolecules* **1996**, *29*, 8948.
[21] Harre, K.; Wegner, G.; *Polymer* **2006**, *47*, 7312.
[22] Fuckel, B.; Hinze, G.; Diezemann, G.; Nolde, F.; Müllen, K.; Gauss, J.; Basche, T.; *The Journal of Chemical Physics* **2006**, *125*, 144903.
[23] Rosenfeldt, S.; Dingenouts, N.; Potschke, D.; Ballauff, M.; Berresheim, A. J.; Müllen, K.; Lindner, P.; Saalwachter, K.; *Journal of Luminescence* **2005**, *111*, 225.
[24] Zhang, H.; Grim, P. C. M.; Foubert, P.; Vosch, T.; Vanoppen, P.; Wiesler, U. M.; Berresheim, A. J.; Müllen, K.; De Schryver, F. C.; *Langmuir* **2000**, *16*, 9009.

[25] Türp, D.; Nguyen, T.-T.-T.; Baumgarten, M.; Müllen, K.; *New Journal of Chemistry* **2012**, *36*, 282.
[26] Marek, T.; Suvegh, K.; Vertes, A.; Ernst, A.; Bauer, R.; Weil, T.; Wiesler, U.; Klapper, M.; Müllen, K.; *Radiation Physics and Chemistry* **2003**, *67*, 325.
[27] Bauer, R. E.; Enkelmann, V.; Wiesler, U. M.; Berresheim, A. J.; Müllen, K.; *Chemistry – A European Journal* **2002**, *8*, 3858.
[28] Wiesler, U.-M.; *Dissertation*, Johannes Gutenberg Universität **2000**.
[29] Kohn, F.; Hofkens, J.; Wiesler, U.-M.; Cotlet, M.; van der Auweraer, M.; Müllen, K.; De Schryver, F. C.; *Chemistry – A European Journal* **2001**, *7*, 4126.
[30] Sakamoto, J.; Müllen, K.; *Organic Letters* **2004**, *6*, 4277.
[31] Bauer, R. E.; Clark, J. C. G.; Müllen, K.; *New Journal of Chemistry* **2007**, *31*, 1275.
[32] Schlupp, M.; Weil, T.; Berresheim, A. J.; Wiesler, U. M.; Bargon, J.; Müllen, K.; *Angewandte Chemie International Edition* **2001,** *40* (21), 4011-4015.
[33] Köhn, F.; Hofkens, J.; Wiesler, U.-M.; Cotlet, M.; van der Auweraer, M.; Müllen, K.; De Schryver, F. C.; *Chemistry – A European Journal* **2001,** *7* (19), 4126-4133.
[34] Sakamoto, J.; Müllen, K.; *Organic Letters* **2004,** *6* (23), 4277-4280.
[35] Kobayashi, S.; Uyama, H.; Kimura, S.; *Chemical Reviews* **2001,** *101* (12), 3793-3818.
[36] Mihov, G.; Grebel-Koehler, D.; Lübbert, A.; Vandermeulen, G. W. M.; Herrmann, A.; Klok, H.-A.; Müllen, K.; *Bioconjugate Chemistry* **2005,** *16* (2), 283-293.
[37] Coates, G. W.; Dunn, A. R.; Henling, L. M.; Dougherty, D. A.; Grubbs, R. H.; *Angewandte Chemie International Edition in English* **1997,** *36* (3), 248-251.
[38] Bauer, R.; Liu, D.; Ver Heyen, A.; De Schryver, F.; De Feyter, S.; Müllen, K.; *Macromolecules* **2007,** *40* (14), 4753-4761.
[39] Mondeshki, M.; Mihov, G.; Graf, R.; Spiess, H. W.; Müllen, K.; Papadopoulos, P.; Gitsas, A.; Floudas, G.; *Macromolecules* **2006,** *39* (26), 9605-9613.
[40] Stangenberg, R.; Saeed, I.; Kuan, S. L.; Baumgarten, M.; Weil, T.; Klapper, M.; Müllen, K.; *Macromolecular Rapid Communications* **2014,** *35* (2), 152-160.
[41] Levy, E.; *Dictionnaire de Physique*; Presses universitaires de France: Paris, **1988**.
[42] Born M.; *Zeitschrift für Physik* **1920**, Vol. 1, 45–48.
[43] Izutsu, K. *Electrochemistry in Nonaqueous Solutions*; WILEY-VCH: Weinheim, **2002**.
[44] Atkins P. W.; MacDermott, A. J.; *J. Chem. Educ.* **1982**, 59(5), 359.
[45] Bjerrum; Wynne-Jones, W. F. K.; Onsager; Fowler; Bronsted; *Transactions of the Faraday Society* **1927**, *23*, 432.
[46] Ebeling, W.; Hilbert, S.; Krienke, H.; *Journal of Molecular Liquids* **2002**, 96-97, 409-423.
[47] Barthel, J.; Krienke, H.; Kunz, W.; *Physical Chemistry of Electrolyte Solutions – Modern Aspects*, Steinkopff, Darmstadt, and Springer, New York (**1998**).
[48] Fouss, R. M.; *J. Am Chem. Soc.* **1958**, 80, 5099.
[49] Debye, P.; Hueckel, E.; *Physik. Z.* **1923**, 185.
[50] Waisman, E.; Lebowitz, J. L.; *J. Chem. Phys.* **1972**, 56, 3086 - 3093.
[51] Blum, L.; *Mol. Phys.* **1975**, 30, 1529.
[52] Holovko, M. F.; Kalyuzhnyi, Y. V.; *Mol. Phys.* **1991**, 73, 1145.
[53] Blum, L.; Bernard, O.; J. Stat. Phys. **1995**, 79, 569.
[54] Wertheim, M. S.; *J. Stat. Phys.* **1984**, 35, 19 - 35.
[55] Wertheim, M. S.; *J. Stat. Phys.* **1986**, 42, 459 - 477.
[56] Holovko, M. F.; *Cond. Matter Phys.* **1999**, 2, 205.
[57] Holovko, M. F.; *J. Mol. Liq.* **2002**, 65, 96 – 97.
[58] Holovko, M. F.; J. Mol. Liq. **1999**, 82, 161-181.

Chapter 2 – Motivation

Since pioneering works made by [redacted] revealed that hydrophobic encapsulation with rigid polyphenylenes by means of divergent dendronization is generally applicable to individual anions in a salt, the well-known structural requirements to lower the coordination ability of anions were substantially modified by a remarkable increase of the anion diameter. Furthermore it has been elucidated that the lipophilic character of these borate anions, up to several nanometers in size, exerts remarkable influence on the physical properties of the electrolytes in such a way that the ionic conductance was increased with increasing anion size. Additionally, the hydrophobic salts exhibited excellent solubility in low permittivity solvents.

In order to amplify the assortment of defined ionic species embedded in a rigid polyphenylene shell, the synthetic strategy has to be discovered to prepare monodisperse, charge-centered cations. This concept is the primary topic within this thesis followed by exploring the preparative methods that provide a pathway towards the spatial expansion of mono-cations. The sparse survey (**Figure 2-1**) of the most common structures of weakly coordinating cations (WCCs) reveals that there are accumulated needs to more efficiently shield the positive charge and to improve the chemical protocols for their preparation.

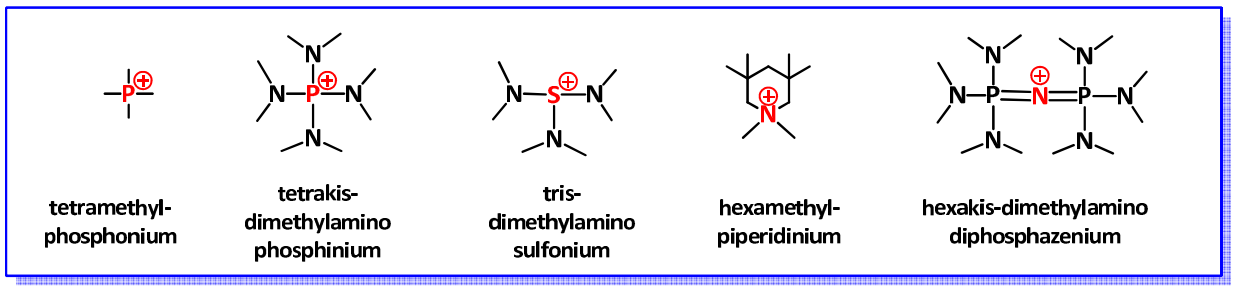

Figure 2-1: Structural overview of the most common weakly coordinating cations (WCCs).

The most effective modification to lower the coordination of cations is a drastic increase of their overall sizes. This is described by Coulomb's law, which states that the attractive force F_C between two oppositely charged ions is inversely proportional to the square of their distance r_{ab}^2 (illustrated in **Figure 2-2**).

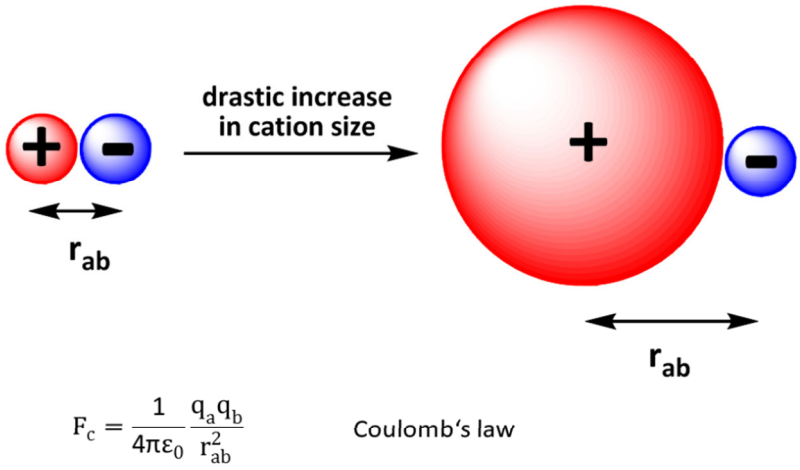

Figure 2-2: Illustration of the drastic increase in cation size leading to a decreased electrostatic attraction.

After carefully choosing the functionality of the cationic species (ammonium, phosphonium, sulfonium, pyridinium…), the synthetic strategy towards large sized ions was elucidated. A particular matter of importance was to clarify whether a drastic increase in cation size proceeds via a divergent dendritic growth or also a convergent assembly of already preformed building blocks leads to the formation of bulky, dendronized phosphonium cations – which are mainly studied within this work.

Moreover, in contrast to WCCs based on alternative dendritic structures, polyphenylene dendrimers fulfill crucial requirements for the structural design of rigid and sterically shielded molecular ions. The advantages of a screening framework solely constituted from phenyl rings are:

- Built from throughout chemically stable moieties
- Hydrophobic scaffold without any basic or nucleophilic sites (nitrogen, oxygen)
- Stiff and rigid framework provides shape persistence

Furthermore, the highly hydrophobic nature of the thus generated spherical polyphenylene shell represents a versatile platform for further site-specific functionalization during the synthesis procedure.

Once the nanoscopic enlargement of cations would proceed with success, the subsequent question arising therefrom is to which extent the size and hydrophobicity of those novel salts is reflected by their physical and chemical properties. Key features that will certainly be affected by the encapsulation are:

- Solubility in organic solvents of low polarity
- Ion conductivity and degree of ion dissociation
- Crystal lattice packing due to the presence of sterically enlarged cations
- Effect on chemical stability

Aside from simply investigating the influence of dendritic growth on the physical properties of electrolytes, a major objective within this work will be to make applicable use of the novel prepared salts and their structural alterations. It is expected that high charge carrier mobility in combination with screened phosphonium groups will avenue a path towards the development of high-performance materials in various application fields.

The selection of phosphonium salts as the main substance class within this thesis comes along with their potential to form phosphorus ylids, which play key roles as reactive intermediates for instance in Wittig reactions. Combining the reactivity of ylids with the structural motif of specifically enlarged dendritic substituents, provides a synthetic approach towards tailor-made building blocks for organic syntheses (illustrated in **Figure 2-3**). It is of particular interest as to which way the presence of spatially demanding polyphenylene-groups influence the stereochemistry of the Wittig reaction. First of all this approach is of synthetic value with regard to the formation of novel alkenes and stilbenes, but also the cognition of mechanistic details may be further elucidated with the help of the benzylphosphonium salts developed throughout of this work.

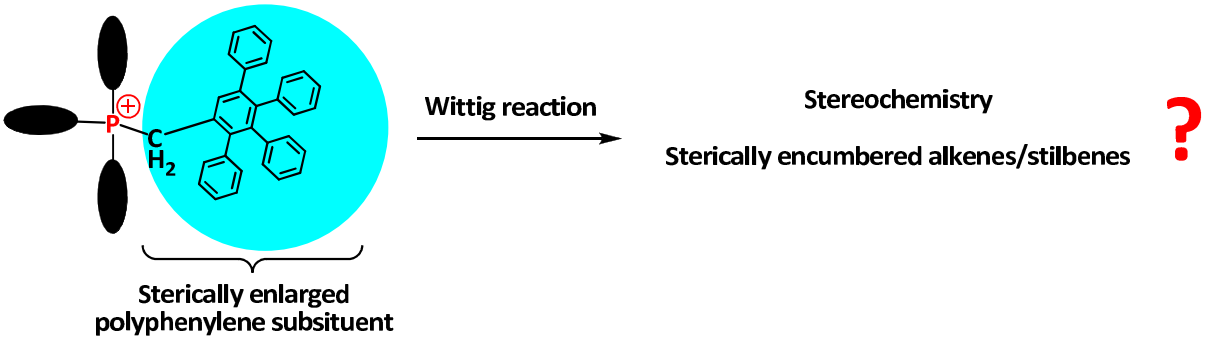

Figure 2-3. Application of phosphonium salts with sterically enlarged benzyl-moieties in the Wittig reaction.

Chapter 3 – Synthesis of Dendronized Polyphenylene Cations

3.1 Introduction

Inspired by the fact that increasing the size and bulkiness of a molecular ion provides a highly efficient pathway to prevent ion association in solution, the subsequent investigation of the resulting physicochemical properties as well as the search for conceivable applications render the hydrophobic encapsulation of organic salts to an attractive field of research. In recent studies, the successful preparation of monodisperse, nanometer-sized tetraphenylborate based polyphenylene-anions were reported by [redacted] via divergent dendritic growth,[1] which represented a new class of organic electrolytes. The resulting salt exhibited outstanding high solubility in low permittivity solvents and their utilization as weakly coordinating anions[2] (WCAs) advises their use in catalysis,[3-6] polymerization,[7-10] electrochemistry,[11-18] stabilization of electrophilic species,[19-23] ionic liquids[24-27] and battery technology.[28-31]

The central synthetic strategy to expand ion sizes beyond the steric constraints of a convergent synthesis approach will be applied within this work for suitable cationic species in order to yield molecularly defined, rigid and hydrophobic electrolytes. First of all the choice of the positive charge center was of particular interest. Most of the commonly known cationic structures are based on onium-derivatives of the pnictogen- (group 15, $R_4M^+ X^-$) or chalcogen-family (group 16, $R_3M^+ X^-$), which are briefly outlined in **Table 3-1**.

Table 3-1: Survey of organic cations with various central elements; * Electronegativity according to Pauling.[41]

Element/Symbol	Covalent Radius [pm]	Electronegativity*	Examples and Applications
Nitrogen (N)	75	3.04	Tetraalkylammonium salts: Common use as surfactants,[32] phase-transfer-catalysts (PTC)[33] and Ionic Liquids (IL)[34]
Phosphorus (P)	106	2.19	Tetraalkylphosphonium based ionic liquids,[35] chiral phosphonium phase-transfer catalysts[36]
Arsenic (As)	119	2.18	Arsenium group as non-viral gene transfection agents[37]
Antimony (Sb)	138	2.05	
Oxygen (O)	152	3.44	Trialkyloxonium salts as alkylating agents,[38] Meerwein Salt $(CH_3)_3O^+ BF_4^-$
Sulfur (S)	180	2.58	Transmethylation in biological systems by S-adenosyl-methionine;[39] application of sulfonium ylides in organic synthesis[40]

The main concept within this work is focused on the synthesis and both physical and chemical properties of large, hydrophobic, rigidly-dendronized cations based on tetraphenyl-phosphonium derivatives with general formula $R_4P^+ X^-$, since phosphorus provides a sufficiently sized covalent radius to align four bulky substituents constituted solely from phenylene rings around the central atom, whereas in the case of ammonium salts even simple tetra-aryl cationic species are not known due to the shortage of space around the nitrogen center. Furthermore, phosphorus is more inclined to delocalize electrons than nitrogen due to its empty 3d orbital.[42] The lower electronegativity of P (2.19) relative to C (2.55) allows the positively charged phosphonium centers to be shielded by partially negative α-carbons, resulting in less interaction between a phosphonium cation and the respective charge-neutralizing anions. In ammonium salts the opposite is the case, since the strong electronegativity of N (3.04) causes partially positive charged α-carbon-substituents surrounding the center, hence increasing the binding to anions.[42], [43]

In addition to the weaker intrinsic ionic interactions, Zhou and Blumstein concluded that phosphonium salts demonstrated better thermal and chemical stability in comparison to ammonium salts with comparable structures.[44]

3.2 Ethynyl-Functionalized Tetraphenylphosphonium Core

The first task to achieve the synthesis of a tetraarylphosphonium cation with polyphenylene dendrons was to prepare an ethynyl-functionalized phosphonium core, which acted as branching unit for subsequent divergent dendritic growth via *Diels-Alder* cycloaddition. Therefore, a suitable procedure started with the preparation of 4-trimethylsilylethynylbromobenzene (**3-1**) via selective Sonogashira coupling[45] of TMS-acetylene to 1-bromo-4-iodobenzene at 0 °C. The subsequent lithium-bromo exchange[46] carried out at -78 °C generated a nucleophilic ligand, which was reacted with phosphorus trichloride in order to yield tris-(4-(trimethylsilylethynyl)phenyl)-phosphine (**3-2**). After the deprotection of **3-2** using K_2CO_3 in methanol, tris-(4-(ethynyl)phenyl)-phosphine (**3-3**) was obtained, which required to be quarternized by a suitable ethynylbenzene-unit for the sake of generating a symmetrical four-coordinated cationic center.

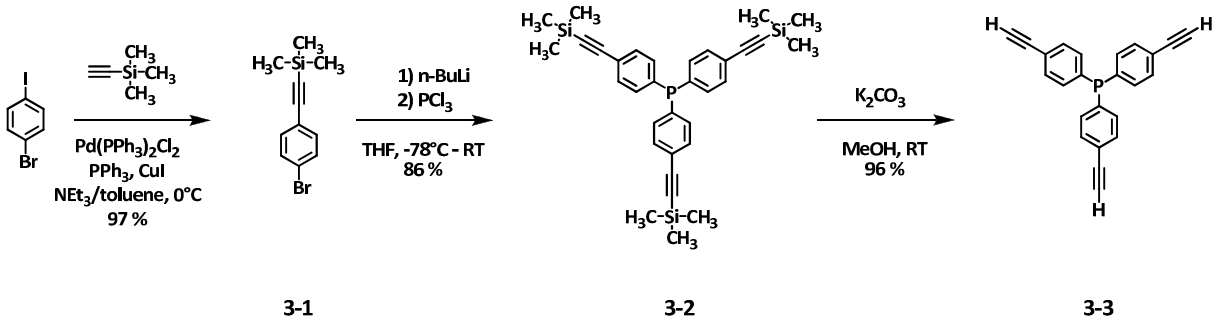

Figure 3-1: Synthesis route to ethynyl-functionalized phosphine **3-3**.

Although there is a variety of general methods for preparing tetraarylphosphonium (TAP)-salts by reacting triarylphosphines with suitable aryl halides in the literature, most commonly supported by the utilization of transition metal catalysts (e.g. palladium, nickel, cobalt), our numerous attempts, however, were not successful via the methods and conditions summarized in **Table 3-2**. Either the starting material was recovered or the corresponding phosphine oxides were obtained as main product for any reaction conditions used in our experiments. The reason for this is most likely attributed to the lowered nucleophilicity of **3-2** and **3-3** in comparison to triphenylphosphine (PPh_3). Also a

disadvantageous interaction of the present TMS-protected (**3-2**) or free alkyne (**3-3**) units with the catalyst is conceivable to explain the failure of the quarternization procedure.

Table 3-2: Reaction conditions for quarternization reaction between phosphine PR_3 and aryl halide. All reactions were carried out in sealed microwave tubes and solvents were degassed and bubbled with argon prior to use.

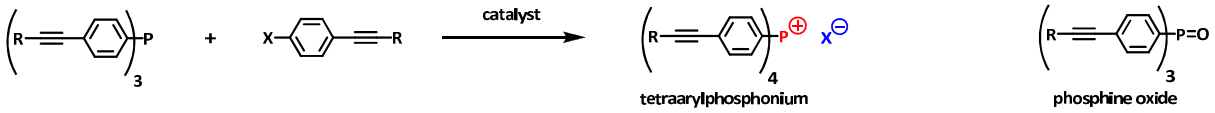

Entry	Catalyst	Reaction Conditions	Product/Comments	Reference
		R = TMS		
1	$Pd_2(dba)_3$ (5 mol %)	X = Br; o-xylene (3 M); 145 °C; 24 h	yield of phosphonium < 10 %; phosphine oxide formation	[47]
2	$Pd_2(dba)_3$ (5 mol %)	X = I; o-xylene (3 M); 145 °C; 24 h	yield of phosphonium < 10 %; phosphine oxide formation	[47]
3	$Pd(OAc)_2$ (5 mol %)	X = I; toluene (0.5 M); 120 °C, 12 - 24 h	starting material recovered; phosphine oxide formation	[48]
4	$NiBr_2$ (5-10 mol %)	X = Br; ethylene glycol (1 M); 180 °C, 4 h	no explicit product assignment was possible	[49]
5	$NiBr_2$ (50 mol %)	X = Br; neat; 250 °C, 24 h	no explicit product assignment was possible	[50]
		R = H		
6	$Pd_2(dba)_3$ (5 mol %)	X = Br; o-xylene (3 M); 145 °C; 24 h	phosphine oxide formation	[47]
7	$NiBr_2$ (50 mol %)	X = Br; neat; 250 °C, 24 h	phosphine oxide formation	[50]

Thus, searching for a more suitable method to obtain **3-3** encouraged us to utilize highly electrophilic reagents to react with phosphine **3-2**. Aromatic diazonium salts represent widely employed reagents for various organic syntheses like *Balz-Schiemann* reactions,[51] *Sandmeyer* chemistry[52] or *Matsuda-Heck* couplings.[53] Since arene diazonium cations Ar-N=N$^+$ exhibit outstanding high reactivity towards forming reactive cationic radical intermediates Ar$^{\bullet+}$ conditioned by the thermal elimination of nitrogen as excellent leaving group, we concluded that a combination of nucleophilic phosphine **3-3** with the aromatic diazonium salt **3-4** might prove as appropriate reaction system for synthesizing the quarternary phosphonium target compound **3-5**. The exact reaction conditions for the selected synthetic route as depicted in **Figure 3-2** were carefully adjusted after realizing that

phosphines and diazonium compounds can react in completely different reaction pathways depending on stoichiometry and solvent resulting in the formation of triaryl-arylhydrazyl-phosphonium salts (Horner et al.[54]) or defunctionalized arenes.[55]

Preparation of 4-ethynylbenzenediazonium tetrafluoroborate **3-4** was achieved by reaction of 4-ethynylaniline in dichloromethane with tert-butyl nitrite according to literature procedure.[56]

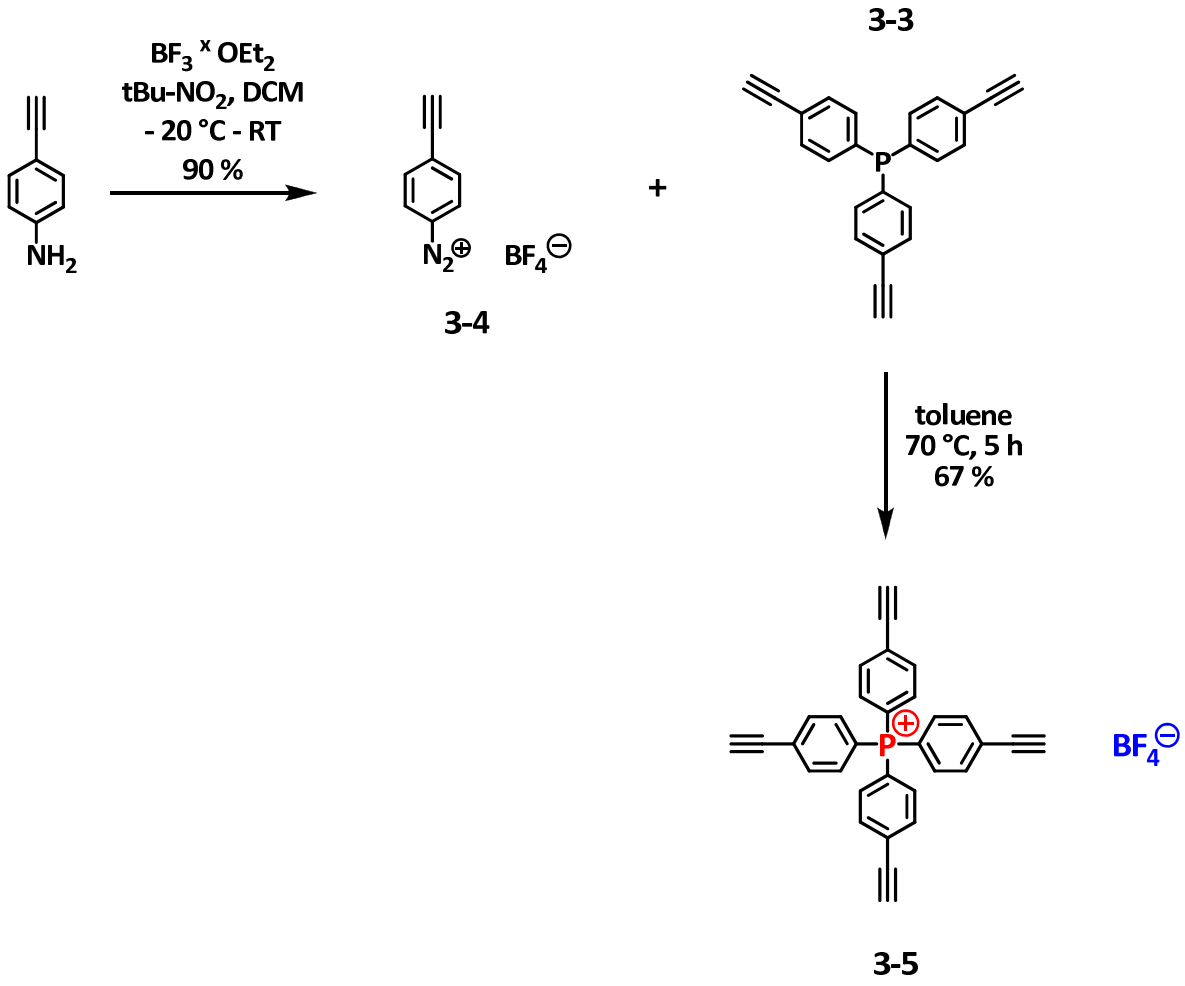

Figure 3-2: Synthesis route to ethynyl-functionalized phosphonium tetrafluoroborate salt **3-5**.

An optimization of the reaction conditions finally yielded the tetrakis-ethynyl-functionalized phosphonium core **3-5**, which was ascertained by MALDI-TOF mass spectrum (m/z = 435.6) and ^{31}P-NMR (δ 21.7, CD_2Cl_2, 298 K, 300 MHz) in good yields (67 %) after column chromatography purification.

3.3 Increase of Cation Size by Divergent Dendritic Growth

With the ethynyl-functionalized phosphonium core **3-5** in hand, a subsequent synthesis of first-generation cationic species was performed by applying the thermal *Diels-Alder* cycloaddition to yield polyphenylene phosphonium salt **3-6** $[P\text{-}G1]^+$ BF_4^- (**Figure 3-3**). In general, the build-up of PPDs is usually carried out in o-xylene at high temperature (150 – 170 °C).

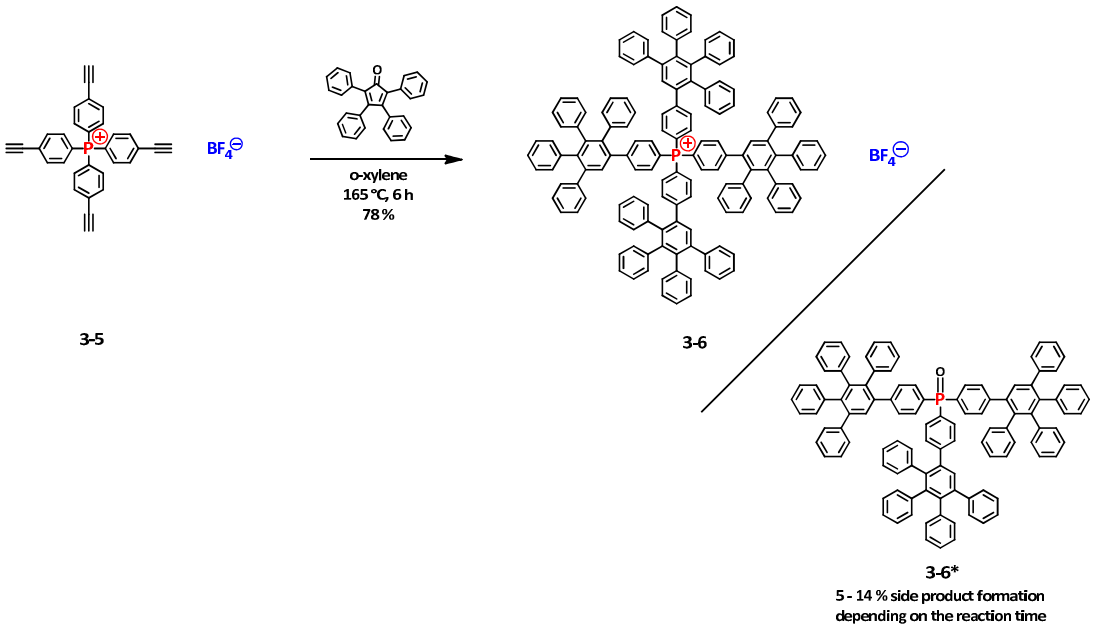

Figure 3-3: Divergent synthesis of a first-generation polyphenylene phosphonium tetrafluoroborate salt **3-6**.

The reaction was monitored by means of MALDI-TOF mass spectrometry and the presence of the fourfold functionalized PPD-phosphonium cation (m/z = 1860.76) was assured after purification via column chromatography (spectrum see **Figure 3-4**). It is noteworthy that the encapsulation of a polar tetraphenylphosphonium core into a hydrophobic polyphenylene shell allowed its elution through a silica gel column due to the remarkably enhanced solubility in organic solvents (DCM/THF mixture, see later in **Table 4-6**). The corresponding phosphine oxide **3-6*** (MALDI-TOF m/z = 1418.56, ^{31}P-NMR δ = 27.56 in CD_2Cl_2 at 298 K) formed during the reaction depicted in **Figure 3-3** could be separately isolated.

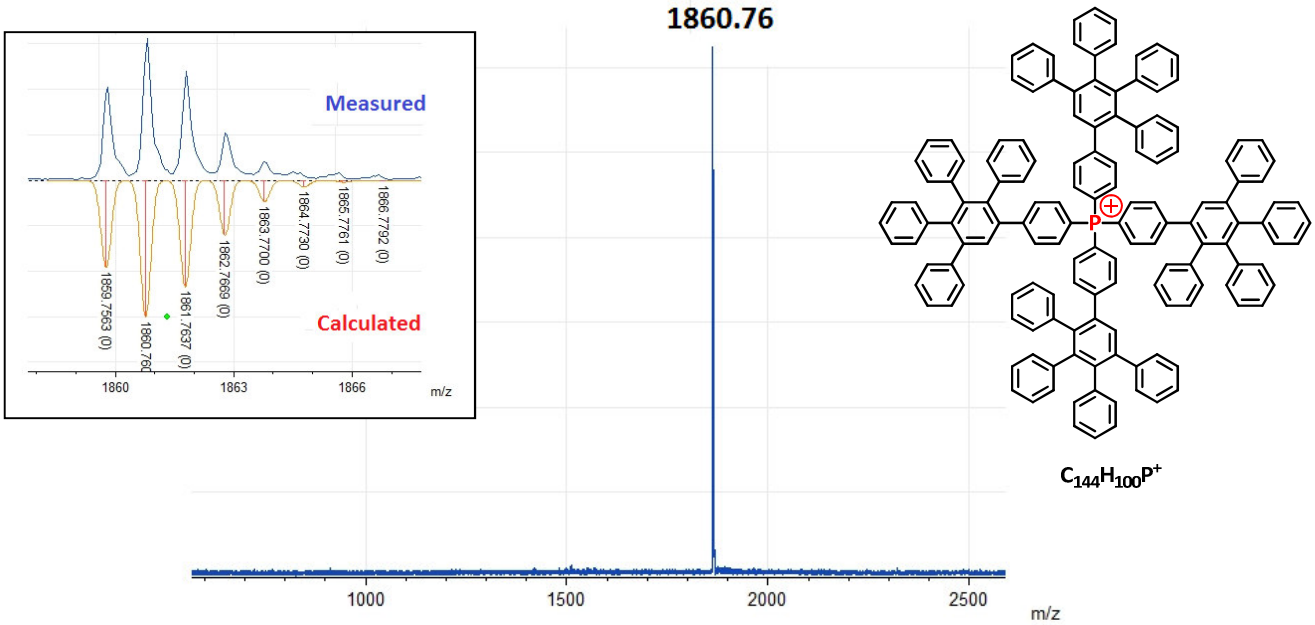

Figure 3-4: MALDI-TOF spectrum of first-generation phosphonium cation **3-6**; inset: comparison of measured and calculated isotope distribution pattern of the peak.

The yield of the undesired side product **3-6*** ranged from 5 % (in a sealed 10 mL microwave vial, diphenylether, DMF, microwave 300 W, 210 °C, 1 h reaction time) to 14 % (bulk batch in a 30 mL microwave vial heated in an oil bath for 6 h to 165 °C as described in the **Experimental Part**). The question raises how this type of side product formation operates in detail. A closer look at the raw mass spectrum recorded from the crude reaction mixture revealed in addition to the main product **3-6** (m/z = 1860.76), two additional peaks attributable to **3-6*** (m/z = 1418.56) and the dendronized tertiary phosphine $\mathbf{C_{108}H_{75}P}$ (m/z = 1402.56). A reasonable assumption based on that postulates an initial cleavage of the G1-phosphonium cation under high temperatures due to the steric overloading by the bulky polyphenylene dendrons. Subsequently the formation of phosphine oxide **3-6*** proceeds via oxidation of that tertiary phosphine $\mathbf{C_{108}H_{75}P}$ by dissolved molecular oxygen. The mole fraction of O_2 in o-xylene present in solution depends on the temperature and the partial pressure of atmospheric oxygen in the reaction vial. This is comprehensively described in the literature for toluene,[57] the solvent which is most similar to o-xylene.

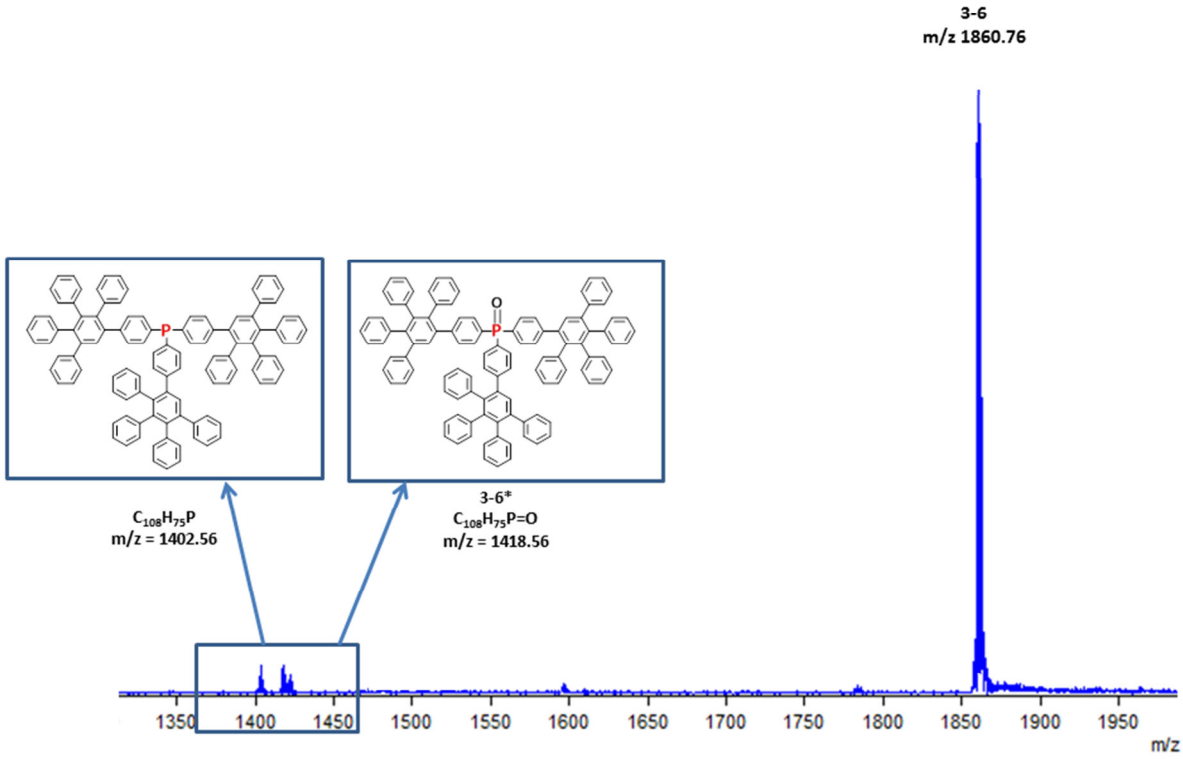

Figure 3-5: MALDI-TOF raw mass spectrum of the formation of **3-6** (reaction and conditions outlined in **Figure 3-3**).

In 2007, *T. E. Barder* examined in his PhD work the oxidation of phosphine ligands under different conditions (0.05 M PR_3-solutions under air- and O_2-atmosphere at 25 °C and 100 °C for 65 h, toluene).[58] In the rationale for the resistance of bulky dialkylbiaryl phosphines toward oxidation by molecular oxygen, electronic and steric factors were considered. The latter were reported to be of decisive importance. Furthermore, *Barder* concluded that in the case of sterically loaded phosphines rather the concentration of O_2 in toluene influences the rate at which phosphine oxide is formed but more essential is the reaction between the initially formed diradical species R_3P-O-O with a second R_3P molecule (rate limiting step in a bimolecular step).[59] This is connected with the rotational energy of the reactive phosphorus center, which directly corresponds to the steric demand of the ligands surrounding the latter. The phosphorus center needs to rotate such that the lone pair of electrons is distal to the shielding ligands.

The results within this work support this rationale and can be particularly observed for the formation of higher generation phosphonium salts (see chapter 3.4), where longer reaction times at elevated temperature (165 °C, 16 – 36 h) facilitate the intrusion of air into the reaction vial on the one side. Additionally, the cleave-off of one dendron to form the respective R_3P phosphine side product during the reactions outlined in **Figure 3-9** and **Figure 3-10** is supposed to be increased due to longer reaction times leading to significant yield losses of the desired phosphonium salts.

Having emphasized the necessity of oxygen-free reaction conditions for the preparation of bulky phosphonium salts, a close view of their analytics will follow. Since the phosphonium cation $C_{144}H_{100}P^+$ of **3-6** possesses a large number of protons in the aromatic region, ^{1}H-NMR spectroscopy is an informative and suitable method for its characterization. A closer look at the low-field region (high chemical shifts) reveals specific signal patterns being typical for ^{1}H-spectra of polyphenylene dendrimers (**Figure 3-6**).

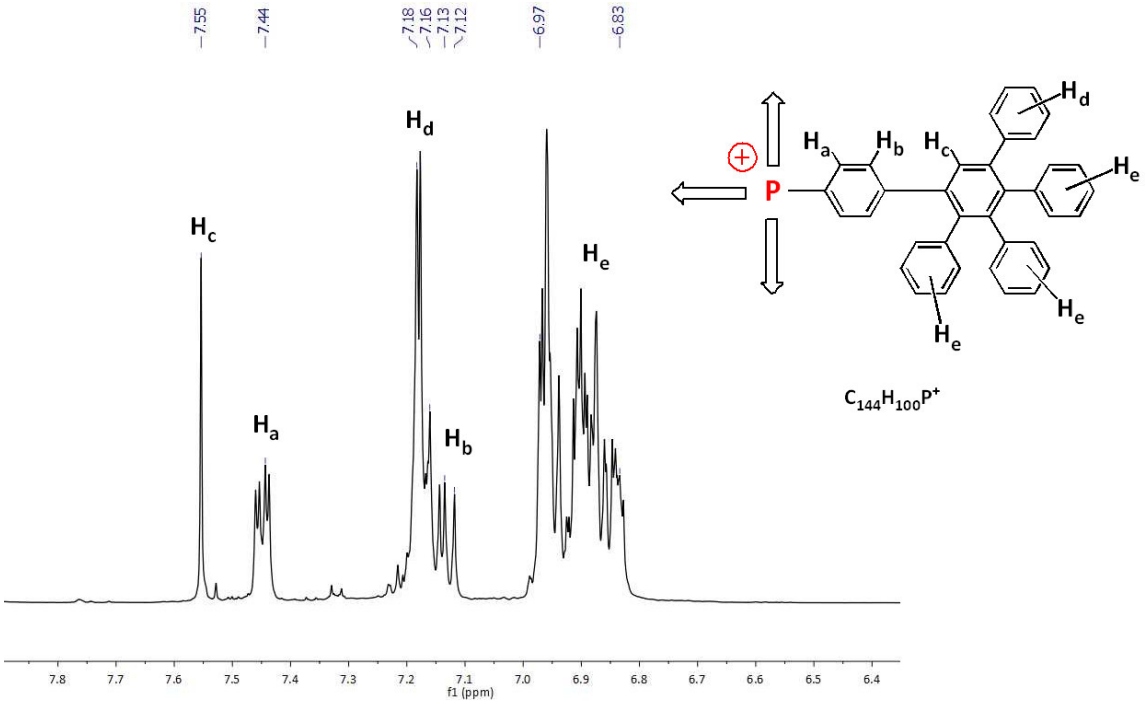

Figure 3-6: ^{1}H-NMR spectrum of **3-6** in CD_2Cl_2 (500 MHz, 298 K).

The sharp low-field singlet at δ 7.55 attributed to the protons H_c at the central "branching" phenyl ring is characteristic for the dendritic polyphenylene structure and is called "**generation proton**", since this structural element is built with every growth step. Higher

generation PPDs possess larger numbers of generation protons and thus more low-field shifted singlets in their ^{1}H-NMR spectra. The signals of the inner phenyl protons H_a at δ 7.44 appear as a well resolved doublet of doublets, which clearly shows the heteronuclear spin-spin coupling between ^{31}P-nucleus and ^{1}H ($^{3}J_{P,H}$ = 8.4 Hz). This is a typical value for vicinal proton coupling to ^{31}P and is observed for all ^{1}H-spectra within this work and serves as valuable way to assign the protons adjacent to the phosphorus center. The signals of the aromatic protons H_d of the phenyl ring next to the generation proton are shifted low-field compared to the other peripheral aromatic protons H_e, since the according phenyl group H_d is less shielded from the magnetic field by neighboring just one direct phenyl ring. Thus, by means of integration a clear distinction of the aromatic protons is possible and structure elucidation is supported by NMR-techniques.

The dendronized salt $[P\text{-}G1]^{+}$ BF_4^{-} (**3-6**) was crystallized in the form of yellow needles and analyzed by X-ray diffraction. Its single crystal structure confirms the formation of a large, rigid and bulky extension of the inner tetraphenylphosphonium core (**Figure 3-7**).

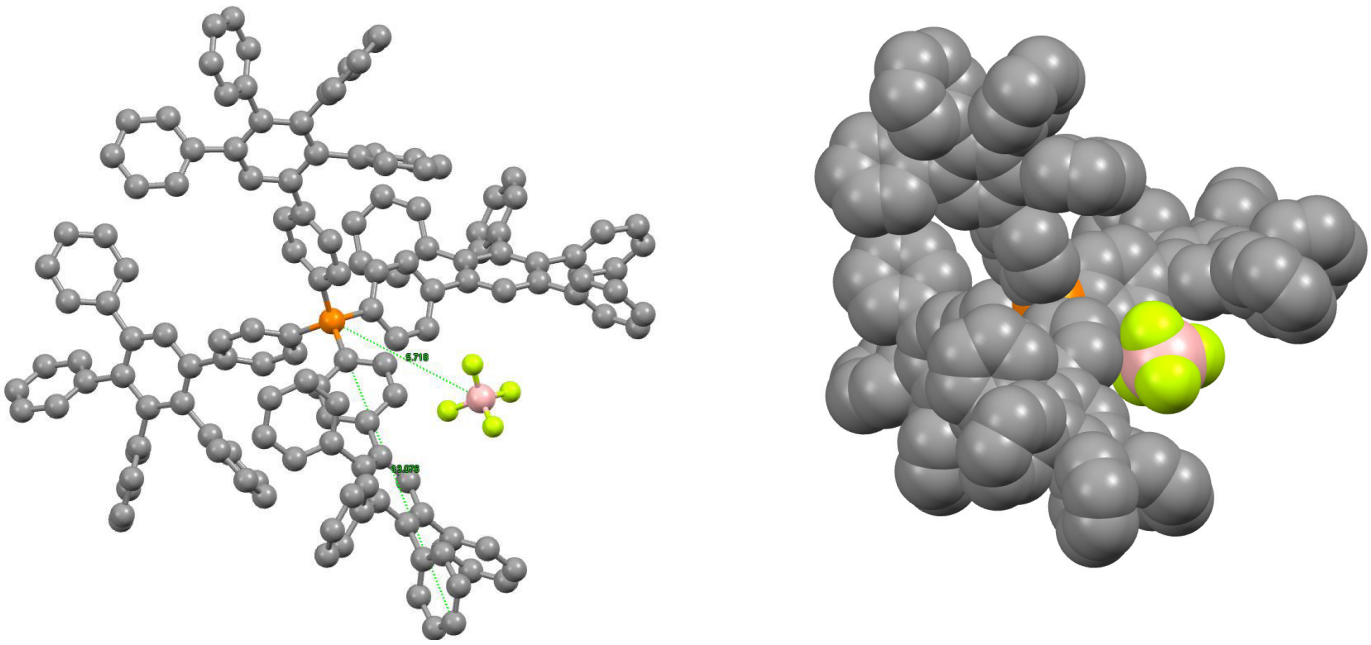

Figure 3-7: (left): Single crystal structure of G1-phosphonium tetrafluoroborate **3-6** (solvents are omitted for clarity). (right): space-filling structure.

The first-generation phosphonium salt crystallized in the tetragonal space group $I4_1/a$. The central P atom occupies the special position (0 ¼ 1/8) – this means the four pentaphenylbenzene ligands are equivalent. The angles between the least square planes of the phenyl ring with respect to the central ring vary from 57.0 to 63.6 °.

Special interest within this work was put on the charge separating ability due to dendronization, which is reflected by the closest distance between cation and anion. From the single crystal of **3-6** it was found that the boron atom from the BF_4^- anion is spatially separated by 0.57 nm from the central cationic phosphorus atom. Thus, there is a significant interdigitation into the hydrophobic polyphenylene scaffold of the phosphonium sphere caused by Coulombic attraction, since the distance from the phosphorus atom to the periphery is 1.39 nm, which is in good agreement with a modelled theoretical cation-radius of 1.4 nm predicted under the assumption of an impervious spherical geometry.

For the purpose of comparison, commercially available tetraphenylphosphonium tetraphenylborate PPh_4^+ BPh_4^- was crystallized under analogous conditions. The distance from the central phosphorus to the closest boron atom was found to be 0.71 nm, so the charges were spatially even more separated though the cation is sterically less encumbered compared to $[P\text{-}G1]^+$ in **3-6**. Despite the fact that the significantly overall augmented cation size of **3-6** had only minor effect on the closest cation – anion contact, the polyphenylene shells largely increased ion distances towards secondary counter ion neighbors to 1.79 nm (compared to 0.87 nm for PPh_4^+ BPh_4^- secondary ion pair distances). This was concluded by analyzing the crystal lattice packing pattern and is depicted in **Figure 3-8**.

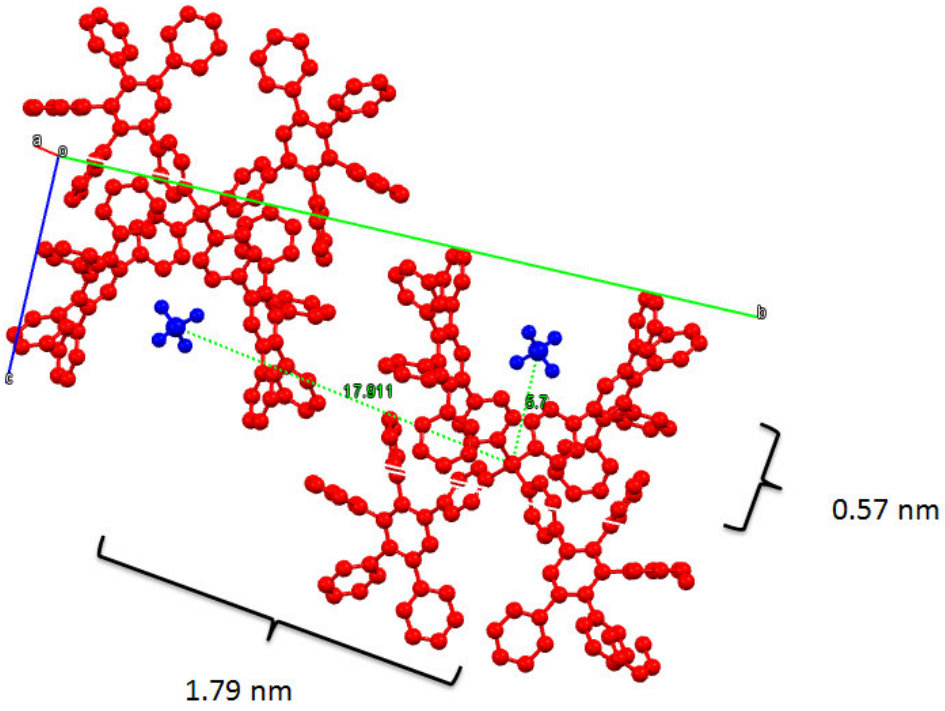

Figure 3-8: Crystal lattice packing of G1-phosphonium tetrafluoroborate **3-6** (cations in red, anions in blue)**.**

As a consequence, the resulting lattice enthalpies of dendronized phosphonium salts can be expected to be significantly lower than those of non-dendronized salts. The achieved increase of steric shielding by polyphenylene dendrons should make dendronized phosphonium salt **3-6** less coordinating compared to non-dendronized tetraphenylphosphonium. Hence, weaker coordination should be reflected in a promotion of ion dissociation, especially in low polarity media. These effects will be tested and compared in paragraph 4.4 of this work.

3.4 Divergent Dendritic Growth towards higher-generation Cations

After it has been shown that the construction of a hydrophobic polyphenylene framework around a phosphonium core could be successfully achieved via thermal *Diels-Alder* reaction with tetracyclone, the subsequent task was to further increase the number of generations and therewith increasing the size and bulkiness of the encapsulating polyphenylene shell. Therefore a branching cyclopentadienone unit capable of continuing the growth step had to be implemented. This was realized by reacting tetracyclone AB_2 building block (**3-7**) with ethynyl-functionalized phosphonium core **3-5**, hence leading to a first-generation phosphonium ion **3-8** bearing 8 TiPS-protected alkyne functionalities on the surface. After deprotection of the silyl groups with tetrabutylammonium fluoride (TBAF), the resulting ethynyl-decorated cation **3-9** could be subjected to a second dendronization step by reaction with tetracyclone yielding the second-generation phosphonium salt $[P\text{-}G2]^+$ BF_4^- (**3-10**). Despite the large steric demand of tetracyclone AB_2 (**3-7**), the cycloaddition reaction towards phosphonium **3-10** was successful also in a complete manner as evidenced by MALDI-TOF mass spectrometry (**Figure 3-9**). However, the yield decreased to 61 % due to the increased reaction time at elevated temperatures (sealed microwave vial, 165 °C, 16 h) and manifold side-products could be detected. For instance the main side product, the neutral phosphine oxide derived from **3-10** by cleaving the inner phosphorus-carbon bond had to be separated by tedious column chromatography purification from the target molecule. The general discussion about the oxidation via molecular oxygen has already been presented in chapter 3.3.

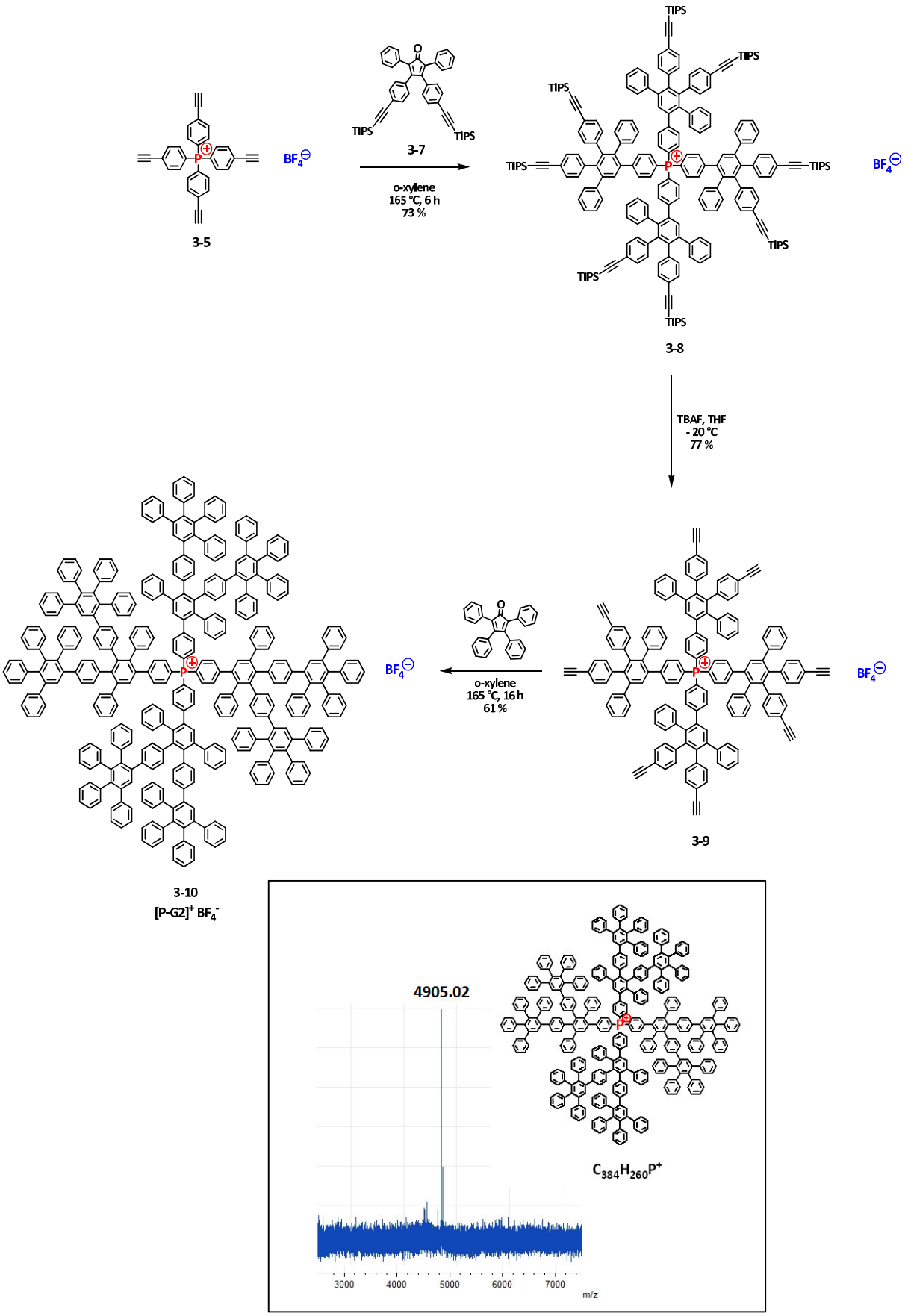

Figure 3-9: Synthesis pathway to G2-phosphonium tetrafluoroborate **3-10**. (inset): MALDI-TOF- spectrum of the corresponding cation **[P-G2]$^+$.**

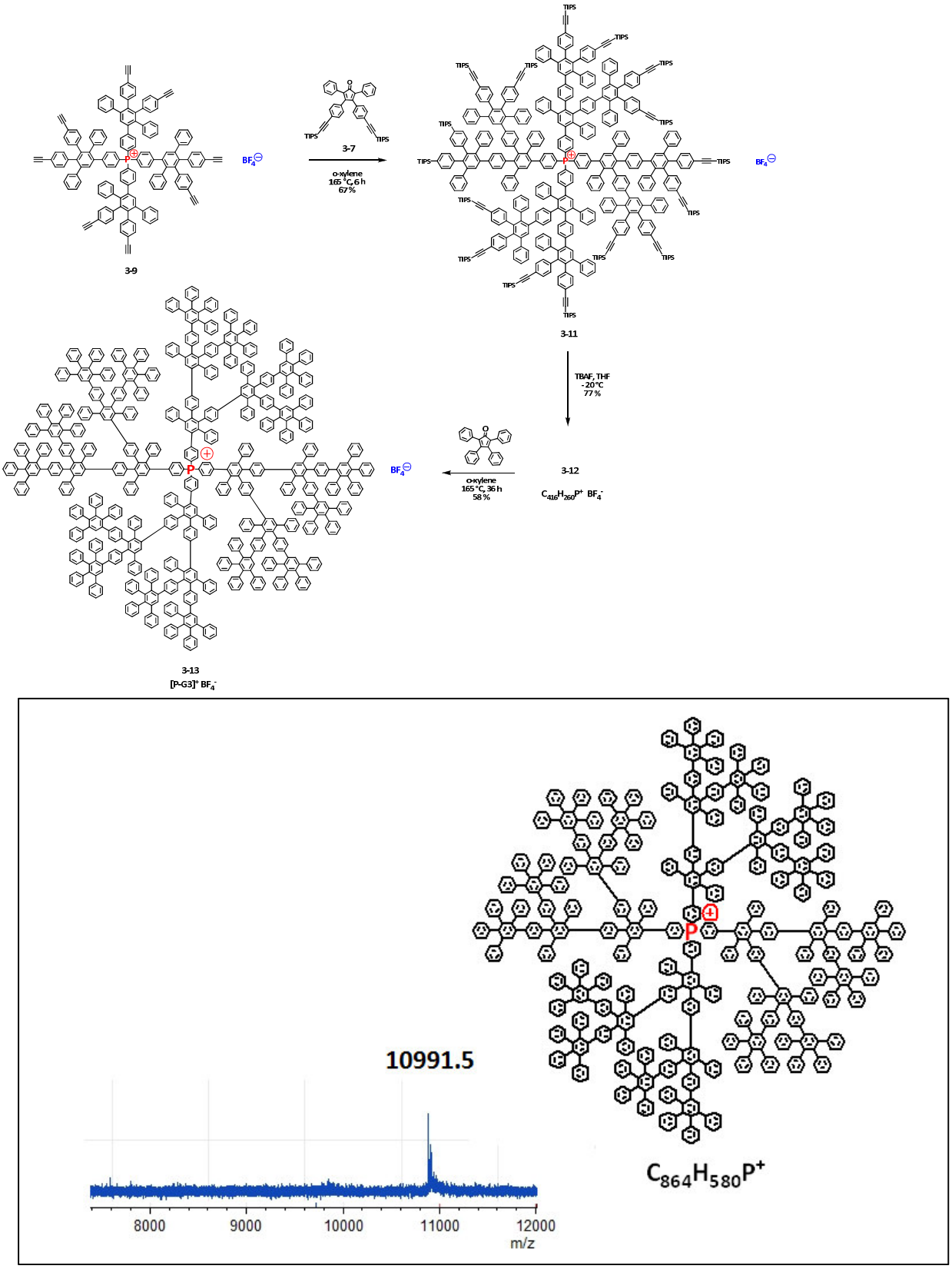

Figure 3-10: Synthesis pathway to G3-phosphonium tetrafluoroborate **3-13**. (inset): MALDI-TOF- spectrum of the corresponding cation **$[P\text{-}G3]^+$.**

The synthetic strategy of repetitive growth step followed by re-activation (deprotection of the silyl-groups via TBAF) was further exploited to synthesize third-generation phosphonium tetrafluoroborate salt $[P\text{-}G3]^+ BF_4^-$ **3-13** (synthesis scheme see **Figure 3-10**). Hence it has been clearly shown that dendronization via thermal *Diels-Alder* cycloaddition represents by all means a valuable method to generate monodisperse macromolecules with molecular weights above 10.000 mass units with no hints of incomplete reaction side products. The impact of the hydrophobic encapsulation and enlargement of the ion radii of the herein synthesized phosphonium salts on the physicochemical properties like solubility, conductivity and ion dissociation in organic solvents will be discussed in greater detail in section 4.4.

3.5 Surface Functionalization

3.5.1 Fluorination

Inspired by the fact that solubility properties of dendritic molecules are essentially dominated by their periphery as works by *Tomalia* and *Fréchet*[60] already pointed out, the applicability of directed surface modification for positively charged phosphonium core structures was investigated. A valuable tool to effectively lower an ion's coordination ability is represented by the fluorination of its periphery. This well-known pattern of either full surface-perfluorination or introduction of 3,5-meta CF_3 aryl functionalities has already been utilized numerous times for generating more weakly coordinating anions.[2] The low polarizability of fluorine causes a suppression of even temporary attractive forces (dispersive interactions) towards other molecules. Thus, fluorinated ions show considerably less tendency towards coordination as compared to their non-fluorinated analogues. An additional consequence of the surface fluorination is the generation of a chemically robust and inert shell.

However, the synthesis of tetrakis-(pentafluorophenyl)phosphonium salts, $P[(C_6F_5)_4]^+ X^-$, is tedious and proceeds according to literature reports by reacting highly electrophilic organoxenium-(II)-salts with the weak nucleophilic fluorinated phosphane $P(C_6F_5)_3$ in the melt.[61, 62] Thus, the distinct delocalization of electron density at the phosphorus hinders the reaction with electrophiles. For that reason a divergent synthesis approach based on the *Diels-Alder* cycloaddition was pursued within this work.

Initially, we attempted to synthesize a first-generation phosphonium derivative **3-15** with a fully perfluorinated surface. Therefore ethynyl-functionalized phosphonium core **3-5** was reacted with fluorine-containing tetracyclone building block **3-14** (synthesized according to literature procedure[63]) under various conditions.

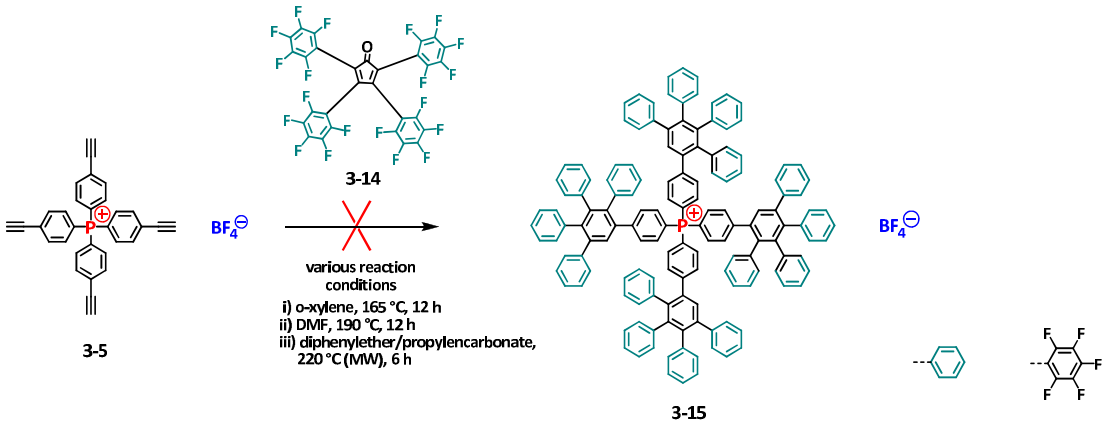

Figure 3-11: Synthesis scheme towards perfluorinated G1-phosphonium tetrafluoroborate **3-15**.

Although high temperature and long reaction times were applied, nevertheless phosphonium salt **3-15** could not be prepared, but instead starting material and non-dendronized phosphine oxide were isolated. Since the thermal pericyclic reaction between diene **3-14** and dienophile **3-5** failed to form the cycloaddition product, the reasons therefore had to be discovered in subsequent experiments. In order to investigate the role of the electronic environment of the reactive acetylene group, first-generation phosphonium cation $[P\text{-}G1\text{-}(ethynyl)_8]^+ BF_4^-$ **3-9** was reacted with perfluoro-tetracyclone **3-14**. Astonishingly this microwave-assisted reaction resulted in the successful preparation of second-generation perfluoro-phosphonium salt **3-16**, as evidenced by MALDI-TOF spectrometry (m/z = 6262.6).

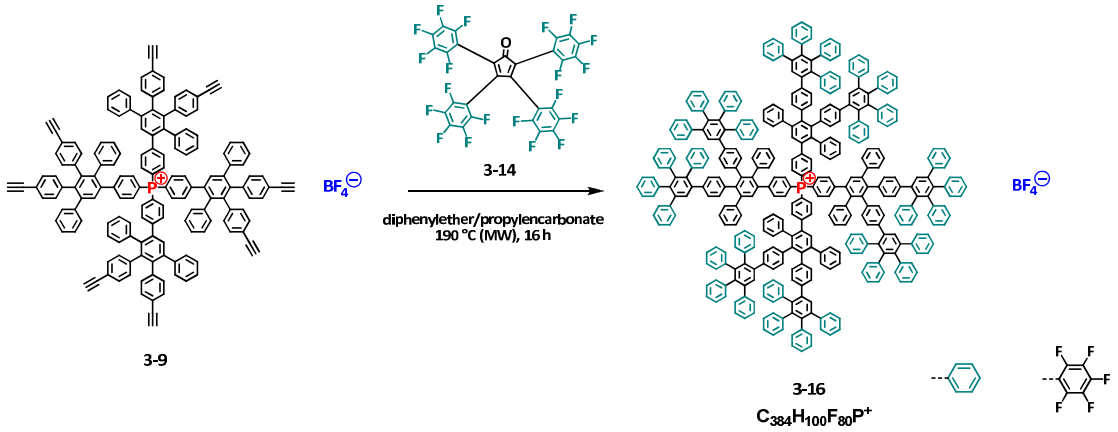

Figure 3-12: Synthesis scheme towards perfluorinated G2-phosphonium tetrafluoroborate **3-16**.

Combining these unexpectedly different reaction outcomes with the fact that the analogous *Diels-Alder* reaction between an ethynyl-functionalized tetraphenylborate **3-17** and fluorine-containing diene **3-14** stated below resulted in the successful preparation of first-generation anion **3-18**,[1] let us come to the conclusion that the rationalization for these observations must be realized by the frontier molecule orbital theory. Further support for our assumption is given by the unavailing attempts to react ethynyl-functionalized perfluoro-borate core **3-19** with diene **3-14** (**Figure 3-13**, bottom), which did not yield the desired first-generation target borate anion **3-20**. [64]

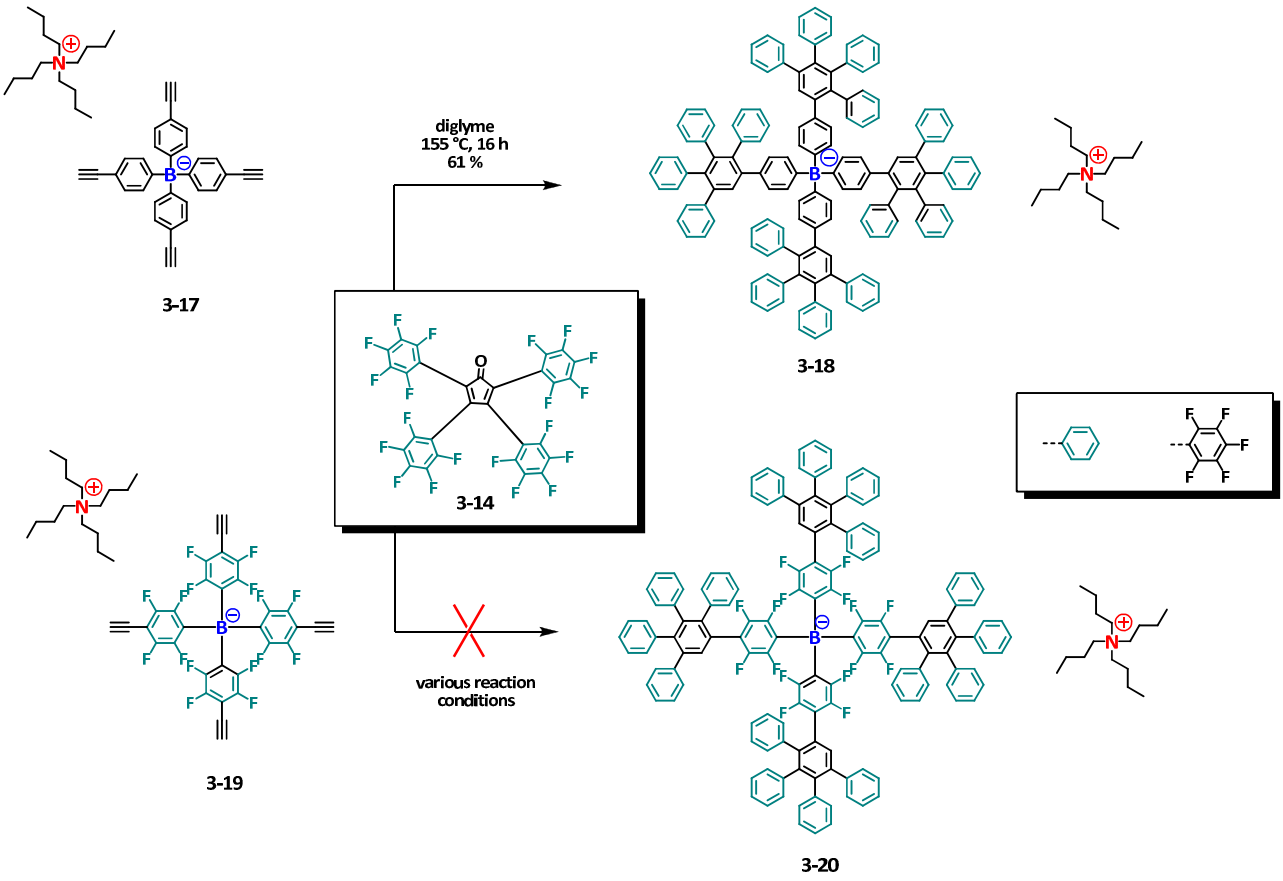

Figure 3-13: Synthesis schemes for the reaction between tetracyclone **3-14** and different borate cores **3-17** and **3-19**.

All the above discussed *Diels-Alder* reactions are orbital symmetry-allowed, thermal [4+2] cycloadditions reactions matching Woodward-Hoffmann rules.[65] In *Diels-Alder* [4+2] cycloadditions with normal electron demand, the MO-interaction occurs between the highest occupied molecule orbital (HOMO) on the diene component and the lowest unoccupied molecule orbital (LUMO) on the dienophile (**Figure 3-14**). The resulting formation of two new σ-bonds (at the expense of two π-bonds) requires disrotatory movement of the participating frontier molecule orbitals.

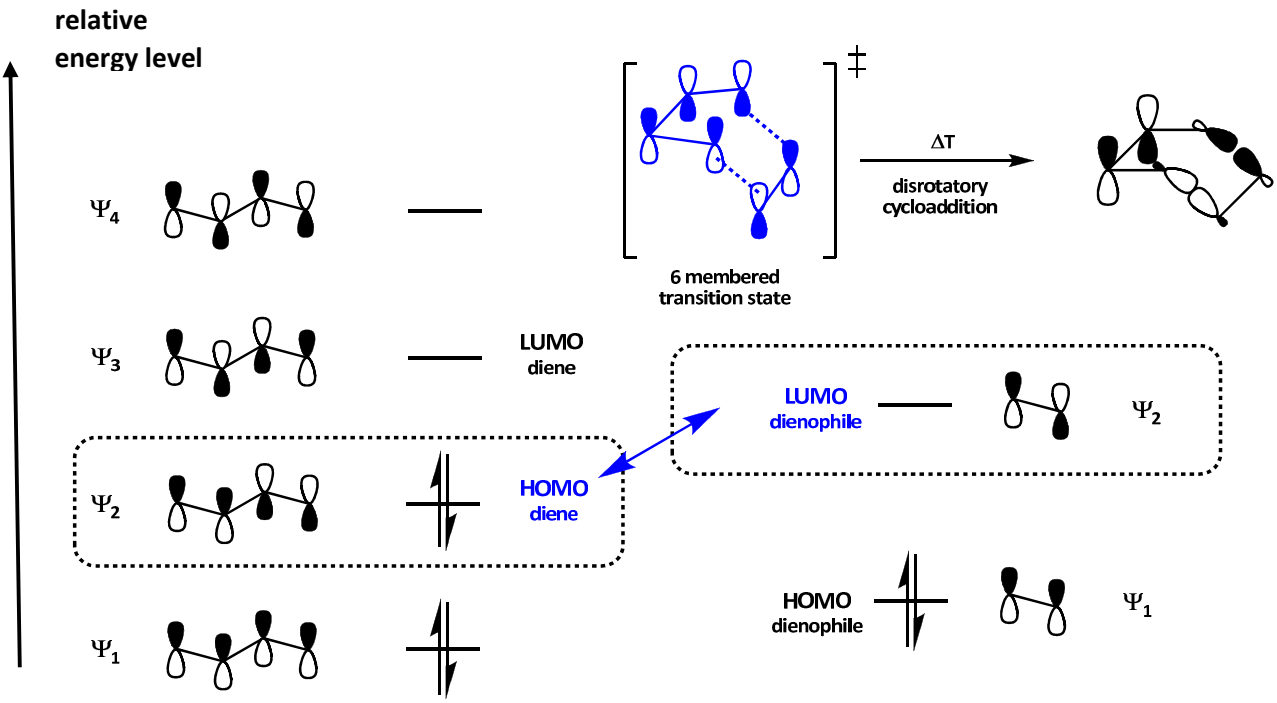

Figure 3-14: Molecule orbital theory scheme for the [4+2] cycloaddition reaction between a diene and a dienophile.

The herein employed tetraphenylcyclopentadienone represents an electron poor diene component with a lowered energy level for its LUMO (LUMO = -2.86 V; HOMO = -5.46 V, obtained from DFT calculations with the B3LYP, G-31G* dataset). In the case of the perfluorinated tetracyclone **3-14** the decrease in LUMO energy is even more pronounced due to the strongly electron-withdrawing pentafluoro-substituents (LUMO = -4.5 V; HOMO = -7.53 V, obtained from DFT calculations with the B3LYP, G-31G* dataset).

For [4+2] cycloadditions of such compounds, however, the orbital interaction between the LUMO on the diene component and the HOMO of the dienophile is of emerging importance in contrast to the opposite situation illustrated above. These type of reactions are termed Diels-Alder reactions with “inverse electron demand”. Studies by Konovalov[66] underline that the reaction rate between tetraphenylcyclopentadienone and substituted styrene derivatives increases with electron-donating functional groups on the dienophile component. This tendency can be rationalized in the energy scheme shown below (**Figure 3-15**) under the presumption of the aforementioned orbital overlap.

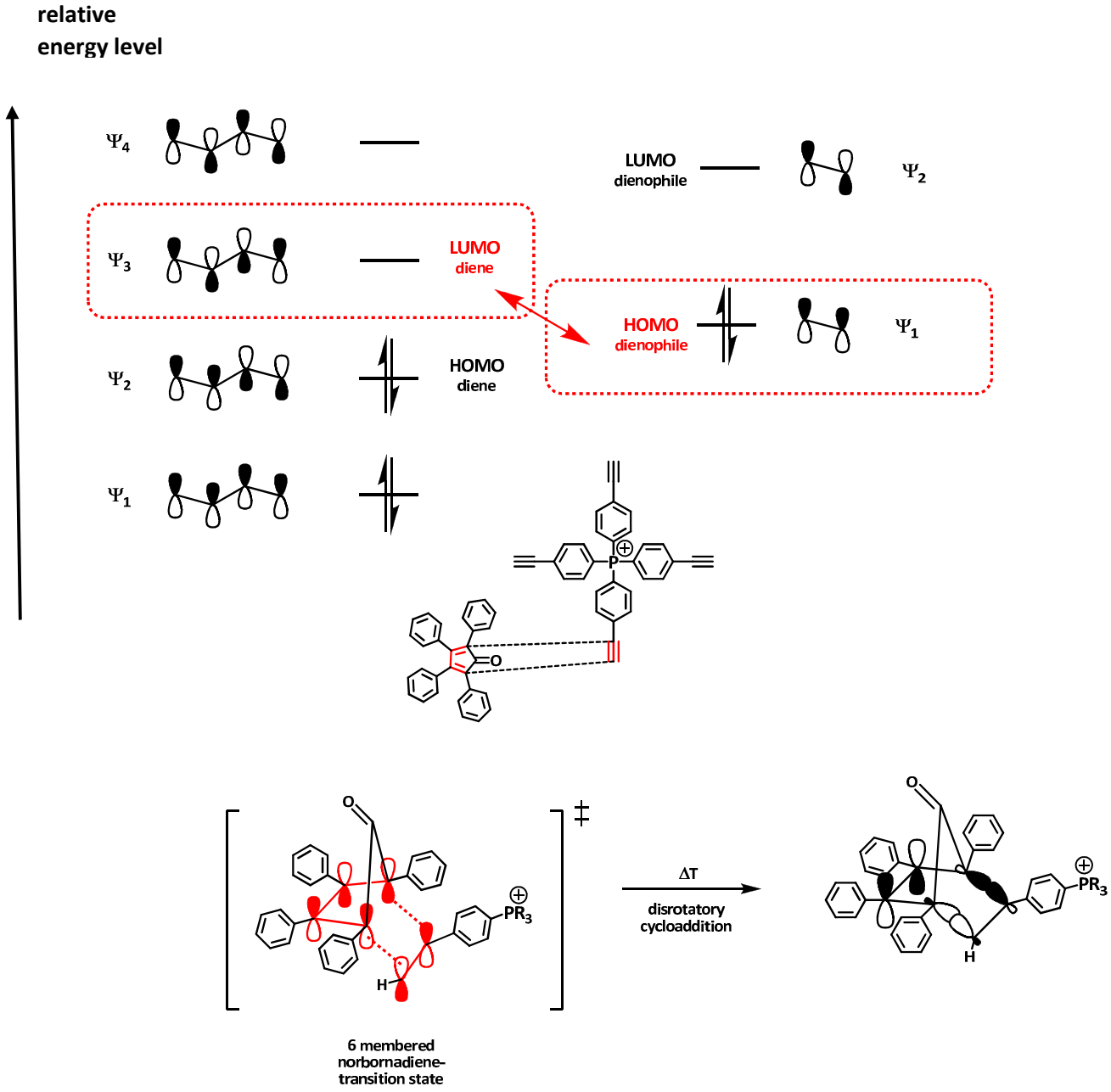

Figure 3-15: Molecular orbital theory scheme for the [4+2] *Diels-Alder* cycloaddition with inverse electron demand. (bottom): Transition state geometry of the reaction between tetraphenylcyclopentadienone and ethynyl-group.

A reasonable estimation of energies and coefficients of frontier molecule orbitals in dependence of the adjacent substituents has been reported in literature.[67] A closer look at the dienophile component (ethynyl-group for the distinct reaction of interest in our case) reveals that electron withdrawing groups (e.g. CHO, PR_3^+ for the phosphonium core **3-5**) produce a lowering of energy of both the $HOMO_{dienophile}$ and $LUMO_{dienophile}$. Vice versa both frontier molecule orbital energies are raised by the introduction of electron-donating groups

(e.g. OMe, BR_3^- for the borate core **3-17**). Substituent effects at C1-postion of the diene components have similar influence on the energy levels of $HOMO_{diene}$ and $LUMO_{diene}$, electron-withdrawal causes a decrease and electron-donation promotes an increase with respect to energy. Thus, the relative MO-energy values of perfluorinated tetracyclone **3-14** are lowered compared to the non-fluorinated analogue. All these tendencies put together are illustrated in **Figure 3-16** with regard to the reactions of interest:

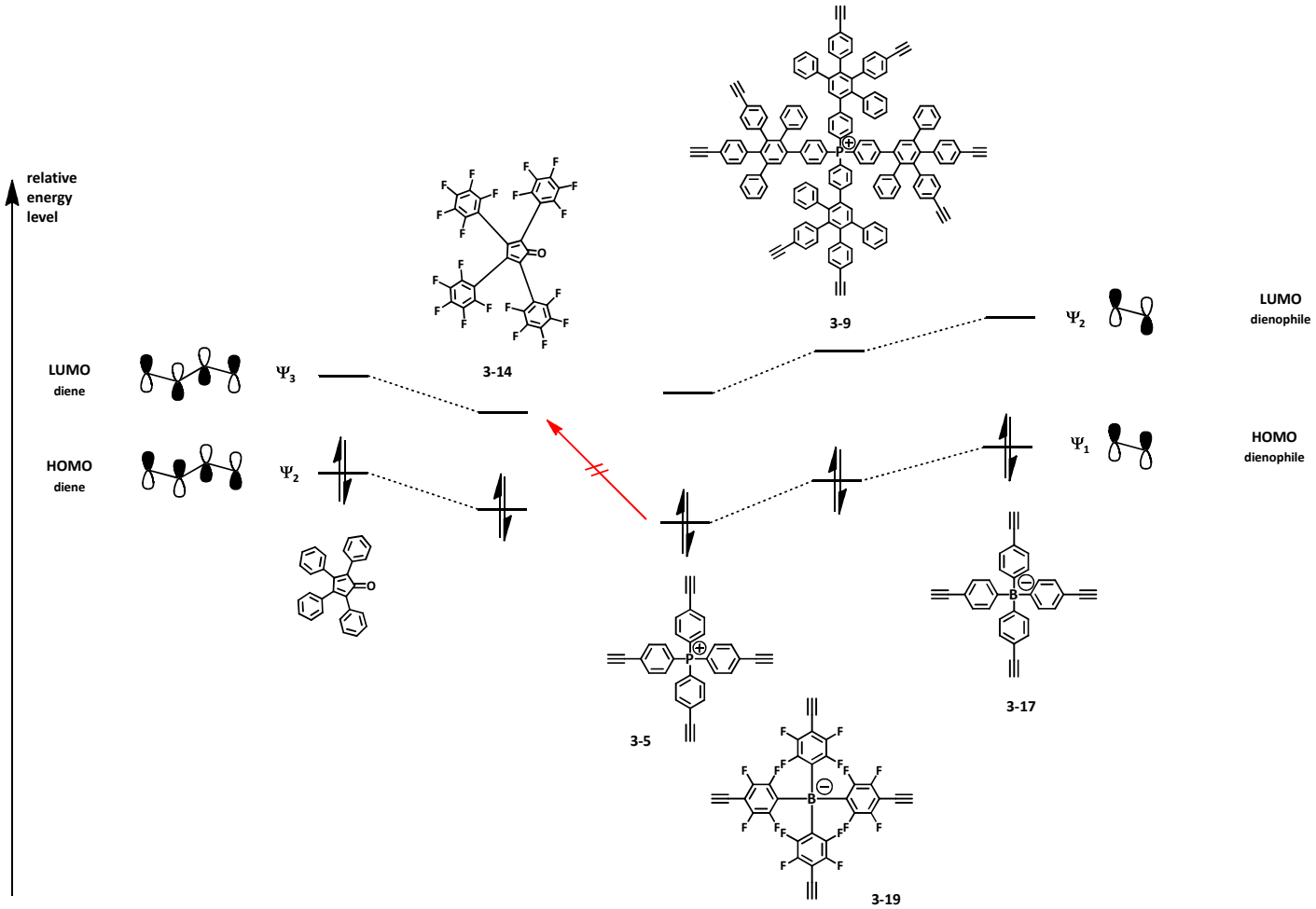

Figure 3-16: Molecule orbital theory scheme with relative energy level estimations for the [4+2] *Diels-Alder* cycloadditions of the reactions between phosphonium cores **3-5**, **3-9** and borates **3-17**, **3-19** with tetracyclones.

It is obvious from the energy level diagram, that the interaction of the lowered $LUMO_{diene}$ of perfluorinated tetracyclone **3-14** with ethynyl-functionalized ionic cores becomes progressively more disfavoured in the order of increasing electron deficiency, meaning also decreasing energy values for the $HOMO_{dienophile}$. This results in an increased energy gap for the crucial frontier orbital interaction (red crossed arrow in **Figure 3-15**) giving a conceivable explanation for the failure of the synthesis of phosphonium cation **3-15** and borate anion **3-20**. Nevertheless, a full explication of all the reaction outcomes above cannot be given solely by the relative molecular orbital energies, but most likely also steric reasons play an important role for the generally observed lowered reactivity of perfluoro-tetracyclone **3-14** compared with its non-fluorinated analogue. However, a by all means smart approach to overcome any steric and electronic restrictions rests upon the expansion of the tetraphenylcyclopentadienone system. An exemplary application of this strategy will be given in the next section.

3.5.2 Bis-(3,5-trifluromethyl)phenyl Surface functionalization

It is a well-known strategy to functionalize an ion's surface with trifluoromethyl-groups (CF_3) for the purpose of minimizing coordinative interaction forces in analogy to the already discussed method of perfluorination.[68] In order to transfer this principle onto the synthesis of phosphonium cations bearing CF_3-groups at the periphery, an adequate functionalized tetracyclone building block **3-22** was prepared via fourfold *Suzuki-Miyaura* coupling reaction between tetrakis-(4-bromophenyl)-cyclopentadienone **3-21** and meta-CF_3-functionalized phenyl boronic acid (**Figure 3-17**).

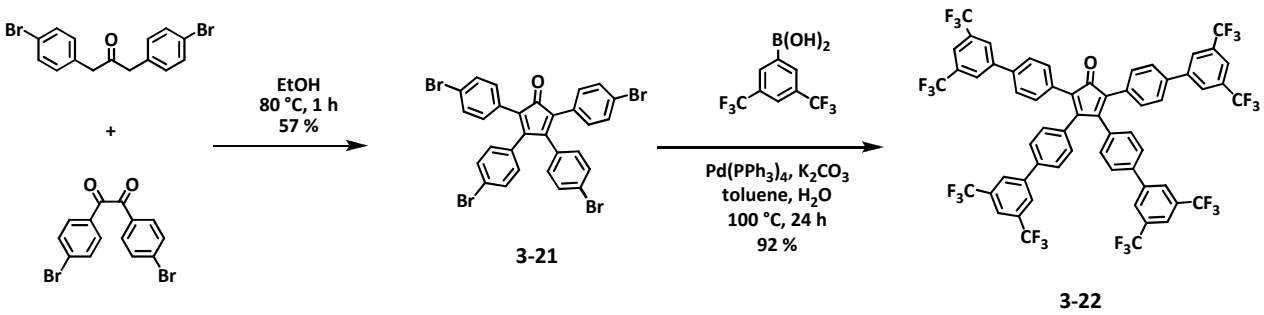

Figure 3-17: Synthetic route to CF_3-functionalized tetracyclone **3-22**.

In addition to being highly fluorinated, building block **3-22** provides a spatially expanded cyclopentadienone system, which proved of particular value for avoiding any steric or electronic restrictions in the generation of CF_3-decorated, large phosphonium cations. Consequent build-up of the first-generation dendrimer **3-23** was successfully performed by standard conditions for thermal *Diels-Alder* reactions between core **3-5** and **3-22**.

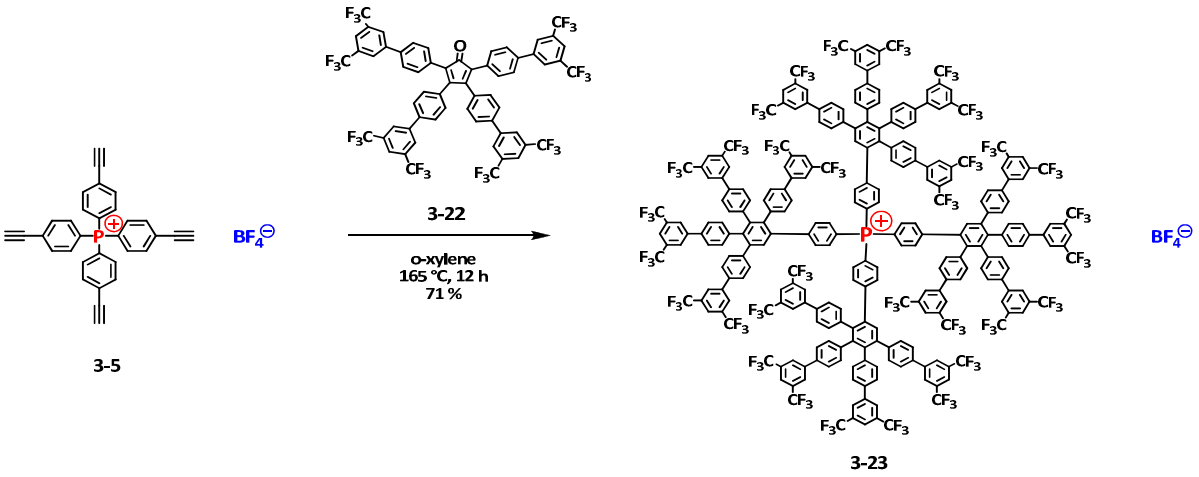

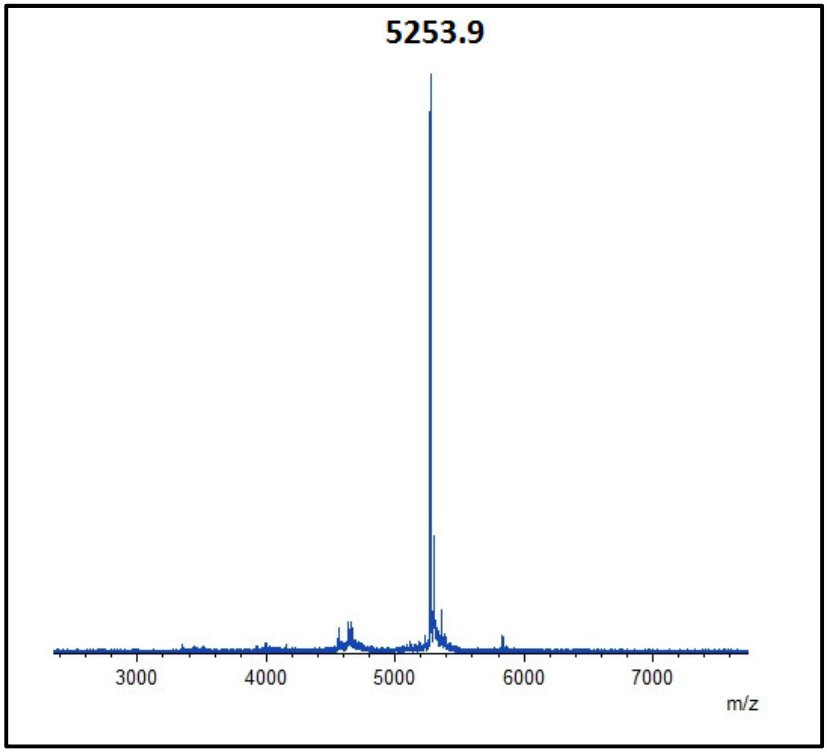

Figure 3-18: Synthesis of first-generation, highly fluorinated phosphonium salt **3-23**. (bottom): MALDI-TOF mass spectrum.

The according MALDI-TOF mass spectrum in combination with heteronuclear NMR techniques of the product **3-23** confirms its complete formation. Hence, the preparation of highly fluorinated phosphonium cation **3-23** serves as illustrative example of the versatile, toolkit-like method of divergent dendritic growth. At first glance, the specific surface modification with fluorine caused synthetic issues, which were easily compensated by simply expanding the diene component by an additional benzene ring. Thereby both, the electron-withdrawing effect as well as the steric hindrance caused by the present meta-CF_3-groups were impinged.

3.6 Synthesis of Aryl-Triazole Hybrid Phosphonium Dendrimers

In order to increase yields and prevent side product formation it is desirable to utilize a dendronization growth step, which proceeds at lower temperatures and milder reaction conditions than the thermal *Diels-Alder* cycloaddition applied so far in the previous sections. For this reason a different synthetic approach on the basis of *Huisgen's* 1,3 - dipolar cycloaddition[69] of azides to terminal alkynes was applied, which results in the formation of substituted triazole-heterocycles. The concerted $[2_s+4_s]$ cycloaddition reaction of a 2 π-electron dipolarophile (e.g. ethynyl-group) and a 4 π-electron dipolar compound (e.g. azide) has been modified by the *Sharpless* group[70] to a copper-(I)-catalyzed, regioselective and stepwise process. This type of "click chemistry", shortly termed copper-(I)-catalyzed azide-alkyne cycloaddition (CuAAC), has already been utilized to synthesize a variety of triazole-rich dendrimers.[71]

Due to its high efficiency and reliability, the CuAAC reaction would provide mild reaction conditions for the synthesis of phosphonium dendrimers. Thereby, the construction of a stiff dendritic framework consisting of benzene- and triazole-rings could be carried out even at room temperature. Our group recently demonstrated the synthesis of shape-persistent hybrid dendrimers[72] with different geometrical architectures. Within this work we further exploited that type of click chemistry for the charged core building block **3-5**.

The construction of the dendritic aryl-triazole framework required the preparation of a bulky aryl azide **3-25** that is capable of reacting with the ethynyl-functionalities of the tetrahedral phosphonium core **3-5**. In principal, such organic azides are easily synthesized via conversion of the according aryl amine.[73]

Thus, commercially available 4-ethynylaniline served as the starting compound, which was reacted with tetracyclone to yield polyphenylene aniline derivative **3-24**. Afterwards, functional group conversion resulted in the preparation of the desired azide building block **3-25**, which was suitable for divergent dendrimer synthesis via Cu-(I)-catalyzed reaction. **3-25** was obtained quantitatively in form of a yellow solid and could be stored for several months at 2 °C without any hints of decomposition.

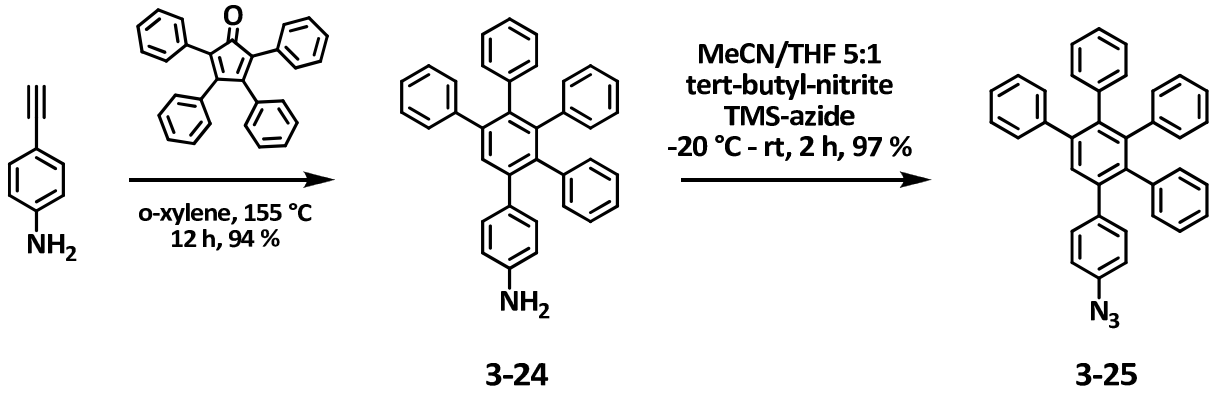

Figure 3-19: Synthetic route to bulky aryl azide building block **3-25**.

First-generation aryl-triazole dendrimer **3-26** was synthesized via copper-(I)-catalyzed azide-alkyne ligation of bulky azide **3-25** and phosphonium core **3-5**. It should be mentioned that acetonitrile was the solvent of choice due to its outstanding solvation and stabilization ability of univalent d^{10}-metal ions.[74] Moreover, the use of tris-(benzyltriazolylmethyl)-amine (TBTA), synthesized according to literature procedure,[75] as the stabilizing ligand turned out to provide the best results. Residual copper was removed by washing with aqueous ammonium chloride solution. Further purification of **3-26** could be achieved via column chromatography owing to the greatly enhanced solubility in organic solvents (DCM, THF, MeCN) in contrast to recently reported phenylene-triazole hybrid dendrimers.[72] This is attributed to the fact, that solubility of dendritic molecules is mainly dominated by their periphery as works by *Tomalia* and *Fréchet* pointed out.[76] Also aggregation of triazole

moieties is hindered due to the attachment of bulky polyphenylene dendrons at the periphery, which is another aspect that might explain the outstanding high solubility of **3-26** in organic solvents.

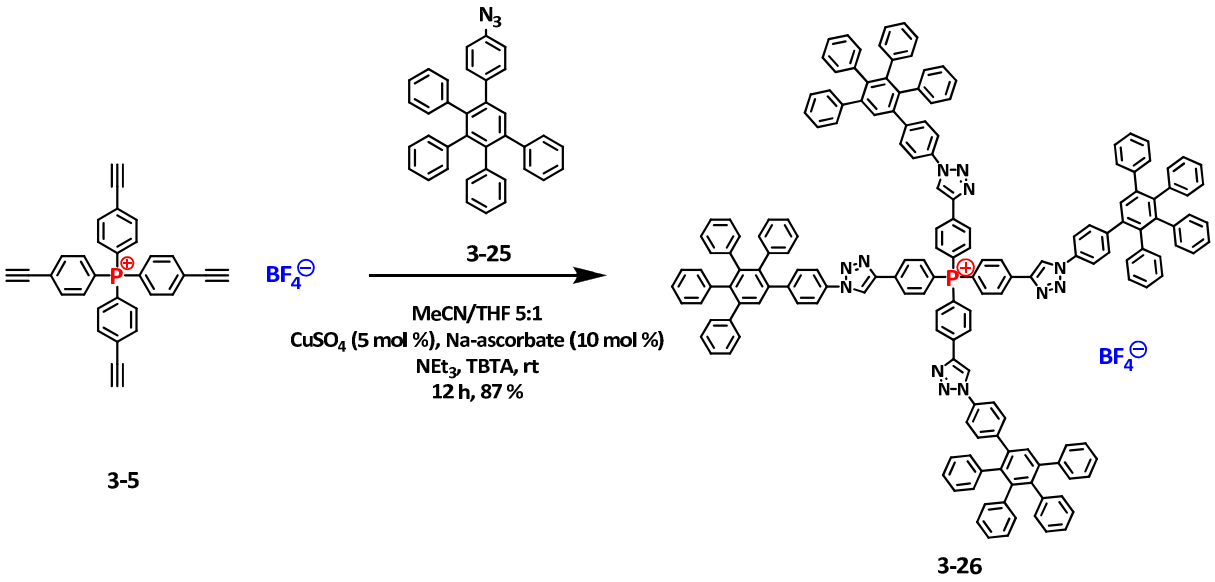

Figure 3-20. Synthetic route to triazole-polyphenylene hybrid dendrimer **3-26**.

^{1}H and ^{13}C NMR signals of dendrimer **3-26** could readily be assigned and were used to confirm complete conversion as well as purity and regioselectivity. A detailed analysis of the proton NMR spectra is given in **Figure 3-21**. Measurements by means of MALDI-TOF mass spectrometry showed the formation of a monodisperse macromolecule (m/z 2434.1), but also demonstrated that polyphenylene-triazole cation **3-26** decomposes easily upon laser irradiation (**Figure 3-22**). The additional signal appearing at a lower m/z ratio of 26 m/z was attributed to a release of nitrogen from a triazole moiety. The yield of triazole-rich phosphonium salt **3-26** was slightly higher (87 %) compared to $[P\text{-}G1]^{+}$ BF_4^{-} (**3-6**) (78 %), which was one of the initial motives for the use of azide building blocks.

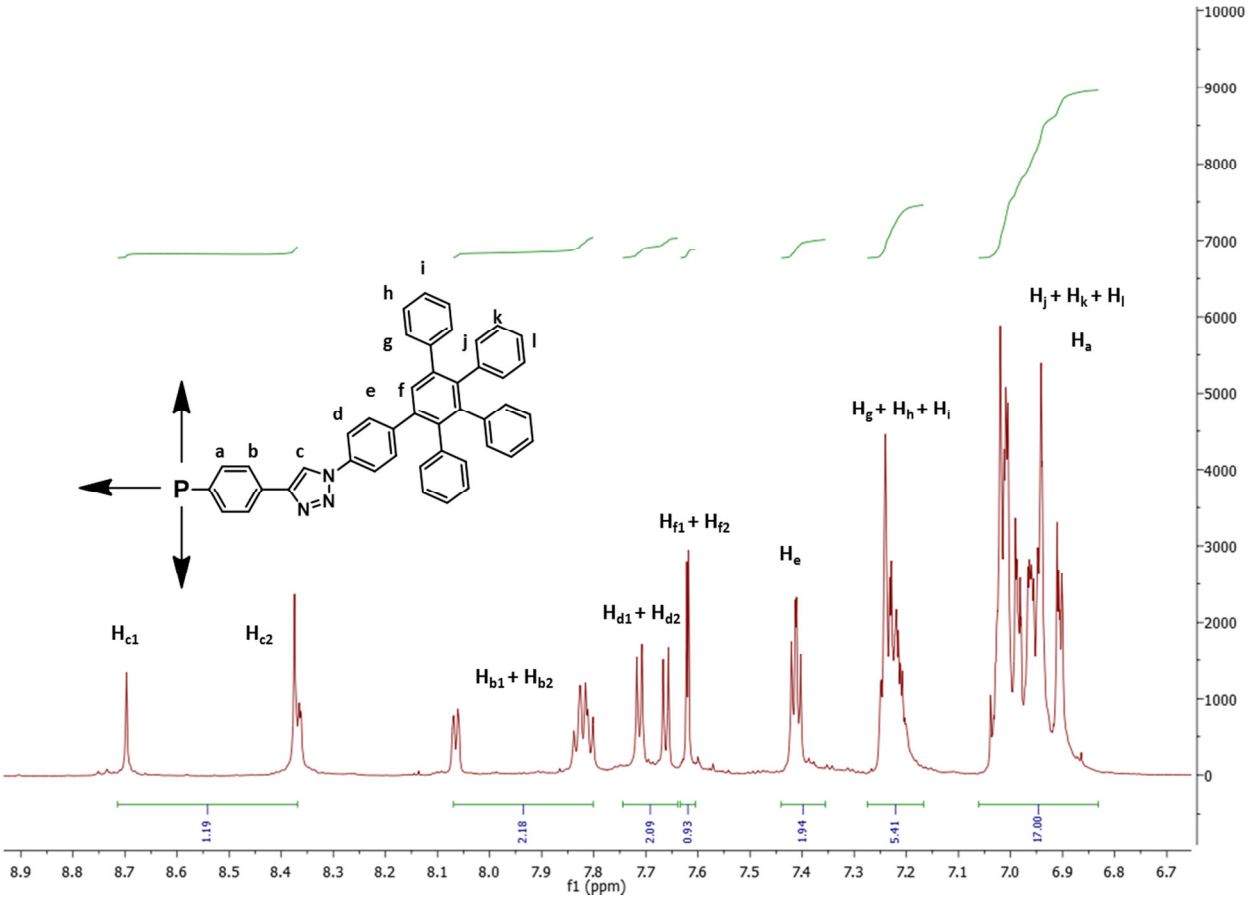

Figure 3-21: Low-field region of ^{1}H-NMR spectrum (850 MHz, CD_2Cl_2, 298 K) of triazole phosphonium salt **3-26**. The complete assignment of the signals was performed with the additional analysis of COSY-, HSQC-, NOESY- and DOSY-NMR spectra. The splitting of the triazole protons and the neighboring ^{1}H cores is attributed to the presence of two atropisomers of compound **3-26** in solution, which is a result of blocked rotation in the rigid molecule. This phenomenum was comprehensively described for first-generation polyphenylene-triazole dendrimers after careful NMR-analysis.[64]

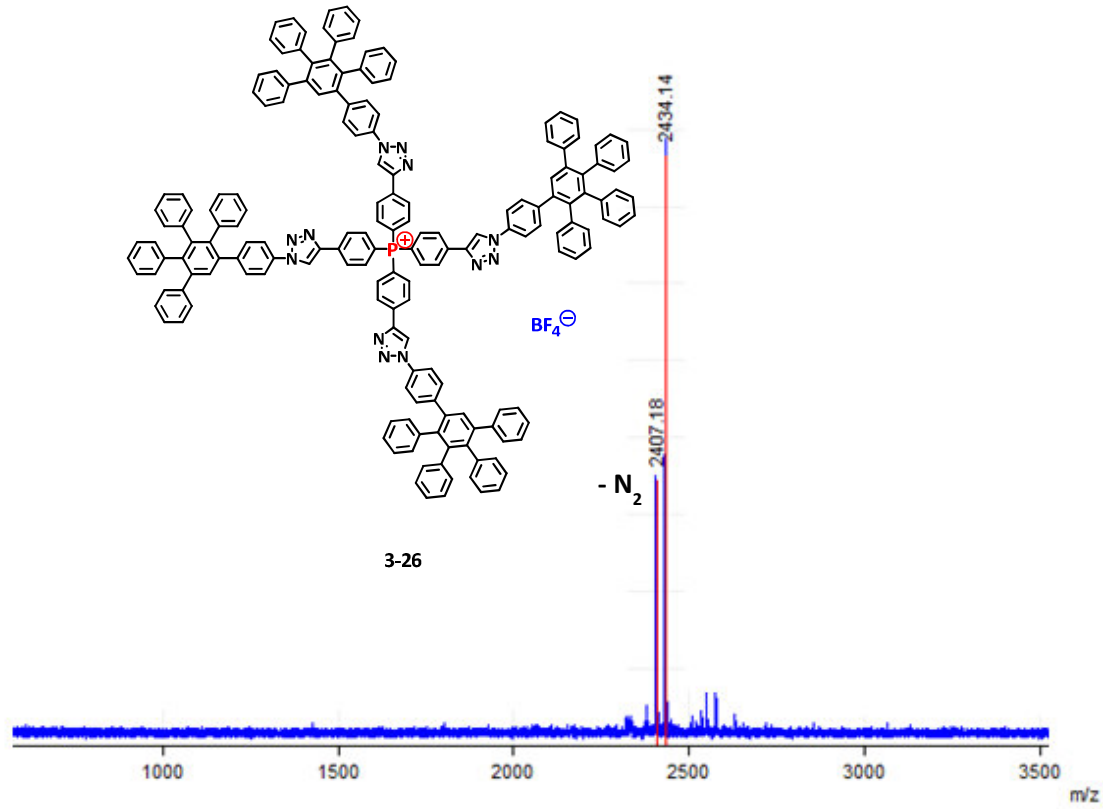

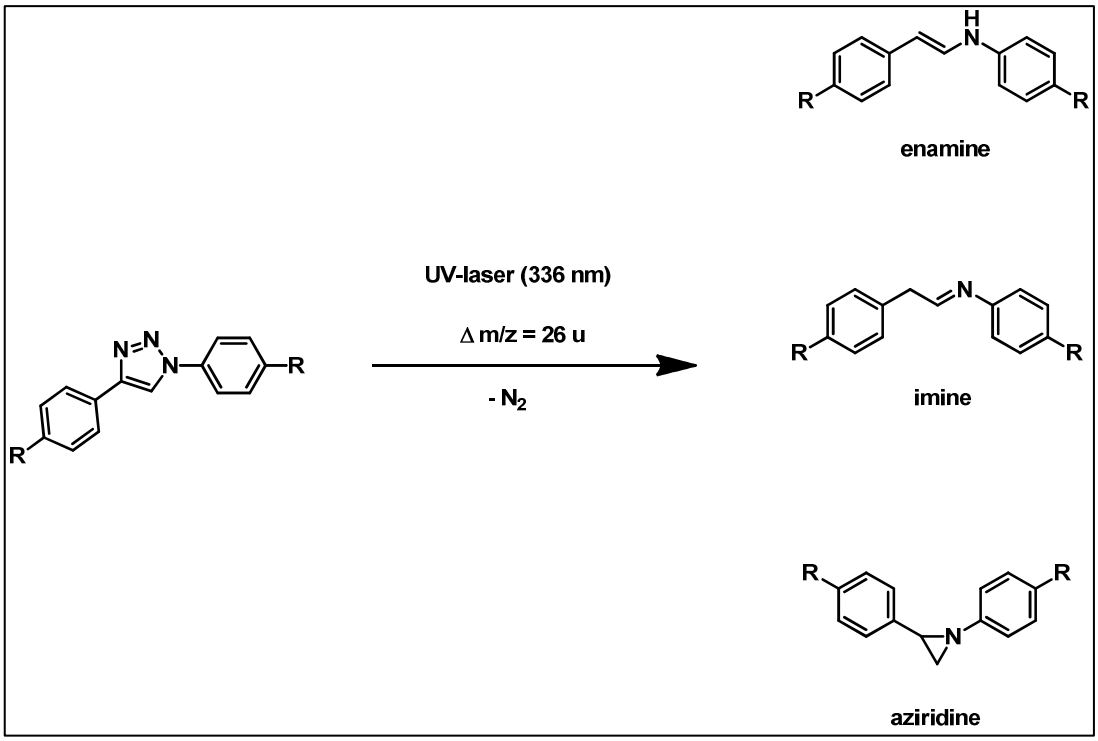

Figure 3-22: MALDI-spectrum of triazole phosphonium-G1 tetrafluoroborate **3-26**. **Bottom:** UV laser induced loss of nitrogen N_2 from triazole rings in aryl-triazole compounds

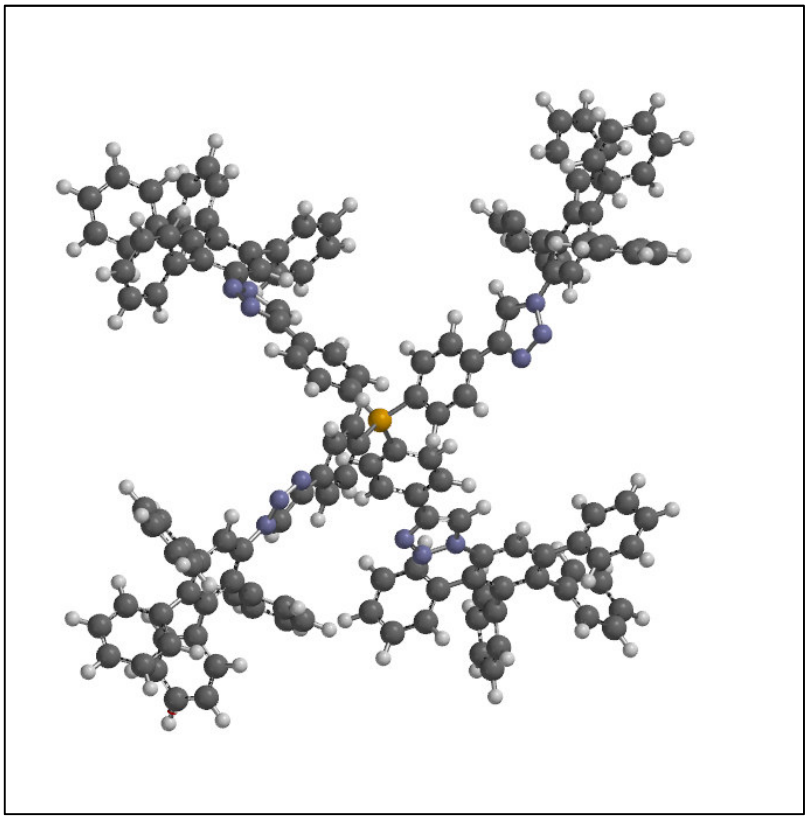

Figure 3-23: Modelled structure of phosphonium cation **3-26** (geometry-optimized via DFT B3LYP, G-31G* calculations).

The hydrodynamic cation-radius r_H of **3-26** was calculated from the experimental diffusion coefficient measured with DOSY-NMR (D^{exp} = 2.51 x 10^{-10} m^2 s^{-1}), CD_2Cl_2, 298 K) and was found to be 2.0 nm. So the size of polyphenylene-triazole hybrid **14** in solution is in between that of second-generation phosphonium **3-10** (P-G_2^+ BF_4-, D^{exp} = 2.81 x 10^{-10} m^2 s^{-1}, r_H = 1.8 nm, CD_2Cl_2, 298K) and third-generation **3-13** (P-G_3^+ BF_4-, D^{exp} = 2.04 x 10^{-10} m^2 s^{-1}, r_H = 2.4 nm, CD_2Cl_2, 298 K). From the geometry-optimized model-structure of the triazole-phosphonium cation **3-26** (see **Figure 3-23**) an ion radius of 1.76 nm was derived, which is close to the experimental value we obtained from DOSY-NMR techniques (2.0 nm). Thus, the assumption of a form-stable shell around the positive charge is valid in the case of triazole moieties being incorporated into the polyphenylene scaffold.

3.7 Discussion and Outlook

All the phosphonium dendrimers synthesized within this chapter originate from a common building block, the ethynyl-functionalized tetraphenylphosphonium derivative **3-5**. The general synthetic step thereto comprises the use of highly electrophilic arenediazonium tetrafluoroborates Ar-N_2^+ BF_4^-, which react with nucleophilic triarylphosphines PR_3 to yield tetraaryl-phosphonium tetrafluoroborates of the general formula $ArPR_3^+$ BF_4^-. Recent literature describes the use of arenediazonium salts as substrates in palladium-catalyzed cross-coupling reaction[77] and the preparation of arylphosphonates[78] from triethylphosphite $P(OEt)_3$.

However, the generality, scope and optimization of reaction parameters for the preparation of quarternary phosphonium salts has been presented for the first time within this thesis. Also a variety of functional groups (bromo, ethynyl, methyl ester) at the diazonium- and phosphine-component was tolerated as the preparation of tetrakis-(4-bromophenyl)-phosphonium tetrafluoroborate **3-29** allocated. The bromo-functionalized cation of **3-29** is only once reported in literature as chloride salt,[79] where it was used to introduce carboxylic acid groups. The idea arose to further modify phosphonium salt **3-29** by means of transition metal catalyzed cross coupling reactions (*Suzuki-Miyaura* and *Sonogashira-Hagihara* standard conditions were tested). Thus, the assortment of conceivable step growth reactions for dendrimers synthesis was meant to be extended.

A schematic overview of the herein obtained intermediates is given in **Figure 3-24** including their intended plans for further modifications**.**

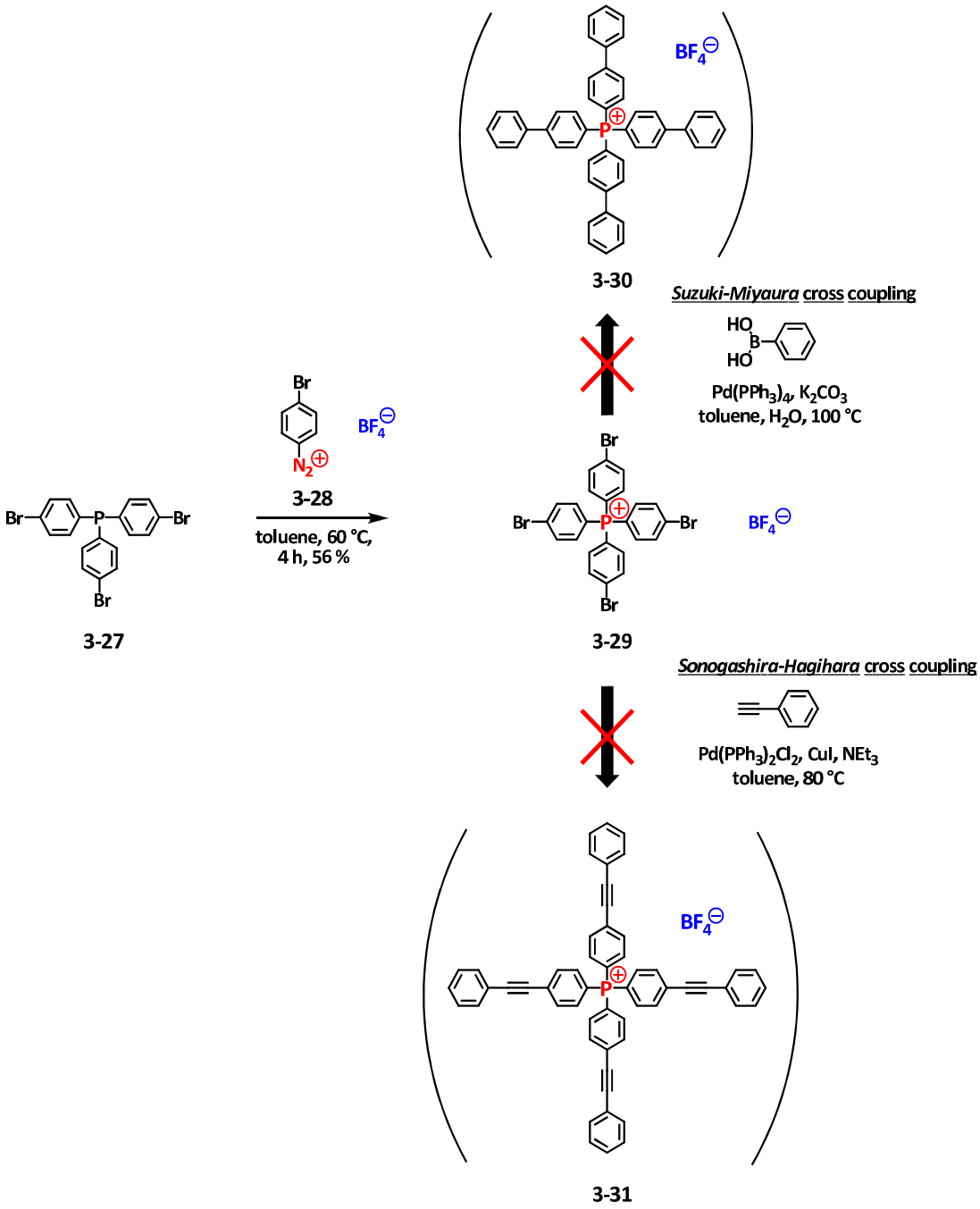

Figure 3-24: Synthetic route to tetrakis-(4-bromophenyl)-phosphonium tetrafluoroborate **3-29**. The subsequent Pd-catalyzed coupling reactions, however, failed. Tris-(4-bromophenyl)-phosphine **3-27** was synthesized according to literature procedure.[80] 4-bromobenzenediazonium tetrafluoroborate **3-28** was produced from p-bromoaniline reacting with BF_3 diethyletherate and tert-butylnitrite (DCM, -20 °C, 90 % yield).

The results of the cross coupling reactions, however, indicate that it is not possible to react phenylboronic acid neither with phenylacetylene nor with the bromo-functionalized phosphonium core **3-29** by means of the selected reaction conditions. Starting material was recovered instead of coupled product **3-30**, which suggests that the oxidative addition of the Pd^0-catalyst to the aryl halide did not proceed. Also target molecule **3-31** was not obtained, but the aryl bromide groups remained unreacted. Obviously the presence of the positive charge on the central phosphorus-atom in para-position to the halide prevents the formation of the palladium-(II)-intermediate.

In contrast to cation **3-29**, the neutral phosphine **3-27** has been successfully coupled with dimethylethynylcarbinol under typical Sonogashira conditions to attach pending ethynyl groups.[80] It is worth mentioning though that there are indeed reported examples in literature, where Pd-mediated cross couplings were performed successfully despite the presence of a para-located positive charge.[81] However, the charges were highly delocalized being incorporated in acridinium and accordingly aza-triangulenium systems. As concluding estimation it should be stated, that the desired expansion of bromo-functionalized tetraphenyl-phosphonium derivatives (e.g. **3-29**) by means of cross couplings is in need of further improvement of the reaction conditions.

Another example that accentuates the versatility of arenediazonium reagents for the preparation of quarternized phosphonium salts is denoted in **Figure 3-25**. Triphenylphosphine was reacted with 4-(methoxycarbonyl)-benzenediazonium tetrafluoroborate **3-32** to yield **3-33**. The subsequent reductions via lithium aluminium hydride ($LiAlH_4$) and also sodium borohydride ($NaBH_4$) though resulted in the degradation of the phosphonium cation **3-33** as evidenced by ^{31}P-NMR of the crude mixture (the absence of the initial PR_4^+ peak at δ 21.5 and the occurrence of a peak of δ - 4.3 strongly indicated the reduction to phosphine PR_3). It is known in the literature[82] that metal hydride reducing agents react with benzyltriarylphosphonium salts $[P(Bn)Ar_3]^+$ to yield the respective triaryl-phosphines PAr_3. The results within this work show that tetraaryl-substituted phosphonium compounds $[PAr_4]^+$ react in the same way under elimination of one ligand.

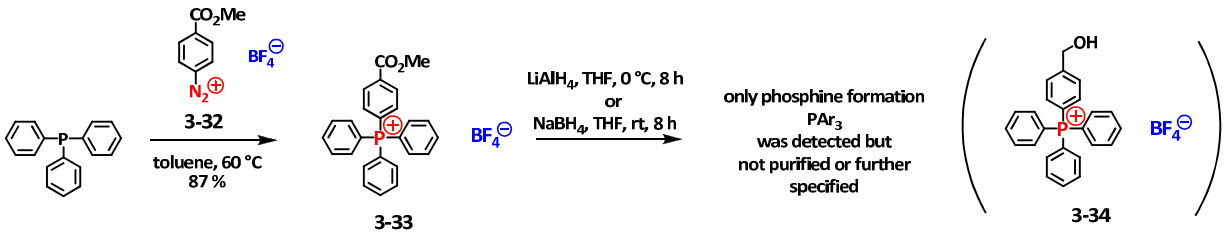

Figure 3-25: Failed synthetic route towards the synthesis of hydroxymethyl-functionalized phosphonium salt **3-34**.

The initial plan was to synthesize phosphonium salt **3-34** functionalized with a methylene hydroxide group (-CH_2OH), that can be further reacted with methacryloyl chloride to produce **3-35**. The latter offers the possibility to be specifically modified by the choice of the initial phosphine. **3-35** is a positively charged phosphonium-methacrylate derivative that results in the formation a hydrophobic poly-cation after radical polymerization. A detailed description of the motivation and propositions for the synthesis of polycations on the basis of charge-shielded phosphonium monomer units will be given in chapter 6.

Admittedly, for the preparation of **3-34** it would be more advisable to select the already literature-known synthetic route based on Ni-(II)-catalysis under high temperature conditions.[49] Nevertheless, also 4-hydroxymethylbenzenediazonium tetrafluoroborate is described in the literature and will most likely yield the intermediate substance **3-34** by reaction with PPh_3. Thus, the application of arenediazonium salts represents a valuable method for the quarternization reaction of phosphines tolerating a variety of functional groups.

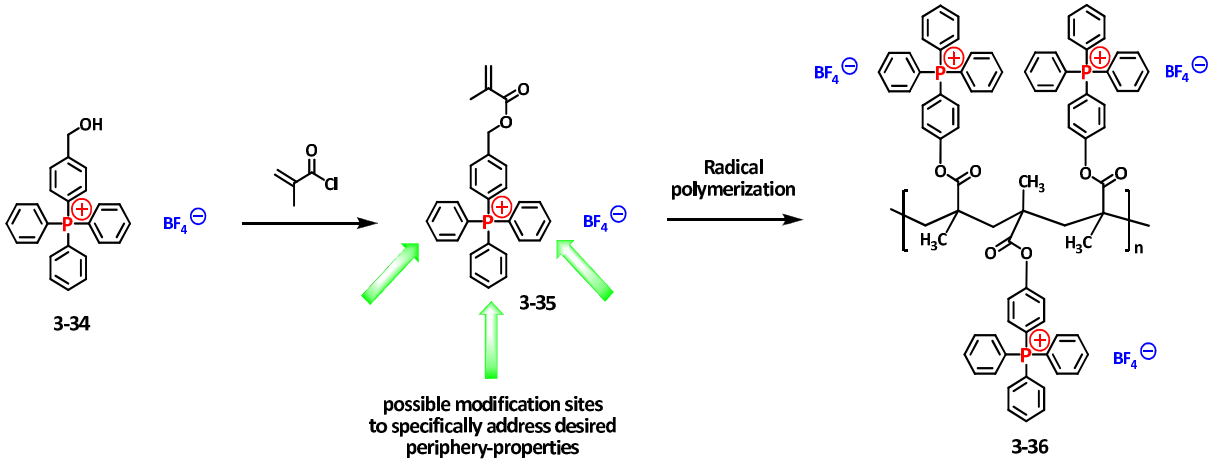

Figure 3-26: Proposed synthetic route towards the synthesis of poly-methacrylate based polyphosphonium **3-36**.

The preparation of bulky azide building block **3-25** represents a breakthrough with respect to the construction of polyphenylene-triazole hybrid dendrimers. Substantial syntheses and characterization of such composite macromolecules were performed by *David Tuerp*.[64], [72] Thereby, the perpetual work-up inconveniences caused by aggregation (and therefrom resulting poor solubility in all common organic solvents) turned the purification of the obtained dendrimers to a time-consuming and tedious procedure (silica gel chromatography, precipitation and recycling GPC was mandatory in order to obtain pure products under significant losses). A useful way to simplify this preparation process is realized by the use of bulky endcapping units (general overview in **Figure 3-27**).

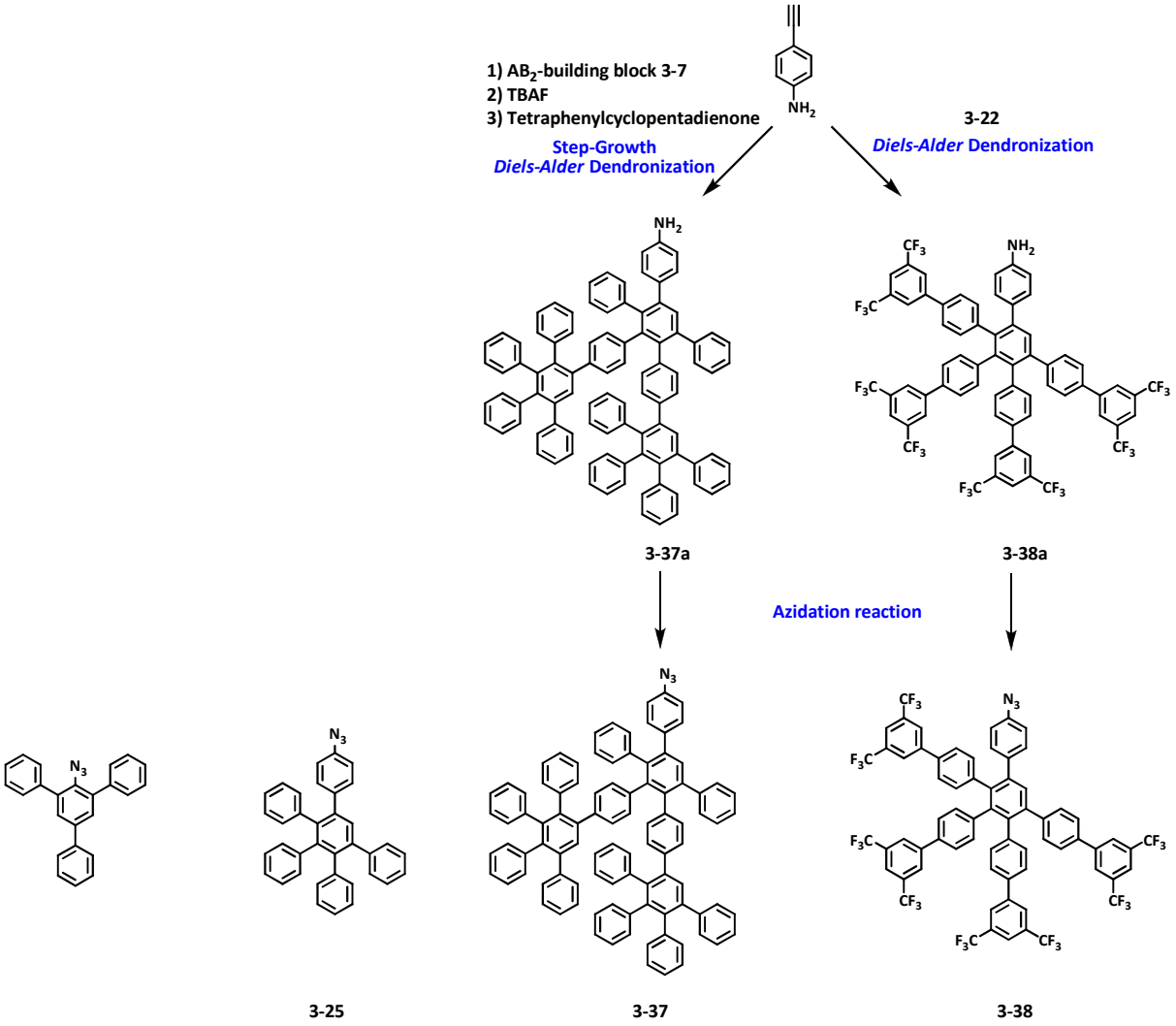

Figure 3-27: Overview of bulky phenylene-rich endcapping azide building blocks. (Left): 2,4,6-triphenylbenzene azide first synthesized by [redacted].

Among those azides, the first-generation derivative **3-25** turned out to be the most effective and reliable reagent for the design and implementation of a globular shaped aryl-triazole dendrimer (**3-26**). Surprisingly, second-generation bulky azide **3-37** and CF_3-functionalized **3-38** were not successfully reacted with positively charged core **3-5** in a convergent synthesis approach (**Figure 3-27**). This observation agrees with the fact that steric hindrance of too large ligands impedes their assembly at the functionalized core. MALDI-TOF analysis of the crude mixtures in both cases showed several peaks in between m/z values of 226 – 700, where solely matrix (dithranol, m/z = 226), starting compound (m/z = 435.7) and phosphine

oxide (m/z = 350.3) could be assigned for sure. Consequently heating these reaction mixtures to 80 °C for 24 h lead to a steady gas evolution and the afterwards recorded mass spectrum displayed even more unattributed peaks. The most obvious side products upon decomposition of azides **3-37** and **3-38** are expected to be amines **3-37a** and **3-38a** respectively.[83] Nevertheless neither FD-mass could indicate their formation nor a TLC comparison with the precursor **3-37a** and **3-38a** as reference materials matched, but a complex mixture of unknown reaction products was present. Furthermore there was even no incomplete reacted intermediate detectable, meaning that only some of the ethynyl-groups would have formed triazole-units by the reaction with the azide group.

In summary, the specially designed large building blocks **3-37** and **3-38** were not suitable to construct a phenyl-triazole-phosphonium hybrid dendrimer in a convergent synthesis approach.

Literature

[1] Tuerp, D.; Wagner, M.; Enkelmann, V.; Müllen, K.; *Angew. Chem. Int. Ed.* **2011**, 50, 4962 – 4965.
[2] Krossing, I.; Raabe, I.; *Angew. Chem. Int. Ed.* **2004**, *43*, 2066.
[3] Moss, S.; King, B. T.; de Meijere, A.; Kozhushkov, S. I.; Eaton, P. E.; Michl, J.; *Organic Letters* **2001**, *3*, 2375.
[4] Barbarich, T. J.; Handy, S. T.; Miller, S. M.; Anderson, O. P.; Grieco, P. A.; Strauss, S. H.; *Organometallics* **1996**, *15*, 3776.
[5] Anderson, L. L.; Arnold, J.; Bergman, R. G.; *J. Am. Chem. Soc.* **2005**, *127*, 14542.
[6] Patmore, N. J.; Hague, C.; Cotgreave, J. H.; Mahon, M. F.; Frost, C. G.; Weller, A. S.; *Chemistry - A European Journal* **2002**, *8*, 2088.
[7] Chen, E. Y.-X.; Marks, T. J.; *Chemical Reviews* **2000**, *100*, 1391.
[8] Chen, M.-C.; Roberts, J. A. S.; Seyam, A. M.; Li, L.; Zuccaccia, C.; Stahl, N. G.; Marks, T. J.; *Organometallics* **2006**, *25*, 2833.
[9] Roberts, J. A. S.; Chen, M.-C.; Seyam, A. M.; Li, L.; Zuccaccia, C.; Stahl, N. G.; Marks, T. J.; *J. Am. Chem. Soc.* **2007**, *129*, 12713.
[10] Zhang, Y.; Ning, Y.; Caporaso, L.; Cavallo, L.; Chen, E. Y. X.; *J. Am. Chem. Soc.* **2010**, *132*, 2695.
[11] LeSuer, R. J.; Geiger, W. E.; *Angew. Chem. Int. Ed.* **2000**, *39*, 248.
[12] Barriere, F.; Camire, N.; Geiger, W. E.; Mueller-Westerhoff, U. T.; Sanders, R.; *J. Am. Chem. Soc.* **2002**, *124*, 7262.
[13] Camire, N.; Nafady, A.; Geiger, W. E.; *J. Am. Chem. Soc.* **2002**, *124*, 7260.
[14] Camire, N.; Mueller-Westerhoff, U. T.; Geiger, W. E.; *Journal of Organometallic Chemistry* **2001**, *637-639*, 823.
[15] Raabe, I.; Wagner, K.; Guttsche, K.; Wang, M.; Gratzel, M.; Santiso-Quinones, G.; Krossing, I.; *Chemistry - A European Journal* **2009**, *15*, 1966.
[16] Stewart, M. P.; Paradee, L. M.; Raabe, I.; Trapp, N.; Slattery, J. S.; Krossing, I.; Geiger, W. E.; *Journal of Fluorine Chemistry* **2010**, *131*, 1091.
[17] Barriere, F.; Geiger, W. E.; *J. Am. Chem. Soc.* **2006**, *128*, 3980.
[18] Geiger, W. E.; Barrière, F. d. r.; *Accounts of Chemical Research* **2010**, *43*, 1030.
[19] Krossing, I.; Reisinger, A.; *Coordination Chemistry Reviews* **2006**, *250*, 2721.
[20] Reisinger, A.; Trapp, N.; Krossing, I.; Altmannshofer, S.; Herz, V.; Presnitz, M.; Scherer, W.; *Angewandte Chemie* **2007**, *119*, 8445.
[21] Mercier, H. P. A.; Moran, M. D.; Schrobilgen, G. J.; Steinberg, C.; Suontamo, R. J.; *J. Am. Chem. Soc.* **2004**, *126*, 5533.
[22] Sarazin, Y.; Hughes, D. L.; Kaltsoyannis, N.; Wright, J. A.; Bochmann, M.; *Journal of the American Chemical Society* **2007**, *129*, 881.
[23] Fang, M.; Wilson, S. R.; Suslick, K. S.; *J. Am. Chem. Soc.* **2008**, *130*, 1134.
[24] Bösmann, A.; Francio, G.; Janssen, E.; Solinas, M.; Leitner, W.; Wasserscheid, P.; *Angewandte Chemie International Edition* **2001**, *40*, 2697.
[25] Larsen, A. S.; Holbrey, J. D.; Tham, F. S.; Reed, C. A.; *J. Am. Chem. Soc.* **2000**, *122*, 7264.
[26] Bejan, D.; Ignat'ev, N.; Willner, H.; *Journal of Fluorine Chemistry* **2010**, *131*, 325.
[27] Timofte, T.; Pitula, S.; Mudring, A.-V.; *Inorganic Chemistry* **2007**, *46*, 10938.
[28] Kita, F.; Sakata, H.; Sinomoto, S.; Kawakami, A.; Kamizori, H.; Sonoda, T.; Nagashima, H.; Nie, J.; Pavlenko, N. V.; Yagupolskii, Y. L.; *Journal of Power Sources* **2000**, *90*, 27.
[29] Strauss, S. H.; Fauber, B. P.; *WO 00/53611* **2000**.

[30] Armand, M.; Johansson, P.; *Journal of Power Sources* **2008**, *178*, 821.
[31] Nolan, B. G.; Tsujioka, S.; Strauss, S. H. in *Fluorinated Materials for Energy Conversion*; Tsuyoshi, N., Henri, G., Eds.; Elsevier Science: Amsterdam, **2005**, p 195.
[32] a) Benrraou, M.; Bales, B. L.; Zana, R. *J.; Phys. Chem. B*, **2003**, 107 (48), pp 13432–13440; b) Kume, G.; Gallotti, M.; Nunes, G*. J.; Surfact. Deterg.* **2008**, 11, 1-11.
[33] a) Starks, C. M.; *J. Am. Chem. Soc.* **1971**, 93, 195; b) Makosza, M.; *Tetrahedron Lett.* **1966**, 4621; c) Makosza, M.; *Tetrahedron Lett.* **1966**, 5489; d) Makosza, M.; *Tetrahedron Lett.* **1969**, 673; e) Brändström, A.; *Adv. Phys. Org. Chem.* **1977**, 15, 267; f) review on asymmetric PTC, see: Ooi, T.; Maruoka, K.; *Angew. Chem. Int. Ed.* **2007**, 46, 4222-4266.
[34] For a representative review on ILs, see: Dupont, J.; de Souza, R. F.; Suarez, P. A. Z.; *Chem. Rev.* **2002**, 102, 3667-3692.
[35] a) Del Sesto, R. E.; Corley, C.; Robertson, A.; Wilkes, J. S.; *Journal of Organometallic Chemistry* **2005**, 690, 2536-2542; b) Gerritsma, D. A.; Robertson, A.; McNulty, J.; Capretta, A.; *Tetrahedron Letters* **2004**, 45, 7629-7631.
[36] He, R.; Ding, C.; Maruoka, K.; *Angew. Chem.* **2009**, 121, 4629-4631.
[37] Mintzer, M. A.; Simanek, E. E.; *Chem. Rev.* **2008**, 109, 259-302.
[38] a) Meerwein, H.; Hinz, G.; Hofmann, P.; Kroning, E.; Pfeil, E.; *J. Prakt. Chem.* **1937**, 147, 257; b) Meerwein, H.; Houben-Weyl „Methoden der Organischen Chemie“ **1965**, 3/6, 325; c) review see: Granik, V. G.; Pyatin, B. M.; Glushkov, R. G.; *Russian Chemical Reviews* **1971**, 40 (9), 747-759.
[39] Cantoni, G. L.; *J. Am. Chem. Soc.* **1952**, **74** (11), 2942.
[40] Trost, B. M.; *Acc. Chem. Res.* **1974**, 7, 85; *Pure Appl. Chem.* **1975**, 53, 563.
[41] Pauling, L.; *J. Am. Chem. Soc.* **1932**, 54 (9), 3570-3582.
[42] Wang, S.-W.; Liu, W.; Colby, R. H.; *Chem. Mater.* **2011**, 23, 1862-1873.
[43] Haav, K.; Saame, J.; Kütt, A.; Leito, I.; *Eur. J. Org. Chem.* **2012**, 2167-2172.
[44] Zhou, P. G.; Blumstein, A.; *Polymer* **1997**, 38, 595-604.
[45] Sonogashira, K.; Tohda, Y.; Hagihara, N.; *Tetrahedron Letters* **1975**, *16*, 4467.
[46] Marvel, C. S.; Hager, F. D.; Coffman, D. D.; *J. Am. Chem. Soc.* **1927**, 49, 2323.
[47] Marcoux, D.; Charette, A. B.; *J. Org. Chem.* **2008**, 73, 590-593.
[48] (a) Migita, T.; Nagai, T.; Kiuchi, K.; Kosugi, M.; *Bull. Chem. Soc. Jpn.* **1983**, *56*, 2869. (b) Migita, T.; Shimizu, T.; Asami, Y.; Shiobara, J.; Kato, Y.; Kosugi, M.; *Bull. Chem. Soc. Jpn.* **1980**, *53*, 1385.
[49] Marcoux, D.; Charette, A. B.; *Adv. Synth. Catal.* **2008**, 350, 2967–2974.
[50] a) Horner, L.; Duda, U.-M.; *Tetrahedron Lett.* **1970**, 5177; b) Horner, L.; Mummenthey, G.; Moser, H.; Beck, P.; *Chem. Ber*. **1966**, 99, 2782; c) Hirusawa, Y.; Oku, M.; Yamamoto, R.; *Bull. Chem. Soc. Jpn.* **1957**, 30, 667.
[51] a) Balz, G.; Schiemann, G. *Chem. Ber.* **1927**, 60, 1186; b) Roe, A. *Org. React.* **1949**, 5, 193.
[52] Hodgon, H. H.; *Chem. Rev.* **1947**, 40(2), 251-277.
[53] Kikukawa, K.; Matsuda, T.; *Chem. Lett.* **1977**, 159.
[54] Horner, L.; Stöhr, H. Nr. 9/1953, 1073-1076.
[55] a) Yasui, S.; Fujii, M.; Kawano, C.; Nishimura, Y.; Ohno, A. *Tetrahedron Lett.* **1991**, *32*, 5601; b) Yasui, S.; Fujii, M.; Kawano, C.; Nishimura, Y.; Shioji, K.; Ohno, A.; *J. Chem. Soc., Perkin Trans. 2* **1994**, 177.
[56] Doyle, M. P.; Bryker, W. J.; *J. Org. Chem*. **1979**, *44*, 1572.

[57] Fischer, K.; Wilken, M.; *J. Chem. Thermodyn.* **2001**, 33, 1285-1308.
[58] a) Barder, T. E.; *PhD thesis*, Massachusettes Institute of Technology, **2007**; b) Barder, T. E.; Buchwald, S. L.; *J. Am. Chem. Soc.* **2007**, 129, 5096-5101.
[59] a) Rauhut, M. M.; Currier, M. H.; *J. Org. Chem.* **1961**, 26, 4626-4628; b) Burkett, H. D.; Hill, W. E.; Worley, S. D.; *Phosphorus and Sulfur* **1984**, 20, 169-172.
[60] a) Grayson S. M.; Fréchet J. M. J.; *Chem. Rev*. **2001**, 101, 3919 –3967; b) Fréchet J. M. J.; *J. Polym. Sci. Part* A **2003**, 41, 3713 –3725.
[61] Frohn, H.-J.; *Organometallics* **2001,** *20,* 4750-4762.
[62] Frohn, H.-J.; Klose, A.; Henkel, G.; *GIT* **1993**, 37, 752.
[63] Bauer, R.; Liu, D.; Ver Heyen, A.; De Schryver, F.; De Feyter, S.; Müllen, K.; *Macromolecules* **2007**, *40*, 4753.
[64] Tuerp, D.; *Dissertation, "Dendronized Ions"*, Mainz **2012**.
[65] Hoffmann, R.; Woodward, R. B.; *J. Am. Chem. Soc.* **1965**, 87 (9), 2046-2048.
[66] Konovalov, A. I.; Solomonov B. N.; *Doklady Akad. Nauk S.S.S.R. Ser. Kim.* **1973**, 211, 1115.
[67] Fleming, I.; „Grenzorbitale und Reaktionen organischer Verbindungen", Verlag Chemie Weinheim.
[68] Kobayashi, H.; *Journal of Fluorine Chemistry* **2000**, 105, 201-203.
[69] Huisgen, R.; *Proceedings of the Chemical Society* **1961**, Centenary Lecture.
[70] Rostovtsev, V. V.; Green L. G.; Fokin, V. V.; Sharpless, K. B.; *Angew. Chem. Int. Ed. Engl.* **2002**, 41 (14), 2596–2599.
[71] Wu P.; Feldman, A. K.; Nugent, A. K.; Hawker, C. J.; Scheel, A.; Voit, B.; Pyun, J.; Fréchet, J. M. J.; Sharpless, K. B.; Fokin, V. V.; *Angew. Chem. Int. Ed. Engl.* **2004**, 43, 3928 - 3932.
[72] Stangenberg, R.; Tuerp, D.; Muellen, K. *Tetrahedron* **2014**, 70, 3178-3184.
[73] Barral, K.; Moorhouse, A. D.; Moses, J. E. *Organic Letters* **2007**, *9*, 1809.
[74] Izutsu, K.; *Electrochemistry in Nonaqueous Solutions*; WILEY-VCH: Weinheim, **2002**.
[75] Chan, T. R.; Hilgraf, R.; Sharpless, K. B.; Fokin, V. V. *Organic Letters* **2004**, *6*, 2853.
[76] a) Grayson, S. M.; Fréchet, J. M. J.; *Chem. Rev*. **2001**, 101, 3919 –3967; b) Fréchet, J. M. J.; *J. Polym. Sci. Part* A **2003**, 41, 3713 –3725.
[77] Roglans, A.; Pla-Quintana, A.; Moreno-Manas, M.; *Chem. Rev.* **2006**, 106, 4622 – 4643.
[78] Berrino, R.; Cacchi, S.; Fabrizi, G.; Goggiamani, A.; Stabile, P.; *Org. Biomol. Chem.* **2010**, 8, 4518 – 4520.
[79] Watabe; Daisuke et al.; Jpn. Kokai Tokkyo Koho, 2011201835.
[80] Grelaud, G.; Argouarch, G.; Paul, F.; *Tetrahedron Letters* **2010**, Vol. 51, Issue 29, 3786 – 3788.
[81] a) Krebs, F. C., *Tetrahedron Letters*, Vol. 44, Issue 1, 17 – 21; b) Krebs, F. C.; Spanggaard, H.; Rozlosnik, N.; Larsen, N. B.; Joergensen, M.; *Langmuir* **2003**, 19, 7873 – 7880.
[82] a) Bailey, W. J.; Buckler, S. A., in Phosphorus Compounds. I. *Reduction of Benzylphosphonium Compounds with Lithium Aluminium Hydride*, **1957**, 3567 – 3569; b) Brophy, J. J.; Gallagher, M. J.; *Australian Journal of Chemistry* **1969**, 22(7), 1399 – 1404.
[83] Sheradsky, T., *Chemistry of the Azido Group*; Patai, S., Ed.; Inter Science: New York, **1971**; 331.

Chapter 4 – Physical and Chemical Properties of Dendronized Salts

4.1 Introduction

A recent publication by [redacted] has reported the synthesis of large dendronized polyphenylene borate anions by divergent dendritic growth.[1] Thereby, the increase in anion size and its specific surface modification had remarkable influence on the physical properties of thereof constituted salts. It was shown by means of conductivity measurements in different organic solvents that the coordinative interactions between oppositely charged ions were effectively reduced. In turn this promoted ion dissociation, which was reflected by increasing ion dissociation degree values (α) as the sizes of the anions were increased. During these studies the charge compensating counter ion was kept constantly tetrabutylammonium ($[N(C_4H_9)_4]^+$, TBA^+).

The central motivation for exploiting the investigation of the electrolyte properties of dendronized salts is based on the successful synthesis of rigid and bulky phosphonium cations presented in chapter 3. Since from then it was possible to investigate salts constituted from both cations and anions with strongly different properties from classical smaller charge carriers (ion size, solubility, charge carrier mobility, ion coordination strength). Therefore required ion exchange techniques will be presented in chapter 4.2 and the results obtained from dielectric spectroscopy measurements are summarized and discussed in section 4.4.

Aside from the influence on physical properties, dendronization also impacts the chemical nature (e.g. reactivity with bases and nucleophiles, redox behavior) of the resulting salts by providing a shape-persistent polyphenylene-shell around the charged core. The way, in which this type of charge screening renders the stability of phosphonium cations with regard to alkaline degradation in solution, oxidation affinity by air and temperature induced decomposition are main issues that will be presented and rationalized in paragraph 4.5.

4.2 Cation Exchange Experiments

The initial development of dendronized salts afforded a series of tetrabutylammonium borates with varying anion sizes (selected structures see **Figure 4-1**).

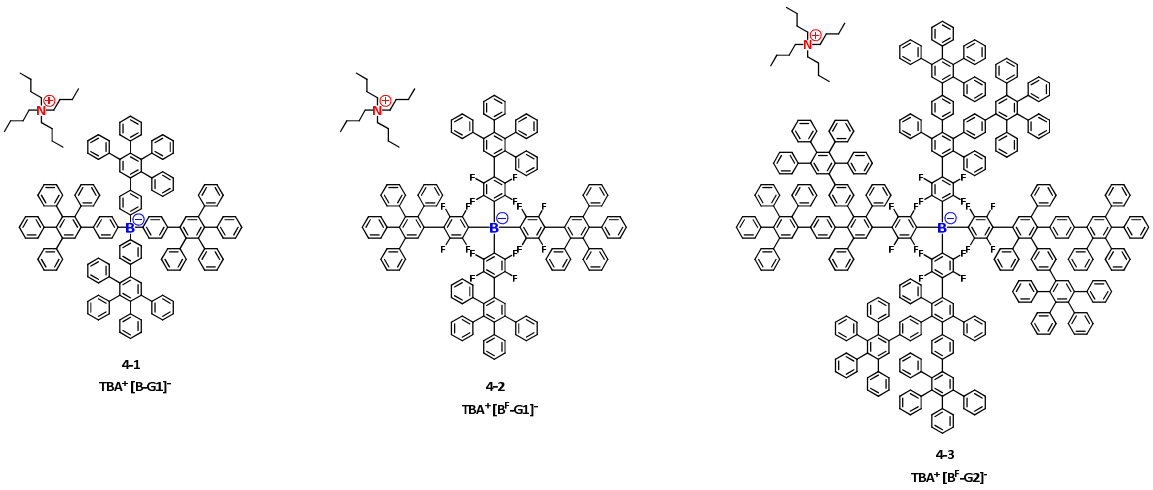

Figure 4-1: Selected Structures of dendronized tetrabutylammonium borates **4-1**, **4-2** and **4-3**.

In order to broaden the scope of dendronized salts, a reliable and practicable method for a clean exchange of tetrabutylammonium to other counter-cations had to be developed. A classical cation metathesis approach was not applicable due to the considerably good solubility of the initial TBA^+ borate dendrimers. Even excess addition of any salt $M^+ X^-$ could not achieve an ion exchange in a satisfying degree. A previous successful suggestion to get rid of the TBA^+-cation was founded on the use of alkyl lithium reagents (n-BuLi) to degrade the tetraalkylammonium-cation in the *Wittig* modification of the *Hofman* elimination.[2] By way of this method though it was not possible to purify and isolate a clean lithium salt of the dendronized borate due to the formation of side products that could not be separated. So the most challenging task was to exchange TBA^+ to smaller cations by employing a versatile technique.

This could be successfully accomplished by the use of a crosslinked polystyrene-based strong acidic cation exchange resin (commercially available in its H^+-form, trade name Amberlite IR 120). In order to load the latter with the according cation of interest (Li^+, Na^+, K^+, Cs^+, Ca^{2+},

Ba^{2+}) for the subsequent ion metathesis step, a typical chromatography glass column was filled with an aqueous suspension of the bead-shaped resin material. After that, a concentrated solution of the respective metal hydroxide salt (M^{n+} n OH- dissolved in H_2O, ~ 3 M – saturated solutions) was slowly rinsed through the column (heat-generation due to the neutralization reaction!) until the pH-value of the collected solution turned basic, which indicated the saturation of the exchange material. The general loading procedure is illustrated in **Figure 4-2** using the example of lithium hydroxide to obtain the Li^+-form of the cation exchanger.

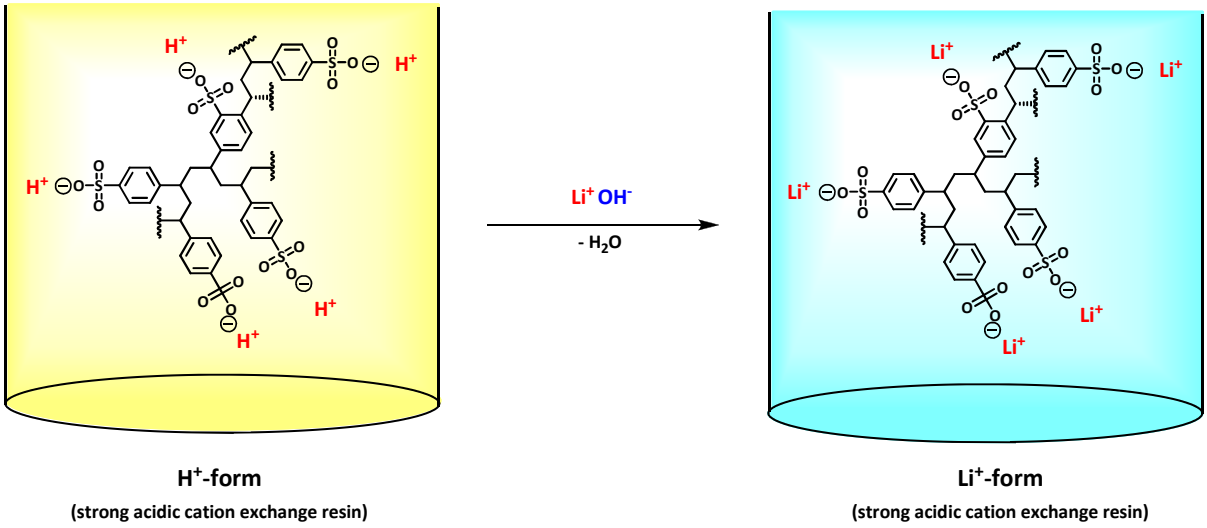

Figure 4-2: Schematic procedure for the generation of the Li^+-form of the strong acidic cation exchange resin.

Some basic principles regarding the affinity of the resin for an ion have to be rationalized before the results from the ion exchange experiments within this chapter are summarized in **Table 4.2**.

In principle the size of an ion in its solvated form (in most common applications the hydrated form is relevant) as well as its charge govern the exchange equilibrium with the resin. For the abovementioned example the resin in the ionic form H^+ is in contact with a solution containing Li^+ ions and the following reaction takes place:

$$R\text{-}H^+ + Li^+ \rightleftharpoons R\text{-}Li^+ + H^+ \qquad \textbf{(Equation 4-1)}$$

During the ion exchange process, H^+ ions will migrate into the solution and be replaced by Li^+ ions from the solution until the equilibrium is reached, which is described by the **mass action law** as follows (under the approximation that the activity coefficients are considered constant):

$$K^{Li+}_{H+} = \frac{R[-Li^+]\,[H^+]}{R[-H^+]\;\;[Li^+]} \qquad \textbf{(Equation 4-2)}$$

In order to gain insight into the correlation between cation size and affinity to the poly-styrene sulfonate (PSS) resin, **Tables 4-1a** and **4-1b** provide relevant data therefore.

Table 4-1a: Ion diameter in the naked form (Van der Waals) and solvated (hydrated) form.

Ion	Hydrated Diameter (Å)	Naked Diameter (Å)
Monovalent		
Li^+	3.82	0.60
Na^+	3.60	0.95
K^+	3.31	1.33
Rb^+	3.28	1.48
Cs^+	3.27	1.69
$[P\text{-}G1]^+$	-	~ 14
$[P\text{-}G2]^+$	-	~ 20
$[P\text{-}G3]^+$	-	~ 24
Divalent		
Be^{++}	4.59	0.31
Mg^{++}	4.26	0.65
Ca^{++}	4.11	0.99
Sr^{++}	4.10	1.13
Ba^{++}	4.05	1.35

Table 4-1b: Relative selectivity coefficients $K(^{x}/_{H+})$ for strong acidic cation exchange resin.

Ion	Selectivity coefficient* (Amberlite IR 120)
Monovalent	
Li^+	0.85
H^+	1.00
Na^+	1.69
K^+	2.46
Cs^+	2.80
Ag^+	7.54
Divalent	
Mg^{++}	0.63
Ca^{++}	1.00
Sr^{++}	1.25
Ba^{++}	2.20

*The resin is a "nominal 8 % divinylbenzene" product. Resins with higher cross-linking will have higher selectivity values, but the order remains unchanged.

Thus it can be clearly concluded from **Equation 4-2** and **Table 4-1b** that high salt concentrations M^{n+} $(OH^-)_n$ are required to fully load the H^+-exchange resin with the respective cation M^{n+}. After the column had been "loaded", the first-generation TBA^+ borate salt **4-2** was slowly passed through the column (in a mixture of THF/H_2O 8:2) to exchange the tetrabutylammonium cation to M^{n+} (illustrated in **Figure 4-3**, monitored by means of ^{1}H-NMR spectra).

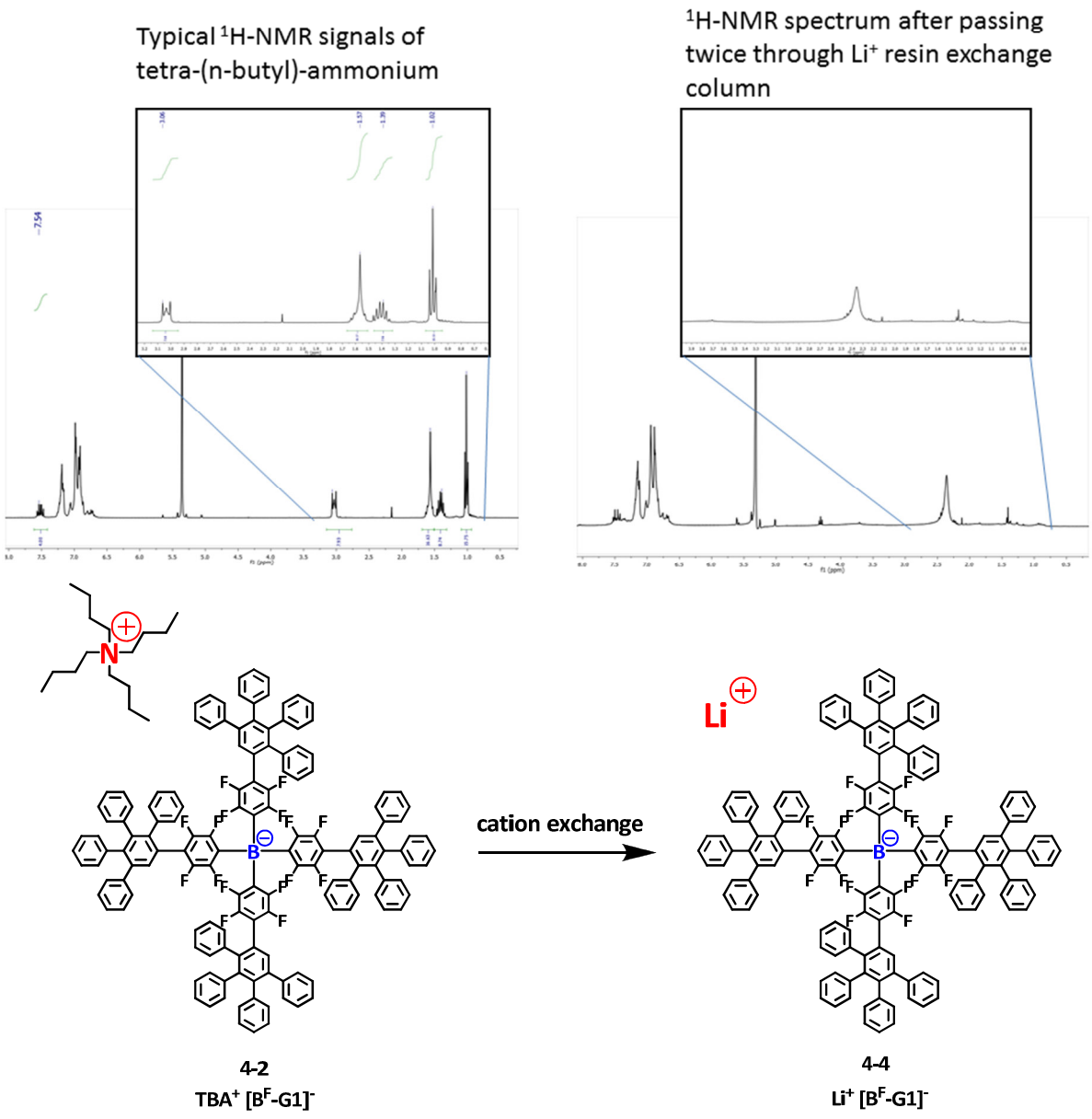

Figure 4-3: ^{1}H-NMR spectra confirm the complete conversion from tetrabutylammonium borate TBA^+ $[B^F\text{-}G1]^-$ **4-2** to lithium borate Li^+ $[B^F\text{-}G1]^-$ **4-4**.

Table 4-2: Summary of the dendronized borate salts ($[B^F\text{-}G1]^-$ anion) with different cations obtained from applying ion exchange resin columns.

Cation	Anion	Compound Number	Preparation Remarks
Monovalent			
Li^+	$[B^F\text{-}G1]^-$	**4-4**	LiOH hydrate as resin-loader
Na^+	$[B^F\text{-}G1]^-$	**4-5**	NaOH as resin-loader
K^+	$[B^F\text{-}G1]^-$	**4-6**	KOH as resin-loader
Cs^+	$[B^F\text{-}G1]^-$	**4-7**	CsOH as resin-loader
Divalent			
Ca^{++}	$[B^F\text{-}G1]^-$	**4-8**	The Na^+-resin was rinsed with $CaCl_2$-solution
Ba^{++}	$[B^F\text{-}G1]^-$	**4-9**	The Na^+-resin was rinsed with $BaCl_2$ solution

The obtained alkaline metal borate salts (Li^+ $[B^F\text{-}G1]^-$ **4-4** and Na^+ $[B^F\text{-}G1]^-$ **4-5**) could be utilized for a subsequent exchange to larger cations including the polyphenylene phosphonium ions developed within this work.

The general approach thereto is illustrated by the preparation of N,N-dimethylanilinium ($DMAH^+$, $Ph\text{-}NH(CH_3)_2^+$) **4-10**: The lithium salt Li^+ $[B^F\text{-}G1]^-$ **4-4** was dissolved in DCM and treated with a moderate excess of N,N-dimethylanilinium chloride. After stirring for 5 hours, water was added to the mixture and the organic phase was collected. After filtration through a silica-gel plug (to remove excess of $DMAH^+$ Cl^-) and precipitation in hexane, the dimethylanilinium borate **4-10** was afforded.

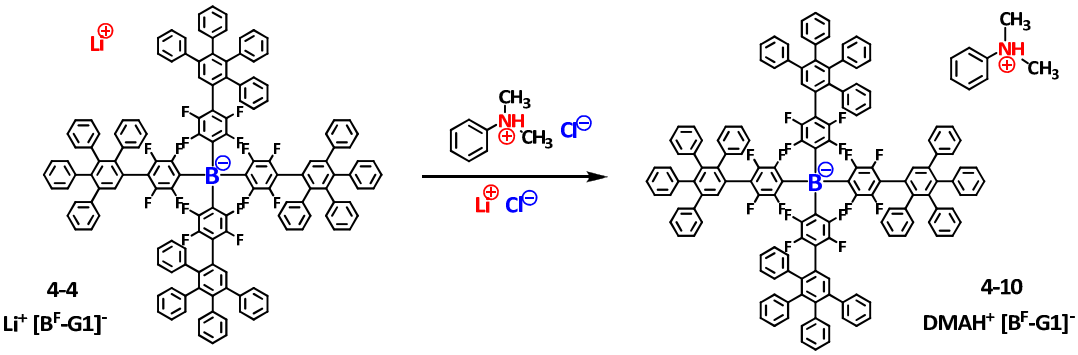

Figure 4-4: Cation exchange towards N,N-dimethylanilinium borate salt **4-10**.

The complete exchange of lithium to the anilinium cation ($DMAH^+$) was confirmed by the signal intensities in the ^{1}H-NMR spectrum of **4-10.** Therefore, the most downfield shifted signal of the borate generation protons at δ 7.45 – 7.42 was related to the characteristic singulet of the cationic methyl groups at δ 3.02 (displayed in detail in **Figure 4-5**).

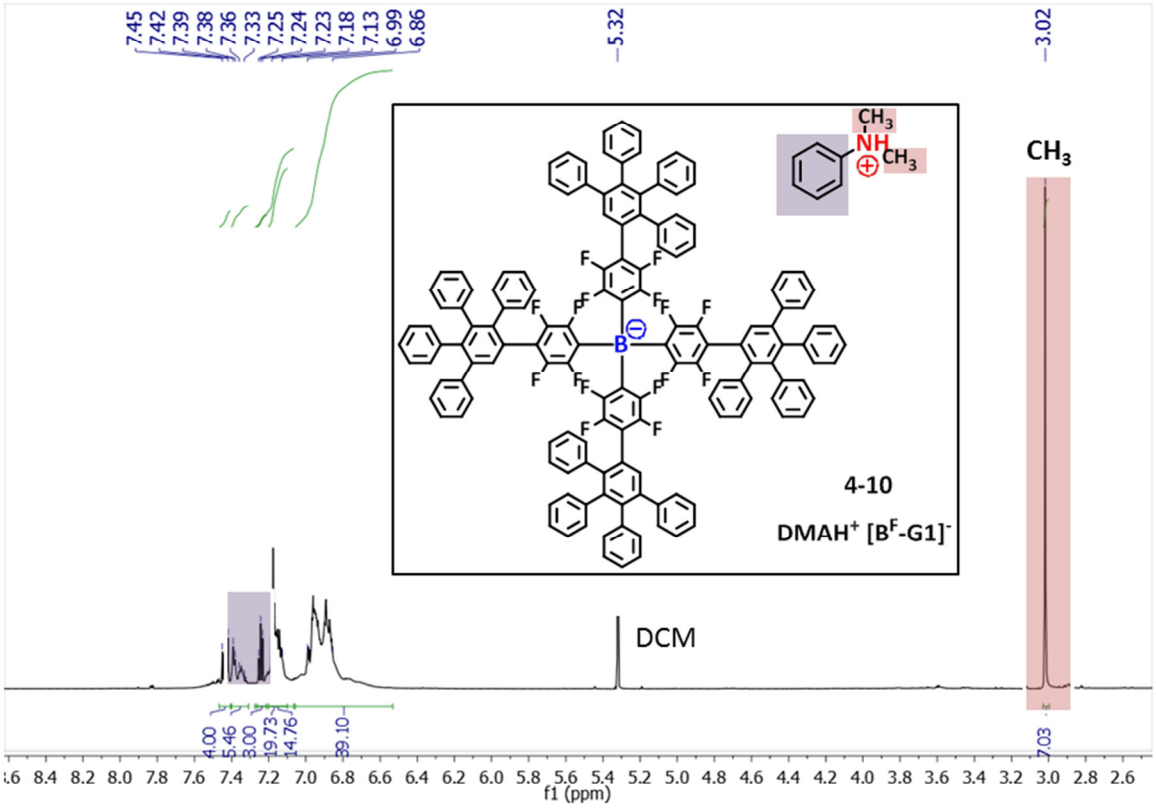

Figure 4-5: ^{1}H-NMR spectrum of $DMAH^+$ $[B^F\text{-}G1]^-$ **4-10** (CD_2Cl_2, 300 MHz, 298 K).

The analogous experimental procedure was successfully applied to replace lithium in **4-4** by larger organic cations (summarized in **Table 4-3**). Particularly the development of hydrophobic salts displaying excellent solubility in low permittivity solvents (like toluene, o-xylene) were accessible via the ion metathesis technique presented in this chapter.

Table 4-3: Summary of the dendronized borate salts ($[B^F\text{-}G1]^-$ anion) with organic cations obtained via ion metathesis reaction.

Cation	Anion	Compound Number	Procedure Remarks
Monovalent 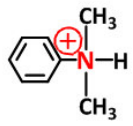 N,N-dimethylanilinium	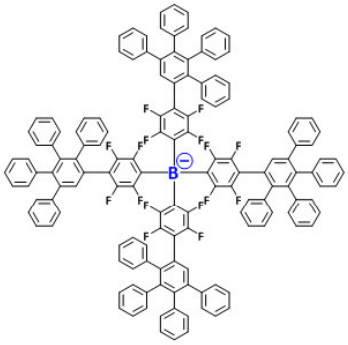 $[B^F\text{-}G1]^-$	**4-10**	ion metathesis reaction between N,N-dimethylanilinium chloride and $Li^+ [B^F\text{-}G1]^-$ (**4-4**)
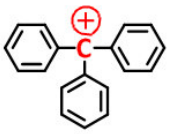 triphenylcarbenium		**4-11**	ion metathesis reaction between triphenylcarbenium chloride (trityl chloride) and $Li^+ [B^F\text{-}G1]^-$ (**4-4**); solution turned yellow upon addition of TrtCl, which indicates formation of the naked trityl cation
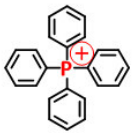 tetraphenylphosphonium		**4-12**	ion metathesis reaction between tetraphenylphosphonium bromide and $Li^+ [B^F\text{-}G1]^-$ (**4-4**)
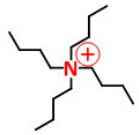 tetrabutylammonium		**4-2**	detailed synthesis is found in literature
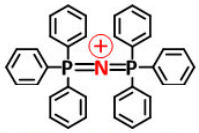 bis(triphenylphosphine) iminium		**4-13**	ion metathesis reaction between bis(triphenylphosphine)iminium chloride ($PPN^+ Cl^-$) and $Li^+ [B^F\text{-}G1]^-$ (**4-4**)
$[P\text{-}G1]^+$		**4-14**	ion metathesis reaction between $[P\text{-}G1]^+ BF_4^-$ and $Li^+ [B^F\text{-}G1]^-$ (**4-4**)
$[P\text{-}G2]^+$		**4-15**	ion metathesis reaction between $[P\text{-}G2]^+ BF_4^-$ and $Li^+ [B^F\text{-}G1]^-$ (**4-4**)
$[P\text{-}G3]^+$		**4-16**	ion metathesis reaction between $[P\text{-}G3]^+ BF_4^-$ and $Li^+ [B^F\text{-}G1]^-$ (**4-4**)
Divalent 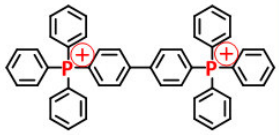 bis(triphenylphosphonium) biphenyl		**4-17**	bis(triphenylphosphonium)biphenyl dibromide was reacted with $Li^+ [B^F\text{-}G1]^-$ (**4-4**); slight excess of lithium borate was used in order to ensure twofold ion exchange

4.3 Hydrodynamic Radii of Dendronized Salts

Diffusion ordered spectroscopy (DOSY) NMR provides a means to directly measure and compare the mobility of different molecular species in solution.[3] The measurement yields a two-dimensional plot in which the ^{1}H NMR signals are spread along an extra dimension. This dimension represents the logarithm of the diffusion coefficient $D = \mu\, k_B\, T$ in solution. Signals of different nuclei that exhibit the same translational mobility in solution appear at the same relative height of the lg D axis. To correlate the obtained mobility $\mu = \frac{D}{k_B T}$ to spatial molecular dimensions, the *Einstein-Stokes* equation is applied:

$$D = \frac{k_B T}{6\pi\eta r_H} \qquad \textbf{(Equation 4-3)}$$

It becomes obvious that ideally spherical particles move slower (values of D decrease) with increasing size (increased hydrodynamic radius r_H) in a given medium with viscosity η.

The DOSY-NMR spectra analysis of the dendronized salts from **Table 4-3** provides information about the size of the molecular species, which is summarized in **Table 4-4** by their respective diffusion coefficient values. The measurements confirmed that hydrodynamic radii r_H of dendronized anions generally increase with increasing dendrimer generation (compare PPh_4^+, which can be regarded as generation 0 to third-generation phosphonium cation $[P\text{-}G_3]^+$). To be very accurate it should be mentioned that the measured – lg D values represent an average value of fully dissociated and associated ion pairs. Thus, the experimental anion radius D_{exp}^- for the first-generation borate anion $[B^F\text{-}G1]^-$ differs slightly depending on the size of the counter cation (illustrated in **Figure 4-7** by the two horizontal dashed lines).

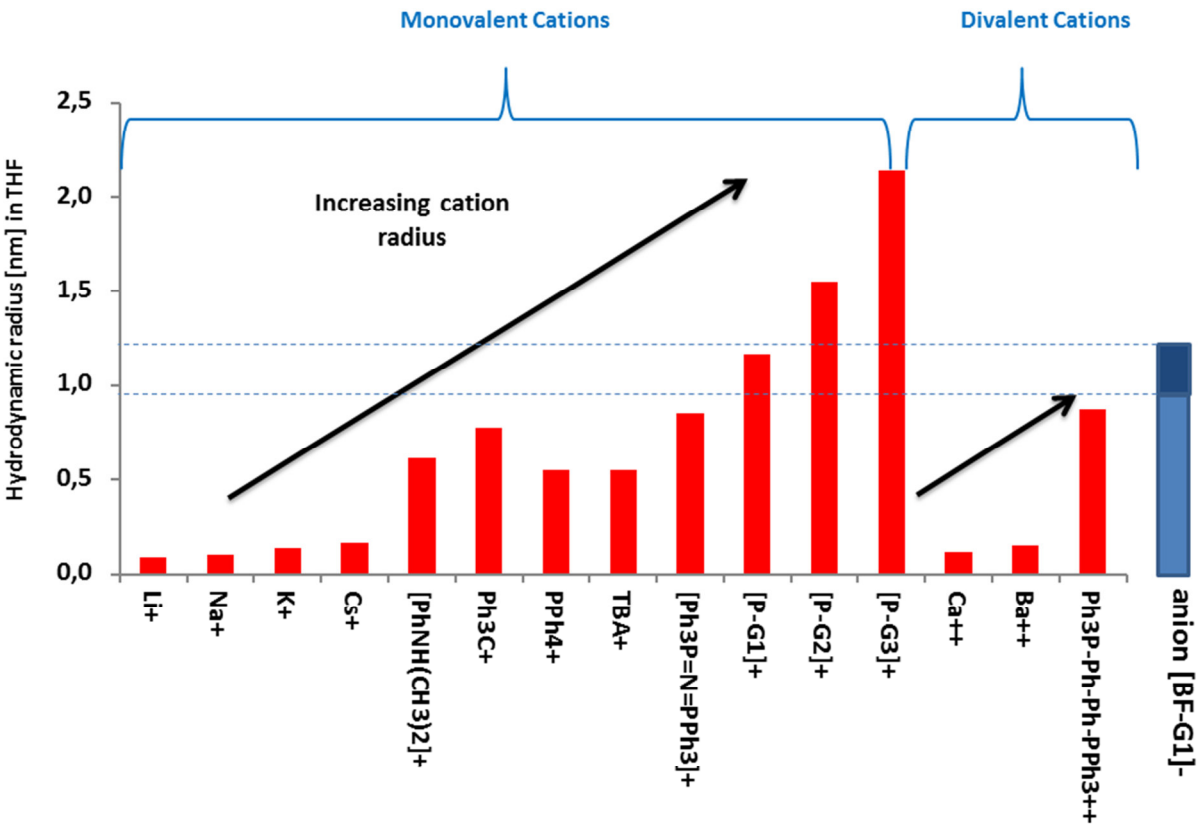

Figure 4-6: Illustration of the cation radii determined by DOSY-NMR measurements (THF-d8, 298 K, 300 MHz).

Table 4-4: Measured diffusion coefficients by means of DOSY-NMR (0.001 M in THF-d8, 298K, 300 MHz). Hydrodynamic radii were calculated by applying the Einstein-Stokes Equation (**Equation 4.3**). All measured data possess a standard deviation of 0.1 nm. Alkali and earth alkali metal radii were obtained from the literature.[6]

Compound	- log D_{exp}+	D_{exp}+ [m^2/s]	hydrodynamic cation radius r_H [nm]	- log D_{exp}-	D_{exp}- [m^2/s]	hydrodynamic anion radius r_H [nm]
Monovalent Cations						
Li^+ [B^F-G1]- (4-4)	nd	nd	0,09	-9,35E+00	4,47E-10	0,98
Na^+ [B^F-G1]- (4-5)	nd	nd	0,10	-9,38E+00	4,17E-10	1,05
K^+ [B^F-G1]- (4-6)	nd	nd	0,14	-9,32E+00	4,79E-10	0,91
Cs^+ [B^F-G1]- (4-7)	nd	nd	0,17	-9,30E+00	5,01E-10	0,87
$PhNH(CH_3)_2^+$ [B^F-G1]- (4-10)	-9,15	7,08E-10	0,62	-9,31E+00	4,90E-10	0,89
Ph_3C^+ [B^F-G1]- (4-11)	-9,19	6,46E-10	0,75	-9,42E+00	3,80E-10	1,15
PPh_4^+ [B^F-G1]- (4-12)	-9,1	7,94E-10	0,55	-9,35E+00	4,47E-10	0,98
TBA^+ [B^F-G1]- (4-2)	-9,1	7,94E-10	0,55	-9,37E+00	4,27E-10	1,02
$Ph_3P{=}N{=}PPh_3$ [B^F-G1]- (4-13)	-9,29	5,13E-10	0,85	-9,44E+00	3,63E-10	1,20
$[P\text{-}G1]^+$ [B^F-G1]- (4-14)	-9,39	4,07E-10	1,17	-9,40E+00	3,98E-10	1,09
$[P\text{-}G2]^+$ [B^F-G1]- (4-15)	-9,55	2,82E-10	1,55	-9,47E+00	3,39E-10	1,29
$[P\text{-}G3]^+$ [B^F-G1]- (4-16)	-9,69	2,04E-10	2,14	-9,42E+00	3,80E-10	1,15
Divalent						
Ca^{++} [B^F-G1]- (4-8)	nd	nd	0,11	-9,25E+00	5,62E-10	0,77
Ba^{++} [B^F-G1]- (4-9)	nd	nd	0,15	-9,28E+00	5,25E-10	0,83
$Ph_3P\text{-}Ph\text{-}Ph\text{-}PPh_3^{++}$ [B^F-G1]- (4-17)	-9,3	5,01E-10	0,87	-9,36E+00	4,37E-10	1,00

The impact of the cation size on the electrolyte properties in terms of ion dissociation and conductivity is of particular interest in the subsequent section.

4.4 Dielectric Spectroscopy of Dendronized Salts

Dielectric spectroscopy (principles explained in the Introduction, chapter 1.7) is the method of choice to investigate the degree of ion dissociation and transport through the measured dc-conductivity.[7-11] The measurements reported within this chapter were thankfully performed by [redacted] in cooperation with [redacted] at the University of Ioannina, Greece. All apparent salts were 0.001 M solutions in THF, so that the mean distance between molecular ions was in the order of the Bjerrum length.[12] The dc-conductivity of an ion-containing medium is the sum of the individual contributions of all charge carriers:

$$\sigma_{dc} = \sum_{i=1}^{n} N_A c_i \mu_i q_i \qquad \textbf{(Equation 4-4)}$$

where N_A is the Avogadro constant, c_i the molar concentration, μ_i the mobility and q_i is the charge of the i^{th} type of charge carrier.

All the measured conductivity values for the different salts (**4-4** to **4-17**) were in the range of $10^{-5}\,\frac{\mathrm{S}}{\mathrm{cm}}$ and are plotted in **Figure 4-8** as a function of cation size (monovalent = blue symbols, divalent = red symbols). Ionic radii of alkali metals were employed from the literature[6] whereas ionic radii for the larger cations and the first-generation anion have been determined by semiempirical AM1 calculations. Again it becomes obvious that the calculated values differ slightly from the experimentally determined values by DOSY-NMR measurements (compare **Table 4-4**).

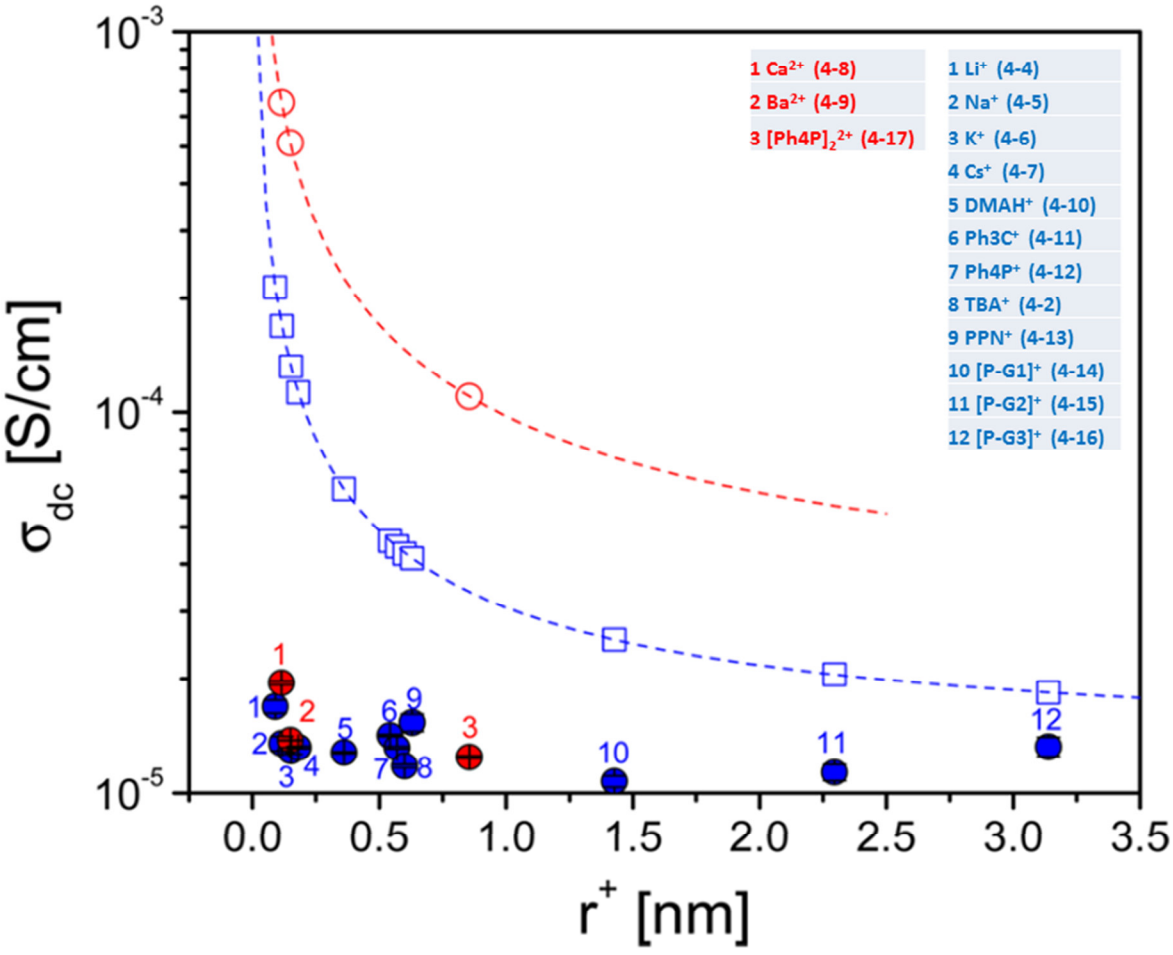

Figure 4-7: Dc-conductivity plotted as a function of cation size at 298 K. Red and blue symbols correspond to divalent and monovalent cations, respectively. Filled symbols give the measured conductivities at 298 K at 0.001 M concentration in THF. Open symbols give the respective calculated conductivities assuming complete dissociation.

The apparent trends upon analyzing the data shown in **Figure 4-7** are as follows. For the smallest cations - the series of the alkali metal salts Li^+ $[B^F\text{-}G1]^-$, Na^+ $[B^F\text{-}G1]^-$, K^+ $[B^F\text{-}G1]^-$, Cs^+ $[B^F\text{-}G1]^-$ - increasing cation size lowers the ionic conductivity. This conforms to a reduced molar ion conductivity Λ_i (mobility) in **tetrahydrofurane** being inverse proportional to the cation radius in the series:

$$r_{Li}+ < r_{Na}+ < r_{K}+ < r_{Cs}+ \quad \rightarrow \quad \Lambda_{Li}+ > \Lambda_{Na}+ > \Lambda_{K}+ > \Lambda_{Cs}+$$

In **aqueous solutions**, however, it is known that the tendency is vice versa and follows:

$$r_{Li^+(H2O)} > r_{Na^+(H2O)} > r_{K^+(H2O)} \rightarrow \Lambda^0_{Li}+ = 36.68\,\frac{cm^2}{\Omega} < \Lambda^0_{Na}+ = 50.11\,\frac{cm^2}{\Omega} < \Lambda^0_{K}+ = 73.5\,\frac{cm^2}{\Omega}$$

To rationalize these findings, the coordination of solvent molecules around the charge centers has to be taken into account. Lithium cations are slower in aqueous solution than potassium cations since the former are more hydrated by water and thus exhibiting a greater effective radius $r_{Li^+(H2O)}$.

In contrast to that the alkali metal borates **4-4** to **4-7** (**1-4** (blue) in **Figure 4-7**) in the herein investigated diluted solutions (10^{-3} M in THF) can reasonably be regarded as solvent separated ion pairs or even fully solvated ion pairs[13] due to the presence of the large non-coordinating borate anion. Our findings support that thereby the cation mobility values follow the size order in the periodic table going from lithium to caesium.

The opposite trend is observed for the phosphonium borates **4-14** to **4-16** (**10-12** in **Figure 4-7**), where the large phosphonium dendrimers with increasing size represent the cations. Thereby an increase of dc conductivity was observed with increasing size of the cations, which is explained in terms of decreasing ion mobility in that order. This clearly reflects the balance between ion dissociation on one hand (promoted by the bulky ions) and charge transport on the other hand (inhibited by the large ions). The dashed lines in **Figure 4-8** show the respective calculated dc conductivities, which were obtained from the mobility $\mu_i = e/6\pi\eta r_i$ according to:

$$\sigma_{\mathrm{calc}} = \frac{p_S e^2}{6\pi\eta}\left[\frac{1}{r^+} + \frac{1}{r^-}\right] \qquad \textbf{(Equation 4-5)}$$

where r_i are the ionic radii, $p_s = \sum \nu i\, zi\, ci$ is the total ion concentration from stoichiometry (0.001 M), and η is the solvent viscosity (η[Pa·s]= 2.1379×10^{-5} exp(910/T)).

The measured dc-conductivity differs from the calculated one, because the paired charges do not contribute to the conduction mechanism. The degree of ion dissociation can be extracted from the ratio of the measured dc-conductivity and the calculated conductivity that assumes complete ion dissociation, as $\alpha = \sigma_{meas}/\sigma_{calc}$, known as the Haven ratio (HR). This ratio is plotted as a function of the cation size in **Figure 4-8**.

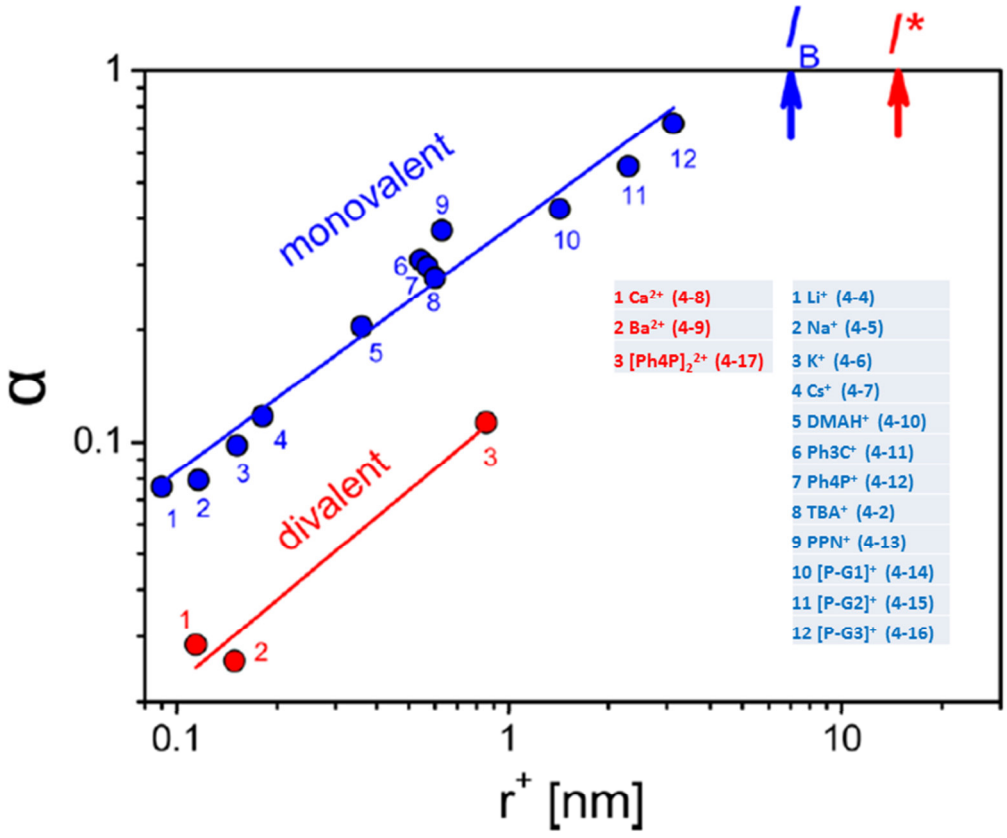

Figure 4-8: Degree of ion dissociation for borate solutions in THF (concentration 0.001 M) at 298 K plotted as a function of cation size. Blue and red symbols refer to monovalent and divalent cations, respectively. Blue arrow gives the estimated Bjerrum length (l_B) for monovalent ions. Red arrow is the estimated escape distance (l*) for the divalent case. Lines represent the result of linear fits.

The systematic variation of the cation size from Li^+ (diameter 0.18 nm) to the much larger dendronized phosphonium cations of **4-14** to **4-16** (**10–12**) (respectively calculated diameters of 2.9, 4.6, and 6.3 nm) follows a power low dependence with an exponent ~2/3. For the cations with r+ ≪ r−, this approach suggests a dependence of the measured conductivity on cation radius as $\sigma_{meas} \sim (r^+)^{-1/3}$. This is actually the case for the cations of the alkali metals (Li^+, Na^+, K^+, Cs^+).

The linear extrapolation in the representation of **Figure 4-8** predicts that a cation of about 7 nm in size would be largely dissociated from the borate anion. This size is within reach of the Bjerrum length (7.4 nm) at this temperature and in the same solvent. This similarity is, at first sight, surprising for two reasons: first borate salts are not point charges and second the borate anion core has a delocalized charge due to the fluorine substitution.[14] In addition to that atomic partial charge distribution, also local solvation effects have to be taken into

account. It is very likely that polyphenylene salts **4-14** to **4-16** (**10–12**) are solubilized well by THF both in the periphery and in the cavities, which is supposed to lead to a reduction of the effective net Coulomb potential mediated by ion-dipole interactions.

Nevertheless, none of these factors seems to alter substantially the escape distance. Hence, this synthetic approach that utilizes very large cations leads to the formation of superweak cations in solvents of low polarity in agreement with the theoretical predictions for the "ideal", i.e., point-like case.

In the divalent case, each cation is attracted by two separate borate anions, thus increasing the calculated conductivity to:

$\sigma_{dc} = p_+\mu_+Z_+e + (2p_-\mu_-e)$ for fully dissociated ions and

the mobility $\mu_+ = Z_+e/6\pi\eta r_+$ ($Z_+ = 2$) resulting in:

$$\sigma_{calc} = \frac{p_S 4e^2}{6\pi\eta}\left[\frac{1}{r^+} + \frac{1}{2r^-}\right]$$

This gives rise to a lower degree of dissociation as compared to the monovalent case (**Figure 4-9**). Nevertheless, the degree of dissociation extrapolates reasonably to the theoretically predicted escape distance from the Coulomb energy. The latter, calculated for a divalent cation with a monovalent anion, gives a characteristic distance of 14.8 nm ($l^* = 2l_B$).

In order to gather additional information on the state of ions, the temperature dependence of the dielectric permittivity was compared for Na^+ [B^F-G1]$^-$ (**4-5**) and [P-G2]$^+$ [B^F-G1]$^-$ (**4-15**) plotted in **Figure 4-10**. In polar liquids the dielectric permittivity decreases with increasing temperature and its value is related to the dipole moment of relaxing units as predicted by Onsager.[15] In evaluating the dipole moments in the solutions we employed the following equation[16]:

$$\varepsilon_S(T) = \mu^2 \frac{N_A(\varepsilon_{THF}+2)({n_{THF}}^2+2)}{27k_B T\varepsilon_0} + (\varepsilon_{THF} - {n_{THF}}^2) + \varepsilon_\infty \qquad \textbf{(Equation 4-6)}$$

where, μ is the dipole moment, c is the concentration ($1*10^{-3}$ mol/m^3), ε_{THF} and n_{THF}, are the measured permittivity and refractive index of the solvent (THF), ε_∞ is the high frequency limit of the dielectric permittivity (obtained from the measured refractive index as $\varepsilon_\infty = n^2$), ε_0 is the permittivity of vacuum, k_B is Boltzmann's constant and N_A is Avogadro's number.

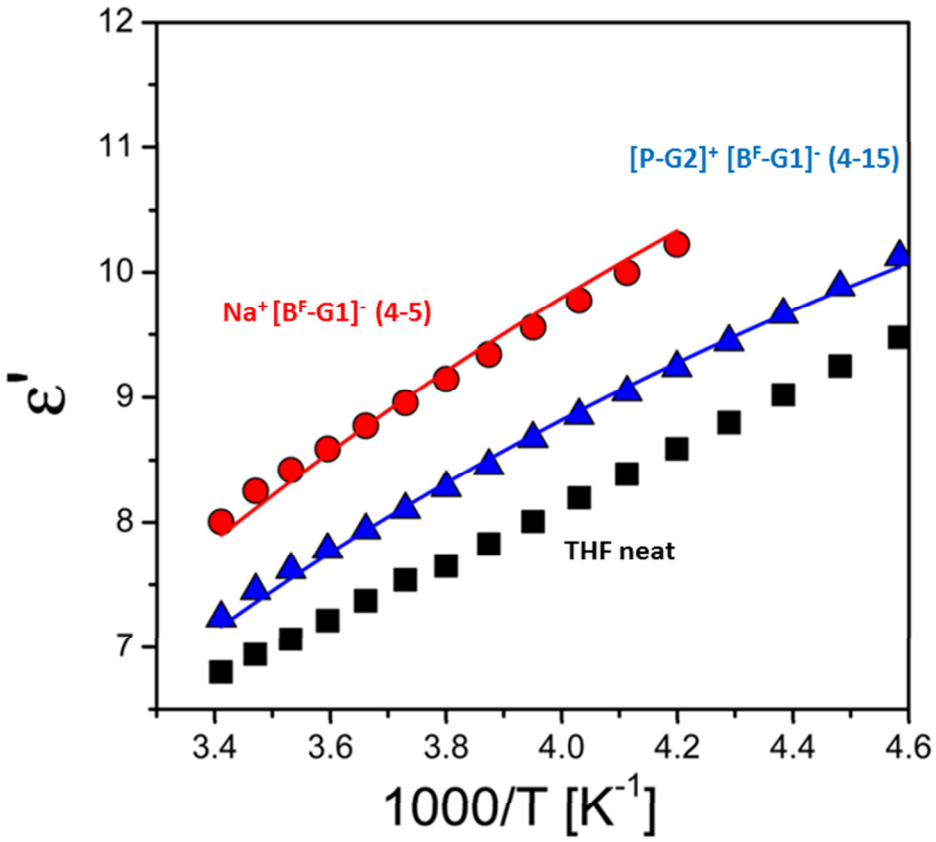

Figure 4-9: Static dielectric permittivity plotted as a function of inverse temperature for the neat solvent THF (squares) and for 0.001 M solutions of Na^+ $[B^F\text{-}G1]^-$ (**4-5**) (circles) and $[P\text{-}G2]^+$ $[B^F\text{-}G1]^-$ (**4-15**) (triangles) in THF.

From the fit to **Equation 4.6**, assuming that all ions form pairs, we obtained dipole moments in the range from 60 to 70 D for **4-5** (Na^+ $[B^F\text{-}G1]^-$) and in the range from 30 to 40 D for **4-14** (**$[P\text{-}G1]^+$ $[B^F\text{-}G1]^-$**, not shown in **Figure 4-10**) and **4-15** (**$[P\text{-}G2]^+$ $[B^F\text{-}G1]^-$**. These are reasonable values in accord with the degree of ion dissociation discussed earlier. For example, in **4-5** (Na^+ $[B^F\text{-}G1]^-$) the dipole moment of an ion pair ($\mu = e(r^+ + r^-)$) is estimated as 74 D, and this values is in good agreement with the experimental values since the majority of ions are associated (**Figure 4-9**). In the larger phosphonium ions the measured dipole moment - under the assumption that all ions form pairs - is below the calculated one for paired ions (~180 D in **$[P\text{-}G2]^+$ $[B^F\text{-}G1]^-$**) since in this case most ions are dissociated (**Figure 4-9**).

Because of ion association, the diffusion coefficients measured by DOSY-NMR (D_{exp}) at 298 K (**Table 4-4**) are not the diffusion coefficients of the free ions but represent some average of the fully dissociated and paired states.[17] This is shown in **Figure 4-10** that compares the

measured diffusion coefficients (symbols) for the different anion sizes/generations at 298 K with the calculated ones (from the Stokes–Einstein relation, $D_i = k_BT/6\pi\eta r_i$) (lines) corresponding to unassociated ions. For the larger cations, the measured and calculated diffusion coefficients are in reasonable agreement, since the degree of ion association is low. For the smaller cations, however, the NMR diffusion coefficients underestimate/overestimate the respective cation/anion diffusion coefficients with regard to the free ions as a result of the stronger ion association.

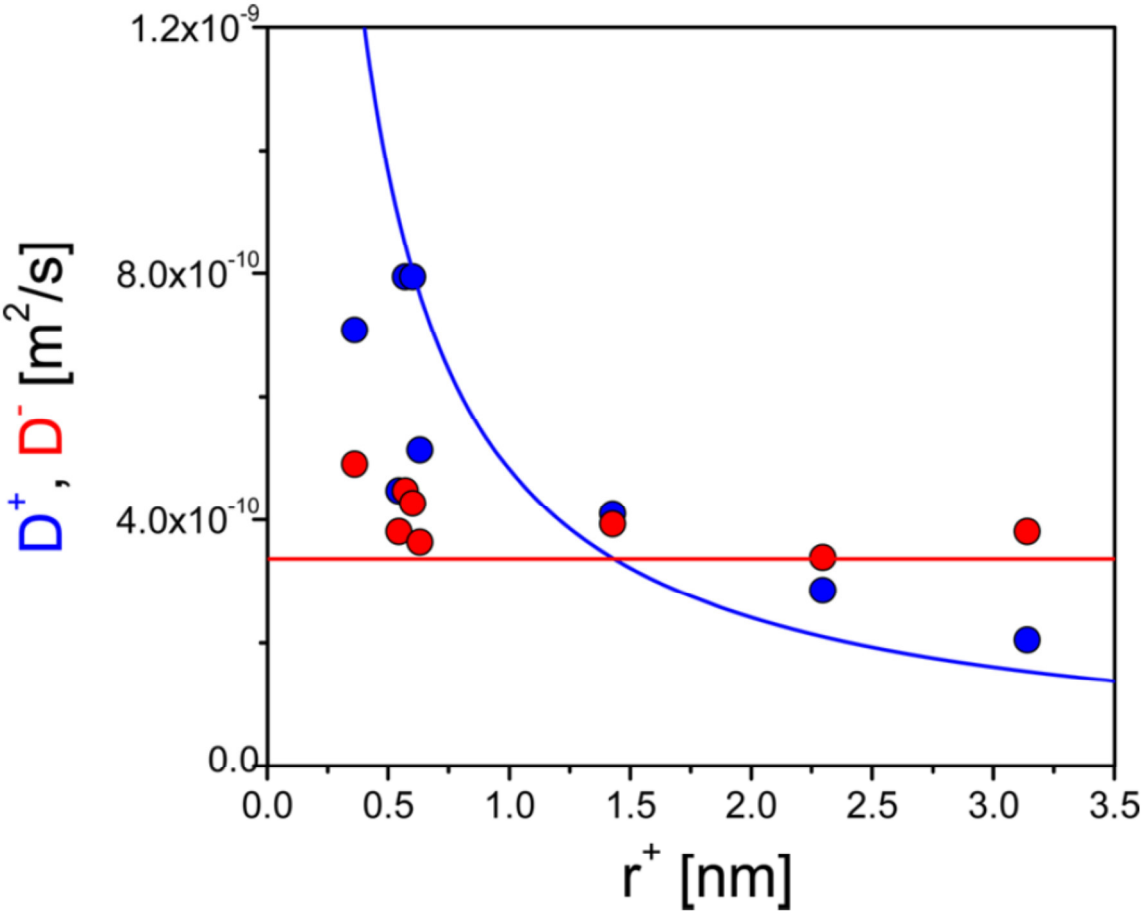

Figure 4-10: Measured (T = 298 K) DOSY-NMR diffusion coefficients for the anion (D^-) (red symbols) and the cation (D^+) (blue symbols) plotted as a function of the cation size. Calculated anion (red) and cation (blue) diffusion coefficients are corresponding to unassociated ions.

4.5 Chemical Properties of Dendronized Phosphonium Salts

The dendritic encapsulation of phosphonium cations leads to a steric shielding of the central positive charge center. This is expected to influence the chemical properties of the dendronized phosphonium salts with respect to thermal stability. First evidence for a remarkable effect of bulky dendrons on the thermal decomposition of monodisperse dendrimer ions was presented in the dissertation of *David Tuerp*.[17] It was discovered that first-generation tetraphenylborate derivative **4-1** undergoes significant thermal decomposition under release of a single polyphenylene dendron generated by the cleavage of the inner boron-carbon bond. It was concluded therefrom that the steric loading caused by bulky dendrons accelerates decomposition reactions for large polyphenylene borates, unless a fluorination of the inner phenyl-groups (like in **4-2**) increases the long-term temperature stability (~ 170 °C in o-xylene for several hours).[1]

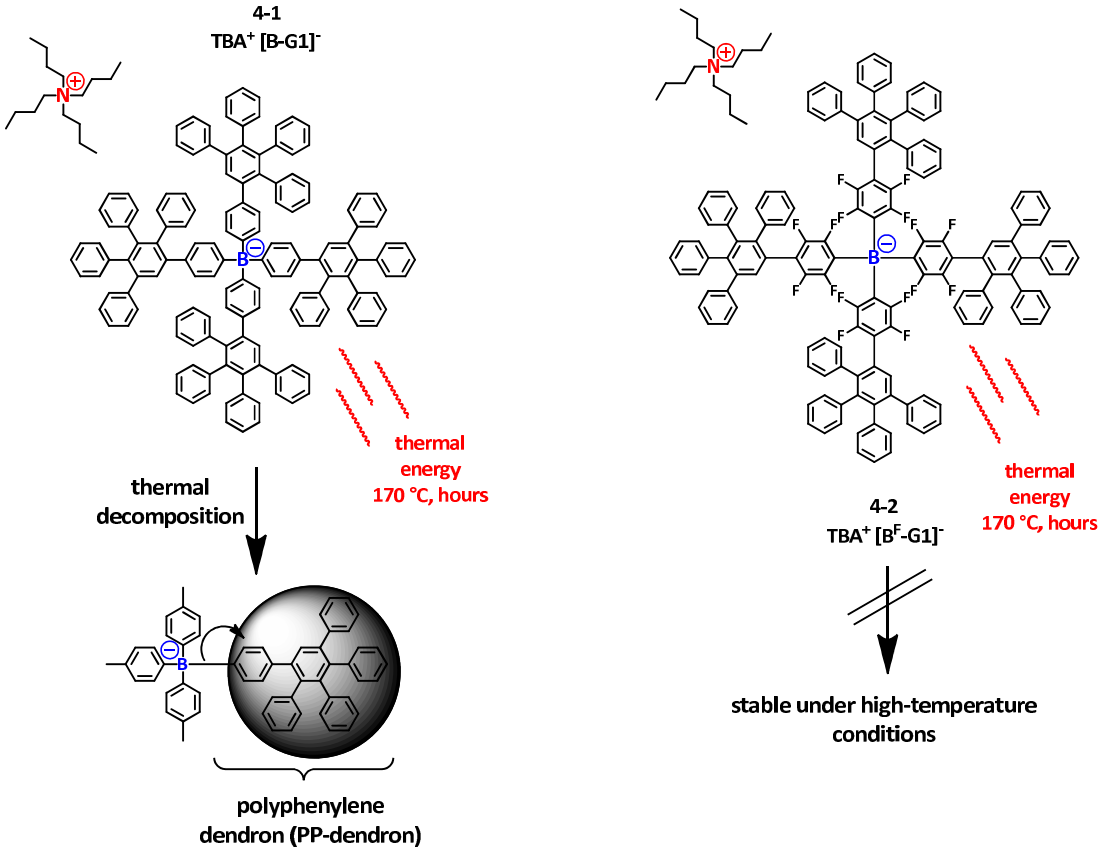

Figure 4-11: Illustrative comparison of first-generation TBA^+ borates **4-1** and **4-2** (inner phenyl rings fluorinated) with regard to thermal decomposition in solution.

The objective within this chapter is to investigate in which way the reported effects for borate anions are transferable to phosphonium cations. For that purpose first-generation phosphonium tetrafluoroborate **4-18** ([**P-G1**]$^+$ **BF$_4^-$**) was compared to non-dendronized tetraphenylphosphonium bromide (**PPh$_4^+$ Br$^-$**) providing that the counter anion is not exerting any influence on the following investigation methods.

By means of thermogravimetric analysis (TGA) the decomposition temperatures of the phosphonium salts **4-18** (350 °C under nitrogen stream, 350 °C under air stream) and **PPh$_4^+$ Br$^-$** (> 400 °C) were determined. Thereby the solid-state thermal stability of the herein compared salts was revealed to be not significantly influenced by the size of the phosphorus ligands. Furthermore, the dried dendronized phosphonium tetrafluoroborate salts synthesized within this work can be stored for long time (several months) even in the presence of air and moisture without decomposition, which agrees with literature known trialkyl- and triarylphosphonium tetrafluoroborates.[18]

Since most chemical reactions and processes of phosphonium salts are performed in solution, the stability of the dissolved salts was of subsequent interest. In particular, the synthesis of phosphonium salts of higher generations in o-xylene, reported in paragraph 3.4, yielded significant amounts of the according phosphine oxide. To understand this finding, a solution of pure **4-18** ([**P-G1**]$^+$ **BF$_4^-$**) (40 mg in 3 mL o-xylene, degassed) in a microwave vial was sealed by a teflon cap and heated at first to 120 °C for 3 days. ^{31}P-NMR indicated no decomposition of the quarternary salt (δ 23.1 as only peak, o-xylene, 202 MHz, 298 K) after that time. However, a further heating of that solution to 150 °C for 2 weeks showed an additional peak in the ^{31}P-spectrum at δ 29.1 (around 1/5 in intensity compared to the still present peak at δ 23.1), which corresponds to the phosphine oxide.

In contrast to that, a suspension of **PPh$_4^+$ Br$^-$** in o-xylene (30 mg in 3 mL) was also heated to 150 °C for 2 weeks and did not show an additional peak in the ^{31}P-spectrum unless the one referred to the starting compound (δ 21.7 in CD_2Cl_2, 202 MHz, 298 K, recorded afterwards due to the poor solubility of PPh_4^+ Br^- in o-xylene). These results suggest a slight decrease of thermal stability due to the presence of large dendrons in neutral o-xylene solution. The reason for the observed oxidation is either caused by residual traces of water or by in-diffusing oxygen.

For practical use of phosphonium salts as stable phase transfer catalysts (PTC),[19] hydroxide ion conducting membranes,[20] and stable sources of naked fluoride ions,[21] the investigation of their stability in alkaline solutions is of substantial interest (or more generally their stability against nucleophiles). Therefore, a series of ^{31}P-NMR kinetic experiments was performed at 25 °C (298 K) and 60 °C (333 K) to compare **4-18** ($\mathbf{[P\text{-}G1]^+\ BF_4^-}$) with $\mathbf{PPh_4^+\ Br^-}$ under the following reaction conditions:

The respective phosphonium salt $\mathbf{PR_4^+\ X^-}$ was prepared as a 0.11 M solution in DMF (Acros Organics, 99.8 %, extra dry, fresh bottle). Furthermore a potassium hydroxide solution (KOH, 0.1 M) in deuterated water (D_2O) was provided. Each sample preparation for a kinetic measurement consisted of adding 0.9 mL of the $\mathbf{PR_4^+\ X^-}$ solution and 0.1 mL of the KOH-solution (both thermostated to the given temperature prior to use) into a glass vial (always kept at constant temperature) at a stirring rate of 400 rpm. At the point of hydroxide addition the measurement started (t = 0 h) with initial concentrations of $c_0[PR_4^+] = 0.1$ M and $c_0[OH^-] = 0.01$ M.

In order to calculate the present concentration of $c[PR_4^+]$, integrable ^{31}P-NMR spectra (process parameters see Experimental Part) were recorded after the given times (see **Figure 4-13** for $[P\text{-}G1]^+\ BF_{4}^-$) and the relative integral ratio of the phosphonium species PR_4^+ (δ 23.5 ppm) and phosphine oxide $O{=}PR_3$ (δ 27 ppm) was determined. The tenfold-molar excess of PR_4^+ compared to OH^- suggests pseudo-first order kinetics according to the alkaline degradation mechanism of phosphonium salts proposed by Ingold (**Figure 4-12**),[22] but our data analysis provided least deviation when assuming a second-order kinetic degradation (fully recorded data sets see Experimental Part).

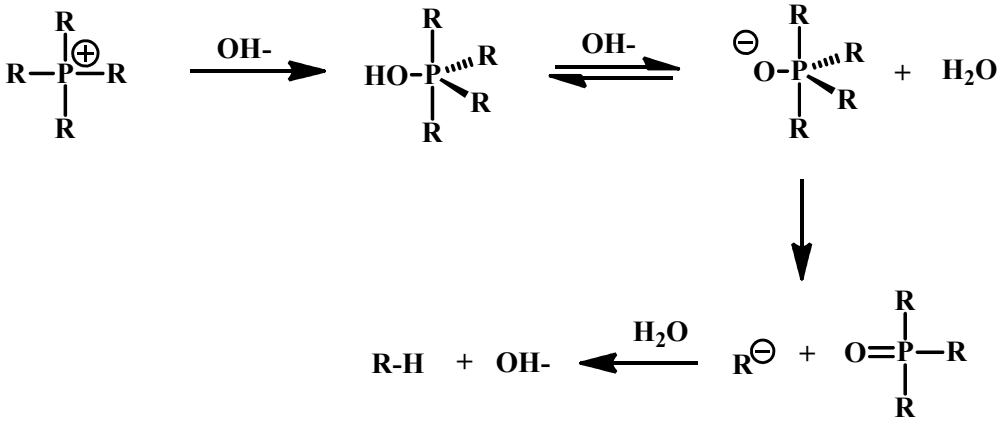

Figure 4-12: Decomposition mechanism of phosphonium cations under basic conditions according to Ingold and coworkers.

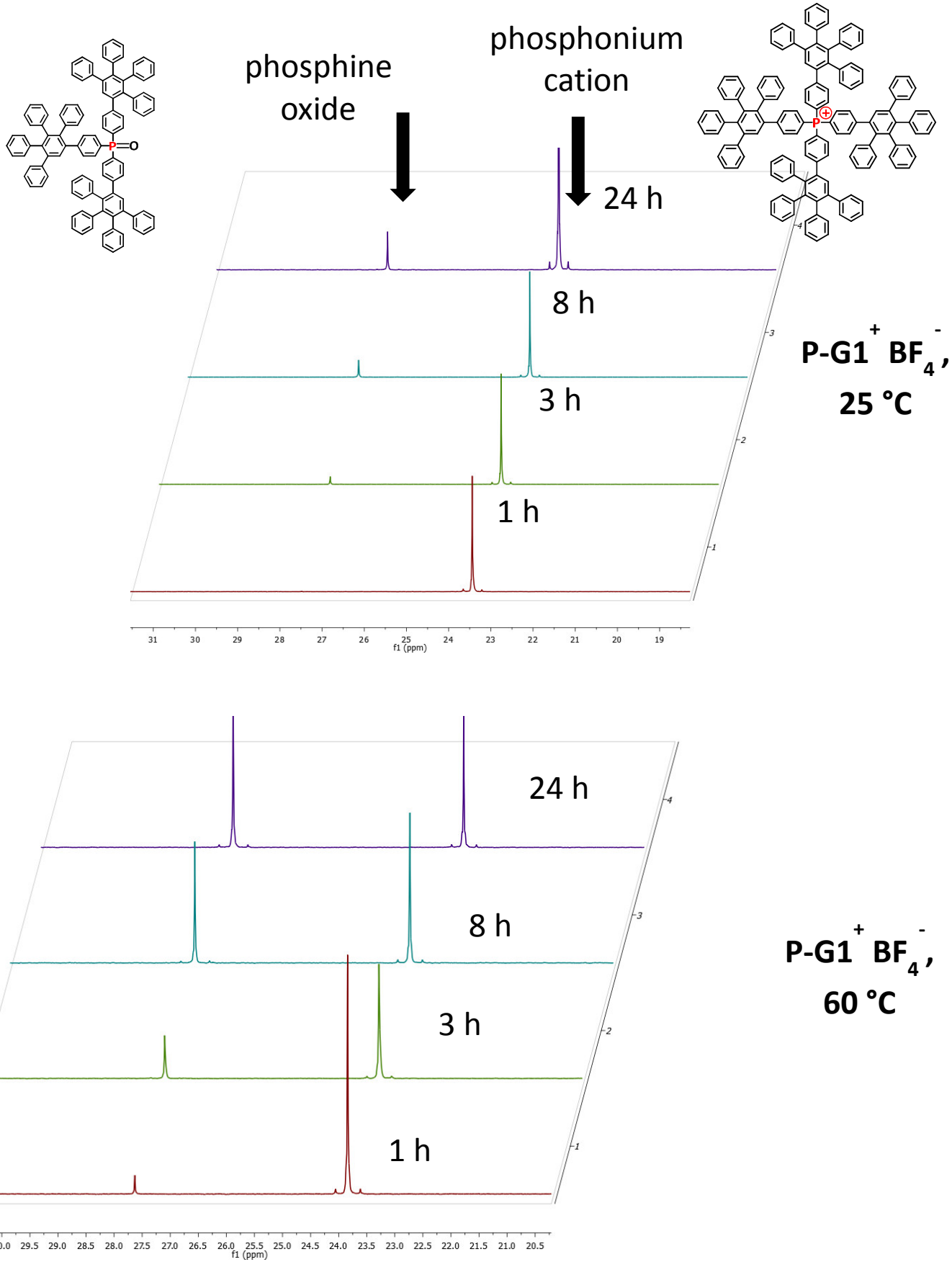

Figure 4-13: Integrable ^{31}P-NMR spectra of $[P\text{-}G1]^+$ BF_4^- (**4-18**) recorded after the given time points. The ratio of the integrals was used to calculate the percentage of residual cationic species c(PR_4^+).

The observed phosphonium cation degradation can be described using **second-order kinetics**.[23] A plot of the reaction time (x-axis) against the reciprocal concentration of the analyte (y-axis) is shown in **Figure 4-14**, which strongly suggests a second-order kinetics for the decomposition of [PR_4^+]. The slope of the graphs provided the rate constant k_2' ($\frac{L}{mol\,h}$). From the rate law the half-life is given by:

$$t_{1/2} = \frac{1}{k\,c0[PR4+]} \qquad \textbf{(Equation 4-7)}$$

It must be noticed that the half-life of a second-order reaction depends on the initial concentration, in contrast to its constancy for a first-order reaction. Thus, the scientific value for comparing reaction rates is only given under exactly the same conditions.

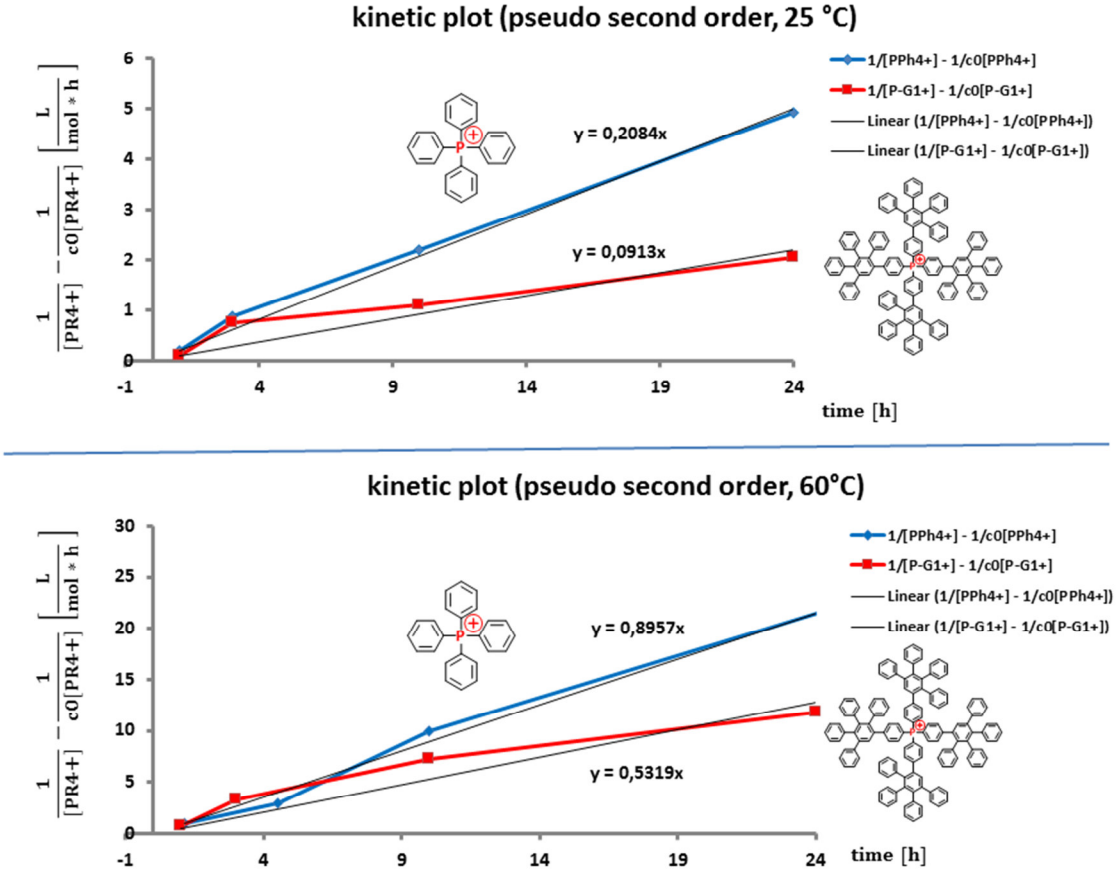

Figure 4-14: Rate constants k_2' of the alkaline degradation of **[PPh_4^+] Br^-** (blue) and **[P-G1$^+$] BF_4^-** (red) assuming pseudo-second order kinetics in a mixture of DMF/D_2O (9:1); $c_0(PR_4^+)$ = 0.1 M; c_0(OH-) = 0.01 M. Data points are averaged and slope is determined via linear regression. Standard deviation is provided in **Table 4.5**.

In order to correlate the chemical reaction rate constants with the temperature T, the Arrhenius Equation[24] was developed and follows:

$$k = A\, e^{\left[\frac{-E_A}{R\,T}\right]} \qquad \textbf{(Equation 4-8)}$$

where A is the pre-exponential factor, E_A is the activation energy of the reaction, R is the gas constant and T the temperature in Kelvin.

With the knowledge of rate constants at different temperatures T (i.e., 298 K and 333 K in the study above), it is possible to rearrange **Equation 4-8** to **Equation 4-9** (assuming that A is temperature independent) and calculate therefrom the activation energy E_A (kJ/mol):

$$E_A = \frac{R \ln\left(\frac{k1}{k2}\right)}{\left(\frac{1}{T2} - \frac{1}{T1}\right)} \qquad \textbf{(Equation 4-9)}$$

Table 4-5: Parameters for the **alkaline degradation** reaction of $PR_4^+\ X^-$ obtained from ^{31}P-NMR kinetic studies assuming pseudo-second-order; $c_0(PR_4^+)$ = 0.1 M; $c(OH^-)$ = 0.01 M; A series of experiments was performed in DMF/D_2O (9:1, v/v) over 24 h.

phosphonium salt	T [°C]	k [L mol^{-1} h^{-1}]	$t_{1/2}$ [h]	activation energy E_A [kJ mol^{-1}]
$PPh_4^+\ Br^-$	25	0.19 ± 0.02	52.8 ± 6.6	35.0 ± 3.0
	60	0.84 ± 0.08	11.9 ± 1.1	
dendrimer P-G_1^+ BF_4^-	25	0.08 ± 0.01	122.5 ± 17.9	45.6 ± 3.0
	60	0.52 ± 0.02	19.4 ± 0.9	

The discussion of the results in this chapter presumes that the tetraphenylphosphonium derivatives ($PPh_4^+\ Br^-$ and P-G1$^+$ BF_4^-) are initially attacked by hydroxyl ions to form a pentavalent intermediate (first step in **Figure 4-12**). The decomposition of the latter is the rate determining step for the hydrolysis according to *McEwen et al.*[25] Taking also into account that this postulation is only valid in dependence of the substituents linked to phosphorus, meaning that for instance highly anion-stabilizing leaving groups (like p-nitrobenzyl), however, render the initial OH- attack to the rate determining step.[26] So compairing the activation energies from **Table 4-5** obtained from our ^{31}P-measurements are only reasonable under the assumption that the leaving of the aryl group (Ph^- and PPD^- respectively) is slower than the attack of the hydroxyl ion. This can be hypothesized in view of the great excess of OH^- used in our experiments. A comparison of the obtained values

(35.0 +/- 3 kJ mol^{-1} for PPh_4^+ Br^-, 45.6 +/- 3 kJ mol^{-1} for P-$G1^+$ BF_4^-) with data from the literature[26] (111.7 – 128.9 kJ/mol for PPh_4^+ Br^- in alcohol-water mixtures) clearly underlines the sensitive dependence of the rate of the hydrolysis upon the dielectric constant of the solution.[27] Postulating a rationale for the slightly increased activation energy of about 10 kJ/mol when first-generation phosphonium salt (P-$G1^+$ BF_4^-) is decomposed in alkaline solution compared to PPh_4^+ Br^- under identical conditions, it is assumed that the initial attack of the highly hydrophilic hydroxide ion at the inner phosphorus is impeded by the large screening of the hydrophobic polyphenylene dendrons.

4.6 Discussion and Outlook

The route towards accessing an extended assortment of salts comprising both unprecedentedly large cations and large anions was extensively described by means of ion exchange techniques by the use of appropriate resins (chapter 4.2). It was shown later on via dielectric spectroscopy measurements that the dendritic encapsulation of a central charge changes the physical properties of organic phosphonium salts in terms of ion mobility and ion dissociation. The construction of a lipophilic polyphenylene shell around the charge centers also influences the chemical properties of the synthesized salts within this work. The obtained dendrimer-salts exhibit excellent solubility in low-polarity solvents, which was observed during the synthesis procedures from chapter 3 and chapter 5. A qualitative overview of the solubility behavior of selected compounds is shown in **Table 4-6**:

Table 4-6: Survey of the most commonly used solvents during the studies of this work. General assessment of solubility refers to dendronized salts from **Table 4-2** and **4-3** as well as phosphonium tetrafluoroborate salts from chapter 3. Special remarks are given for the respective solvent.

Solvent	relative permittivity ε_R	Remarks
H_2O	80.1	non-solvens for dendronized ions; even Li+ [BF-G1]- (**4-4**) precipitates in water
dimethyl sulfoxide DMSO	46.7	very good solvent
acetonitrile CH_3CN	37.5	very good solvent
N,N-dimethylformamide DMF	36.7	very good solvent
dichloromethane CH_2Cl_2	8.93	very good solvent; most commonly used for all work-up-procedures to redissolve the crude products in a minimum amount of solvent
THF	7.58	good solvent; especially for dendronized salts with phsophonium cations (G1 and G0) lower solubility than DCM
chloroform $CHCl_3$	4.81	very good solvent
diethylether Et_2O	4.33	poor solvent; only high generation phosphonium salts (G2 and G3) fairly dissolve; **4-14**, **4-15** and **4-16** displayed moderate solubiltiy
o-xylene	2.57	good solvent
o-toluene	2.38	good solvent; ~ 0.1 M solutions can be prepared
hexane	1.88	non-solvens for all dendronized salts within this work; the dendrimer surface has to be modified with alkyl chains in order to achieve solubility in aliphatic solvents

Furthermore, the results from **section 4.5** suggest that dendritic encapsulation increases the chemical stability of phosphonium salts with regard to decomposition by nucleophilic reagents.

Combining the greatly enhanced solubility in organic solvents, the effective charge separation in low-polarity solvents and their increased chemical stability, dendronized phosphonium salts excite special interest as ionic groups in anion exchange membrane (AEM) for alkaline fuel cell (AFC) applications.[28] Therefore the results from this and the previous chapter have to be implemented to a polymer matrix with the goal to obtain an anion conducting material with the following prerequisites:

- high ionic conductivity (~ 10^{-1} S cm^{-1}), hydroxyl charge carrier
- barrier to electrons to provide effective separation between anode and cathode
- good mechanical and thermal stability to facilitate processing
- scalability and low cost of materials

The judicious selection of the cationic group is of substantial importance to reach a high concentration of charges, to ensure a high ionic mobility and to get a chemically robust membrane. Most AEM suffer from decomposition in alkaline media caused by the nucleophilic attack of hydroxide ions on the cationic group. Based on the results of this work (see chapter 4.5), the toolkit-like concept of dendronization in combination with specific functionalization may be considered to develop more suitable ionic groups for AEM-materials with the desired properties highlighted above. A conceivable strategy therefore is proposed in the following and illustrated in **Figure 4-16**:

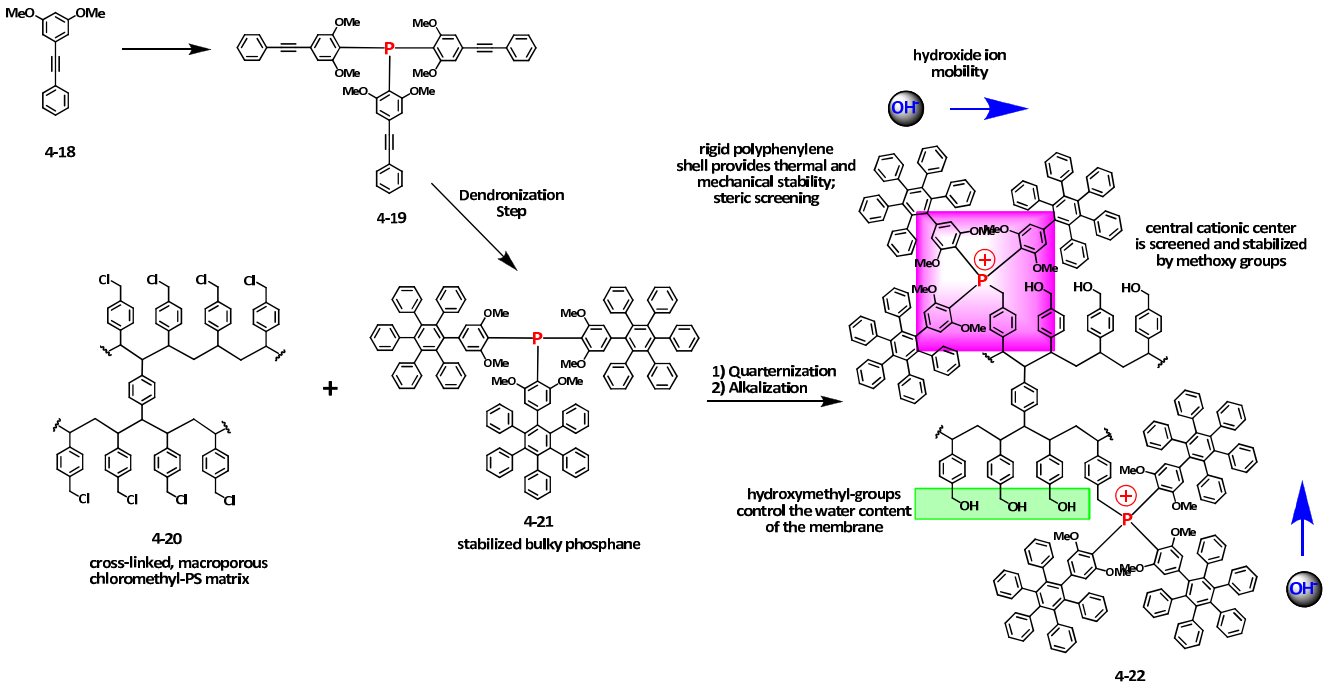

Figure 4-15: Schematic demonstration of the proposed synthetic pathway towards an alkaline exchange membrane (AEM) for effective alkaline fuel cells (AFCs).

Feasible membranes **4-22** with good mechanical stability and suitable water uptake can be processed similar to literature procedures from *Varcoe* and *Slade*.[29] Thereby, cross-linked chloromethyl styrene is grafted onto preformed ethylene-tetrafluoroethylene ETFE) polymer films.[29b] Most commonly followed is a quarternization step with trimethylamine (TMA). In contrast to that, the approach presented herein utilizes a bulky phosphane **4-21** with stabilizing ortho methoxy-groups and sterically screening polyphenylene dendrons (the practicability of this quarternization step will be shown in section 5.2). The focus on this tethered type of stabilized phosphonium ions is highly appreciable since they turned out to be more stable towards the attack by hydroxide ions than the conventional quarternary ammonium groups.[30] The main degradation pathways, being well studied for ammonium and sulfonium head groups,[31] are Sommelet-Hauser and Stevens rearrangement,[32] Hofmann degradation[33] or E1 elimination[34] for bulky substituents or by nucleophilic substitution resulting from a hydroxyl attack on the alpha-hydrogens of the cationic group. All of the above listed degradation mechanisms are avoided at its best by the proposed membrane structure **4-22**.

Furthermore, Chempath et al. showed that membranes with a poor water solvation exhibited a faster degradation of the cationic groups, since less hydrated OH^- ions become much more reactive.[35] For that reason a simultaneous generation of hydroxymethyl groups is considered during the alkalization step towards **4-22** to promote water uptake. It should be noted that the latter structural guidelines are not yet experimentally verified results but just postulates. In this work only the slightly increased stability of polyphenylene phosphonium groups against hydroxide attack was discovered (see chapter 4.5). This was rationalized by an impeded pass of OH^- through the hydrophobic environment of the dendritic scaffold. Additionally, it must be taken into account that the enhanced steric loading caused by the bulky dendrons is supposed to weaken the central phosphorus – carbon bond. This can be estimated by analyzing the binding lengths of recently synthesized phosphine ligands having a 2,3,4,5-tetraphenylphenyl (TPPh) moiety on one of the phenyl rings (at the ortho, meta, and para position) of triphenylphosphine.[36]

Literature

[1] Tuerp, D.; Wagner, M.; Enkelmann, V.; Müllen, K.; *Angew. Chem. Int. Ed.* **2011**, 50, 4962 – 4965.
[2] Bach, R. D.; Bair, K. W.; Andrzejewski, D.; *J. Am. Chem. Soc.* **1972**, *94*, 8608.
[3] Mpoukouvalas, K.; Tuerp, D.; Wagner, M.; Müllen, K.; Butt, H.-J.; Floudas, G.; *J. Phys. Chem. B* **2011**, 115 (19), 5801–5806.
[4] a) Jerschow, A.; Müller, N.; J. Magn. Res. A **1996**, 123, 222-225; b) Jerschow, A.; Müller, N.; *J. Magn. Res. A* **1991**, 125, 372-375.
[5] Einstein, A.; *Annalen der Physik* **1905**, 17, 549.
[6] Shannon, R. D.; *Acta Cryst.* **1976**, Vol. 32, Part 5, 751-767.
[7] Broandband Dielectric Spectroscopy; Kremer, F., Schönhals, A., Eds.; Springer-Verlag: Berlin, **2003**.
[8] Floudas, G. Dielectric Spectroscopy. In *Polymer Science: A Comprehensive Reference*; Matyjaszewski, K., Möller, M., Eds.; Elsevier BV: Amsterdam, **2012**; Vol. 2.32, pp 825−845.
[9] Dyre, J. C.; *J. Appl. Phys.* **1988**, 64, 2456−2468.
[10] Fragiadakis, D.; Dou, S.; Colby, R. H.; Runt, J.; *J. Chem. Phys.* **2009**, 130, 064907.
[11] Serghei, A.; Tress, M.; Sangoro, J. R.; Kremer, F.; *Phys. Rev. B.* **2009**, 80, 184301.
[12] Moritz, R.; Zardalidis, G.; Butt, H.-J.; Wagner, M.; Müllen, K.; Floudas, G.; *Macromolecules* **2014**, 47, 191−196
[13] Reich, H. J.; Borst, J. P.; Dykstra, R. R.; Green, P. *J. Am. Chem. Soc.* **1993**, 115, 8128-8741.
[14] Krossing, I.; Raabe, I.; *Angew. Chem. Int. Ed.* **2004**, 43, 2066.
[15] Onsager, L.; *J. Am. Chem. Soc.* **1936**, 58, 1486.
[16] Guggenheim, E. *A.; Trans. Faraday Soc.* **1949**, 45, 714.
[17] Tuerp, D.; *Dissertation*, Universität Mainz **2011**.
[18] Netherton, M. R.; Fu, G. C. Org. Lett. **2001**, Vol. 3, No. 26, 4295-4298.
[19] a) Sasson Y. et al. (eds.), *Handbook of Phase Transfer Catalysis,* Chapman & Hall **1997**; b) Landini, D.; Maia, A.; Rampoldi, A.; *J. Org. Chem.* **1986**, 51, 3187 – 3191.
[20] Tang, D.; Pan, J., Lu, S.; Zhuang, L., Lu, J.; *Sci China Chem* **2010**, Vol. 53, No. 2, 357-364.
[21] Borrmann, T.; Lork, E.; Mews, R.; Stohrer, W.-D.; *Journal of Fluorine Chemistry* **2004**, 125, 903-916.
[22] Fenton, C. W.; Ingold, C. K.; *J. Chem. Soc.* **1929**, 2312.
[23] a) Atkins, P. W.; De Paula, J.; *Physical Chemistry for the Life Sciences* **2006***.* New York, NY: W. H. Freeman and Company; b) Petrucci, R. H., Harwood, W. S., Herring, F. G. *General Chemistry: Principles and Modern Applications* **2002***.* Upper Saddle River, NJ: Prentice-Hall, Inc.
[24] a) Laidler, K.; "The Development of the Arrhenius Equation." *J. Chem. Educ.* **1984**, 61 (6), 494; b) Logan, S. R.; "The orgin and status of the Arrhenius Equation." *J. Chem. Educ.* **1982**, 59 (4), 279.
[25] McEwen, W. E.; Vander Werf, C. A.; Zander, M. J.; *J. Am. Chem. Soc.* **1959**, 81, 3806.
[26] Aksnes, G.; Songstad, J.; *Acta Chem. Scand.* **1962**, 16, No. 6, 1426-1432.
[27] Scatchard, G.; *Chem. Revs.* **1932**, 10, 229.
[28] Merle, G.; Wessling, M.; Nijmeijer, K.; Anion exchange membranes for alkaline fuel cells: A review, *Journal of Membrane Science* **2011**, 377, 1– 35.
[29] a) Varcoe, J.; Slade, R.; Lam How Yee, E.; Poynton, S.; Driscoll, D.; Apperley, D. Chem. Mater. **2007**, 19, 2686; b) Poynton, S. D.; Kizewski, J. P.; Robert, C. T.; Slade, J.; Varcoe, R.; *Solid State Ionics* **2010**, 181, 219-222.

[30] Gu, S.; Cai, R.; Luo, T.; Chen, Z. W.; Sun, M. W.; Liu, Y.; He, G,; Yan, Y. S.; *Angew. Chem. Int. Ed.* **2009**, 48, 6499-6502.
[31] a) Cope, A. C.; Trumbull, E. R.; *Olefins from Amines: The Hofmann Elimination Reaction and Amine Oxide Pyrolysis in Organic Reactions*, R. E. Krieger Publ. Co.; Huntington, New York, 1975; b) Trostyanskaya, E. B.; Makarova, S. B. *Zhurnal Prikladnoi Khimii* **1966**, 39, 1754.
[32] Ghigo, G.; Cagnina, S.; Maranzana, A.; Tonachini, G.; *J. Org. Chem.* **2010**, 75, 3608-3617.
[27] Chempath, S.; Boncella, J. M.; Pratt, L. R.; Henson, N.; Pivovar, B. S.; *Journal of Physical Chemistry* **2010**, C 114, 11977-11983.
[33] Cope, A. C.; Mehta, A. S.; *J. Am. Chem. Soc.* **1963**, 85, 1949-1952.
[34] a) Chempath, S.; Einsla, B. R.; Pratt, L. R.; Macomber, C. S.; Boncella, J. M.; Rau, J. A.; Pivovar , B. S.; *Journal of Physical Chemistry* **2008**, C 112, 3179-3182; b) Chempath, S.; Einsla, B. R.; Boncella, J. M.; Pivovar, B. R., Pratt, L. R. in *AIChE Annual Meeting* **2007**; c) Einsal, B. R.; Chempath, S.; Pratt, L. R.; Boncella, J. M.; Rau, J.; Macomber, C.; Pivovar, B. S.; *ECS Transactions* **2007**, 1173-1180.
[35] Iwasawa, T.; Komano, T.; Tajima, A.; Tokunaga, M.; Obora, Y.; Fujihara, T.; Tsuji, Y.; *Organometallics* **2006**, 25, 4665-4669.

Chapter 5 – Application of Dendronized Benzylphosphonium Salts in the Wittig Reaction

5.1 Introduction

The synthesis of dendronized tetraphenylphosphonium derivatives yielded symmetric tetrahedral coordinated bulky cations (**chapter 3**). As already outlined, the crucial quarternization step was accomplished by the use of diazonium salts. However, the most common approach to prepare quarternary phosphonium salts consists of the nucleophilic reaction between a phosphine and an alkyl halide or benzyl halide.[1] The benzylphosphonium salts developed within this work were prepared similar to Kröhnke's procedure[2] by reacting the corresponding benzyl halide with phosphines (**chapter 5.2**). Both the divergent and convergent approach for dendritic growth were deployed and turned out to be suitable for the preparation of sterically crowded benzylphosphonium salts. In a versatile manner this method of quarternization provided differently constituted phosphonium salts, whose crystal structures gave insight into their ion packings (**chapter 5.3**).

The main issue within this chapter is the application of benzylphosphonium salts with large polyphenylene α-substituents of unprecedented size in the Wittig reaction. In addition to envisage currently accepted explanations for the source of the stereoselectivity of the Wittig reactions and bring these in line with the findings gathered during this work, the preparation of novel alkenes and stilbenes with bulky polyphenylene substituents proceeded by this way under mild reaction conditions (**chapter 5.4**).

5.2 Divergent Synthesis of Dendronized Benzylphosphonium Salts

The preparation of first-generation benzylphosphonium bromide **5-6** was performed in a divergent synthetic approach (full synthetic route see **Figure 5-1**). Therefore, commercially available 4-ethynylbenzyl alcohol **5-1** was reacted with phosphorus tribromide to yield 4-ethynylbenzyl bromide **5-2**. The latter served as electrophile to react with tris-(4-ethynylphenyl)-phosphine **5-4** in a nucleophilic substitution under mild conditions to afford 4-ethynylbenzyl-tris-(4-ethynylphenyl)-phosphonium bromide (**5-5**). Thus, a phosphonium core with four pending ethynyl groups and one alpha-methylene moiety was generated, which enables a further dendritic growth via thermal [4+2] *Diels-Alder* reaction. This was subsequently achieved in a microwave assisted reaction between core **5-5** and tetraphenylcyclopentadienone (300 W, 180 °C, 3 bar pressure). In contrast to the traditional heating via oil bath it was purposed to shorten the reaction time and to increase the yield of the phosphonium bromide **5-6**.[3] However, the mandatory use of DMF made the purification of the latter difficult. For that reason the yield of **5-6** could not be remarkably improved compared to the same reaction performed in o-xylene heated via oil bath.

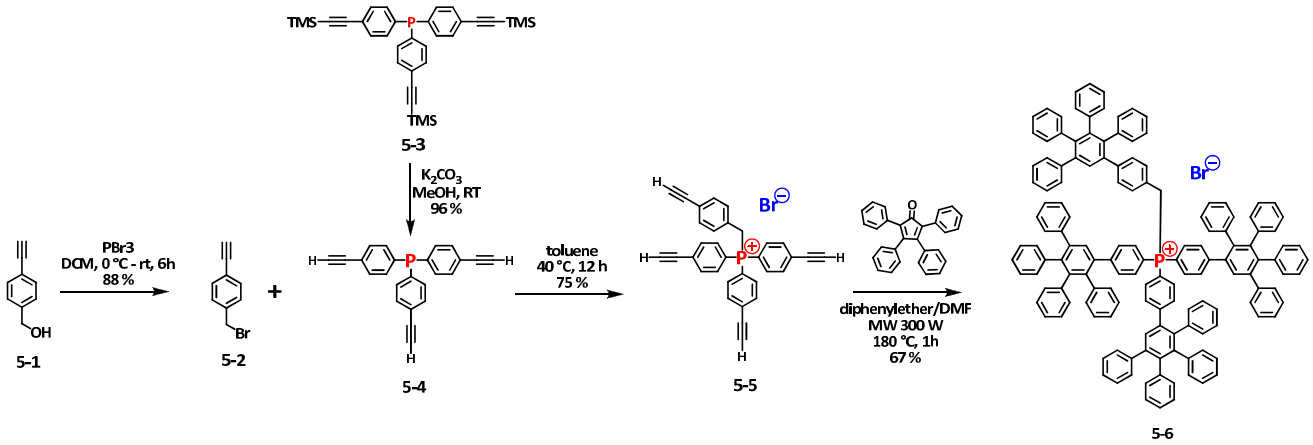

Figure 5-1: Synthetic route towards fully dendronized benzylphosphonium bromide **5-6** ($[P^{CH2}\text{-}G1]^+$ Br^-)

The presented reaction path offers a versatile variation of the counter halide ion. For instance, benzylalcohol derivative **5-1** could easily be converted to 4-ethynylbenzyl iodide **5-7** by treatment with triphenylphosphine, imidazole and iodine,[4] which allowed for the generation of dendronized phosphonium iodide **5-10**. Also the transformation of **5-1** to 4-

ethynyl-benzylchloride **5-8** was possible via concentrated hydrochloric acid.[5] This type of functional group conversion was not particularly performed in the course of this work, but demonstrates the versatility of the herein developed synthesis strategy.

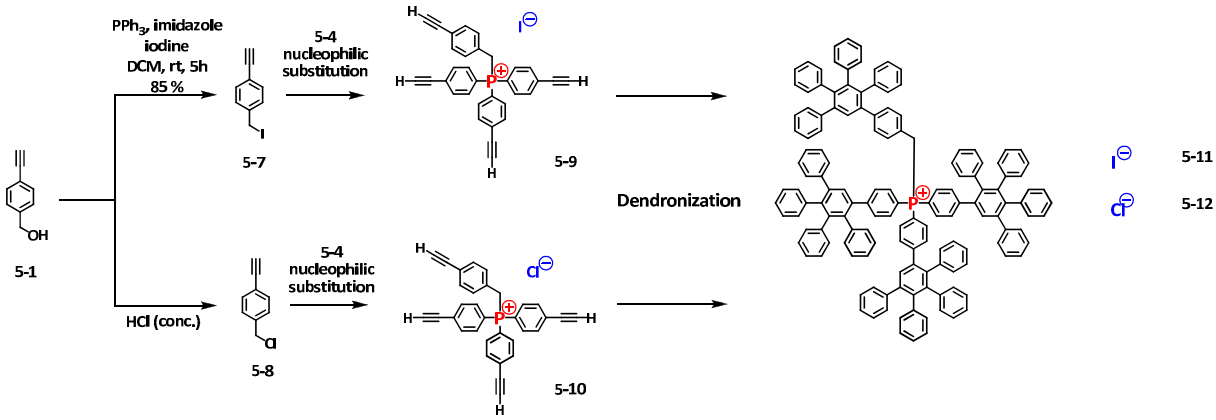

Figure 5-2: Synthetic scheme towards benzylphosphonium halides **5-11** (**[P^{CH2}-G1]$^+$ I$^-$**) and **5-12** (**[P^{CH2}-G1]$^+$ Cl$^-$**).

5.3 Convergent Synthesis of Dendronized Benzylphosphonium Salts

Every divergent synthetic approach to construct a shielding polyphenylene framework around the cationic phosphorus center requires a high-temperature Diels-Alder cycloaddition step, hence promoting side reactions and lowering the yield of the target cations. Thus, a convergent synthesis approach was pursued, where bulky building blocks comprising polyphenylene dendrons are already preformed and assembled in the final step. For this reason, polyphenylene benzylbromide **5-13** (PPD-CH_2Br) and dendronized phosphane **5-14** ($P(Dendr)_3$) were prepared as key intermediates. Reacting those two reagents in a nucleophilic substitution reaction yielded first-generation benzylphosphonium bromide **5-15** in excellent yields. The ease of purification and the practicability of this convergent synthesis strategy is superior to all the previous reported methods to synthesize dendronized quarternary phosphonium salts within this work (**Figure 5-3**). Simple precipitation in cold diethylether (twice) provides the target phosphonium salt **5-15** in analytical pure form.

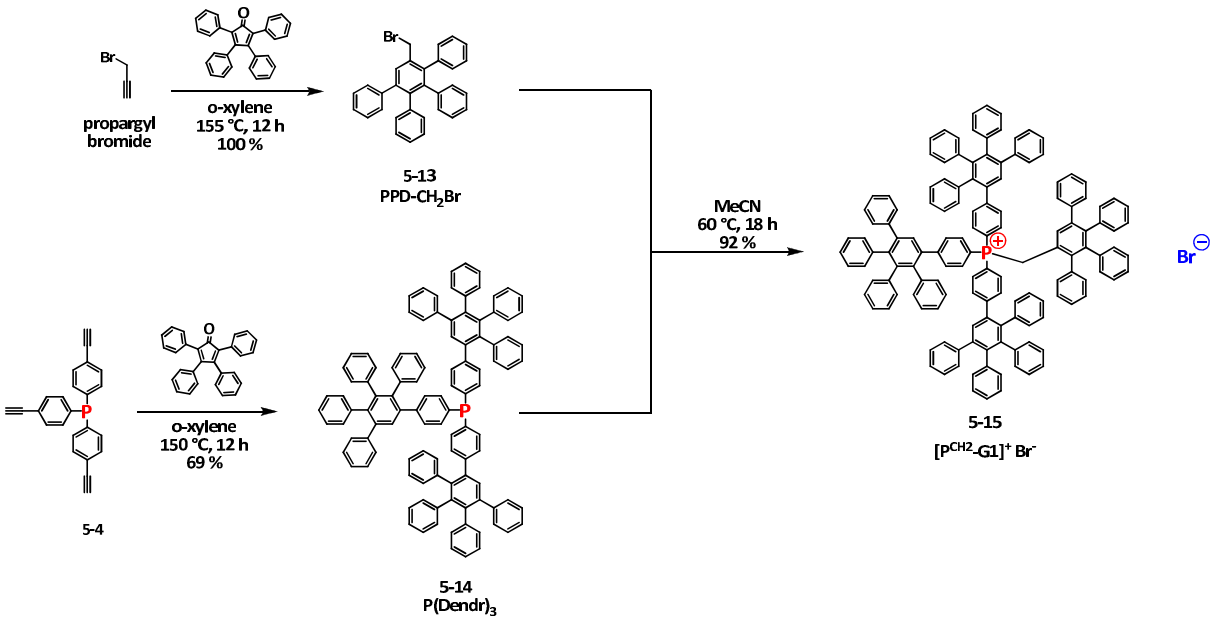

Figure 5-3: Synthesis route to first generation benzylphosphonium bromide **5-15** (**[P^{CH2}-G1]$^+$ Br$^-$**) employing a convergent preparation method.

By way of the above shown reaction pathway, the sterically congested benzylphosphonium salt **5-6** is accessible, which raises the question about the chemical reactivity of the α-methylene group. By treatment with base, benzylphosphonium cations are typically known to form benzylidenephosphoranes of general formula **L_3P=CHR'**, which exists in a tautomeric equilibrium with the corresponding zwitterionic phosphorus ylide **$(L_3P)^+$-$(CHR')^-$**. The relative reactivity and stereoselectivity in the Wittig reaction due to the presence of unprecedentedly large polyphenylene dendrons is the subject of research in the following section. In order to investigate more comprehensively the effect of the ylide nature, the series of benzylphosphonium bromides was expanded by use of the synthesis protocol according to the reaction scheme in **Figure 5-4**. Therefore, triphenylbenzylphosphonium bromide **5-16** and tris(n-butyl)benzylphosphonium bromide **5-17** were prepared:

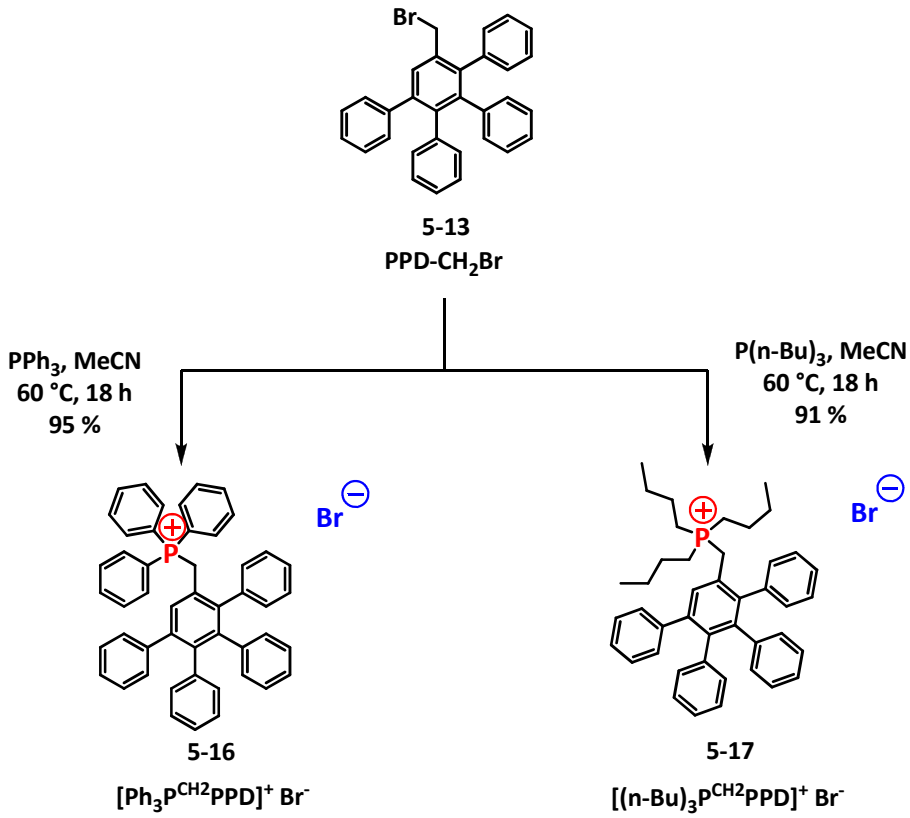

Figure 5-4: Synthetic scheme towards benzylphosphonium bromides **5-16** (**[Ph_3P^{CH2}PPD]$^+$ Br**) and **5-17** (**[$(n\text{-}Bu_3)P^{CH2}$PPD]$^+$ Br^-**).

Whereas **5-16** produces the semi-stabilized ylide **5-19** upon treatment with base, the benzylphosphonium bromide **5-17** results in the formation of ylide **5-20**. A complete survey of the obtained ylides and the investigation of the subsequent Wittig reactions with different aldehydes will be covered in more detail in the next section. But before that, the crystal structures of **5-16** and **5-17** are depicted to assess the spatial assembly of the ligands at the phosphorus and the bulky polyphenylene moiety. This becomes of particular interest, since the stereoselectivity of the Wittig reaction is reported to be strongly dependent on the size, angles, and geometry of the phosphorus ylide.

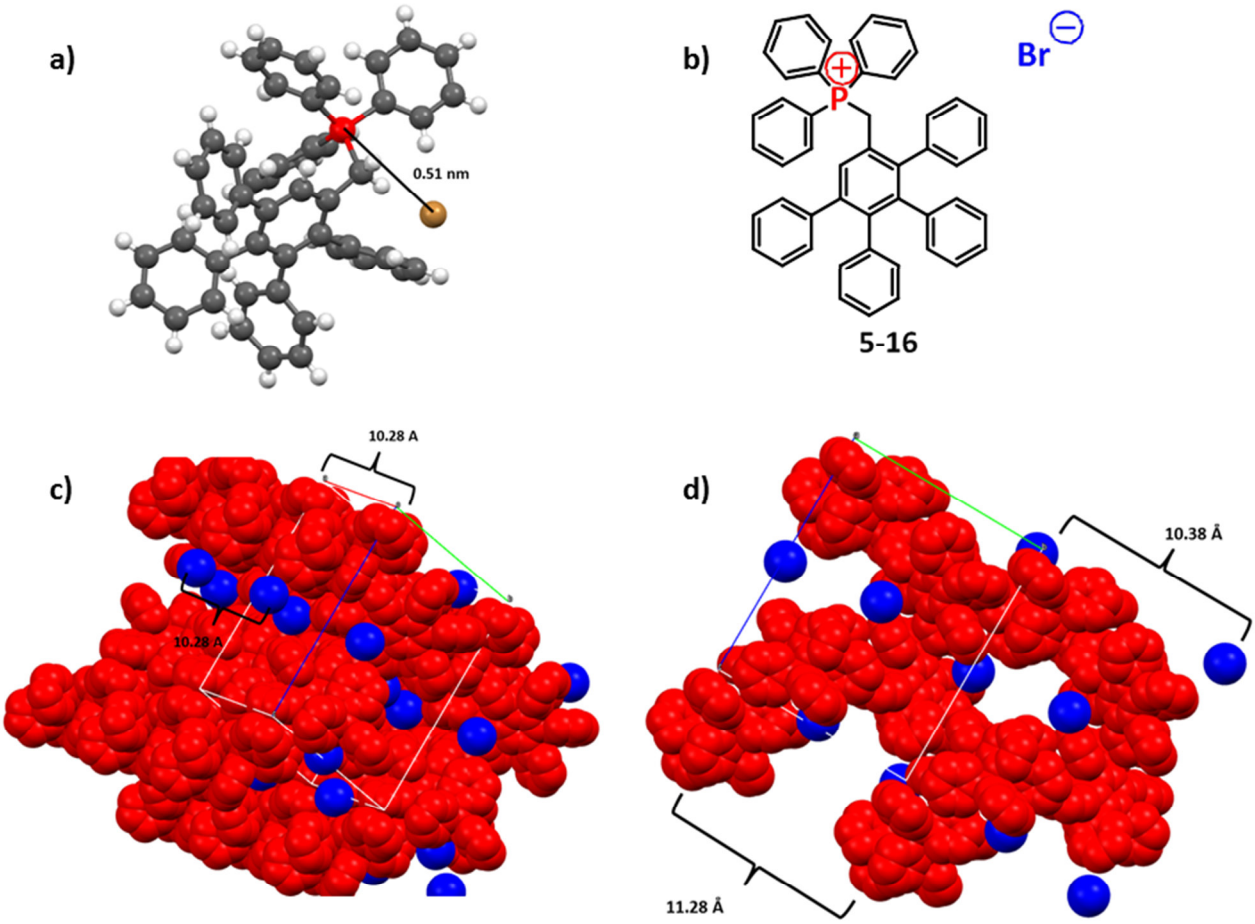

Figure 5-5: Single crystal structure of benzylphosphonium bromide **5-16** (a); (b) 2D-formula structure; (c) crystal lattice packing with cations in red, anions in blue; (d) view along the b-axis.

Single crystals of **5-16** **$[Ph_3P^{CH2}PPD]^+$ Br^-** were obtained by slow evaporation of a concentrated solution (in a 5:1 mixture of DCM/hexane) in a sealed glass vial. X-ray diffraction analysis revealed that the phosphonium cations arrayed in staggered columns with the closest cation-cation distance of 10.28 Å (see **Figure 5-5**). The charge-compensating bromide-anions aligned in the void places of the cation lattice and their closest distance to the cation was determined to 5.1 Å (0.51 nm). The closest anion-anion spacing was found to be 10.28 Å, so identical to the cations.

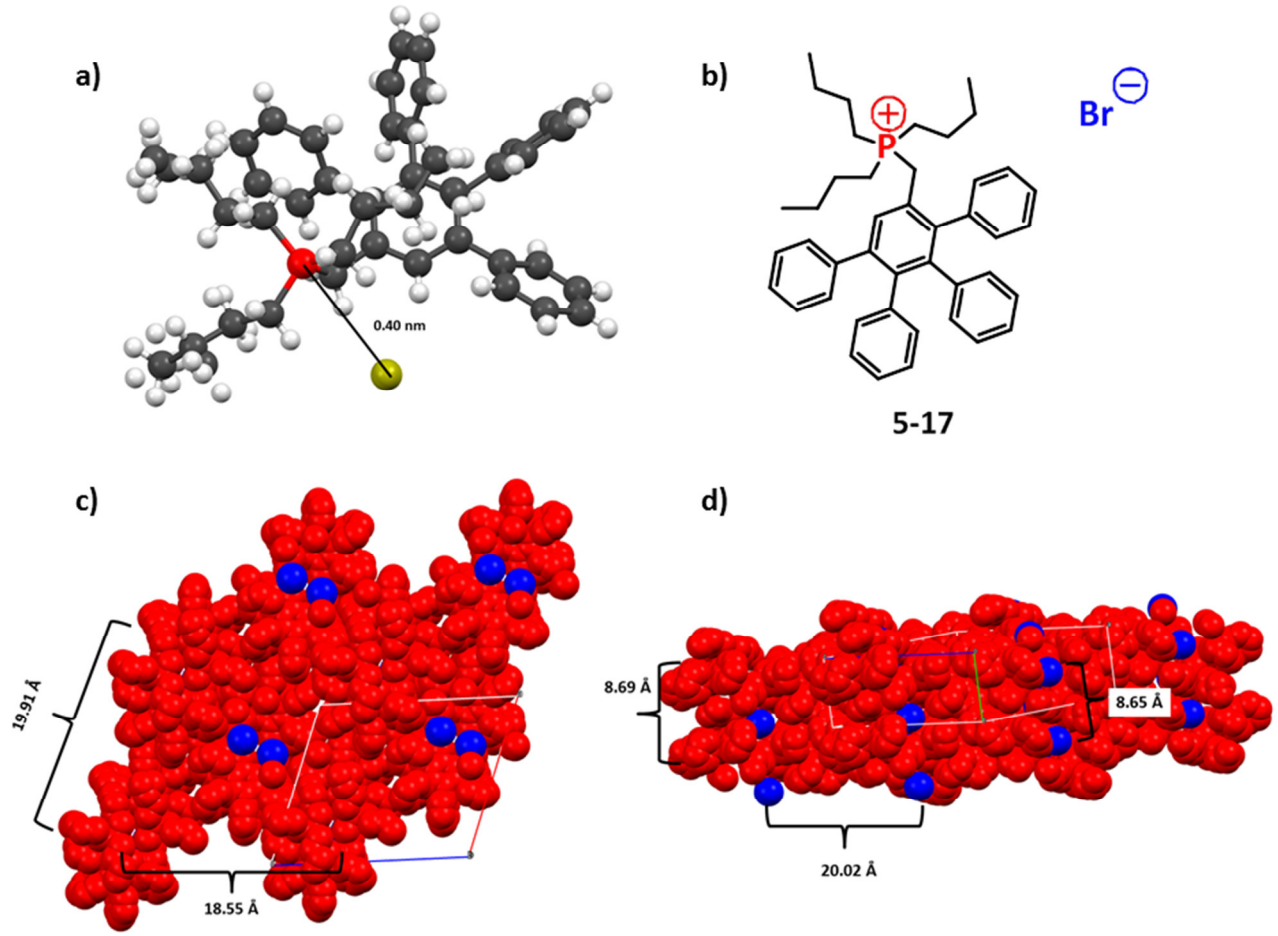

Figure 5-6: Single crystal structure of benzylphosphonium bromide **5-17** (a); (b) 2D-formula structure; (c) crystal lattice packing with cations in red, anions in blue; (d) view along the b-axis.

Single crystals of **5-17** **$[(n\text{-}Bu_3)P^{CH_2}PPD]^+$ Br^-** were obtained by slow evaporation of a concentrated solution (in a 5:1 mixture of DCM/hexane plus addition of small amounts of Na_2CO_3 to promote crystallization) in a sealed glass vial. X-ray diffraction analysis revealed that the phosphonium cations likewise arrayed in staggered columns with closest cation-cation distances of 8.69 Å (see **Figure 5-6**). The intercolumnar distances were determined to be 18.55 Å and 19.91 Å respectively. The bromides are spatially separated by 8.65 Å and located in the cation lattice voids. The intercolumnar distance of the anions was determined to be 20.02 Å (see **Figure 5-6**).

5.4 Wittig Reaction of Dendronized Benzylphosphonium Salts

The focus of this chapter is on the application of dendronized benzylphosphonium salts as Wittig reagents, bearing bulky substituents of unprecedented size in the α-position to the phosphorus. Since its introduction about 60 years ago,[7], [8] the Wittig reaction has become of particular interest with regard to the stereochemistry of the initial adduct formation and the resultant (*E/Z*) olefin ratio.[9], [10] A variety of factors including temperature, solvent, choice of the carbonyl reagent, the type of ylide as well as the presence and concentration of lithium salts were demonstrated to influence the resulting (*E/Z*) alkene ratio.[11], [12] Detailed mechanistic studies by Vedejs et al.[13] investigated the role of substituents at phosphorus ylids and attributed the relevant stereochemistry to a kinetically controlled formation of *cis*- or *trans*-oxaphosphetanes. However, among the substituent effect reported so far, the group R' in the α -position of the ylide (**Figure 5-7**) was mostly limited to a simple CH_3-moiety or slightly larger alkyl homologues. Hence, we considered dendronization as a valuable tool for the introduction of an unprecedented large and rigid polyphenylene substituent at the phosphonium component. By employing this approach, novel alkenes with markedly large substituents became accessible.

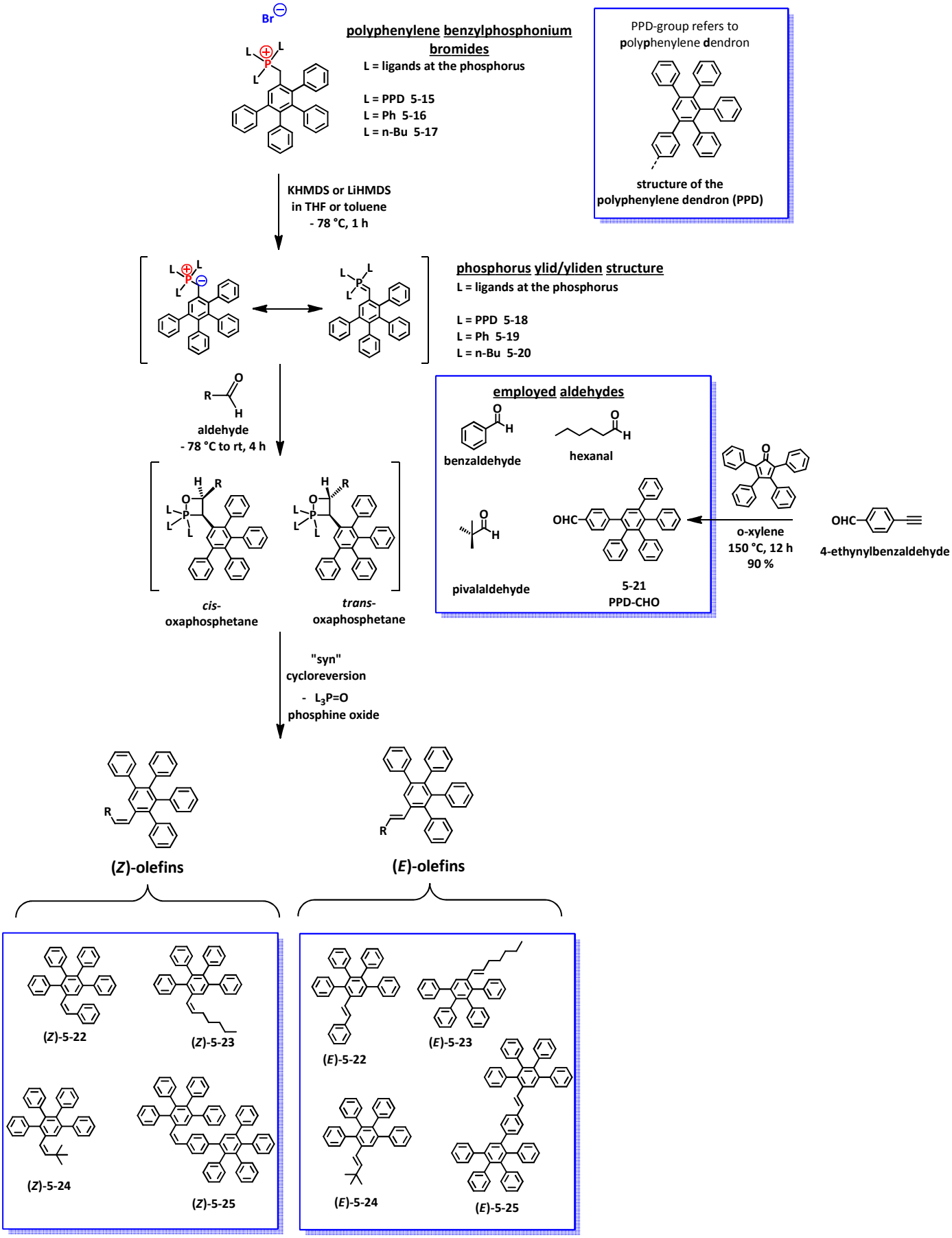

Figure 5-7: Reaction conditions, intermediates and final products of the Wittig reaction between benzylphosphonium bromides **5-15** to **5-17** and aldehydes R-CHO.

The stereochemistry of the Wittig olefination in the presence of bulky α-substituents was investigated. Therefore, the formation of a **semi-stabilized ylides Ph_3P=CH-PP** (**5-19**), **(n-Bu_3)P=CH-PP** (**5-20**) and **sterically shielded ylide $(PPD)_3$P=CH-PP** (**5-18**) was initiated by treatment of the according benzylphosphonium bromide with potassium hexamethyldisilazide (KHMDS, salt-free conditions) and LiHMDS (lithium halide present) as bases at -78 °C (THF or toluene). After addition of aldehydes (benzaldehyde, hexanal, pivalaldehyde and polyphenylene benzaldehyde derivative **5-21 PPD-CHO)** to the ylide suspensions, the (*E/Z*) ratio of the obtained alkenes was determined via the coupling constant of the two vinylic protons (reaction conditions see **Figure 5-7**, results see **Table 5-1**). Typical $^3J_{HH}$-values for the (*E*)-olefins were observed to be 16 – 17 Hz and 11 - 12.5 Hz for the (*Z*)-olefins, which is in agreement with experimental data of unsymmetrical substituted stilbenes.[14]

Table 5-1: Results of the Wittig reactions[a] according to the scheme in **Figure 5-7**

entry	phosphonium ylide L_3P=CHPP	base	solvent	aldehyde	(E/Z)-ratio	Literature reported (E/Z) ratio for R' = CH_3	isolated yield[b], %
			Semi-stabilized Ylide, Ph_3P=CH-PP 5-19				
1	L = Ph	LiHMDS	THF	PhCHO	1/99	17/83 [10a]	84
2	L = Ph	LiHMDS	toluene	PhCHO	1/99		82
3	L = Ph	KHMDS	THF	PhCHO	1/99	8/92 [13]	63
4	L = Ph	LiHMDS	THF	n-C_5H_{11}CHO	50/50	14/86 [10a]	78
5	L = Ph	KHMDS	THF	n-C_5H_{11}CHO	40/60	6/94 [10a]	61
6	L = Ph	LiHMDS	THF	$(CH_3)_3$CCHO	37/63		82
7	L = Ph	LiHMDS	toluene	$(CH_3)_3$CCHO	41/59		80
8	L = Ph	KHMDS	THF	$(CH_3)_3$CCHO	n.d.	1/99 [10a]	0[c]
9	L = Ph	LiHMDS	THF	PPD-CHO	1/99		74
10	L = Ph	LiHMDS	toluene	PPD-CHO	1/99		70
11	L = Ph	KHMDS	THF	PPD-CHO	1/99		59
			Semi-stabilized Ylide, n-Bu_3P=CH-PP 5-20				
12	L = n-Bu	LiHMDS	THF	PhCHO	1/99		88
13	L = n-Bu	LiHMDS	toluene	PhCHO	1/99		84
14	L = n-Bu	KHMDS	THF	PhCHO	1/99	83/17 [10a]	76
15	L = n-Bu	LiHMDS	THF	n-C_5H_{11}CHO	72/28		83
16	L = n-Bu	KHMDS	THF	n-C_5H_{11}CHO	85/15	67/33 [10a]	71
17	L = n-Bu	LiHMDS	THF	$(CH_3)_3$CCHO	81/19		69
18	L = n-Bu	KHMDS	THF	$(CH_3)_3$CCHO	71/29	90/10 [10a]	64
19	L = n-Bu	LiHMDS	THF	PPD-CHO	1/99		86
20	L = n-Bu	LiHMDS	toluene	PPD-CHO	1/99		76
21	L = n-Bu	KHMDS	THF	PPD-CHO	1/99		59
			Sterically Shielded Ylide, PPD_3P=CH-PP 5-18				
22	L = PPD	LiHMDS	THF	PhCHO	1/99		62
23	L = PPD	LiHMDS	THF	n-C_5H_{11}CHO	52/48		55

[a] Exact reaction procedure is described in the **Experimental Part**. [b] After purification and isolation via column chromatography. [c] Product **5-26** was isolated in 86 % yield (structure see in the reaction scheme in Figure **5-9**). [d] polyphenylene aldehyde **5-21** (**PPD-CHO**) was synthesized to incorporate an uncommonly large substituent at the aldehyde (**Figure 5-7**). [e] Given that Me-groups in the α-position were not found in the literature, the shortest primary alkyl-chain analog was selected.

PP-group refers to bulky **poly**phenylene moiety

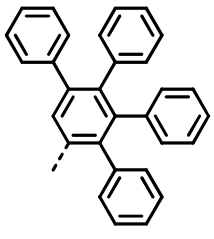

In salt-free Wittig reactions, non-stabilized ylides usually react with aldehydes to yield preferably (*Z*)-alkenes.[10a] The results within this work revealed the exclusive formation of (*Z*)-olefins when aromatic aldehydes (benzaldehyde and **PPD-CHO 5-21**) were reacted with all type of semi-stabilized ylides **L_3P=CH-PP** (**5-18** to **5-20**). Even the presence of Li^+ cations (c = 0.05 M) and the use of nonpolar toluene as solvent did not affect the (*Z*)-selectivity (see entries 1-3 and 9-11 in **Table 5-1**).

Stabilized ylides, however, are generally known to result in the preferential formation of (*E*)-alkenes.[10a], [13a] The Wittig reaction of semi-stabilized ylide **n-Bu_3P=CH-PP (5-20)** with hexanal and pivaldehyde likewise predominantly yielded (*E*)-alkenes **5-23** and **5-24** (see entries 15–18 in **Table 5-1**), however upon reacting with benzaldehyde and **PPD-CHO 5-21**, exclusively (Z)-stilbenes **5-22** and **5-25** were obtained.

It is known that *cis*- or *trans*-disubstituted oxaphosphetanes represent the initially formed intermediates for the reaction between phosphorus ylides and aldehydes.[13a] The *cis*/*trans* ratio depends on the size and spatial arrangement of the substituents at the phosphorus. Inspired by the non-planar cycloaddition mechanism proposed by Vedejs et al.,[13b] we suggested the most likely transition state geometries in **Figure 5-8**.

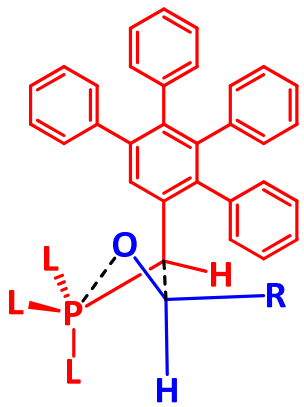

***cis*-oxaphosphetane transition state**

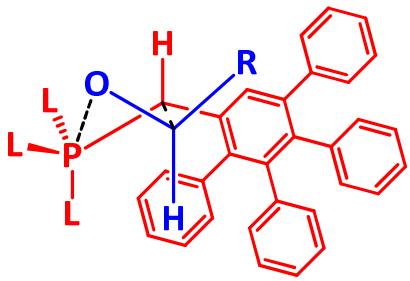

***trans*-oxaphosphetane transition state**

Figure 5-8: Proposed transition state geometries for Wittig reactions between polyphenylene-ylides (**5-18** to **5-20**, red) and aldehyde RCHO (blue).

The bulky polyphenylene dendron in pseudo-axial orientation experiences minimal repulsion from the ligands on the phosphorus center by rotation of the PPD-C_α axis. Thus, two possible configurations for the incoming aldehyde are reasonable. For the *cis*-configuration, the group R aligns in a pseudo-equatorial position in order to minimize destabilizing steric repulsion from the bulky PP-moiety. For the case of trans-orientation, however, the aldehyde substituent R encounters even more unfavorable steric interaction with the PPD-moiety, since both large groups are arranged in the equatorial plane. Hence, this rationalization explains the increased degree of *Z*-selectivity for all olefins formed during the experiments in the presence of bulky substituents at α-position compared to literature-known ylids with smaller groups.

Nevertheless, there is still a matter of ambiguity regarding the performed Wittig reactions within this work. It was observed that the yields of the resulting olefins were generally lower when KHMDS was employed as base rather than LiHMDS. This was attributed to the formation of product **5-26** ($C_{31}H_{24}$, toluene derivative) and **5-27** ($C_{62}H_{44}$, symmetrical stilbene with bulky polyphenylene substituents), which were detected by means of FD-mass (m/z 396.5 and 788.7 respectively). **5-26** could even be isolated via column chromatography. For that purpose a suspension of **5-16** in THF reacting with KHMDS (1 eq) for 5 hours at room temperature provided compound **5-26** in 70 % isolated yield (of course no aldehyde component was added). At the moment it is not fully clear how to answer the arising question what was the reason therefore. Most likely the presence of the weaker coordinating potassium cation K^+ (compared to the oxophilic lithium cation Li^+) exerts its influence on the ylide stability and promotes an alternative degradation pathway to **5-26**. It can be assumed that hexamethyldisilazide anion is less coordinated by use of KHMDS rather than LiHMDS and therefore more reactive. Furthermore, if one considers the present phosphonium halides **$[L_3P\text{-}CH_2\text{-}PP]^+$ Br^-**, it becomes apparent that there exist two possible sites where the anion **$N\{Si(CH_3)_3\}^-$** might attack: most likely the α-hydrogens of the benzyl group, whose acidity is enhanced by the adjacent positive charge. But literature reports also clearly point out the direct attack of alkoxides[15] and organolithium reagents[16] at the phosphorus atom itself followed by a release of a hydrocarbon leaving group (e.g. toluenes for benzylphosphonium salts). Thus, a plausible mechanism to explain the formation of toluene derivative **5-26** is described, nevertheless it is not clear whether this assumption accounts for the experiments during this work.

Also the formation of admittedly small quantities of symmetrically substituted stilbene derivative **5-27** could be detected for some experiments performed within the present studies (e.g. entry 11 and 21 in **Table 5-1**). The search for a valuable explanation therefore is most likely based on transylidation reactions[17] and/or rapid dimerization equilibria.[18] The importance of a sophisticated choice of the base for the Wittig reactions within this thesis is best illustrated by the reaction between phosphonium salt **5-16** $\mathbf{[Ph_3P^{CH2}PPD]^+\ Br^-}$ with pivaldehyde (compare entry 6 and 8 from **Table 5-1**). The use of LiHMDS leads to the formation of the expected olefin **5-24** (*E/Z* ratio 37/63) in 82 % yield and about 10 % toluene side product **5-26** could be isolated. However, the employment of KHMDS as base did not result in the formation of any alkene product (the reaction was performed three times), but instead of that about 70 % **5-26** and 20 % stilbene **5-27** could be obtained after column chromatography. Current investigations focus on preventing the formation of any undesired side product and shall help to clarify the mechanism of their emergence.

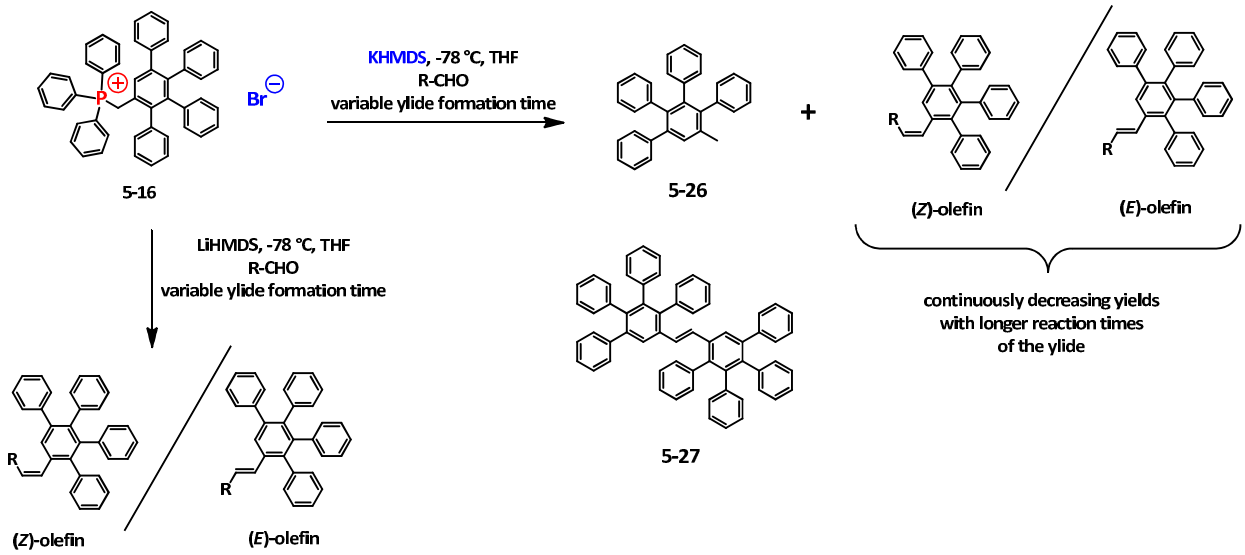

Figure 5-9: Experimentally observed degradation pathways of ylide **5-19** yielding toluene derivative **5-26** and symmetrically substituted stilbene **5-27** in dependence of the reaction conditions (LiHMDS or KHMDS as base).

5.5 Synthesis of Dendronized Methylphosphonium Iodide (5-28)

During this work various methods and reaction conditions for the quarternization of phosphines (PR_3) were carried out (diazonium salts, transition metal catalyzed couplings of aryl halides, SN_2-reactions of benzyl halides). A very popular method for the preparation of methylphosphonium salts has been studied by Kusabayashi et al.[19] by reacting iodomethane (CH_3I) with triphenylphosphine in different solvents. Following this procedure it was apparent to prepare first-generation methylphosphonium salt **5-28** by reacting bulky phosphine **5-14** with CH_3I under mild reaction conditions (see reaction scheme in **Figure 5-10**). The pure methylphosphonium iodide **5-28** is obtained by simple precipitation of the crude reaction mixture in cold hexane and filtration.

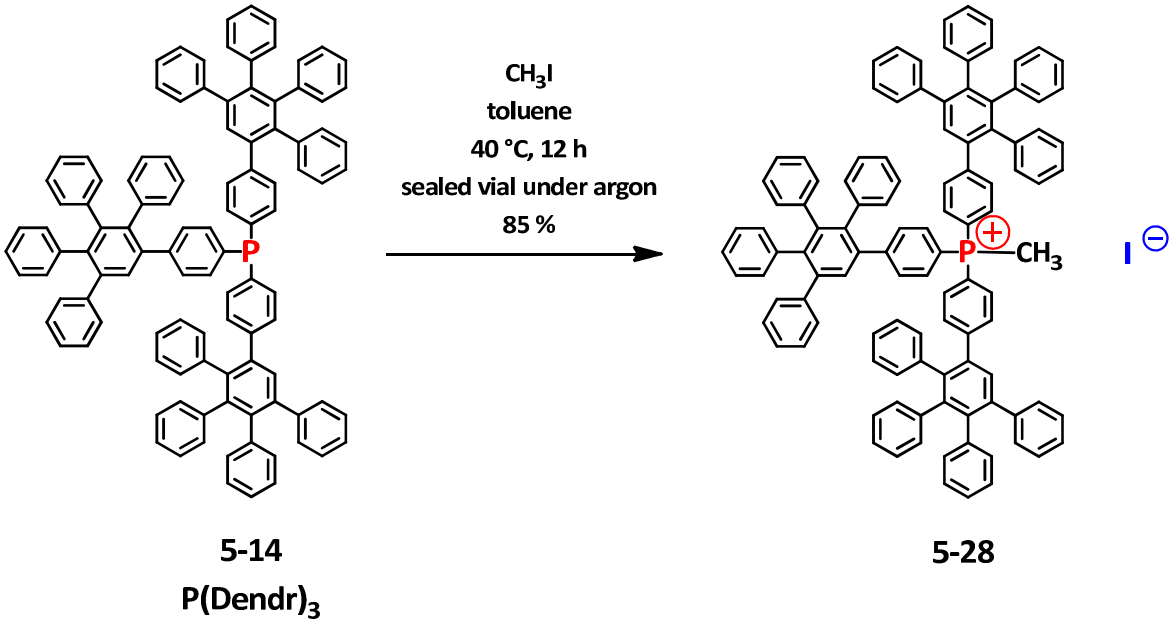

Figure 5-10: Methylation of first-generation phosphine **5-14** via iodomethane yielded methylphosphonium iodide **5-28**.

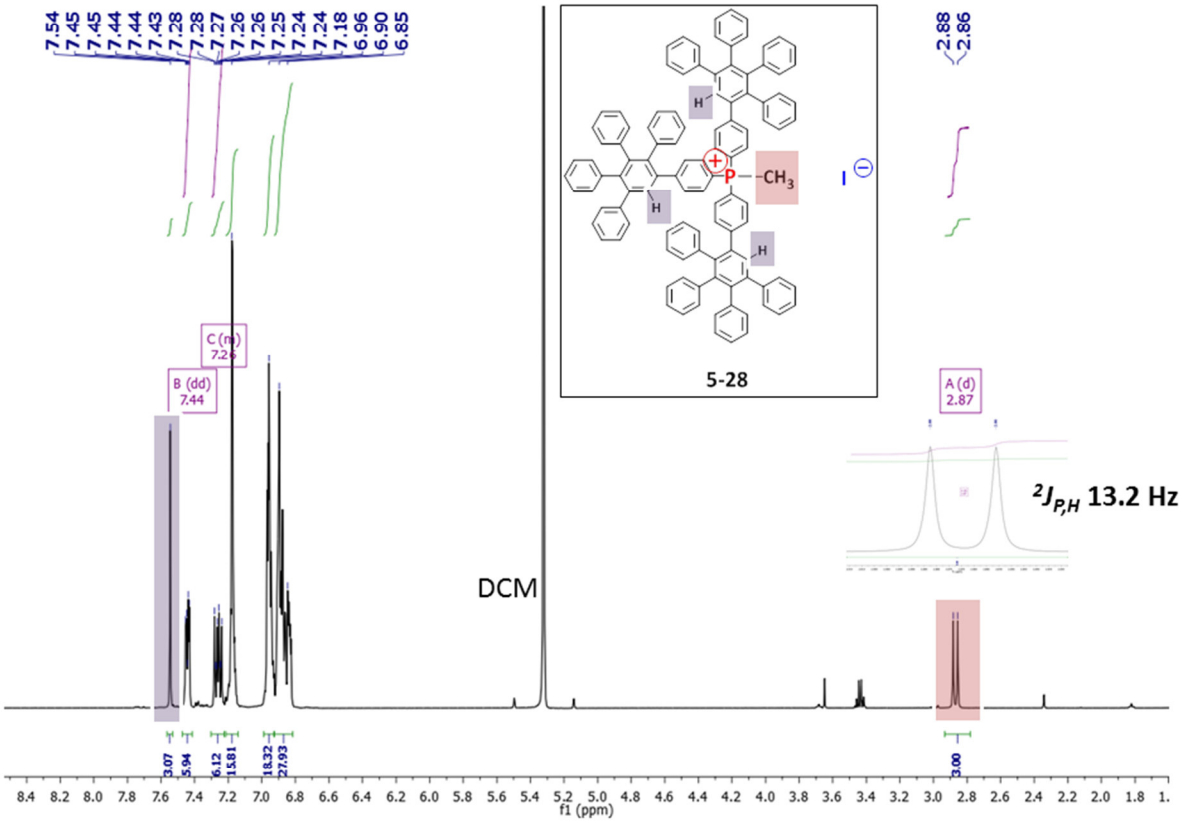

Figure 5-11: ^{1}H-NMR spectrum of methylphosphonium iodide **5-28** after recrystallization from DCM/EtOAc.

The geminal heteronuclear spin-spin coupling between ^{31}P and ^{1}H ($^2J_{PH}$ 13.2 Hz) becomes obvious from the ^{1}H-NMR spectrum of **5-28** (**Figure 5-11**) and has also been determined for the characteristic methylene-groups for the benzylphosphonium salts from the previous chapter (see **Experimental Part**). The values of the coupling constants are in agreement with literature reports.[20]

Methylphosphonium iodide **5-28** could be grown into large, cubic crystals of up to 0.5 cm length, which were suitable for structure elucidation by means of X-ray diffraction (see **Figure 5-12**). The closest cation – anion distance could hence be determined to 0.46 nm.

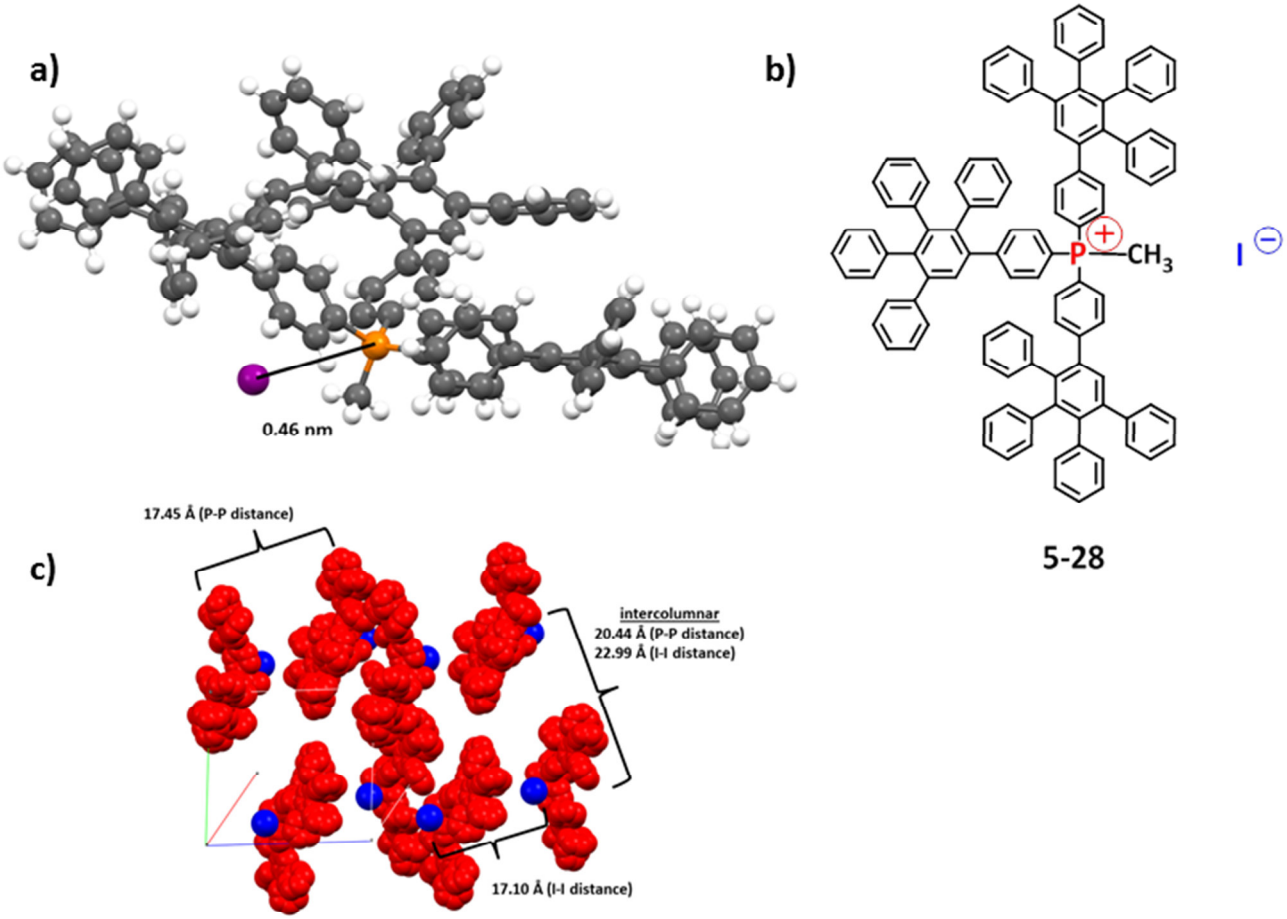

Figure 5-12: (a) Single crystal structure of methylphosphonium iodide **5-28**; (b) 2D-formula structure; (c) crystal lattice packing with cations in red, anions in blue; (d) view along the b-axis.

The methylphosphonium cation forms a bowl-shaped trigonal pyramid with the methyl group in the apical position.

We recognized the potential of phosphonium iodide **5-28** for further chemical transformations, more particularly C-alkylation, to extend the structural variety of dendronized phosphonium salts. Thus it was possible to synthetically introduce two benzyl

groups in the α-position as shown by the preparation of **5-29**. Also the functionalization with an electron-poor pentafluorophenyl group has been achieved as the formation of perfluoro-benzylphosphonium iodide **5-30** certifies.

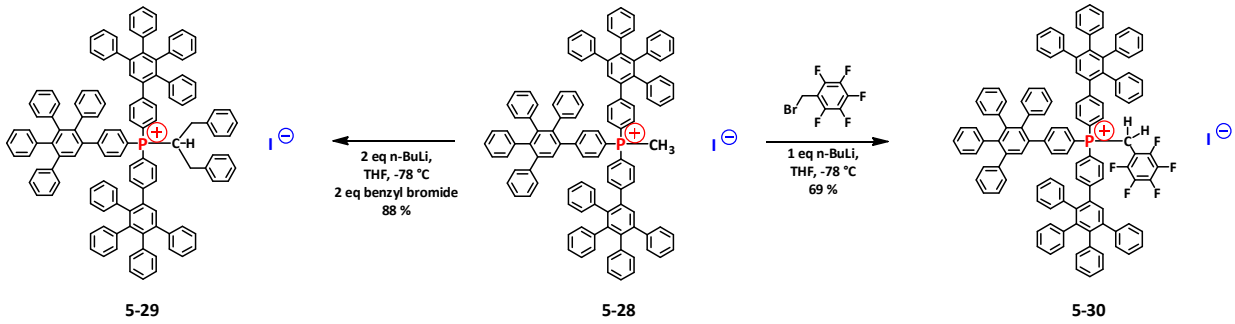

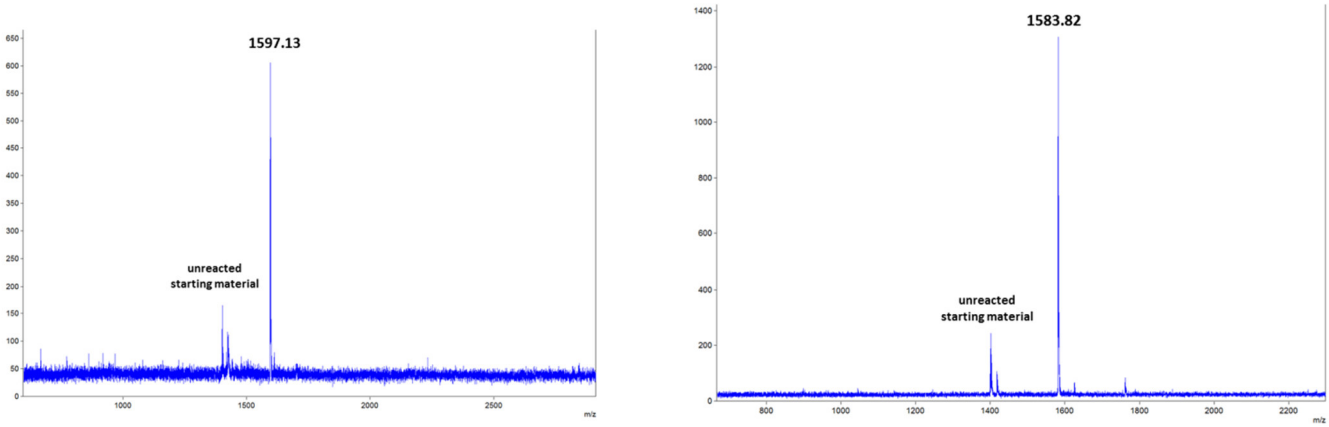

Figure 5-13: Reaction scheme towards benzylphosphonium ylids **5-29** and **5-30**. bottom: MALDI-TOF spectrum of the obtained phosphonium salts.

5.6 Synthesis of Oligo-cationic Phosphonium Salts

The route towards sterically congested benzylphosphonium salts was successfully committed by means of divergent and convergent dendritic growth. Both synthetic approaches resulted in the formation of first-generation phosphonium-polyphenylene dendrimers, which were accessible under mild reaction conditions. The crucial building block herein was the implementation of the sterically crowded phosphane **5-14** ($PDendr_3$). A promising deployment of the latter involves its use as nucleophilic reagent in order to construct a precise polyphenylene architecture with a defined number of charges. First experiments in that direction were performed to prepare the bis-phosphonium dibromide **5-31** and the tris-phosphonium tribromide **5-32** (see **Figure 5-14**), however there is no proof of their complete quarternization, yet. ^{31}P-NMR measurements suggested the desired conversion of bulky phosphane (used in stoichiometric excess) to the benzylphosphonium group (the initial single peak at δ - 8.75 disappeared and a set of peaks in the region between 21.82 and 21.52 attributable to PR_4^+ species was detected in the ^{31}P-NMR spectrum of **5-31** and **5-32**, see **Figure 5-15** and **Figure 5-16**). The reason for the incomplete quarternization reactions is presumably attributed to a steric overcrowding of the large polyphenylene dendrons, since the electron density at the nucleophilic phosphorus atom in **5-14** is not substantially altered compared to spatially less demanding PPh_3.[21] This was evaluated by theoretical calculations (B3LYP/6-31G(d,p) level) of the molecular electrostatic potential minimum (V_{min}) according to the method of *Koga et al*.[22]

In the literature there are several reports regarding the complete reaction between PPh_3 and a,a'-dibromo-p-xylene towards a di-cation with varying reaction conditions (DMF, 4 h, room temperature, 98 % yield[23] ; DMF, 12 h, 160 °C, 50 % yield[24]). In order to establish a successful route towards **5-31** and **5-32** (**Figure 5-14**) it is according to the many reports advisable to elevate the reaction temperature to 160 °C and switch to DMF as solvent. Furthermore, the use of silver-(I)-salts (e.g. silver carbonate) is suggested to activate the benzylbromo-moiety similar to the carbohydrate chemistry in the Koenigs-Knorr reaction.[25]

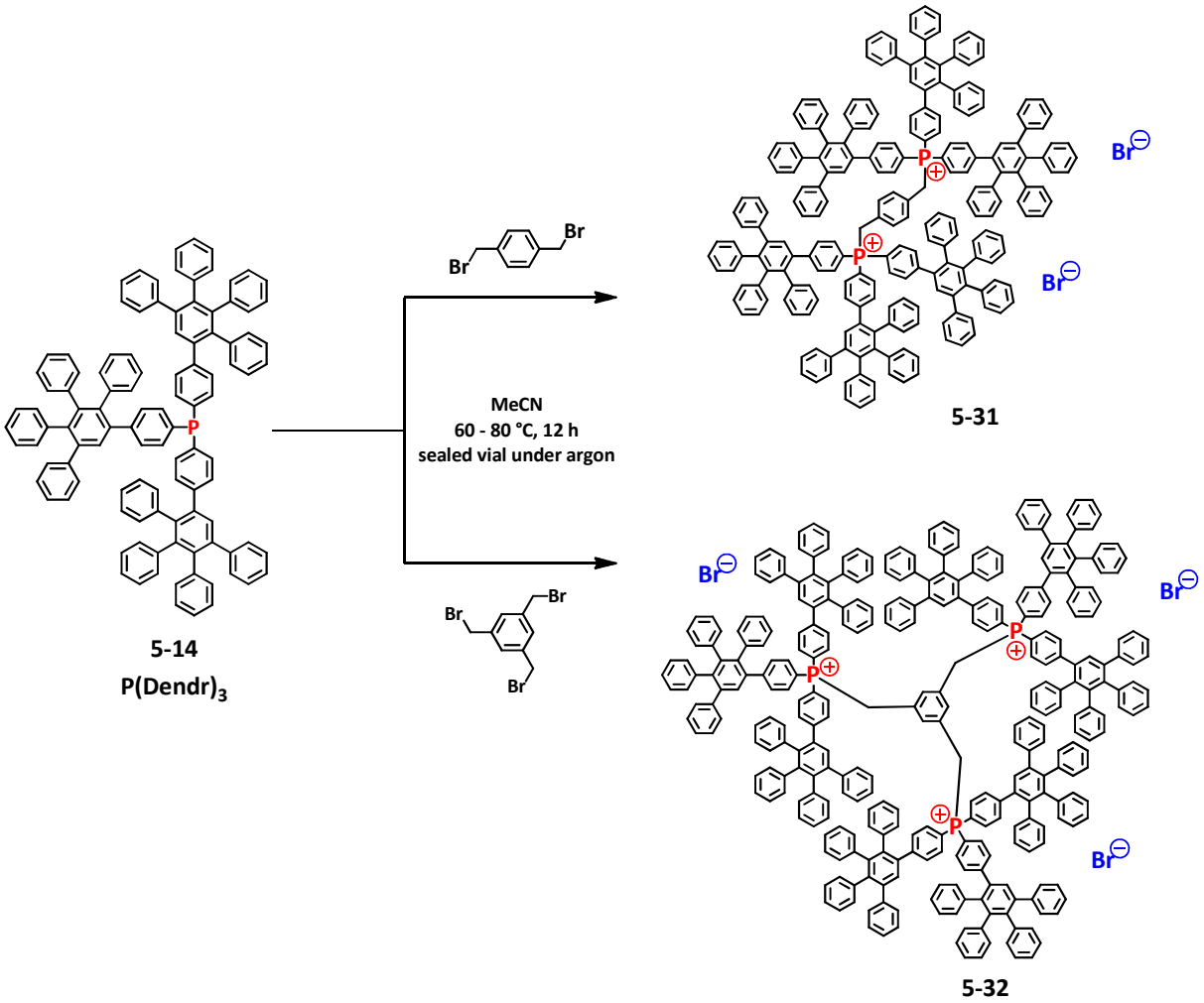

Figure 5-14: Synthesis scheme towards bis-phosphonium dibromide **5-31** and tris-phosphonium tribromide **5-32**.

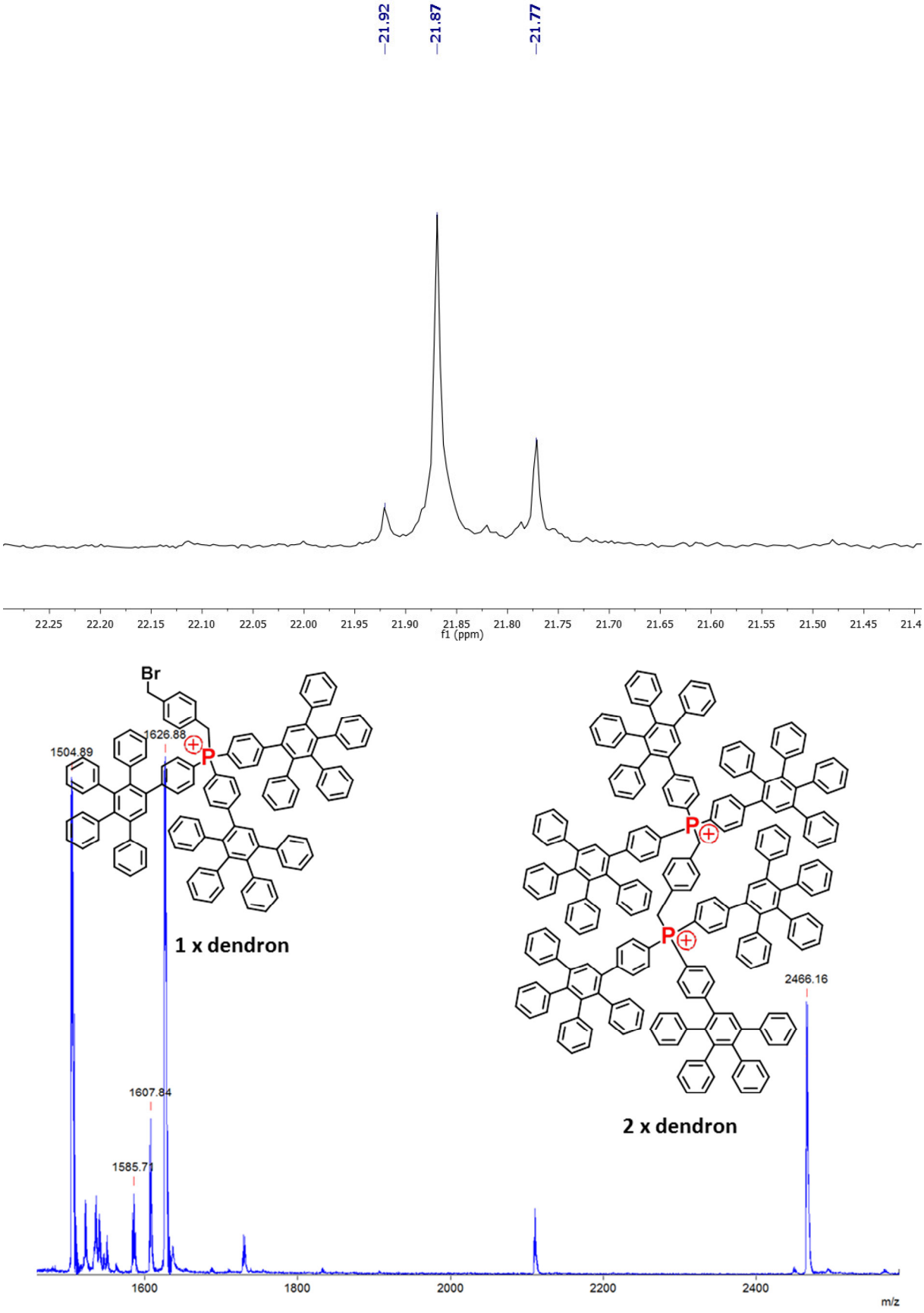

Figure 5-15: ^{31}P-NMR spectrum of bis-phosphonium dibromide **5-31**. (bottom): MALDI-TOF mass spectrum of **5-31**.

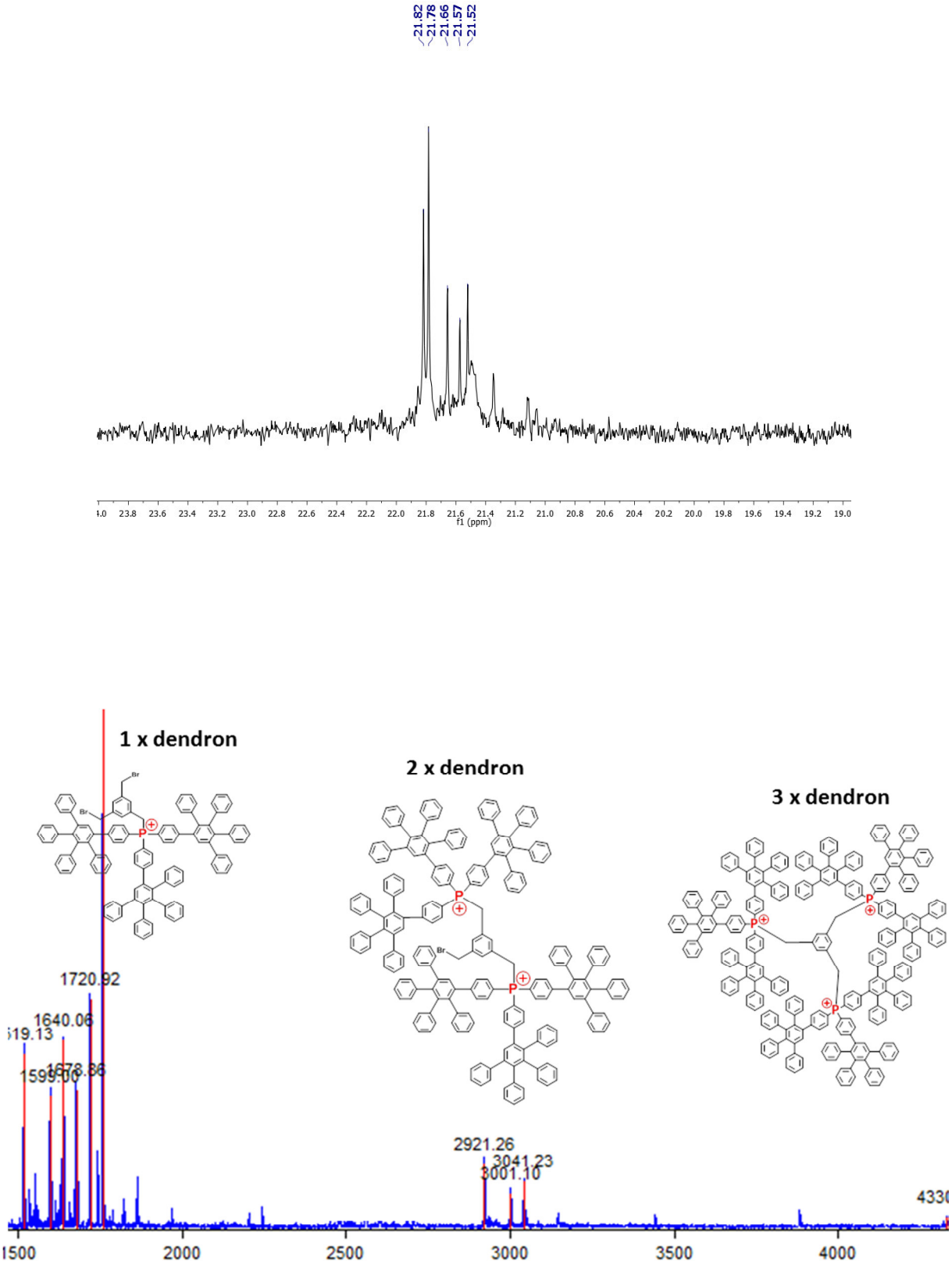

Figure 5-16: ^{31}P-NMR spectrum of tris-phosphonium dibromide **5-32**. (bottom): MALDI-TOF mass spectrum of **5-32**.

5.7 Discussion and Outlook

A promising subject of future research is the structural optimization of first-generation phosphine **5-14**. This becomes particularly evident by recent literature reports, where bulky and rigid phosphine ligands are applied for the synthesis of five-membered heterocycles by means of palladium-catalyzed amidation.[26] Also electron-rich, large phosphine ligands are employed to facilitate the preparation of diaryl ethers.[27] It has been postulated that Pd^{II}-catalyst inhibition is prevented and the reductive elimination step is accelerated due to the enhanced rigidity and screening around the active palladium-(II) center. Furthermore, functionalized phosphines bearing sterically encumbering substituents have a profound impact of low-coordinated chemistry of phosphorus. For instance, the employment of 2,4,6-Me_3-C_6H_2 (mesityl, Mes) and 2,4,6-^{t}Bu_3-C_6H_2 (supermesityl) permitted the isolation of stable phosphaalkenes[28] and diphosphenes.[29] Recent developments of more sophisticatedly designed bulky aryl substituents led to the isolable compounds of the heavier elements of the periodic table with low-coordination numbers.[30]

The versatile concept of dendronization can be utilized for an accurate design of phosphines displaying the demanded structural features. **Figure 5-15** illustrates schematically the conceivable modifications in terms of size (higher generation, degree of branching), accessibility of the nucleophilic phosphorus (e.g. by reacting an internal alkyne with a tetraphenylcyclopentadienone building block; by introduction of ortho- or meta-functionalities at the inner phenyl rings) and the optional site-specific introduction of various functional groups within the polyphenylene scaffold.

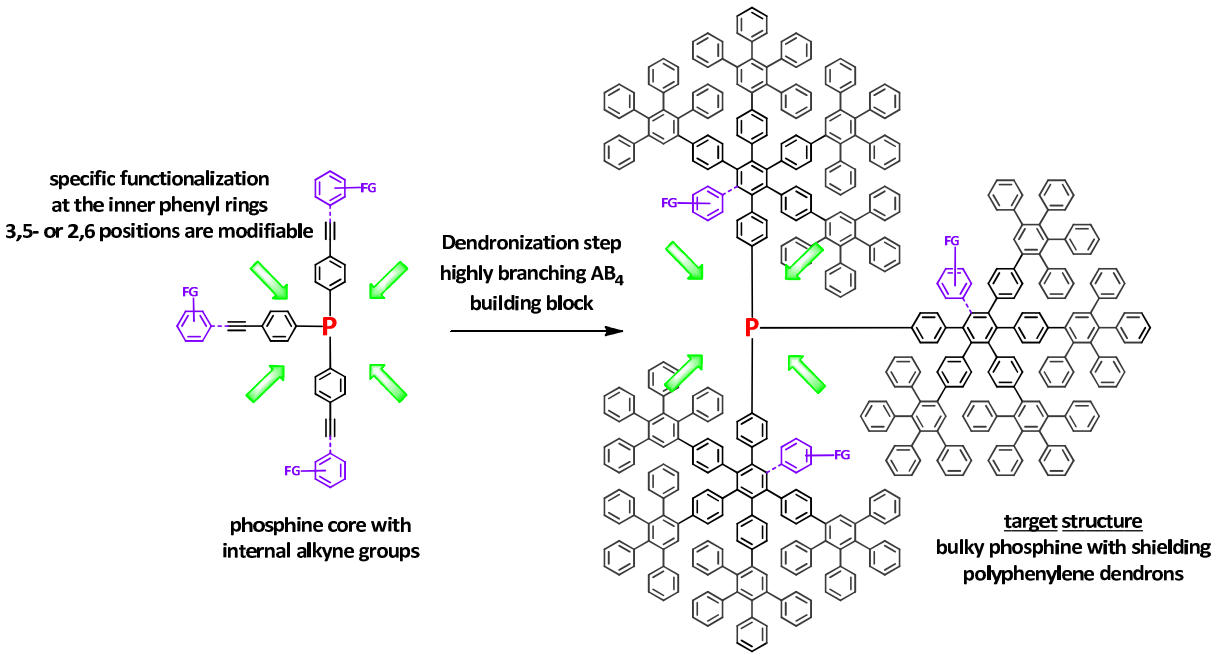

Figure 5-17: Schematic overview presenting the synthesis route towards a series of phosphines with unprecedented large aryl substituents.

Furthermore, it is of particular importance within this chapter that the formation of bulky stilbenes **5-22** and **5-25** occurred peculiarly in their *Z*-configuration regardless of the utilized phosphorus ylide (**Ph_3P=CH-PP** (**5-19**), **(n-Bu_3)P=CH-PP** (**5-20**) and **(PPD)$_3$P=CH-PP** (**5-18**)). According to the modern interpretation of the Wittig reaction mechanism,[31] this finding is rather surprising:

Supposed that all the ylides employed within these studies can be regarded as semi-stabilized, the experimentally observed selectivities for Wittig reactions reveal that the most (*Z*)-selective reactions proceed with bulky triarylphosphine-derived semi-stabilized ylides (like **Ph_3P=CH-PP** and **(PPD)$_3$P=CH-PP**), but trialkylphosphine-derived ylides (like **(n-Bu_3)P=CH-PP**) usually exhibit more pronounced (*E*)-selectivity. Furthermore, tertiary aldehydes are generally displaying highest (*Z*)-selectivity compared to primary and aromatic aldehydes upon reacting with a given semi-stabilized ylide. Since our results ensued the exclusive formation of (*Z*)-stilbenes for the Wittig reaction of benzaldehyde and bulky aromatic aldehyde (**PPD-CHO 5-21**) with any type of semi-stabilized ylide, the logical consequence would be the development of a **stabilized ylide 5-33** with a large carbon ester polyphenylene α-substituent (proposed synthetic route to **5-33** suggested in **Figure 5-18**).

Employing the latter in Wittig reactions and analyzing the stereochemical outcome of the products will provide a more detailed conclusion of the role of bulky substituents. This idea follows from the fact that stabilized ylides react through a late transition state with a puckered *trans*-configuration, which undergoes [2+2] cycloreversion to the respective (*E*)-alkene.[13b], [32]

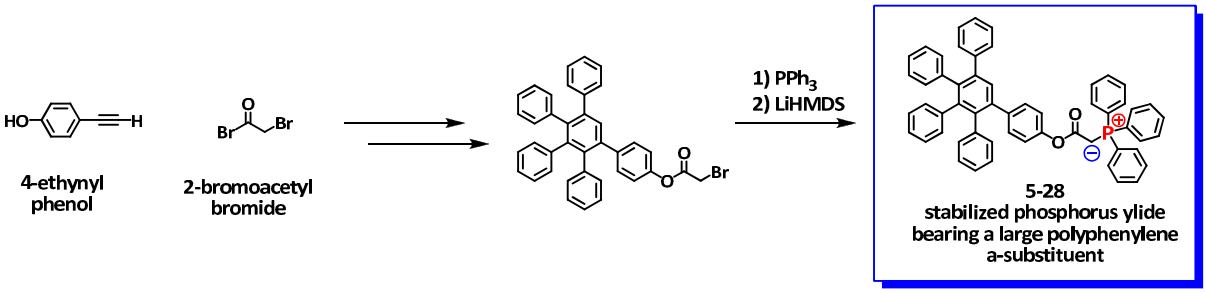

Figure 5-18: Proposed synthetic pathway towards the synthesis of the stabilized phosphorus ylide **5-33**.

Aside from the synthetic point of view the particular value of producing polyphenylene-based stilbene dendrimers is founded in their photoisomerization and fluorescence behavior.[33] It has been reported that the sterically shielding of a photoactive *cis*-stilbene site by use of rigid polyphenylene dendrons exhibited strong room temperature fluorescence (20 % quantum yield) and a long fluorescence life time (1.6 ns). Furthermore it has been observed for the first time that the dendronized *cis*-stilbene analogue showed a longer lifetime than its corresponding *trans*-isomer.[34]

The preparative versatility realized in the high-yielding Wittig reactions presented within this work substantially improved the former tedious synthesis of encapsulated stilbene-derivatives and moreover allows for a site-specific functionalization.

Literature

[1] for a general review of phosphines and phosphonium ions see: Trippett, S.; Allen, D. W.; "Phosphines and Phosphonium Salts", *Organophosphorus Chemistry*: Volume 8, **1977**, 8, 1-30.
[2] Kröhnke, F.; *Chem. Ber.* **1950**, 83, 291.
[3] Lidstroem, P.; Tierney, J.; Wathey, B.; Westman, J. "Microwave assisted organic synthesis – a review", *Tetrahedron* **2001**, 57, 9225-9283.
[4] Garegg, P. J.; Regberg, T.; Stawiński, J.; Strömberg, R.; *J. Chem. Soc., Perkin Trans. 2* **1987**, 271-274.
[5] Norris, J. F.; *American Chemical Journal* **1907**, 38, 627-642.
[6] Vedejs, E.; Marth, C. F.; *J. Am. Chem. Soc.* **1988**, 110 (12), 3948–3958.
[7] Wittig, G.; Geissler, G.; *Liebigs Ann. Chem.* **1953**, 580, 44.
[8] Wittig, G.; Schöllkopf, U.; *Chem. Ber.* **1954**, 87, 1318.
[9] For general reviews of the Wittig reaction, see: a) Gosney, I.; Rowley, A. G.; *Organophosphorus Reagents in Organic Synthesis*; Cadogan, J. I. G., Ed.; Academic Press: New York **1979**, 7-153; b) Schlosser, M.; *Top. Stereochem.* **1970**, 5, 1; c) Bestmann, H. J; *Pure Appl. Chem.* **1980**, 52, 771; d) Trippett, S.; *Quart. Rev.* **1963**, 17, 406; e) Trippett, S.; *Pure Appl. Chem.* **1964**, 9, 255; f) Maercker, A.; *Org. React.* **1965**, 14, 270; g) LeBigot, Y.; Delmas, M.; Gaset, A.; *Inf. Chim.* **1984**, 251, 123; h) Bergelson, L. D.; Shemyakin, M. M.; *Angew. Chem. Int. Ed. Engl.* **1964**, 3, 250; i) Bestmann, H. J.; *Pure Appl. Chem.* **1979**, 51, 515.
[10] a) Schlosser, M.; Schaub, B.; *J. Am. Chem. Soc.* **1982**, 104, 5821; b) Bestmann, H. J.; *Bull. Soc. Chim. Belg.* **1981**, 90, 519; c) Vedejs, E.; Meier, G. P.; Snoble, K. A. J.; *J. Am. Chem. Soc.* **1981**, 103, 2823; d) Olah, G. A.; Krishnamurthy, V. V.; *Ibid.* **1982**, 104, 3987; e) McEwen, W. E.; Beaver, B. D.; Cooney, J. V.; *Phosphorus Sulfur* **1985**, 25, 255.
[11] a) Vedejs, E.; Snoble, K. A. J.; Fuchs, P. L.; *J. Org. Chem.* **1973**, 38, 1178; b) Vedejs, E.; Fuchs, P. L.; *J. Am. Chem. Soc.* **1973**, 95, 822; c) Vedejs, E.; Snoble, K. A. J.; *J. Am. Chem. Soc.* **1973**, 96, 5778; d) Vedejs, E.; Marth, C.; *Tetrahedron Lett.* **1987**, 28, 3445; e) Vedejs, E.; Huang, W. F.; *J. Org. Chem.* **1984**, 49, 210.
[12] a) Maryanoff, B. E.; Reitz, A. B.; Duhl-Emswiller, B. A.; *J. Am. Chem. Soc.* **1985**, 107, 217-226; b) Maryanoff, B. E.; Reitz, A. B.; Mutter, M. S.; Inners, R. R.; Almond, H. R.; Whittle, R., R.; Olofson, R. A.; *J. Am. Chem. Soc.* **1986**, 108, 7664-7678; c) Reitz, A. B.; Nortey, S. O.; Jordan Jr., A. D.; Mutter, M. S.; Maryanoff, B. E.; *J. Org. Chem.* **1986**, 51, 3302-3308.
[13] a) Vedejs, E.; Marth, C. F.; Ruggeri, R.; *J. Am. Chem. Soc.* **1988**, 110, 3940-3948; b) Vedejs, E., Marth, C. F.; *J. Am. Chem. Soc*. **1988**, 110, 3948-3958.
[14] Kvaran, Á.; Konrádsson, E.; Evans, C.; Geirsson, J. K. F.; *Journal of Molecular Structure* **2000**, 553, 79 – 90.
[15] Grayson, M.; Keough, P. T.; *J. Am. Chem. Soc.* **1960**, 82 (15), 3919–3924.
[16] Seyferth, D.; Hughes, W. B.; Heeren, J. K.; *J. Am. Chem. Soc.* **1965**, 87 (13), 2847-2854.
[17] a) Bestmann, H. J.; *Chem. Ber.* **1962**, 95, 58; b) Bestmann, H. J.; Liberda, H. G.; Snyder, J. P.; *J. Am. Chem. Soc.* **1968**, 90 (11), 2963–2964.
[18] Bestmann, H. J.; Snyder, J. P.; *J. Am. Chem. Soc.* **1967**, 89 (15), 3936-3938.
[19] Kondo, Y.; Zanka, A.; Kusabayashi, S.; *J. Chem. Soc. Perkin Trans 2*, **1985**, 827.
[20] Manatt, S. L.; Juvinall, G. L.; Wagner, R. I.; Ellemann, D. D.; *J. Am. Chem. Soc.* **1966**, 88(12), 2689-2697.
[21] Iwasawa, T.; Komano, T.; Tajima, A.; Tokunaga, M.; Obora, Y.; Fujihara, T.; Tsuji, Y.; *Organometallics* **2006**, 25, 4665-4669.
[22] Suresh, C. H.; Koga, N.; *Inorg. Chem.* **2002**, 41, 1573-1578.

[23] Harrowven, D. C.; Nunn, M. I. T.; Fenwick, D. R.; *Tetrahedron Letters* **2002**, 43(41), 7345-7347.
[24]Ran, K.; Hui-Jun, Y.; Mi-Hye, Y.; Sung-Chul, S.; Soon-Ki, K.; Yun-Hi, K.; *Bulletin of the Korean Chemical Society* **2012**, 33, (2), 420-425.
[25] Koenigs, W.; Knorr, E.; *Chemische Berichte* **1901**, 34, , 957.
[26] Su, M.; Buchwald, S. L.; *Angew. Chemie Int. Ed.* **2012**, 51, 4710-4713.
[27] Aranyos, A.; Old, D. W.; Kiyomori, A.; Wolfe, J. P.; Sadighi, J. P.; Buchwald, S. L.; *J. Am. Chem. Soc.* **1999**, 121 (18), 4369–4378.
[28] Klebach, T. C.; Lourens, R.; Bickelhaupt, F.; *J. Am. Chem. Soc.* **1978**, 100, 4886–4888.
[29] Yoshifuji, M.; Shima, I.; Inamoto, N.; Hirotsu, K.; Higuchi, T.; *J. Am. Chem. Soc.* **1981**, 103, 4587–4589.
[30] See, for example: a) Mizuhata, T.; Sasomori, T.; *Chem. Rev*. **2009**, 109, 3479–3511; b) Rivard E.; Power, P. P.; Dalton Trans. 2008, 4336–4343; c) Sasomori, T.; Tokitoh, N.; *Dalton Trans.* **2008**, 1395–1408; d) Shah, S.; Protasiewicz, J. D.; *Coord. Chem. Rev.* **2000**, 181–201; (e) Robinson, G. H.; *Acc. Chem. Res.* **1999**, 32, 773–782.
[31] Byrne, P. A.; Gilheany, D. G.; *Chem. Soc. Rev.* **2013**, 42, 6670.
[32] Vedejs, E.; Fleck, T.; *J. Am. Chem. Soc.* **1989**, 111, 5861.
[33] Imai, M.; Ikegami, M.; Momotake, A.; Nagahata, R.; Arai, T.; *Photochem. Photobiol. Sci.* **2003**, 2, 1181-1186.
[34] Tabuchi, M.; Momotake, A.; Kanna, Y.; Nishimura, Y.; Arai, T.; *Photochem. Photobiol. Sci.* **2011**, 10, 1521.

Chapter 6 – Dendronized Polyelectrolytes

6.1 Introduction

Polyelectrolytes (PEs) are defined as polymers carrying either positively or negatively charged ionizable functional groups. The properties of such polysalts in solution and at charged surfaces substantially depend on the fraction of dissociated ionic groups, the dielectric constant of the parent solution, the salt concentration, and the polymer-substrate interactions.[1]

The specific design of the charged functionality as well as the molecular weight of such polymers leads to the production of materials for the use in a wide range of industrial applications – water purification, oil recovery, paper-making and mineral processing are just a few of them to mention. Thus, the demand for flocculants (coagulants), rheology-modifiers and dispersants can be satisfied by synthetic polyelectrolytes.[2]

Since the continuous motif within this work rests on the formation of a defined number of charges followed by an extensive hydrophobization of the so generated electrolytes by means of dendritic encapsulation, the indispensable question emerges in which way this principle suits for the synthesis of polyelectrolytes. This gives rise to a variety of properties that will be influenced by exceedingly increasing the spatial dimension and rigidity of the charge-carrying ionic group (such as charge density and ionic conductivity, thermal and mechanical stability, viscosity and self-assembly). Initial efforts within this chapter envisaged the quantitative exchange of small chloride anions (diameter 334 pm) to large, hydrophobic borate anions (diameter ~ 2200 pm) in a polycation (poly-MEMTA chloride). Furthermore, approaches to generate sterically shielded charges along a polymer backbone in a controlled fashion are postulated, which result in the formation of stiff, rod-like poly-phosphonium cations. For that reason the building blocks developed within this work are of particular value.

6.2 Hydrophobization of a Polycation

Most synthetically available polycations are derived from positively charged acrylic acid or methacrylic acid monomers. Therefore, [2-(methacryloyloxy)ethyl]trimethylammonium chloride (METMA Cl-) served as starting material to produce water-soluble poly-METMA chloride (**6-1**) in a free radical polymerization reaction.

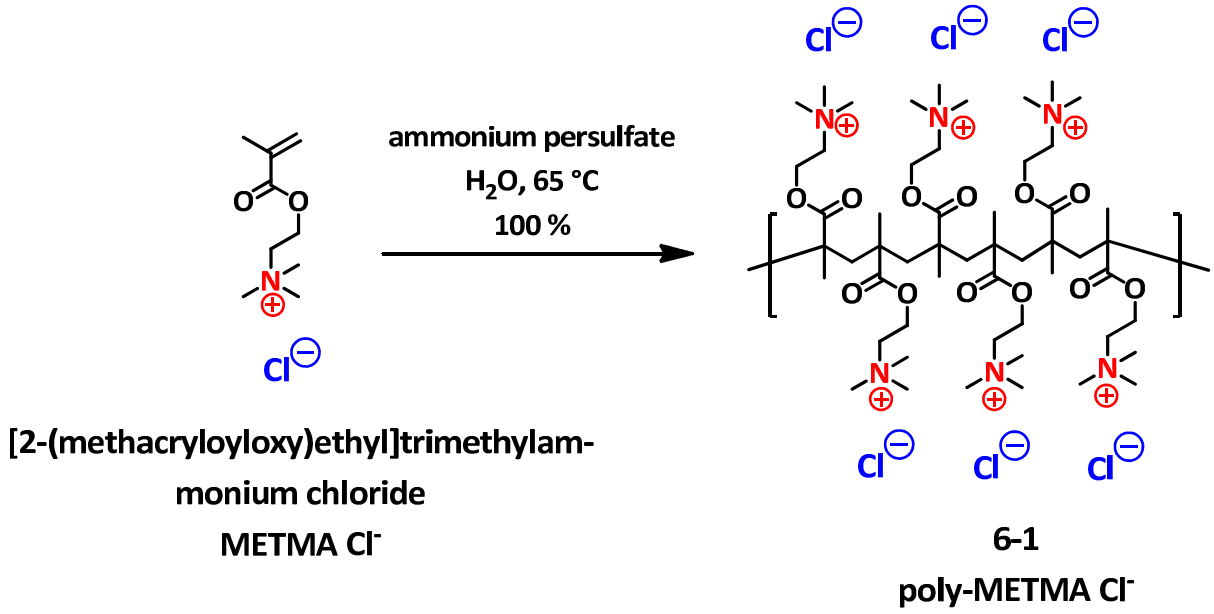

Figure 6-1: Free radical polymerization of METMA chloride initiated by ammonium persulfate in aqueous solution.

It has been reported in the literature[3] that varying the counter-anions for the polycation poly-METMA significantly influences its solubility range and the resulting thermal stability. Thereby, the anion exchange reaction was facilitated by a phase-separation of the resulting products. For that reason it was of particular interest, whether unprecedentedly large and hydrophobic borates can be exchanged as feasible charge compensating counter-anions. First of all, tetraphenyl borate $[BPh_4]^-$ and tetrakis pentafluorophenyl borate $[B(C_6F_5)_4]^-$ were utilized as anions to yield the hydrophobic polyelectrolytes **6-3** (poly-METMA $[BPh_4]^-$) and **6-4** (poly-METMA $[B(C_6F_5)_4]^-$) respectively. A quantitative exchange of the chloride ions to tetraphenyl borate could be assumed by integration of the ^{1}H-NMR signals of the resultant product (**6-3**, poly-METMA $[BPh_4]^-$).

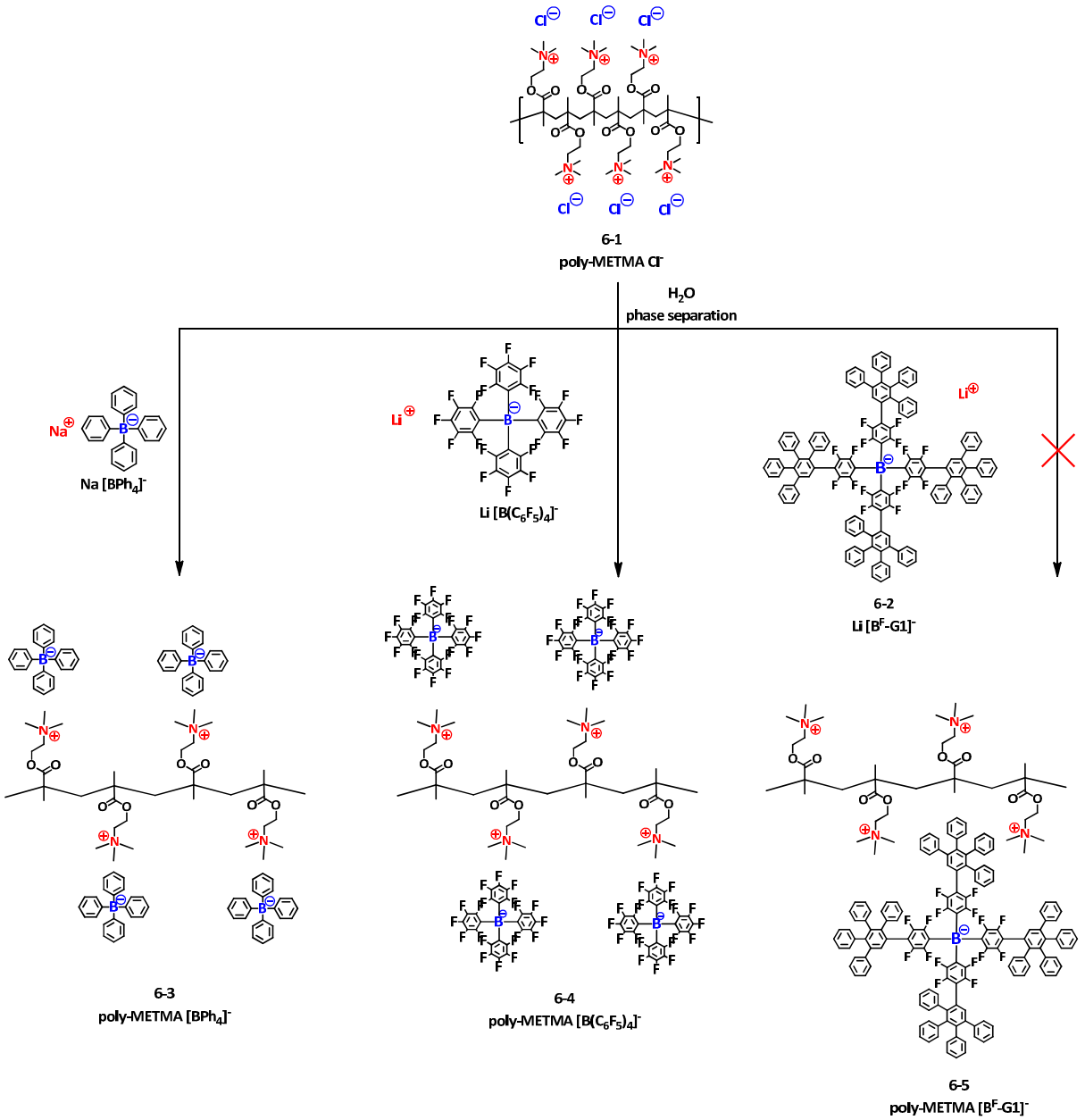

Figure 6-2: Anion exchange experiments to exchange chloride to large and hydrophobic borate anions in poly-METMA chloride **6-1**.

Whereas the preparation of **6-3** and **6-4** proceeded in a smooth way similar to the literature procedures,[3] the formation of **6-5** did not succeed. The starting material poly-METMA chloride (**6-1**) was dissolved in water and to that was slowly dropped a solution of lithium G1-borate (**6-2**, Li^+ $[B^F\text{-}G1]^-$). Instantaneous formation of a precipitate suggested a successful anion metathesis. NMR-analysis of both the precipitate and the remaining solution, however, revealed that the solid consisted solely of precipitated lithium borate (**6-2**), which is not soluble in water.

For that reason the subsequent step to achieve an anion exchange was pursued by employing the silver(I)-salt of the dendronized borate, Ag^+ $[B^F\text{-}G1]^-$ (**6-6**), which was obtained by cation exchange similar to the well-established procedure presented in chapter 4.2 (**Figure 6-3**) . It is known that AgCl exhibits very low solubility in polar organic solvents[4] (K_{sp} = $[Ag^+]$ $[Cl^-]$ in $mol^2\ L^{-2}$; $10^{-10.4}$ in DMSO, $10^{-12.4}$ in CH_3CN, $10^{-18.0}$ in MeOH, $10^{-16.4}$ in acetone, $10^{-21.1}$ in nitroethane), so it was expected that treatment of poly-METMA chloride with Ag^+ $[B^F\text{-}G1]^-$ (**6-6**) will promote the precipitation of silver-(I)-chloride and thus enable a successful anion exchange towards **6-5**. The presence of Ag^+ $[B^F\text{-}G1]^-$ (**6-6**) was unambiguously evidenced by ^{1}H-NMR analysis and the quantitative spectrophotometric detection of a ternary silver(I)-complex of 1,10-phenanthroline and eosin (2,4,5,7-tetrabromofluoresceine). The solution spectra of the so generated mixed-ligand complexes are characterized by high-intensity metal-to-ligand charge-transfer bands at 540-555 nm (**Figure 6-4**).[5]

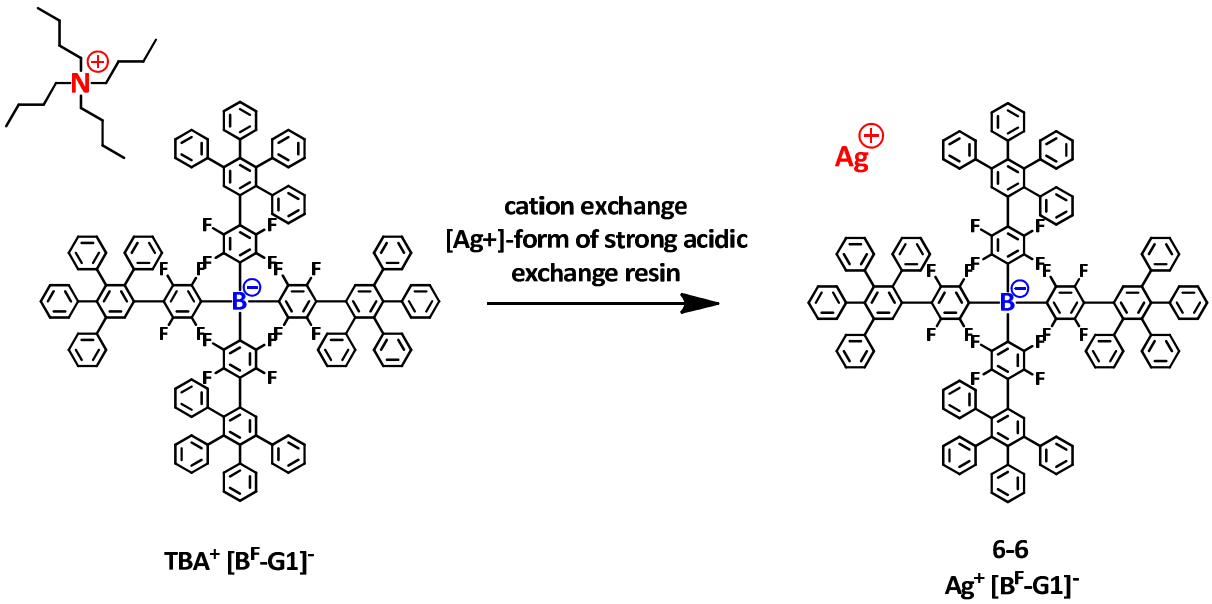

Figure 6-3: Anion exchange experiments to exchange chloride to large and hydrophobic borate anions in poly-METMA chloride **6-1**.

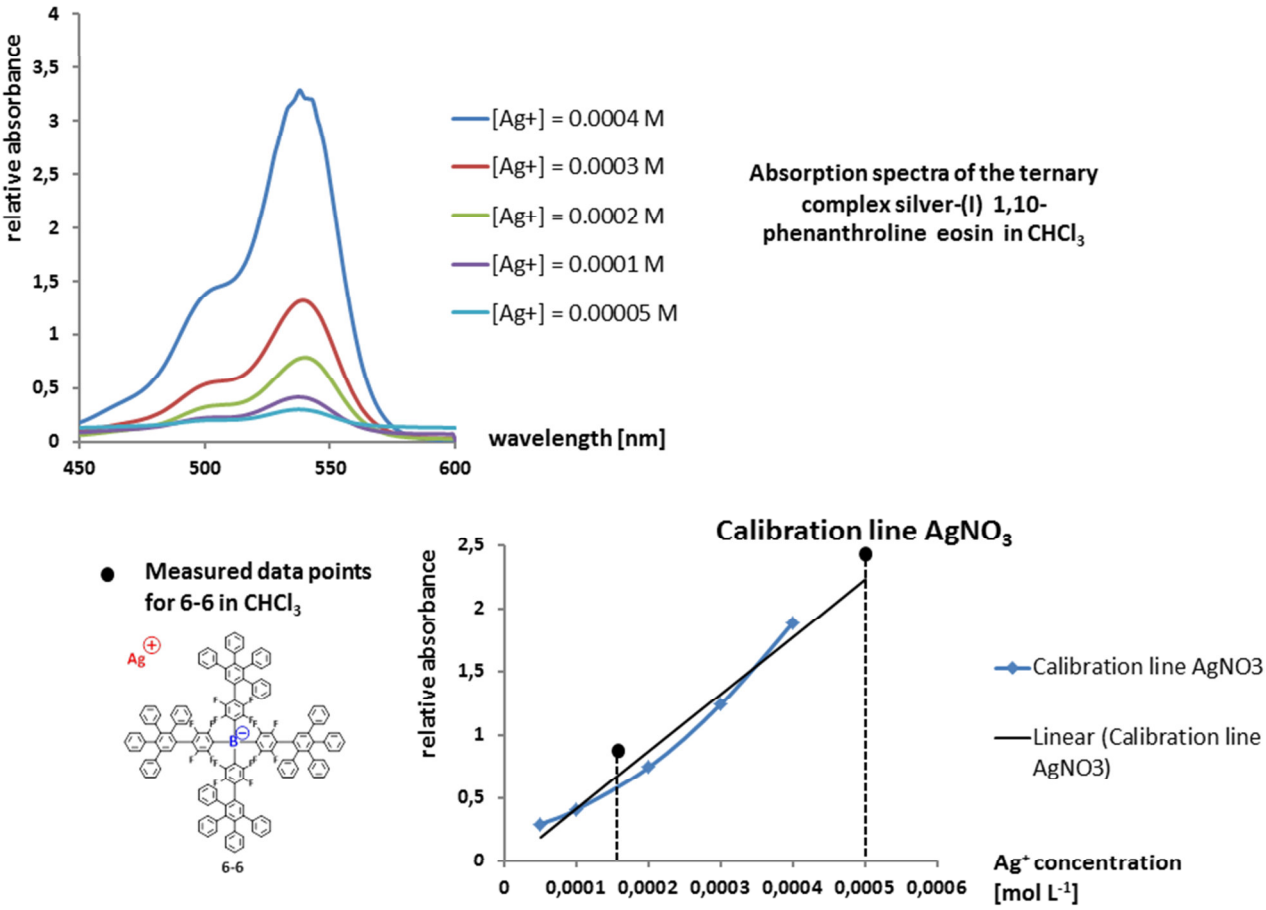

Figure 6-4: Photometric analysis of Ag^+ in **6-6** apparent as ternary dye complex.

With the silver-(I)-borate salt **6-6** in hand, the subsequent anion metathesis was targeted by dissolving poly-METMA chloride **6-1** in methanol followed by slow addition of Ag^+ $[B^F\text{-}G1]^-$ (**6-6**) (1.1 eq in methanol). An immediate precipitation indicated the successful anion exchange at first glance. However, after the solid residue was filtered and dried, the ^{1}H-NMR analysis (CD_2Cl_2, 298 K) of the filtrate revealed more than confusing results: the appearance of ^{1}H-NMR signals in the aromatic region (δ 7.53 – 6.57) clearly accounts for the presence of the dendronized borate anion. The signals in the aliphatic region, however, were not to reconcile with the expected target compound **6-5**. Neither the chemical shifts nor the signal intensities (integrals) could provide unambiguous information about the identity of the apparent polymer. An attempt to explain the data is based on an incomplete exchange of chloride to bulky borate $[B^F\text{-}G1]^-$. But even in this case too many unclarified questions remain unacknowledged, e.g. the tremendous shift and the coincidence of the poly-METMA signals. It is not likely that the solvent change from MeOD to CD_2Cl_2 and the presence of the weaker

coordinating counter-anion $[B^F\text{-}G1]^-$ can fully explain the discrepancies illustrated in **Figure 6-5a** and **Figure 6-5b**.

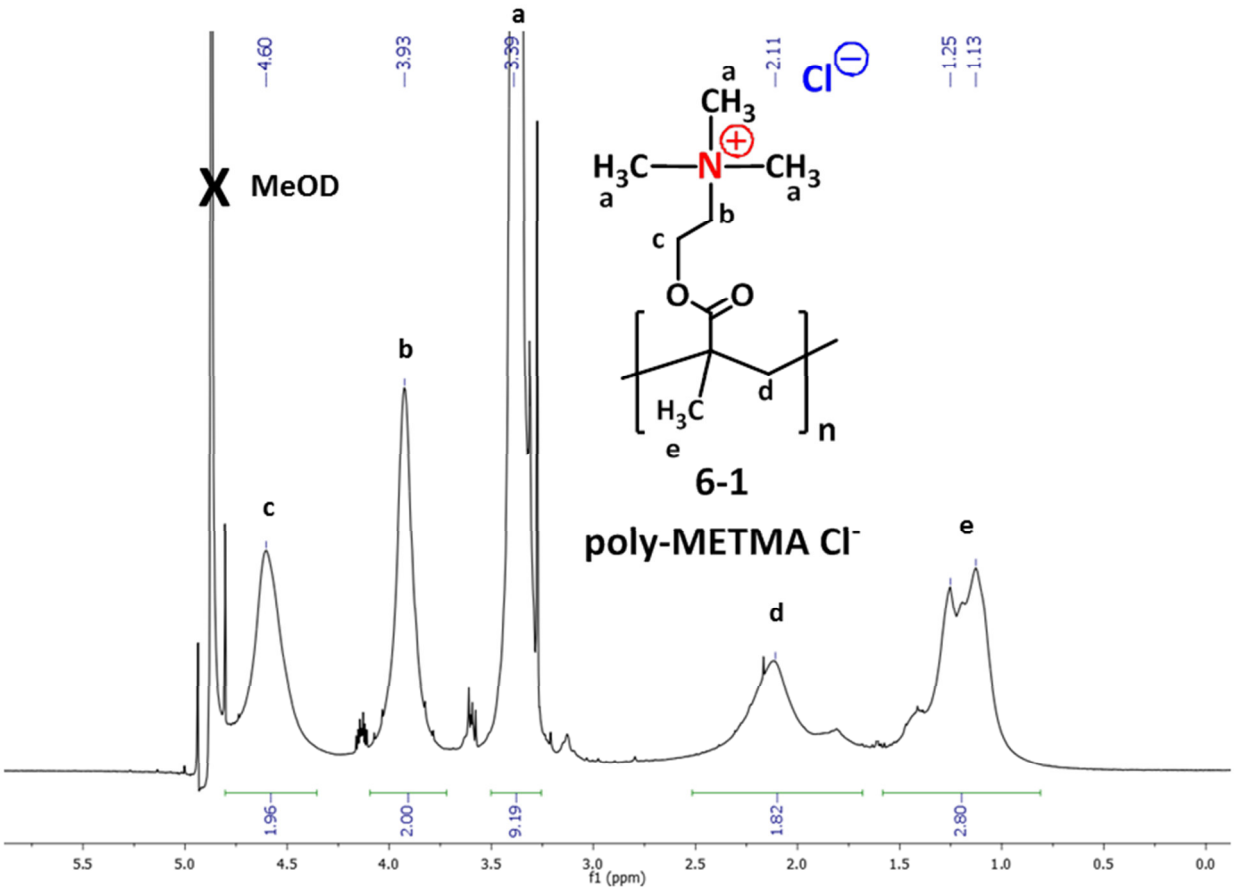

Figure 6-5a: ^{1}H-NMR spectrum of the anion exchange starting material poly-METMA chloride **6-1** (MeOD, 298 K).

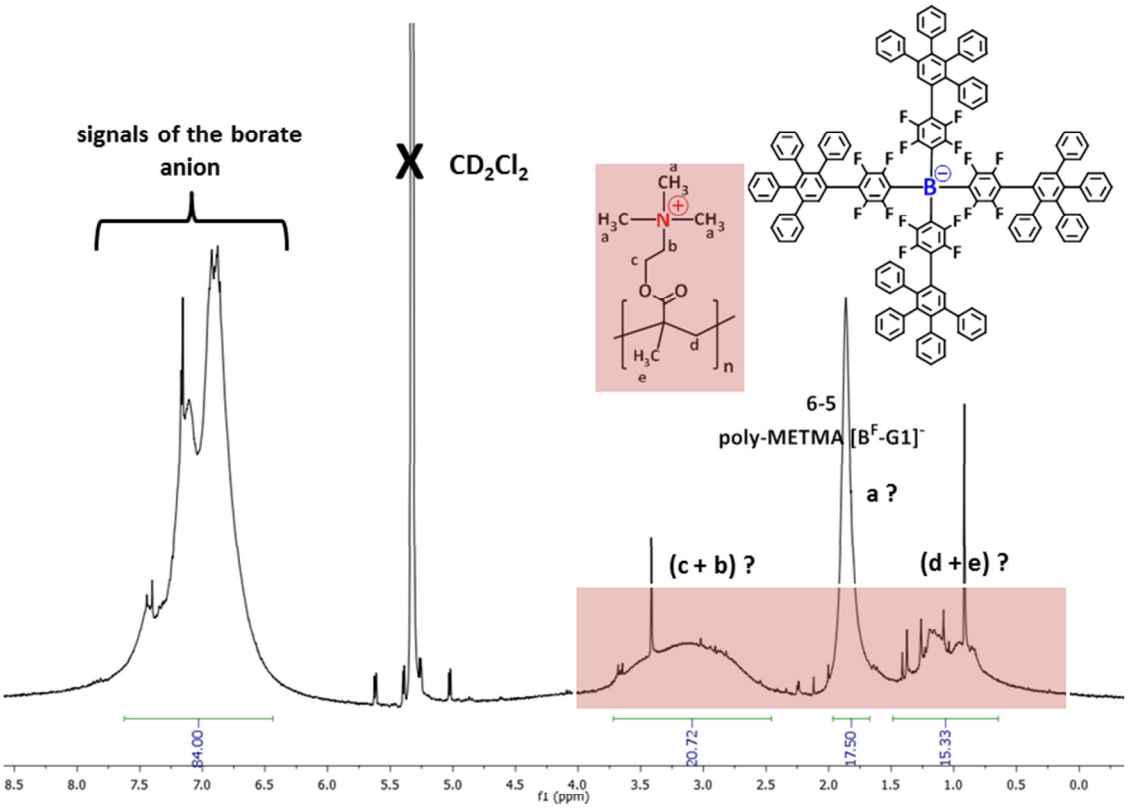

Figure 6-5b: ^{1}H-NMR analysis after the attempted anion exchange employing poly-METMA chloride **6-1** and silver-(I)-borate Ag^{+} $[B^{F}\text{-}G1]^{-}$ to yield **6-5** (CD_2Cl_2, 298 K).

Several further experiments employing Ag^{+} $[B^{F}\text{-}G1]^{-}$ (**6-6**) were repeated with poly-METMA chloride **6-1** and also different polycation halides (poly-4-N-methylvinylpyridinium iodide for instance) were subjected to anion exchange attempts to introduce large, hydrophobic borate counter-anions. Though none of the experiments performed within this work were explicitly operating satisfactory.

The most sophisticated rationale for the observed results within this section is given by applying the cell-model and its Poisson-Boltzmann solution to the case of the linear polyelectrolyte **6-1**.[6] According to the latter the macro-ions are regarded as rod-like objects interacting with the small surrounding ions in cells with cylindrical geometry. In this case one may look at the cylindrical tube enclosing the molecule and simply neglect the fact that it is bent on scales larger than the persistence length of the polyelectrolyte, provided that the cell diameter R_0 is small compared to the latter. A descriptive illustration therefore is shown in **Figure 6-6**.

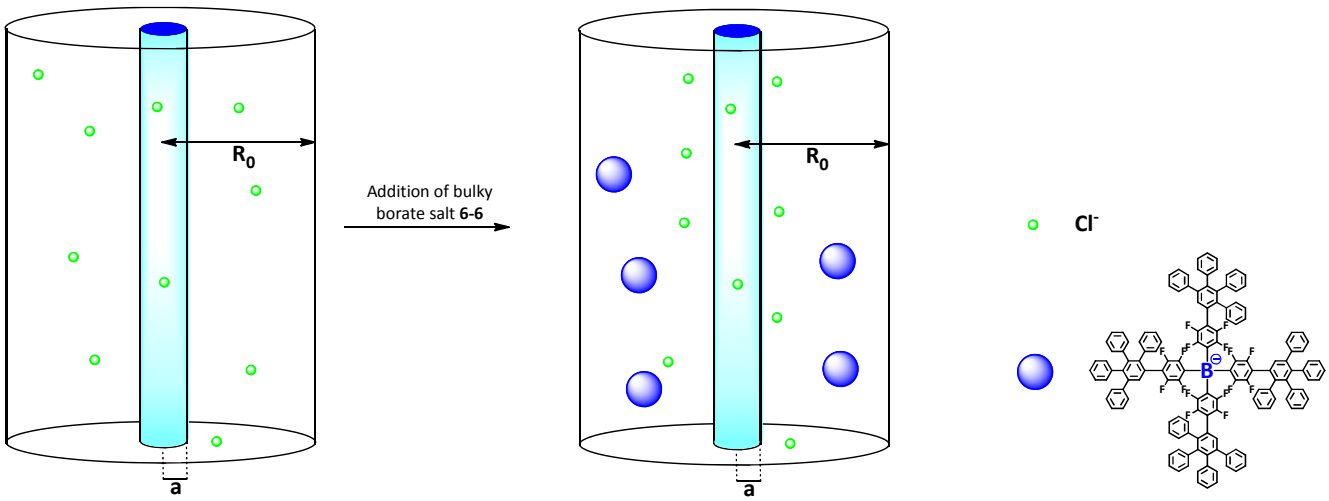

Figure 6-6: Illustration of the cylindrically symmetric geometry of the cell-model for rodlike polyelectrolytes. The polyion is regarded as a charged rod with infinite length and radius a in a cylinder of radius R_0. The charge neutrality is ensured by a corresponding number of counterions.

Thus, the calculation of the counterion distribution is reduced to the components of one cell.[7] The polyelectrolyte-rod is characterized by ξ, which is defined by the ratio of the Bjerrum length l_B (0.715 nm in H_2O at 298 K) and the axial distance b of the charges along the polymer chain.

$$\xi = \frac{l_B}{b} \qquad \textbf{(Equation 6-1)}$$

In order to explain the results from this section, the investigation of the colligative properties of polyelectrolyte solutions in the form of the counterion condensation has to be reflected.[8] The observation that the measured osmotic pressure Π of PE-solutions is significantly lower than the ideally calculated Π_{id} by means of the *Van't Hoff Equations*,[9], [10] provides a measure of the proportion of "non-condensed" to the polymer chain – the osmotically active counterions. The physical background of this effect is the competition between the energy gain due to electrostatic interactions and the entropy change in the free energy by condensation of the counterions.

This term of "condensation" was initially reported by *Oosawa*[11] and further developed in *Manning*'s theory.[12] If the repulsive electrostatic interaction energy of two adjacent charges on the polymer chain is greater than the thermal energy k_BT, an initially free counterion condenses to reduce the repulsive interaction ($\xi > 1$) as illustrated in **Figure 6-7**.

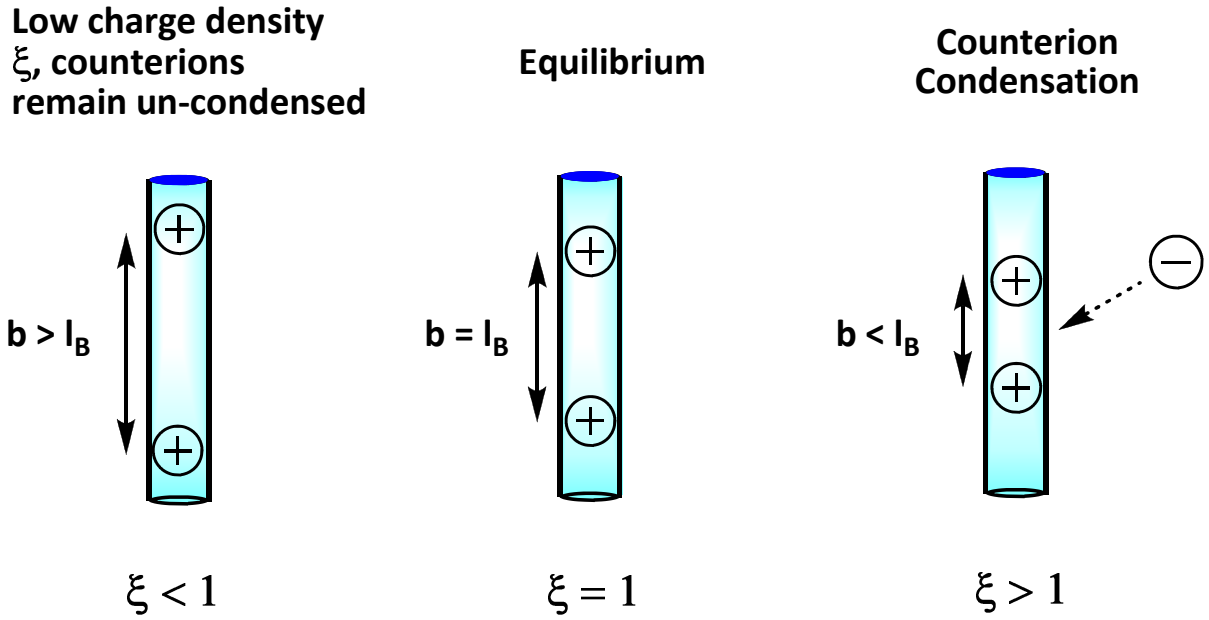

Figure 6-7: Schematic representation of the counterion condensation on the polyelectrolyte chain in dependence of the charge density ξ.

Considering that the addition of Ag^+ $[B^F\text{-}G1]^-$ (**6-6**) (1.1 eq in MeOH) to poly-METMA chloride **6-1** in methanol leads to an immediate formation of an AgCl precipitate with the free chloride ions in solution. The fraction of these un-condensed Cl^- is given by the so called Manning-fraction f_ξ[13], [14]:

$$f_\xi = 1 - \frac{1}{\xi} \qquad \textbf{(Equation 6-1)}$$

The remaining fraction of the large $[B^F\text{-}G1]^-$ ions remains in solution and interacts with the condensed polycation **6-1** according to the *Debye-Hückel* approximation.[15], [16] It is assumed that the addition of the large dendronized borate salt is not resulting in a further charge compensation of the polymer chain due to its intrinsic spatial demand (so no typical polyelectrolyte effect).[17], [18] But instead the precipitation of the condensed poly-METMA chloride **6-1** caused by the local charge clouds of the $[B^F\text{-}G1]^-$ anions is postulated.

6.3 Dendritically Shielded Ionic Group at a Polycation

Within this chapter the main focus was on the question in which way the distinct polymer architecture of a polyelectrolyte can be influenced by dendritically shielding the ionic groups with polyphenylene dendrons. The idea was inspired by comprehensive reviews reporting the attachment of wedgelike dendrimers to linear polymer chains to create anisotropic "nanocylinders".[19-21] Thus, polymer conformations all the way from random-coil to fully stretched linear can be attained by implementing dendrons with different structure, size and molecular stiffness along a conventional polymer backbone. This rigidification of the backbone is caused by steric repulsion between the pendant dendrons. For that reason the whole matter is referred to as shape control by implementation of steric strain.
One striking example in the literature where particularly polyphenylene dendrons served as solubilizing group and efficiently suppressed aggregation was the modification of polyfluorenes towards blue-light emitting polymers.[22] This illustrates the unprecedented ability of a rigid PP-shell to maintain a certain shape. Hence, we regarded the attachment of charged side chain polyphenylene moieties to a poly-styrene based main chain as valuable means to permit spatial control and produce a stiff, rod-like poly-phosphonium cation.

The first approach thereto was based on the divergent construction of a sterically shielded phosphonium group attached to the reactive sites along a polymer backbone. Therefore, initially the free radical co-polymerization of styrene and 4-vinylbenzyl chloride to yield co-polymer **6-7** bearing statistically distributed electrophilic chloromethyl-groups (20 mol %) as anchor points. The subsequent quarternization step proceeded by reacting **6-7** with tris-(4-ethynylphenyl)-phosphine in a S_N2-reaction. Thus, polyphosphonium chloride **6-8** was generated, which comprises of ethynyl-functionalized cationic groups. This enables a dendronization step via the well-established thermal [4+2] *Diels-Alder* cycloaddition (**Figure 6-8**).

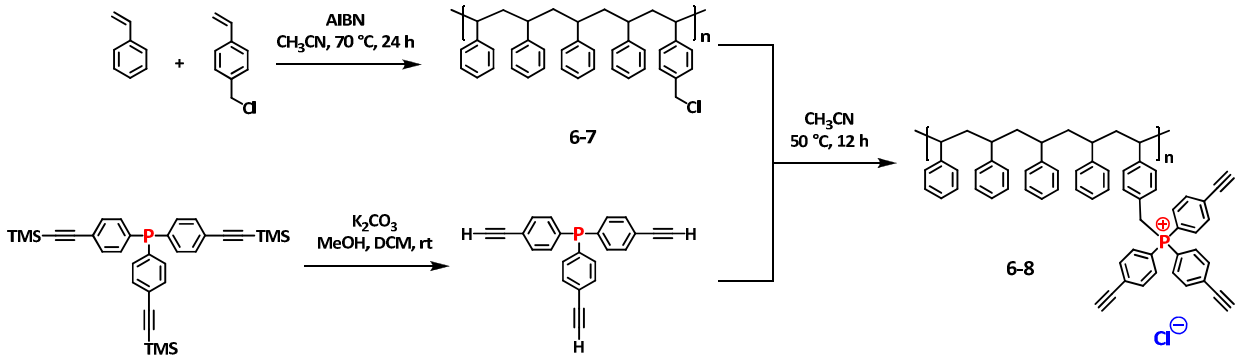

Figure 6-8: Synthetic route towards the ethynyl-functionalized polyphosphonium chloride **6-8**.

The quarternization reaction could be monitored by ^{31}P-NMR. **Figure 6-9** illustrates the consumption of the phosphine (disappearing signal at δ – 5.87) under simultaneous generation of the cationic triarylbenzyl-moiety (indicated by the appearance of the peak at δ 23.66). After 24 hours reaction time the target compound **6-8** exhibited a broad signal-distribution in the ^{31}P-NMR spectrum around δ 22.72, which is characteristic for polydisperse phosphonium salts.

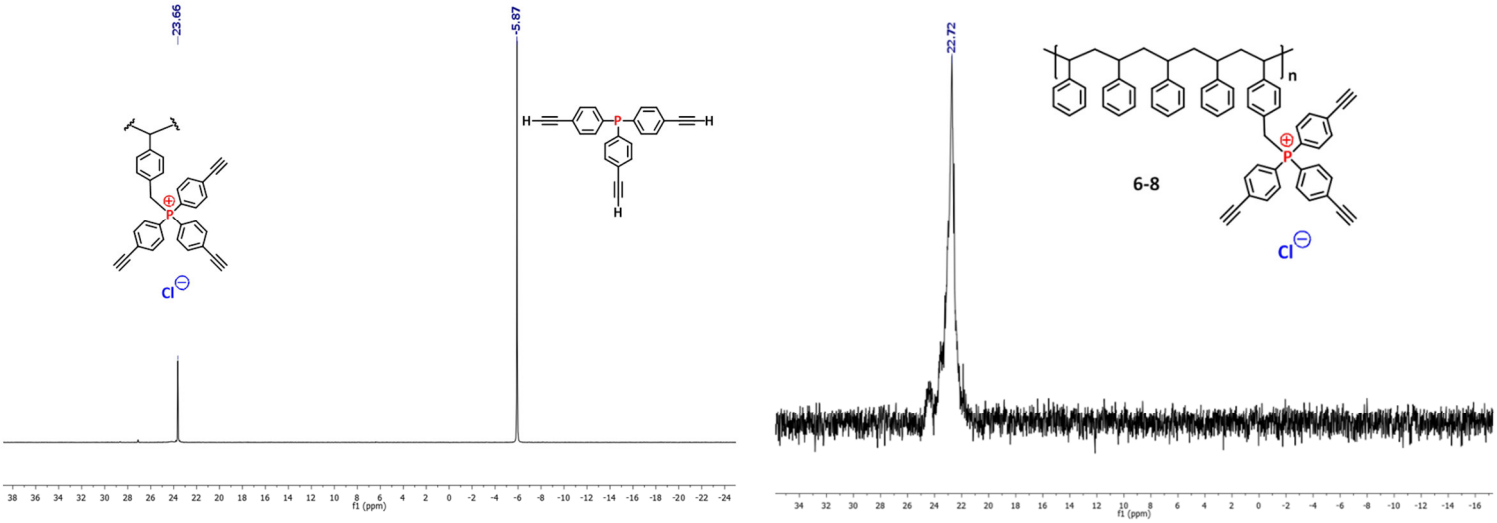

Figure 6-9: Comparison of the ^{31}P-NMR spectra (CD_2Cl_2, 298 K) towards the synthesis of polyphosphonium chloride **6-8**. left: after 1 h reaction time. right: after 24 h reaction time.

Reacting the polycationic core **6-8** with tetraphenylcyclopentadienone in o-xylene at high temperature (round bottom flask, 150 °C, 24 h, solvent degassed by freeze-pump-thaw technique and condenser placed) was supposed to provide the dendronized polyphosphonium salt **6-9**. After working up the reaction mixture and purifying the target compound (filtration through a celite pad and subsequent precipitation in hexane), the ^{1}H-NMR analysis revealed additional peaks in the aromatic region accounting for a successful introduction of the polyphenylene dendrons. However, the observed narrow distribution of the signals is somewhat untypical for a polydisperse electrolyte material. For that reason the additional analysis of the corresponding ^{31}P-NMR spectrum revealed a single, sharp peak at δ 27.76. This clearly refers to a monodisperse phosphine oxide being formed during the reaction. Taking both NMR-spectra of the obtained product mixture shown in **Figure 6-8** into account, the formation of first-generation phosphine oxide (**6-10**) occurred. So it became evident that the benzylic position next to the phosphorus in **6-8** was prone to break upon exposure to high temperature. Comparing the synthesis conditions of **6-9** with the ones for the preparation of the monodisperse benzylphosphonium salt **5-6** (presented in chapter 5.2) imparts the assumption that the prolonged reaction time caused the cationic groups along the polymer chain in **6-9** to be cleaved off under formation of the oxidation product **6-10**. It must be noted that the reaction towards **6-9** was performed in degassed o-xylene but with solely a condenser placed on the round bottom flask and not being sealed.

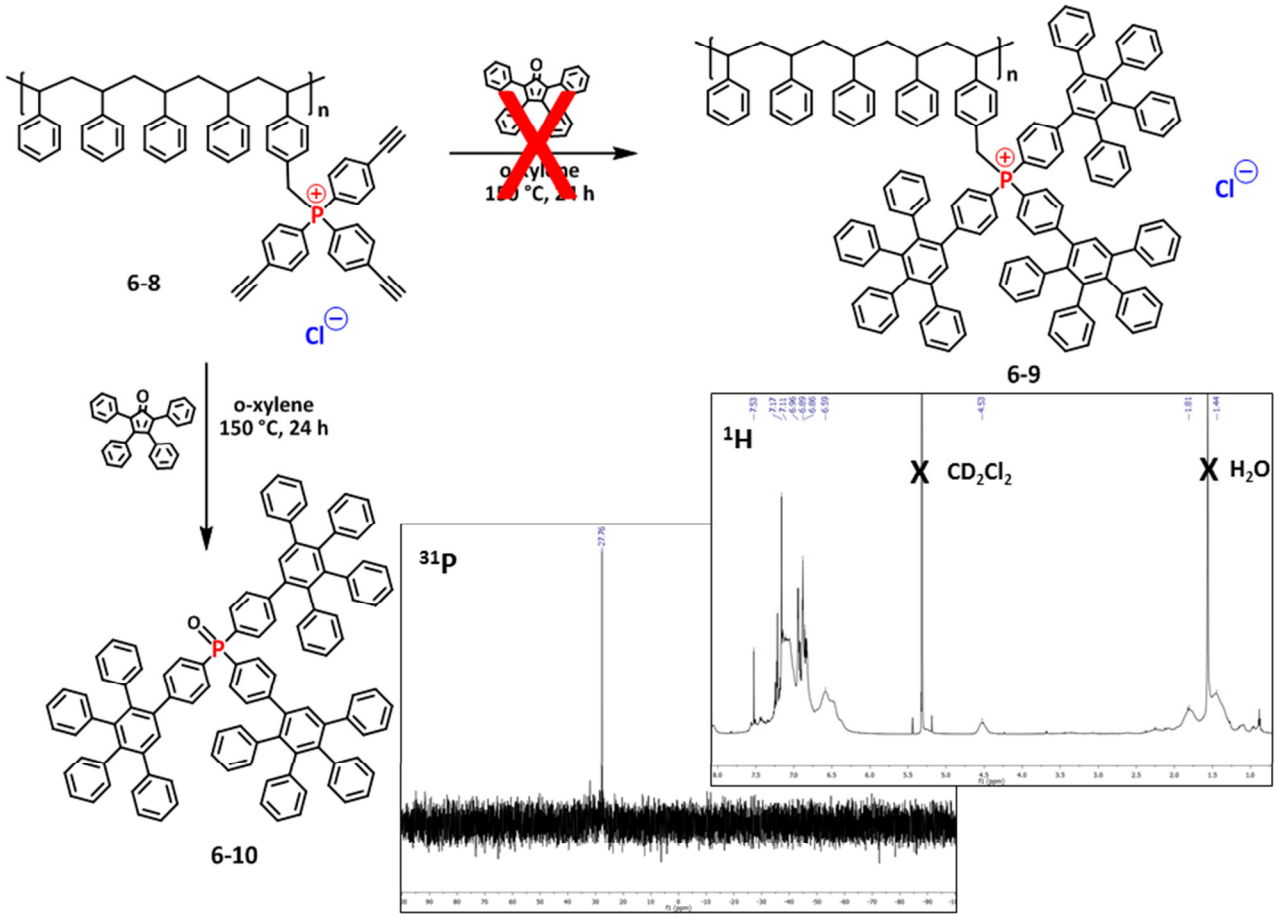

Figure 6-10: Reaction route towards dendronized polyphopshonium chloride **6-9**. Insets: ^{1}H- and ^{31}P-NMR spectrum (CD_2Cl_2, 298 K) of the isolated product.

In view of the oxidation reported herein for the performed divergent synthesis, it is of interest to rationalize these findings in scope of former results gained within that work. The thermogravimetric analysis (TGA) of phosphonium compound **5-16** ($[Ph_3P^{CH2}PPD]^+$ Br^-, synthesis and structure shown in chapter 5.2) reveals a decomposition temperature of 301.5 °C under air stream. The latter can be regarded as simplest model-structure of the benzylphosphonium groups present in the target polymer **6-9**. This clearly underlines that the P-benzyl-bond is thermally more easily cleaved than the P-aryl-bond (compare the solid-state decomposition temperature of 469.9 °C of dendronized tetraphenylphosphonium P-G1$^+$ BF_4^-, section 4.5).

The presence of additional bulky polyphenylene-dendrons, however, is supposed to exert steric strain and mechanical tension on the system. Furthermore, the increased charge density of the cationic groups during the intermediate formation of **6-9** leads to an electrostatic repulsion. Those two effects might lead to a significant decrease in the stability of the crucial P^+-benzyl-bond and thus explain the formation of phosphine oxide **6-10** (as shown in the reaction scheme in **Figure 6-10**) at already 150 °C (24 h reaction time). So the concluding critical issue associated with the divergent route proposed herein is the growth step via thermal *Diels-Alder* reaction. A promising method to prevent the thermal decomposition in future studies was explored within this work in chapter 3.6 by employing the copper-(I)-catalyzed azide-alkyne cycloaddition (CuAAC).

An alternative synthetic principle towards the generation of polymers encapsulated by dendrons starts with already functionalized dendrimer-monomers, which are subjected to a polymerization or polycondensation reaction (macromonomer route).[21] Thus, the embedment of sterically encumbered cationic phosphonium groups into a polymer chain was pursued using this synthetic strategy. Therefore, dendronized phosphonium salt **6-12** bearing a single polymerizable vinyl-group was synthesized by reacting bulky phosphine **6-11** with 4-vinylbenzyl chloride in good yield.

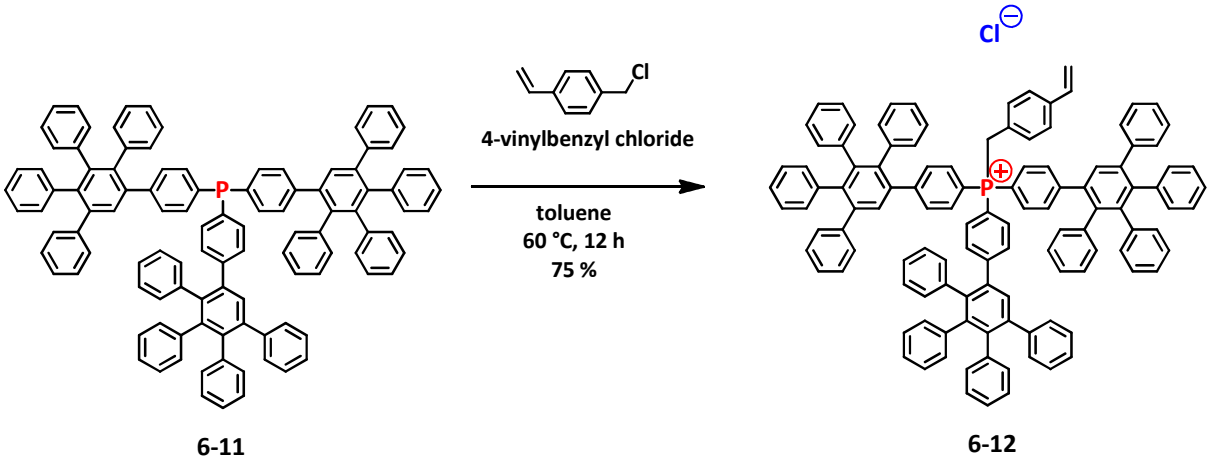

6-11 **6-12**

Figure 6-11: Synthesis of dendronized vinylphosphonium chloride **6-12**.

It was of substantial interest whether such styrene-based monomer **6-12** was still capable of undergoing a free radical polymerization despite the presence of the three large and shielding polyphenylene dendrons. A thoroughly degassed solution of **6-12** in MeCN (60 °C, 12 h, freeze-pump-thaw technique in a sealed microwave tube with a teflon cap) did not show any hints of a radical reaction after addition of 10 mol % of AIBN (argon atmosphere). This was clearly evidenced by analyzing the ^{1}H-NMR spectrum of the obtained product, which still displayed the characteristic vinyl proton signals at δ = 6.70 (dd, 1 H, $^{3}J_{HH}$ (trans) = 17.6 Hz, $^{3}J_{HH}$ (cis) = 9.9 Hz) and δ = 5.93 – 5.76 (2 x d, 2 H, $^{3}J_{HH}$ (trans) = 17.6 Hz, $^{3}J_{HH}$ (cis) = 9.4 Hz). To test the principal accessibility of the double bond in vinylphosphonium chloride **6-12**, a DMF-solution of the latter was prepared and 50 mol % of AIBN were added. After carefully degassing the solution, the vial was sealed and heated to 110 °C for 24 h (freeze-pump-thaw technique in a sealed microwave tube with a teflon cap). Under these harsh reaction conditions the vinylic proton-signals were indeed no more detectable in the ^{1}H-NMR spectrum of the purified product. Rather oligomers of the former monomer **6-12** were formed, which could be verified by means of DOSY-NMR (-lg D = - 9,71, r_H ~ 2.8 nm) and GPC-analysis (Mn = 2409.72 g/mol, Mw = 2603.2 g/mol, PDI = 1.08, polystyrene as standard, solvent DMF, spectra see **Experimental Part**). The problems associated with the route proposed in **Figure 6-11** are due to steric hindrance. Here the critical point is the spatial demand of both monomer and chain end. Incoming monomer will only be connected to the chain end if the steric hindrance is not too high. Otherwise this process will be slowed or even rendered impossible. The radical polymerization applied within this work is known to undergo many side reactions, such as termination of the reactive end or auto-initiation. Although there are plenty of literature reports where functionalized dendritic monomers where polymerized employing the analogous approach under radical polymerization conditions,[23-30] however all that monomers bear a more flexible dendrimers-scaffold and the reactive functional group is more distal to the latter. Furthermore, the concentration of the reaction medium plays an absolutely important role in the polymerization of macromonomers. There are reports in the literature[28], [31] showing that below a certain weight concentration of monomers, c_m, the polymerization is rendered rather impossible. At too high concentrations, however, the viscosity of the medium increases, which limits the mobility of large monomers and thus favors termination.[32] Thus, the investigation of the

optimum concentration range is impressingly important for the polymerization proposed for **6-12**, which means the optimization of the reaction conditions is subject of further research.

6.4 Discussion and Outlook

Considering the inconveniences in the present chapter to produce dendronized polymers with rigid phosphonium groups, and also taking the results from the previous chapters into account, an elaborated approach thereto will be presented in the following. In the literature several examples pointed out the great potential of Suzuki polycondensation (SPC) reactions even for cases where steric congestions have to be considered.[33] The goal is to synthetically access a molecular nanoobject created by sterically demanding and charged dendrimer-monomers (conceivable structural motif is given by phosphonium di-cation **6-15**, **Figure 6-12**). Therefrom results the investigation of the coiling behavior and the possibility to form a medium-independent and shape-persistent target poly-ion cylinder (illustrated by structure **6-17**). Thus, the backbone is reported to get stiffened and fully stretched. The question remains at which charge density the polyphenylene phosphonium dendrimers can be tightly aligned along the polymer chain and will the resulting polyelectrolyte be stable in spite of extreme physical (high temperature, high electric potentials applied) and chemical conditions (base-stability, resistance against nucleophiles).

Once the successful preparation of stiff polyelectrolyte rods based on the polyphenylene phosphonium chemistry investigated within this work would be established, a fundamental research progress towards the design of artificial ion channels with shape-persistence can be forwarded.[34]

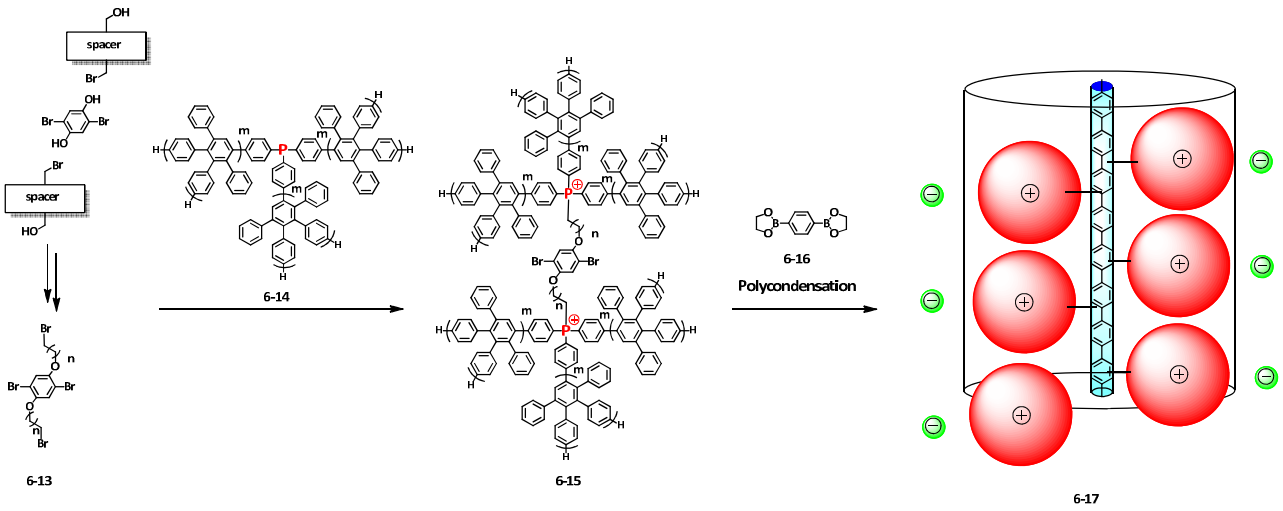

Figure 6-12: Synthesis scheme of dendronized, rod-like polyphosphonium structures **6-17**.

The proposed synthesis route shown in **Figure 6-12** is mainly based on the pioneering works by *Rehahn*, *Schlüter* and *Wegner*,[35-39] where transition metal catalyzed polycondensation reactions in heterogeneous solvent mixtures provided rod-shaped polymers on the basis of poly-(para-phenylene) (PPP, as represented by the central axis in structure **6-17**, colored in blue). Conveivable drawbacks in the reaction scheme proposed in **Figure 6-12** might encounter with respect to the stability of the dendronized electrolyte-functionality during the process of Pd-catalyzed SPC. Also the analytical characterization of the charged polymers is known to be difficult.[40] The versatility of the postulated synthesis route, however, is due to the possibility to initially synthesize the neutral PPP-precursor by reacting the dibromo-compound **6-13** with diboron-benzene **6-16**. Thus, the uncharged polymers can be analyzed by conventional methods (e.g. NMR, GPC, light-scattering, viscosimetry, osmometry) and afterwards being quarternized in a polymer-analogous reaction with **6-15** in a selective and complete manner (most likely depending on the careful choice of the length of the alkyl spacer in **6-13**). There are numerous reports in the literature employing this postsynthetic approach for the formation of polyelectrolytes, which bear sensitive charged groups with respect to the polycondensation conditions.[40-45]

Aside from encapsulating the positive charge of a phosphonium group into a large polyphenylene scaffold at the side chain of a polymer backbone, *Long et al*. has recently reported the synthesis of phosphonium ionomers employing a multiple Menschutkin reaction to provide polymers with controlled charge density. Ionenes represent a unique class of polyelectrolytes with the cationic charges located within the polymer main chain. The step-growth polymerization of bifunctional bis-phosphonium derivatives and dihalides was used to produce high molecular weight phosphonium ionenes.[46] By employing a systematic variation of the employed monomer building blocks (ditertiary phosphine and di-benzyl halides) based on the rigidified dendrimer-structures presented within this work, novel phosphonium ionenes with a stiff framework structure and a distinct charge localization can be generated as outlined schematically in **Figure 6-13**. This approach will be inter alia topic of further research by *Li Zeyu*.

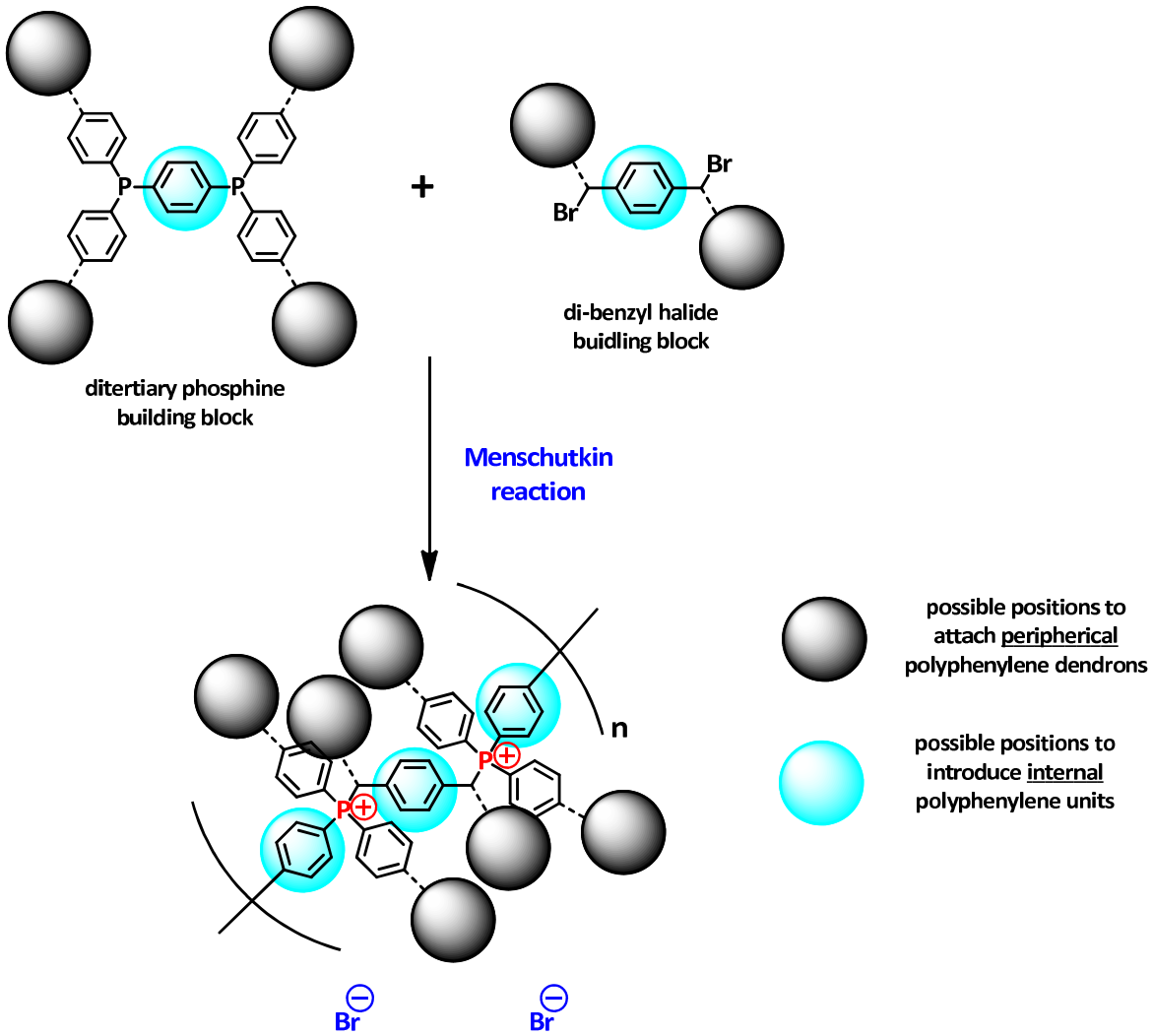

Figure 6-13: Synthesis scheme towards rigid polyphosphonium ionenes.

Literature

[1] for a review on the theoretical model description of polyelectrolytes, see: Dobrynin, A. V.; Rubinstein, M.; „Theory of polyelectrolytes in solutions and at surfaces“; *Prog. Polym. Sci.* **2005**, 30, 1049 – 1118; b) Tripathy, S.; Kumar, J.; „Handbook of Polyelectrolytes and their Applications'', American Scientific Publishers, Stevenson Ranch **2002**.
[2] Mortimer, D. A.; "Synthetic Polymers – A review"; *Polymer International* **1991**, 25, 29-41.
[3] Marcilla, R.; Blazquez, J. A.; Fernandez, R.; Grande, H.; Pomposo, J. A.; Mecerreyes, D.; *Macromol. Chem. Phys.* **2005**, 206, 299-304.
[4] Luehrs, D. C.; Iwamoto, R. T.; Kleinberg, J.; *Inorg. Chem.* **1966**, 5(2), 201-204.
[5] Idriss, K. A.; Seleim, M. M.; Abu-Bakr, M. S.; *Proc. Indian Acad. Sci. (Chem. Sci.)* **1980**, Vol. 89, No. 6, 519 – 523.
[6] Holm, C.; K´ekicheff, P.; Podgornik, R.; eds. Electrostatic Effects in Soft Matter and Biophysics, Proceedings of the Les Houches NATO-ASI, Oct. 1-13, **2000**, NATO Science Series II - Mathematics, Physics and Chemistry, Vol. 46, Kluwer, Dordrecht (**2001**).
[7] Deserno, M.; Dissertation, Mainz **2000**.
[8] Gray, F. M.; „Solid Polymer Electrolytes“ **1991**, VCH Publishers, New York. MacCallum, J. R., Vincernt, C. A.; „Polymer Electrolyte Reviews“ **1991**, Elsevier, London.
[9] Kern, W.; *Z. Phys. Chem.* **1938**, *181*, 249.
[10] Kern, W.; *Z. Phys. Chem.* **1939**, *184*, 197.
[11] Oosawa, F.; „Polyelectrolytes" **1971**, Marcel Dekker, Inc., New York; b) Oosawa, F.; *J. Polym. Sci.* **1957**, *23*, 421.
[12] Manning, G. S.; *J. Chem. Phys.* **1969**, *51*, 924; 934; 3249.
[13] Manning, G. S., *Ber. Bunsenges. Phys. Chem.* **1996**, *100*, 909.
[14] Le Bret, M.; Zimm, M.; *Biopolymer* **1984**, *23*, 287.
[15] Debye, P.; Hückel, H.; *Phys. Z.* **1923**, *24*, 185.
[16] Barrow, G. M.: „Physikalische Chemie“ **1984**, Vieweg & Sohn, Wiesbaden.
[17] Brodowski, G.; Dissertation, Karlsruhe **1999**.
[18] Wittemann, M.; Dissertation, Karlsruhe **2000**.
[19] Frey, H.; *Angew. Chem.* **1998**, 110, 2313-2317; *Angew. Chem. Int. Ed.* **1998**, 37, 2193-2197.
[20] Schlüter, A. D.; *Top. Curr. Chem.* **1998**, 197, 165-191.
[21] Schlüter, A. D.; Rabe, J. P.; *Angew. Chem.* **2000**, 112, 860-880.
[22] Setayesh, S.; Grimsdale, A. C.; Weil, T.; Enkelmann, V.; Müllen, K.; Meghdadi, F.; List, E. J. W.; Leising, G.; *J. Am. Chem. Soc.* **2001**, 123, 946-953.
[23] Draheim, G.; Ritter, H.; *Macromol. Chem. Phys.* **1995**, 196, 2211-2222.
[24] Percec, V.; Ahn, C. H.; Ungar, G.; Yeardley, D. J. P.; Möller, M.; Sheiko, S. S.; *Nature* **1998**, 391, 161-164.
[25] Chen, Y. M.; Chen, C. F.; Liu, W. H.; Xi, F.; *Macromol. Rapid Commun.* **1996**, 17, 401- 407.
[26] Neubert, I.; Klopsch, R.; Claussen, W.; Schlüter, A. D.; *Acta Polym.* **1996**, 47, 455-459.
[27] Neubert, I.; Schlüter, A. D.; *Macromolecules* **1998**, 31, 9372-9378.
[28] Shu, L.; Schlüter, A. D.; *Macromol. Chem. Phys.* **2000**, 201, 239-245.
[29] Zistler, A.; Koch, S.; Schlüter, A. D.; *J. Chem. Soc. Perkin Trans.* **1999**, 1, 501-508.
[30] Neubert, I.; Amoulong-Kirstein, E.; Schlüter, A. D.; *Macromol. Rapid Commun.* **1996**, 17, 517-527.

[31] a) Tsukahara, Y.; Tsutsumi, K.; Yamashita, Y.; Shimada, S.; *Macromolecules* **1990**, 23, 5201-5208; b) Wintermantel, M.; Gerle, M.; Fischer, K.; Schmidt, M.; Wataoka, I.; Urakawa, H.; Kajiwara, K.; Tsukahara, Y.; *Macromolecules* **1996**, 29, 978-983.
[32] Percec, V.; Ahn, C.-H.; Barboin, B.; *J. Am. Chem. Soc.* **1997**, 119, 12978-12979.
[33] Percec, V.; Schlüter, A. D.; Ronda, J. C.; Johansson, G.; Ungar, G.; Zhou, J. P.; *Macromolecules* **1996**, 29, 146 -1472.
[34] Koert, U.; *Chemie in unserer Zeit* **1997,** Vol**.** 31, Issue 1, 20–26**.**
[35] Rehahn, M.; Schlüter, A. D.; Feast, W. J.; Wegner, G.; *Polymer* **1989**, *30*, 1054.
[36] Rehahn, M.; Schlüter, A. D.; Feast, W. J.; Wegner, G.; *Polymer* **1989**, *30*, 1060.
[37] Rehahn, M.; Schlüter, A. D.; Wegner, G.; *Makromol. Chemie* **1990**, *191*, 1991.
[38] Rehahn, M.; *Dissertation*, Mainz **1990**.
[39] Schlüter, A. D.; Wegner, G.; *Acta Polymerica* **1993**, *44*, 59.
[40] Rulkens, R.; Schulze, M.; Wegner, G.; *Macromol. Rapid Commun.* **1994**, *15*, 669.
[41] Rau, U.; Rehahn, M.; *Macromol. Chem.* **1993**, *195*, 2225.
[42] Rau, U.; Rehahn, M.;*Polymer* **1993**, *34*, 2889.
[43] Rau, U.; *Dissertation*, Karlsruhe **1993**.
[44] Rulkens, R.; *Dissertation*, Mainz **1996**.
[45] Brodowski, G.; Horvat, A.; Ballauf, M.; Rehahn, M.; *Macromolecules* **1996**, *29*, 6962.
[46] Hemp, S. T.; Zhang, M.; Tamami, M.; Long, T. E.; *Polym. Chem.* **2013**, 4(12), 3582-3590.

Chapter 7 – Summary and Outlook

The central objective of this work was to generate weakly coordinating cations of unprecedented molecular size providing an inherently stable hydrophobic shell around a central charge. It was hypothesized that divergent dendritic growth by means of thermal [4+2] *Diels-Alder* cycloaddition might represent a feasible synthetic method to circumvent steric constraints and enable a drastic increase in cation size.

This initial proposition could be verified: applying the divergent dendrimer synthesis to an ethynyl-functionalized tetraphenylphosphonium derivative afforded monodisperse cations with precisely nanoscopic dimensions for the first time. Furthermore, the versatile nature of the applied cascade reactions enabled a throughout flexible design and structural tuning of the desired target cations. The specific surface functionalization as well as the implementation of triazolyl-moieties within the dendrimer scaffold could be addressed by sophisticated variation of the employed building block units (see chapter 3).

Due to the steric screening provided by their large, hydrophobic and shape-persistent polyphenylene shells, rigidly dendronized cations proved more weakly coordinating compared to their non-dendronized analogues. This hypothesis has been experimentally confirmed by means of dielectric spectroscopy (see chapter 4). It was demonstrated for a series of dendronized borate salts that the degree of ion dissociation α increased with the size of the cations. The utilization of the very large phosphonium cations developed within this work almost achieved to separate the charge carriers about the Bjerrum length in solvents of low polarity, which was reflected by approaching near quantitative ion dissociation even at room temperature. In addition to effect the electrolyte behavior in solution, the steric enlargement of ions could be visualized by means of several crystal structure analyses. Thus an insight into lattice packing under the effect of extraordinary large cations could be gathered.

An essential theme of this work focused on the application of benzylphosphonium salts in the classical Wittig reaction, where the concept of dendronization served as synthetic means to introduce an exceptionally large polyphenylene substituent at the α-position. The straightforward influence of this unprecedented bulky group on the Wittig stereochemistry was investigated by NMR-analysis of the resulting alkenes. Based on the obtained data a

valuable explanation for the origin of the observed selectivity was brought in line with the up-to-date operating [2+2] cycloaddition mechanism. Furthermore, a reliable synthesis protocol for unsymmetrically substituted polyphenylene alkenes and stilbenes was established by the design of custom-built polyphenylene precursors (see chapter 5).

Finally, fundamental experiments to functionalize a polymer chain with sterically shielded ionic groups either in the pending or internal position were outlined within this work. Thus, inherently hydrophobic polysalts shall be formed so that future research can invesigate their physical properties with regard to counter ion condensation and charge carrier mobility.

In summary, this work demonstrates how the principles of dendrimer chemistry can be applied to modify and specifically tailor the properties of salts. The numerously synthesized dendrimer-ions shown herein represent a versatile interface between classic organic and inorganic electrolytes, and defined macromolecular structures in the nanometer-scale. Furthermore the particular value of polyphenylene dendrimers in terms of a broad applicability was illustrated. This work accomplished in an interdisciplinary manner to give answer to various questions such as structural modification of ions, the resulting influence on the electrolyte behavior, as well as the stereochemical control of organic syntheses via polyphenylene phosphonium salts.

One of the most challenging tasks for the future will be the construction of rigid and nanoscopically structured materials with oppositely charged ionic groups in an alternating pattern within a hydrophobic polyphenylene framework. First of all the synthesis approach thereto has to be explored, which is schematically proposed in **Figure 7-1** on the basis of the findings within this work.

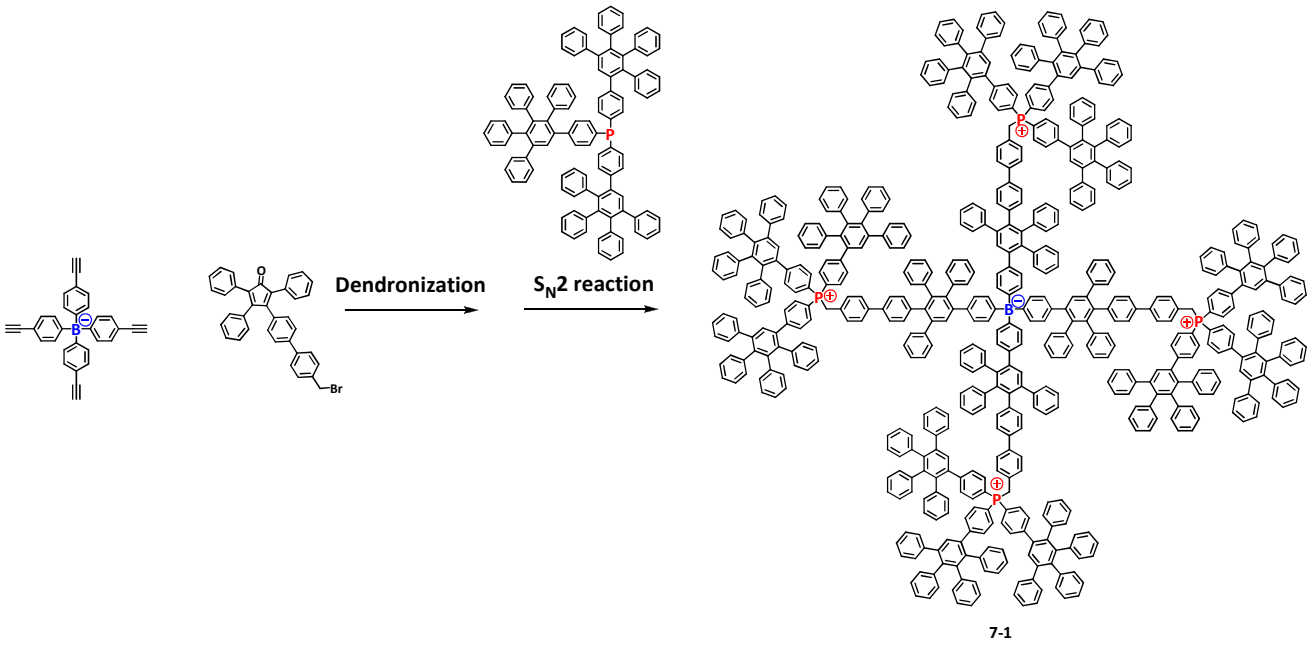

Figure 7-1: Suggested synthesis scheme towards the zwitterionic key structure **7-1**.

Along these lines the question in which way the electrostatic interaction of the charge-compensating counter ions with both the aromatic scaffold and among each other is organized. A suitable combination of analytical techniques (NMR, dielectric spectroscopy, electrophoresis, UV-absorbance measurements) shall provide information about the effect of internal ionic groups on the structural conformation and chemical stability of the desired polyelectrolyte materials. Furthermore, the charge density distribution throughout the aromatic system represents a perpetual motif within this work and could not be clarified at that moment. For that reason zwitterionic structures similar to the architecture **7-1** proposed herein will contribute to answer this regard. The possibility to suitably functionalize this key architecture once more underlines the powerful versatility of the tool-kit-like dendrimer chemistry.

Chapter 8 - Experimental Part

8.1 Materials and Methods

All starting materials were purchased from Sigma-Aldrich, Acros Organics, ABCR Chem, Alfa Aesar, Fisher Scientific, Synthonix and TCI Europe and used as received without further purification. AB_2 and AB_4 cyclopentadienone building blocks were synthesized according to literature procedures.[1], [2] All syntheses were carried out under argon atmosphere using anhydrous solvents. All air and water sensitive reactions were performed under dry argon atmosphere using standard Schlenk techniques. Solvents were dried and deoxygenated prior to use and stored under argon with activated 4 Å molecular sieves. Given reaction temperatures refer to the temperature of the oil bath used for heating. Thin layer chromatography was performed on silica coated aluminum sheets from Machery-Nagel. Column chromatography was done with silica gel (particle size 0.063-0.200 mm) from Merck.

All the compounds synthesized within this work were characterized by NMR (measurements performed by [redacted] and [redacted]) and mass spectroscopy. The NMR experiments were performed with a 5 mm triple resonance TXI $^{1}H/^{13}C/^{15}N$ probe equipped with a z-gradient on the 850 MHz spectrometer, with a BBI $^{1}H/X$ probe with a z gradient on the 700 MHz system, with a BBFO $^{1}H/BB/^{19}F$ probe on the 500 MHz magnet system and with a BBI $^{1}H/X$ probe (300 MHz) all with Bruker Avance I - III working units.
For a ^{1}H NMR spectrum 32 transients were typically used with a 9.3 µs long 90° pulse and a 13600 Hz spectral width together with a recycling delay of 5s.

The ^{19}F NMR data was collected with 32 scans were the 90° pulse was 14.6 µs long and a 60000 Hz spectral width together with a recycling delay of 5s.

The ^{13}C NMR measurements were made with a J-modulated (coupling constant of 145Hz ^{1}H-^{13}C was used) spin-echo for C-nuclei coupled to protons to determine the number of attached protons and proton decoupling during acquisition. The 90° pulse for carbon was between 12 -14 µs long (depending on the probe unit) and 2048 number of scans was taken with a relaxation delay of 2 s.

The integrable ^{31}P NMR (202 MHz) measurements were obtained with the invers gated decoupling technique[1] (30° degree flip angle was used), which had a 11 µs long 90° pulse for phosphor with a relaxation delay of 5s and between 64 and 256 scans.

The proton, carbon, phosphorous and fluorine spectra were measured in CD_2Cl_2 at 298.3 K and the spectra were referenced as follows: for the residual $CHDCl_2$ at $\delta(^1H)$ = 5.32 ppm, CD_2Cl_2 $\delta(^{13}C$ quintett) = 53.8 ppm, CD_2Cl_2 $\delta(^{31}P$ quintett) = 53.8 ppm and CD_2Cl_2 $\delta(^{19}F$ quintett) = 53.8 ppm.

The assignment was accomplished by $^1H,^1H$ COSY (correlated spectroscopy) and $^1H,^1H$ NOESY (nuclear overhauser enhancement spectroscopy). The spectroscopic widths of the homo-nuclear 2D COSY and NOESY experiments were typically 13600 Hz in both dimension (f1 and f2) and the relaxation delay 2 s. The mixing time used in the 2D NOESY was kept at 300 ms.

The 2D $^1H,^{13}C$-HSQC (heteronuclear single quantum correlations via double inept transfer and phase sensitive using Echo/Antiecho-TPPI gradient selection with decoupling during acquisition) experiments were recorded with 2048 points in f2 and 512 points in f1 dimension. Before Fourier transformation, the data were zero filled to 1024 points in f1 and multiplied by a window function (q-sine bell or sine bell) in both dimension.

For all 2D $^1H,^{13}C$-HSQC a coupling constant of $^1J_{CH}$ = 145 Hz was used for optimizing observable intensities of cross peaks from one bond ^1H-^{13}C correlation.

Diffusion Ordered NMR Spectroscopy (DOSY-NMR) experiments were thankfully performed by [redacted] using a 5 mm BBI ^1H/X z-gradient probe with a gradient strength of 5.350 [G/mm] on a Bruker Avance-III 700 NMR Spectrometer. The gradient strength of probes was calibrated by analysis of a sample of $^2H_2O/^1H_2O$ at a defined temperature and compared with the theoretical diffusion coefficient of $^2H_2O/^1H_2O$ (values taken from Bruker diffusion manual) at 298.3 K. The temperature was held constantly at 25 °C and defined with a standard ^1H methanol NMR sample. The control of the temperature was realized with a VTU (variable temperature unit) and an accuracy of +/- 0,1 K, which was checked with the standard Bruker Topspin 3.1 software.

In this work, the diffusion time (d20) was optimized for the BBI probe to 60 ms while the gradient pulse length was kept at 2.0 ms. The optimization was realized by comparing the remaining intensity of the signals at 2% and 95% gradient strength. The intensity loss of the

echo was in the range of 90 %. Using longer diffusion time, a loss of signal intensity (from the echo) occurred due to a short spin lattice relation time (T_1), which was measured with the inversion recovery method[3] before the diffusion measurements were made. The diffusion measurements were done with a 2D DOSY sequence[4] by incrementing in 32 linear steps from 2% to 100% with the BBI probe and 16 gradient linear steps with the diffusion probe. The 2D NMR sequences for measuring diffusion coefficient using echoes for convection compensation and longitudinal eddy current delays to store the magnetization in the z-axis, and only be dependent on T_1-relaxation. The calculation of the diffusion value was automatically done with the mono exponential function:[5]

$$\ln\left(\frac{I(G)}{I(0)}\right) = -\gamma^2\delta^2G^2\left(\Delta - \frac{\delta}{3}\right)D$$

where I(G) and I(0) are the intensities of the signals with and without gradient, γ the gyromagnetic ratio of the nucleus (^{1}H in this measurements), G is the gradient strength, δ the duration of the pulse field gradient (PFG), D the diffusion value in m^2/s and Δ the "diffusion time" between the beginning of the two gradient pulses. The relaxation delay between the scans was 2s. Denoted mobilities μ equal measured diffusion coefficients D divided by k_BT with T = 298 K. Hydrodynamic radii r_H were calculated from measured diffusion coefficients D via the *Einstein-Stokes* relation.[6]

Dielectric spectroscopy measurements were thankfully performed by [redacted], University of Ioannina, in a liquid sample cell (Novocontrol BDS1308) consisting of two gold-coated electrodes with 20 mm in diameter. Teflon spacers having a thickness of 100 µm were used between the electrodes**.** For each measurement approximately 0.5 mL solution was necessary to fill the sample cell. Different concentrations of the salts in THF were used with concentrations in the range from 10^{-5} to 10^{-1} M and the linear concentration regime was established (**Figure 8-1**).

Once the solution was placed in the liquid sample cell the temperature was immediately dropped to 173 K to avoid any possible solvent evaporation. The dielectric measurements were performed in a cryostat at different temperatures in the range from 173.15 to 293.15 K at atmospheric pressure, and for frequencies in the range from 10^{-2} – 10^7 Hz using a Novocontrol High Resolution Alpha Analyzer. Temperature was controlled by a Novocontrol

Quatro Cryosystem, which uses N_2 to heat and cool the sample with an accuracy of +/- 0.1 K.

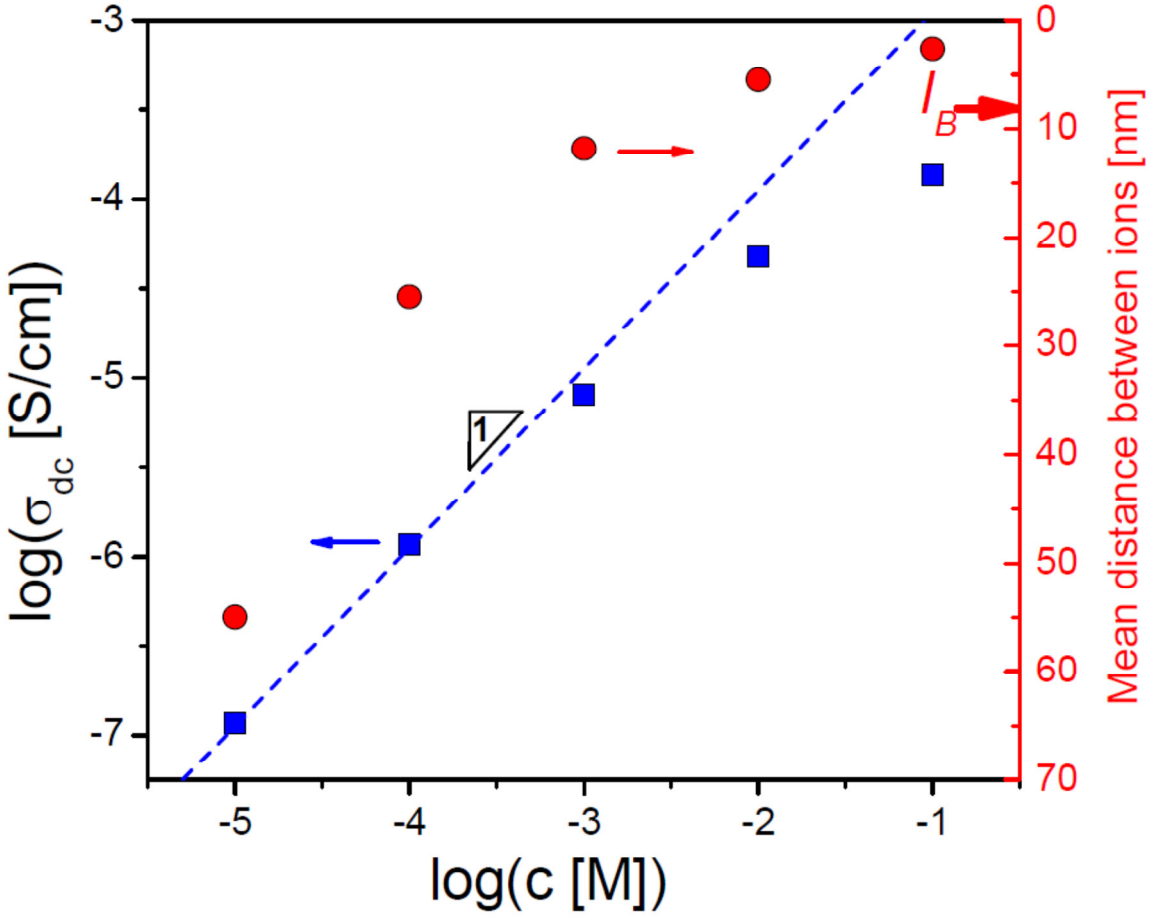

Figure 8-1: (Left) Concentration dependence of the dc-conductivities of **4-11** in THF solutions at 243.15 K. **A** line with slope 1 is shown. (Right) Concentration dependence of the mean-distance between molecular ions. The Bjerrum length in THF is shown with an arrow.

The complex dielectric function, $\varepsilon^* = \varepsilon' - i\varepsilon''$, where ε' is the real and ε'' is the imaginary part, is in general, a function of frequency f (or the radial frequency $\omega = 2\pi f$), temperature T, and pressure P, $\varepsilon^* = \varepsilon^*(\omega,T,P)$. $\varepsilon^*(\omega)$, is related to the complex electric conductivity, $\sigma^*(\omega)$, through

$$\sigma^*(\omega) = \sigma' + i\sigma'' = i\omega\varepsilon\,\varepsilon^*(\omega) \Rightarrow \sigma' = \omega\varepsilon_0\varepsilon'',\ \sigma'' = \omega\varepsilon_0\varepsilon'$$

For pure electronic conduction no contribution arises to ε' while $\varepsilon''(\omega)=\sigma_{dc}/\varepsilon_0\omega$ increases linearly with decreasing frequency. The "transition" from dc- to ac-conductivity is given by a frequency independent to a frequency-dependent $\sigma'(\omega)$. After having established the critical frequency, measurements at a fixed frequency (f ~ 17 kHz) were made over the same

temperature range with a heating/cooling rate of 5 K/min. **Figure 8-2** shows the temperature dependence of the dc-conductivities.

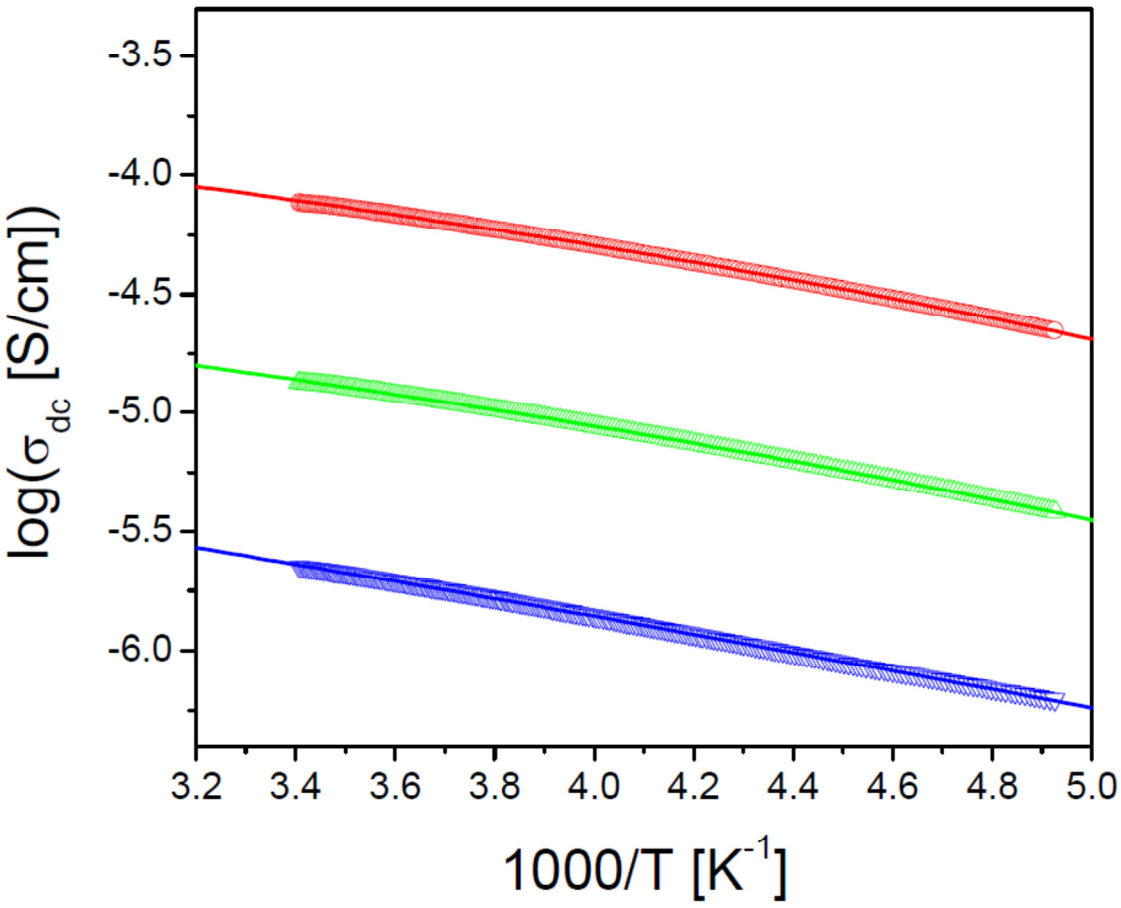

Figure 8-2: Temperature dependence of the dc-conductivities of **4-11** in 10^{-2} M (circles), 10^{-3} M (up triangles) and 10^{-4} M (down triangles) THF solutions. Lines are fits to the VFT equation.

Field desorption (FD) mass spectrometry was performed on a VG Instruments ZAB 2-SE-FPD using 8 kV accelerating voltage. MALDI-TOF mass spectrometry was performed by [redacted] on a Bruker Reflex spectrometer with a 337 nm nitrogen-laser, calibrated with poly ethylene glycol (3000 g/mol). Samples for MALDI-TOF MS were prepared by mixing the analyte with dithranol as matrix in THF or DCM in a ratio of 1/250. Negatively charged ions were detected using the appropriate polarity of the field.

Thermogravimetric analyses (TGA) and differential scanning calorimetry (DSC) measurements were performed on a Mettler TG 50 device by [redacted].

Single crystal diffraction data were recorded using a STOE IPDS2T diffractometer by [redacted]. Data were collected at 193 K using graphite-monochromated Mo Kα radiation (λ_α = 0.71073 Å). The strategy for the data collection was evaluated by using the STOE software. The data were collected by the standard omega scan techniques, and were scaled and reduced using XRED software. The structures were solved by direct methods using SIR-2004, and refined by full matrix least-squares with SHELXL-2014, refining on F^2. The positions of all the atoms were obtained by direct methods. All non-hydrogen atoms were refined anisotropically. The remaining hydrogen atoms were placed in geometrically constrained positions, and refined with isotropic temperature factors, generally 1.2U_{eq} of their parent atoms.

Elemental analyses of solid samples were performed on a Foss Heraeus Vario EL and measured as service at the Institute of Organic Chemistry, University of Mainz. All samples were dried over night at high vacuum (10^{-3} mbar, rt) in order to remove any traces of solvent molecules. The values for polyphenylene dendrimers exhibited deviations > 0.40 % from the calculated elemental composition due to the property of dendrimers to act as host-molecules. Thus, the complete removal of residual solvents and atmospheric gases (N_2, CO, CO_2, H_2O) was not possible for all samples. Compounds with high content of carbon tend to combust in an incomplete manner.

Melting points were recorded using a Büchi B-545 melting point apparatus (Flawil, Switzerland) with a heating rate of 5 °C/min.

8.2 Syntheses

Synthesis protocol of substances from chapter 3

((4-Bromophenyl)ethynyl)trimethylsilane (3-1)

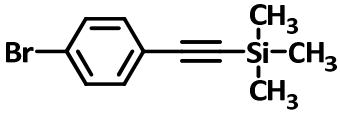

20.0 g (70 mmol) 1-bromo-4-iodobenzene, 1.83 g (7 mmol) PPh_3, 1.33 g (7 mmol) CuI and 2.45 g (3.5 mmol) $Pd(PPh_3)_2Cl_2$ were dissolved in a mixture of 150 mL triethylamine and 150 mL toluene. The mixture was cooled to 0 °C under argon. Then 7.1 g (10.3 mL, 72.3 mmol) TMS-acetylene was added dropwise over 30 min. Afterwards the mixture was allowed to warm to room temperature overnight. Water was added to the reaction mixture and the organic phase was washed with saturated NH_4Cl (aq), 1 N HCl (aq), 10 % Na_2CO_3, and dried over Na_2SO_4. After evaporation of the solvent under reduced pressure, the crude product was purified by column chromatography using hexane as eluent to yield 23.3 g (92 % yield) of the pure compound as colorless needles (after recrystallization from EtOAc).

^{1}H-NMR (300 MHz, CD_2Cl_2, 298 K) δ 7.35 (d, 2 H, *J* = 8.2 Hz), 7.14 (d, 2 H, *J* = 8.2 Hz), 0.26 (s, 9 H, TMS).

^{13}C-NMR (76 MHz, CD_2Cl_2, 298 K) δ 139.20, 132.00, 129.35, 120.39, 105.51, 93.50, 0.29.

FDMS (m/z): calcd. for $C_{11}H_{13}BrSi$: 253.21, found: 253.4 [M+] bromo isotope pattern; white crystalline solid (yield 92 %).

Melting point: 112 °C (uncorrected); literature: 115 – 116 °C.[7]

Tris(4-((trimethylsilyl)ethynyl)phenyl)phosphine (3-2)

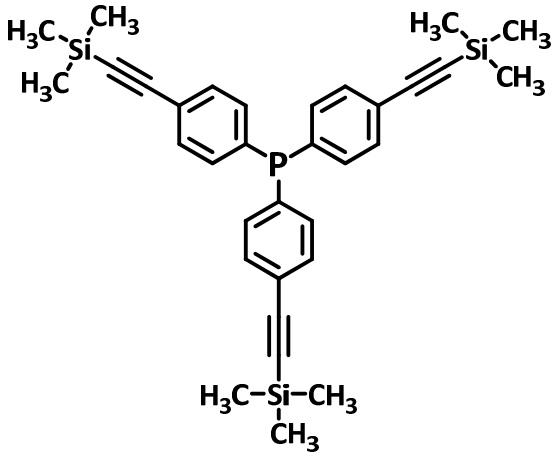

A 250 mL round bottom flask was charged with ((4-bromophenyl)ethynyl)trimethylsilane (12.65 g, 50 mmol) and dissolved in 40 mL dry THF. After cooling to – 78 °C with an acetone dry ice bath, 31.25 mL n-butyllithium (1.6 M solution in hexane, 50 mmol) was added dropwise to the solution at that temperature. The mixture was stirred at -78 °C under argon atmosphere for 1 h. After that time 2.3 g phosphorus trichloride (8.3 mL, 2.0 M solution in DCM, 16.6 mmol) was added dropwise. Stirring overnight at RT completed the reaction. Saturated brine solution (20 mL) was added to the mixture and the organic phase was dried over $MgSO_4$. After evaporation of the solvent under reduced pressure, the crude product was purified by column chromatography using a mixture of hexane : ethylacetate (4 : 1) as eluent to yield 7.85 g (86 %) of the pure target compound as a white solid.

^{1}H-NMR (300 MHz, CD_2Cl_2, 298 K) δ 7.45 (dd, $^3J_{HH}$ = 8.4 Hz, 4JPH = 1.7 Hz, 6 H), 7.23 (dd, $^3J_{PH}$ = 7.9 Hz, $^3J_{HH}$ = 7.74 Hz, 6 H), 0.27 (s, 27 H, TMS).

13C-NMR (76 MHz, CD_2Cl_2, 298 K) δ 137.60 (d, $^3J_{PC}$ = 13.9 Hz) 133.98 (d, $^3J_{PC}$ = 20.3 Hz), 132.21(d, $^2J_{PC}$ = 6.6 Hz), 124.30, 104.81, 96.43, 0.02.

^{31}P-NMR (202 MHz, CD_2Cl_2, 298 K) δ -5.13 ppm.

FDMS (m/z): calcd. for $C_{33}H_{39}PSi_3$: 550.89, found: 550.78 [M+]; white solid (yield 86%).

Melting point: 202.4 °C

Elemental analysis: found: 71.97 % C, 7.06 % H (calculated: 71.95 % C, 7.14 % H)

Tris(4-ethynylphenyl)phosphine (3-3)

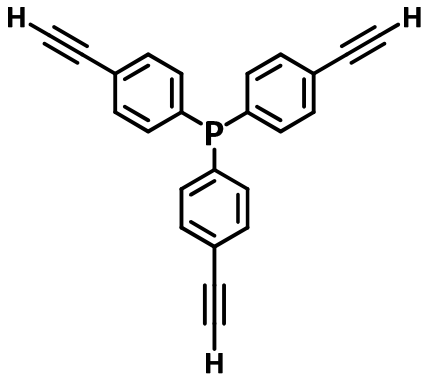

5.5 g of tris(4-((trimethylsilyl)ethynyl)phenyl)phosphine (10 mmol) was dissolved in a mixture of DCM and MeOH (100 mL, 1:1 v/v). 552 mg K_2CO_3 (50 mmol) was added in portions and the mixture was stirred at room temperature under argon atmosphere for 5 h. The reaction mixture was diluted with additional 50 mL DCM and the organic phase was washed with water (2 x 20 mL) and dried over $MgSO_4$. After removal of the solvent under reduced pressure the crude product was purified by column chromatography using a mixture of hexane : ethylacetate (9:1) as eluent to yield 3.15 g (96 %) of the pure compound as a white solid.

^{1}H-NMR (300 MHz, CD_2Cl_2, 298 K) δ 7.41 (dd, $^3J_{HH}$ = 8.6 Hz, $^4J_{PH}$ = 1.9 Hz, 6 H), 7.19 (dd, $^3J_{PH}$ = 8.3 Hz, $^3J_{HH}$ = 7.5 Hz, 6 H), 3.09 (s, 3 H, ethynyl).

^{13}C-NMR (76 MHz, CD_2Cl_2, 298 K) δ 138.21 (d, 3JPC = 14.01 Hz) 134.12 (d, $^3J_{PC}$ = 19.9 Hz), 132.07(d, $^2J_{PC}$ = 7.3 Hz), 125.28, 105.67, 97.69.

^{31}P-NMR (202 MHz, CD_2Cl_2, 298 K) δ - 5.42.

FDMS (m/z): calcd. for $C_{24}H_{15}P$: 334.35, found: 333.98 [M+].

Melting point: 62.3 °C

4-Ethynylbenzenediazonium tetrafluoroborate (3-4)

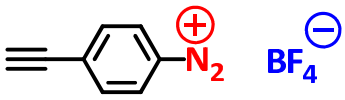

1.17 g of 4-ethynylaniline (10 mmol) was dissolved in 30 mL dry DCM and cooled to – 20 °C. To the solution was added dropwise 3.55 g bortrifluoride diethyletherate (3.2 mL, 25 mmol) and 2.06 g tert-butyl nitrite (2.4 mL, 20 mmol) over 30 min. The mixture was stirred at – 20 °C for 2 h and then allowed to slowly warm to room temperature. Slow addition of Et_2O (50 mL) followed by filtration of the precipitate yielded the crude product, which was further purified by dissolving the slightly brown solid in acetone and dropping it into cold Et_2O. The final product was filtered off, dried under vacuo for 12 h and was used without further purification for the next synthetic step.

Yield: 1.95 g (90 %) of a brown-white solid.

Tetrakis(4-ethynylphenyl)phosphonium tetrafluoroborate (3-5)

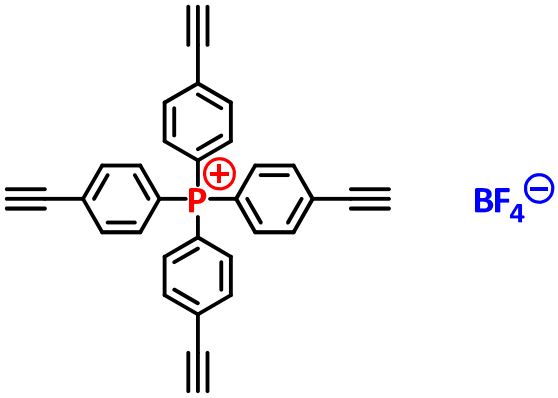

A microwave vial was charged with 668 mg tris(4-ethynylphenyl)phosphine (2 mmol), 450 mg of 4-ethynylbenzenediazonium tetrafluoroborate (2.2 mmol) and 6 mL of toluene (dry). The vial was sealed with an alumina cap and the solvent was thoroughly degassed by repeated freeze-pump-thaw technique. The reaction mixture was heated to 70 °C for 5 h. After removal of the solvent under reduced pressure the crude product was purified by column chromatography using a mixture of DCM and THF (4:1) as eluent. The residue was taken up in a minimum amount of DCM, precipitated Et_2O, filtered and dried to yield 700 mg (67 %) of the pure compound as a white solid.

^{1}H-NMR (700 MHz, CD_2Cl_2, 298 K) δ 7.89 – 7.50 (m, 8 H), 3.46 (s, 4 H).

^{13}C-NMR (76 MHz, CD_2Cl_2, 298 K) δ 146.89, 145.89, 144.09, 141.23, 137.18, 136.26, 135.97 (d, $^{3}J_{PC}$ = 10.3 Hz), 135.15 (d, $^{3}J_{PC}$ = 10.6 Hz), 131.67, 131.44, 131.23 (d, $^{2}J_{PC}$ = 13.0 Hz), 130.58 (d, $^{2}J_{PC}$ = 13.3 Hz), 129.90, 129.34, 128.75, 128.70, 128.20, 127.88, 127.61, 126.93, 126.79, 126.39, 125.74, 118.31, 118.14.

^{31}P-NMR (202 MHz, CD_2Cl_2, 298 K) δ 23.15 ppm.

MALDI-TOF (m/z): calcd. for $C_{32}H_{20}P^{+}$: 435.47, found: 435.11 [M^{+}].

Phosphonium-G1 tetrafluoroborate (3-6)

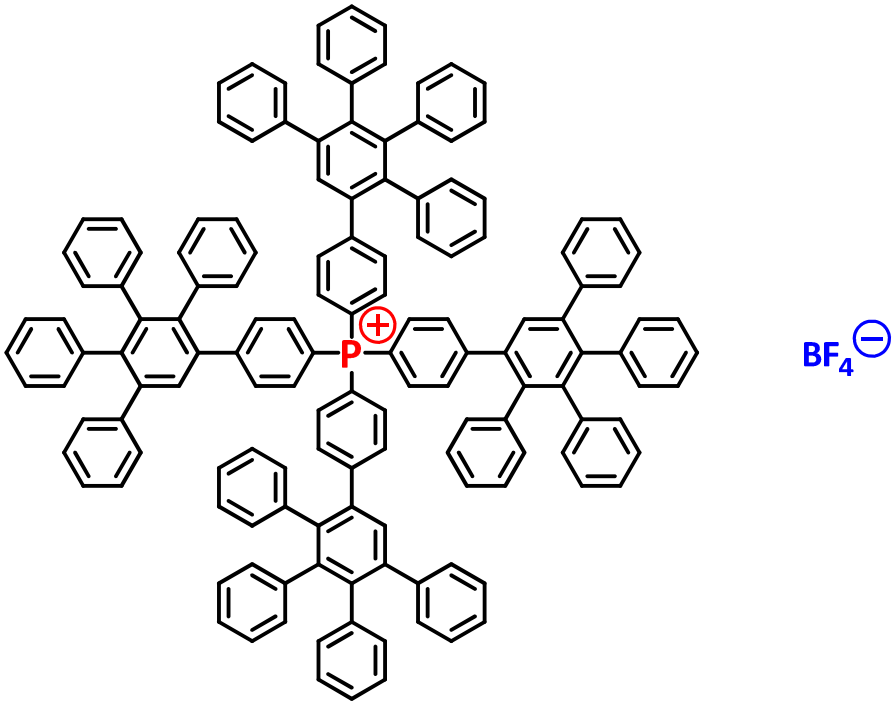

522 mg (1 mmol) of tetrakis(4-ethynylphenyl)phosphonium tetrafluoroborate and 1.7 g tetraphenylcyclopentadienone (4.4 mmol) were dissolved in o-xylene (15 mL) in a microwave tube. The vial was sealed and degassed by freeze-pump-thaw technique. The mixture was heated to 165 °C in an oil bath and stirred for 6 h. After cooling to room temperature the mixture was purified by column chromatography using firstly a mixture of hexane and ethyl acetate (4:1) and then a mixture of DCM and THF (4:1) as eluent. After removal of the solvent, the crude product was dissolved in methylene chloride, precipitated in Et_2O, filtered and dried in vacuum to afford 1.52 g (0.78 mmol, 78 %) pure target compound as a beige powder.

^{1}H-NMR (700 MHz, CD_2Cl_2, 298 K) δ 7.59 (s, 4 H), 7.48 – 7.47 (dd, $^{3}J_{HH}$ = 8.5 Hz, $^{4}J_{PH}$ = 3.2 Hz, 8 H), 7.33 – 7.30 (dd, $^{3}J_{PH}$ = 13.5 Hz, $^{3}J_{HH}$ = 8.1 Hz, 8 H), 7.23 – 7.16 (m, 20 H), 7.00 –6.87 (m, 60 H).

^{13}C NMR (176 MHz, CD_2Cl_2) δ 142.00, 140.66, 140.21, 139.04, 138.87, 132.02,131.87, 131.82, 131.45, 131.18, 130.79, 130.26, 120.71, 120.66, 120.21, 119.93, 119.79, 119.74.

^{31}P-NMR (202 MHz, CD_2Cl_2, 298 K) δ 21.97 ppm.

ESI-MS (m/z): calcd. for $C_{144}H_{100}P^{+}$: 1861.31, found: 1861.01 [M+].

Phosphonium-((ethinyl-TIPS)$_8$)-G1 tetrafluoroborate (3-8)

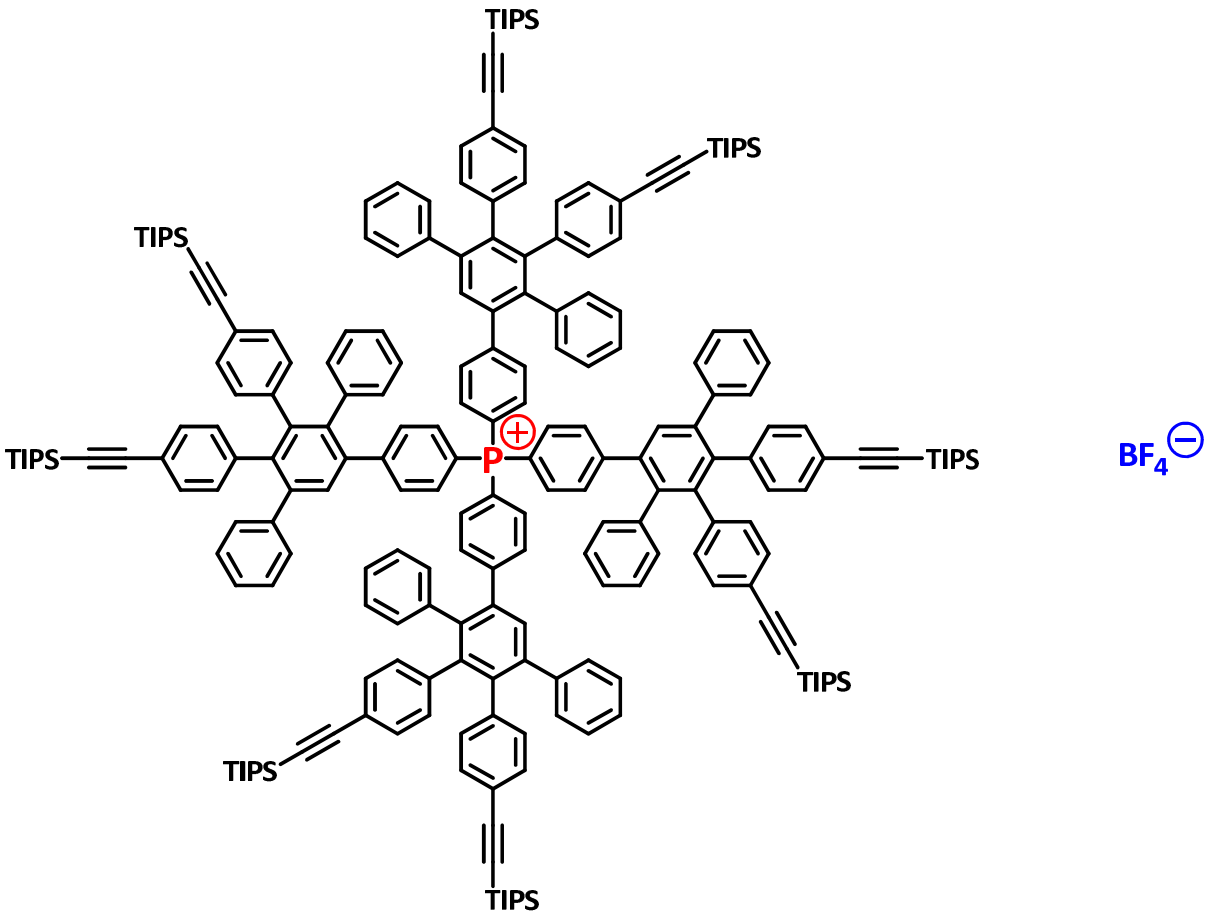

522 mg (1 mmol) of tetrakis(4-ethynylphenyl)phosphonium tetrafluoroborate **(3-5)** and 3.28 g AB_2 building block (4.4 mmol) were dissolved in o-xylene (25 mL) in a microwave tube. The vial was sealed and degassed by freeze-pump-thaw technique. The mixture was heated to 165 °C in an oil bath and stirred for 6 h. After cooling to room temperature the mixture was purified by column chromatography using a mixture of hexane and ethyl acetate (4:1) and then a mixture of DCM and THF (4:1) as eluent. After removal of the solvent, the crude product was dissolved in methylene chloride, precipitated in Et_2O, filtered and dried in vacuum to afford 2.61 g (0.73 mmol, 73 % yield) pure target compound as a beige powder.

^{1}H-NMR (700 MHz, CD_2Cl_2, 298 K) δ 7.53 (s, 4 H), 7.24 – 6.95 (m, 52 H), 6.86 – 6.79 (m, 28 H), 1.09 (s, TIPS, 168 H).

^{13}C NMR (176 MHz, CD_2Cl_2, 298 K) δ 142.53, 141.66, 140.74, 139.89, 139.37, 132.25, 131.61, 130.98, 130.68, 130.18, 121.41, 120.86, 120.21, 119.84, 119.72, 119.36, 19.15(CH), 12.03 (CH_3).

^{31}P-NMR (202 MHz, CD_2Cl_2, 298 K) δ 22.17 ppm.

ESI-MS (m/z): calcd. for $C_{232}H_{260}Si_8P^+$: 3302.83, found: 3302.02 [M^+].

Phosphonium-(ethinyl)$_8$)-G1 tetrafluoroborate (3-9)

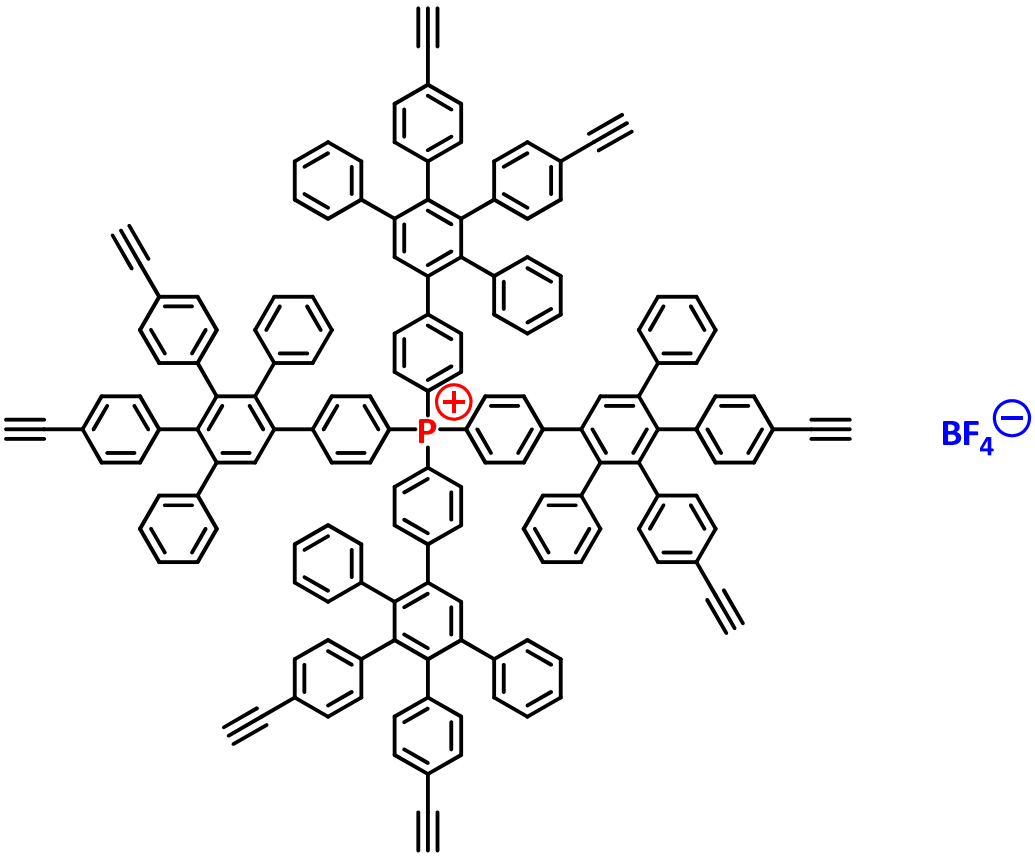

To a solution of 1.69 g (0.5 mmol) of phosphonium-((ethinyl-TIPS)8)-G1 tetrafluoroborate **(3-8)** in 25 mL dry DCM was added dropwise a solution of tetrabutylammonium fluoride (2 mL, 1.0 M in THF, 2 mmol) in THF (25 mL). The mixture was stirred at – 20 °C for 2 h under argon. After washing 6 times with a concentrated aqueous solution of sodium chloride, the solution was filtered over silica and the solvent removed under vacuum. The remainder was dissolved in methylene chloride, precipitated in hexane, filtered and dried to afford 812 mg (0.38 mmol, 77 % yield) of the product as white powder.

^{1}H-NMR (700 MHz, CD_2Cl_2, 298 K) δ 7.54 (s, 4 H), 7.23 – 6.94 (m, 52 H), 6.84 – 6.76 (m, 28 H), 4.31 (s, ethynyl, 4 H).

^{13}C NMR (176 MHz, CD_2Cl_2, 298 K) δ 145.66, 141.44, 141.27, 140.96, 140.59, 139.73, 139.57, 139.32, 131.78, 131.23, 130.97, 130.19, 128.17, 127.52, 127.03, 126.48, 119.94, 119.67, 83.74 (ethynyl), 77.37 (ethynyl).

^{31}P-NMR (202 MHz, CD_2Cl_2, 298 K) δ 22.34 ppm.

MALDI-TOF (m/z): calcd. for $C_{160}H_{100}P^+$: 2052.76, found: 2053.05 [M^+].

Phosphonium-G2 tetrafluoroborate (3-10)

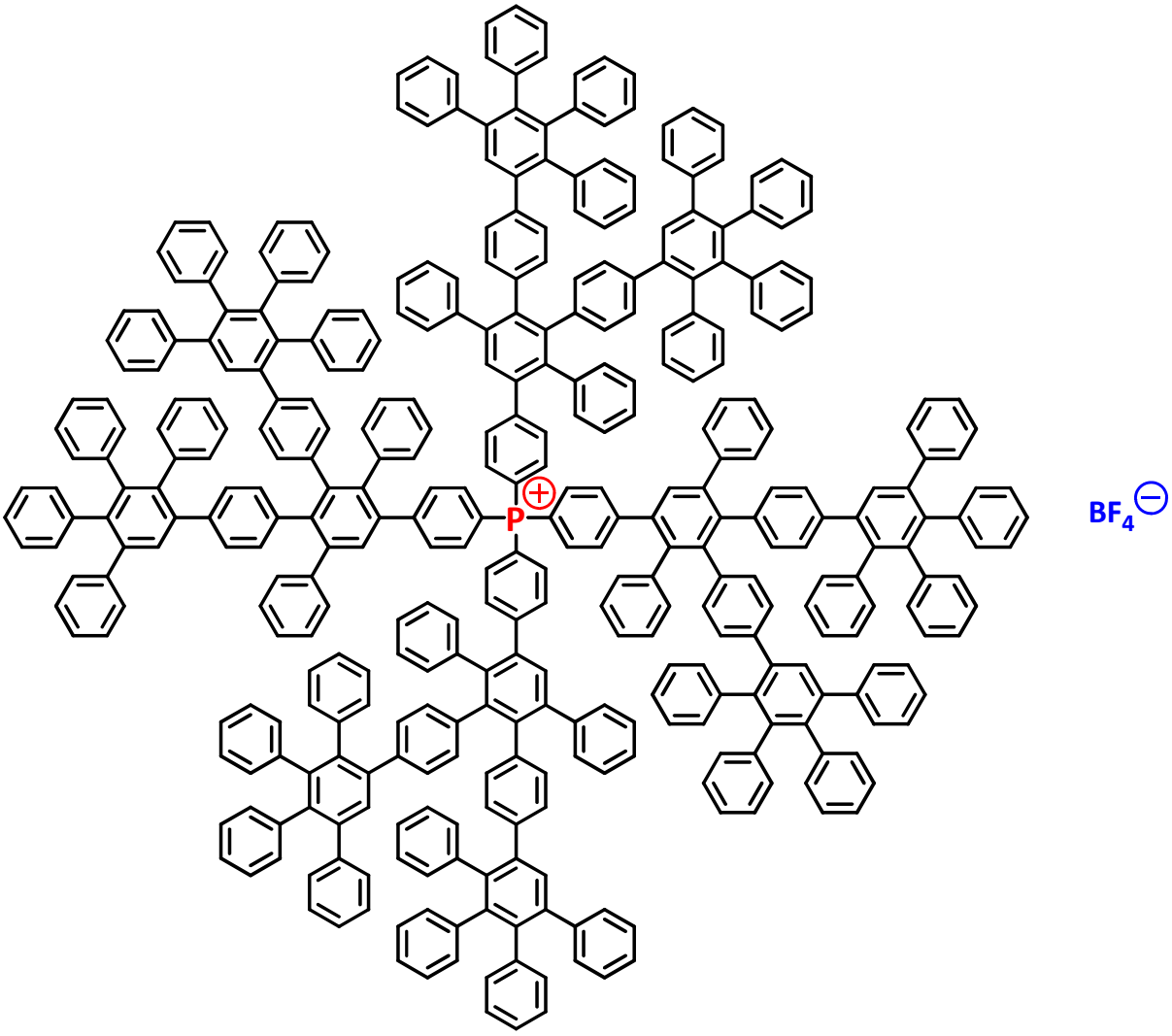

214 mg (0.1 mmol) of phosphonium-(ethinyl)8)-G1 tetrafluoroborate **(3-9)** and 338 mg tetraphenylcyclopentadienone (0.88 mmol) were dissolved in o-xylene (3 mL) in a microwave vial. The vial was sealed and degassed by freeze-pump-thaw technique. The mixture was heated to 165 °C in an oil bath and stirred for 16 h. After cooling to room temperature the mixture was purified by column chromatography using firstly a mixture of hexane and ethyl acetate (4:1) and afterwards a mixture of DCM and THF (4:1) as eluent. After removal of the solvent, the crude product was dissolved in methylene chloride, precipitated in Et_2O, filtered and dried in vacuum to afford 403 mg (0.08 mmol, 61 %) pure target compound as a beige powder.

^{1}H-NMR (700 MHz, CD_2Cl_2, 298 K) δ 7.56-7.32 (m, 12 H), 7.24 – 7.09 (m, 60 H), 6.99 – 6.49 (m, 172 H).

^{13}C NMR (176 MHz, CD_2Cl_2, 298 K) δ 142.26, 142.11, 141.29, 141.11, 140.98, 140.59, 140.41, 139.85, 139.77, 139.65, 139.52, 139.02, 138.34, 135.78, 131.89, 131.44, 131.04, 130.29, 129.80, 129.65, 129.05, 128.69, 128.51, 128.33, 127.99, 127.89, 127.65, 127.19, 126.85, 126.59, 125.94, 125.63, 124.27.

^{31}P-NMR (202 MHz, CD_2Cl_2, 298 K) δ 23.54 ppm.

MALDI-TOF (m/z): calcd. for $C_{384}H_{260}P^+$: 4905.02, found: 4904.85 [M^+].

Phosphonium-((ethinyl-TIPS)$_{16}$)-G2 tetrafluoroborate (3-11)

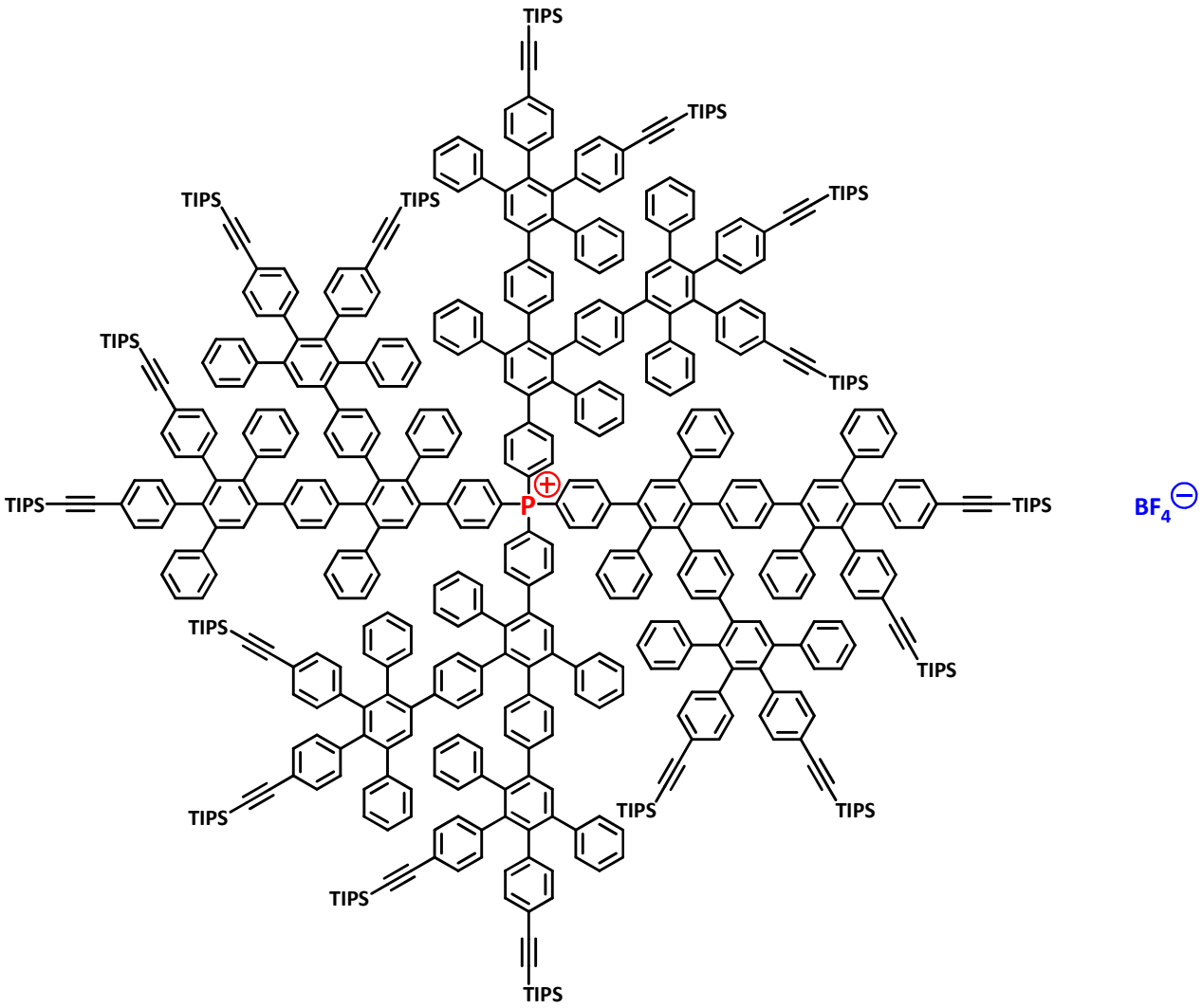

428 mg (0.2 mmol) of phosphonium-(ethinyl)$_8$)-G1 tetrafluoroborate **(3-9)** and 1.31 g AB_2 building block (1.76 mmol) were dissolved in o-xylene (5 mL) in a microwave tube. The vial was sealed and thoroughly degassed by freeze-pump-thaw technique. The mixture was heated to 165 °C in an oil bath and stirred for 16 h. After cooling to room temperature the mixture was purified by column chromatography using a mixture of hexane and ethyl acetate (4:1) and afterwards a mixture of DCM and THF (4:1) as eluent. After removal of the solvent, the crude product was dissolved in methylene chloride, precipitated in Et_2O, filtered and dried in vacuum to afford 1.05 g (0.13 mmol, 67 %) pure compound as a beige powder.

^{1}H-NMR (700 MHz, CD_2Cl_2, 298 K) δ 7.53 – 7.35 (m, 12 H), 7.24 – 6.95 (m, 68 H), 6.86 – 6.79 (m, 164 H), 1.09 (s, TIPS, 336 H).

^{31}P-NMR (202 MHz, CD_2Cl_2, 298 K) δ 22.17 ppm.

MALDI-TOF (m/z): calcd. for $C_{560}H_{580}Si_{16}P^+$: 7790.94, found: 7790.4 [M^+].

Phosphonium-(ethinyl)$_{16}$)-G2 tetrafluoroborate (3-12)

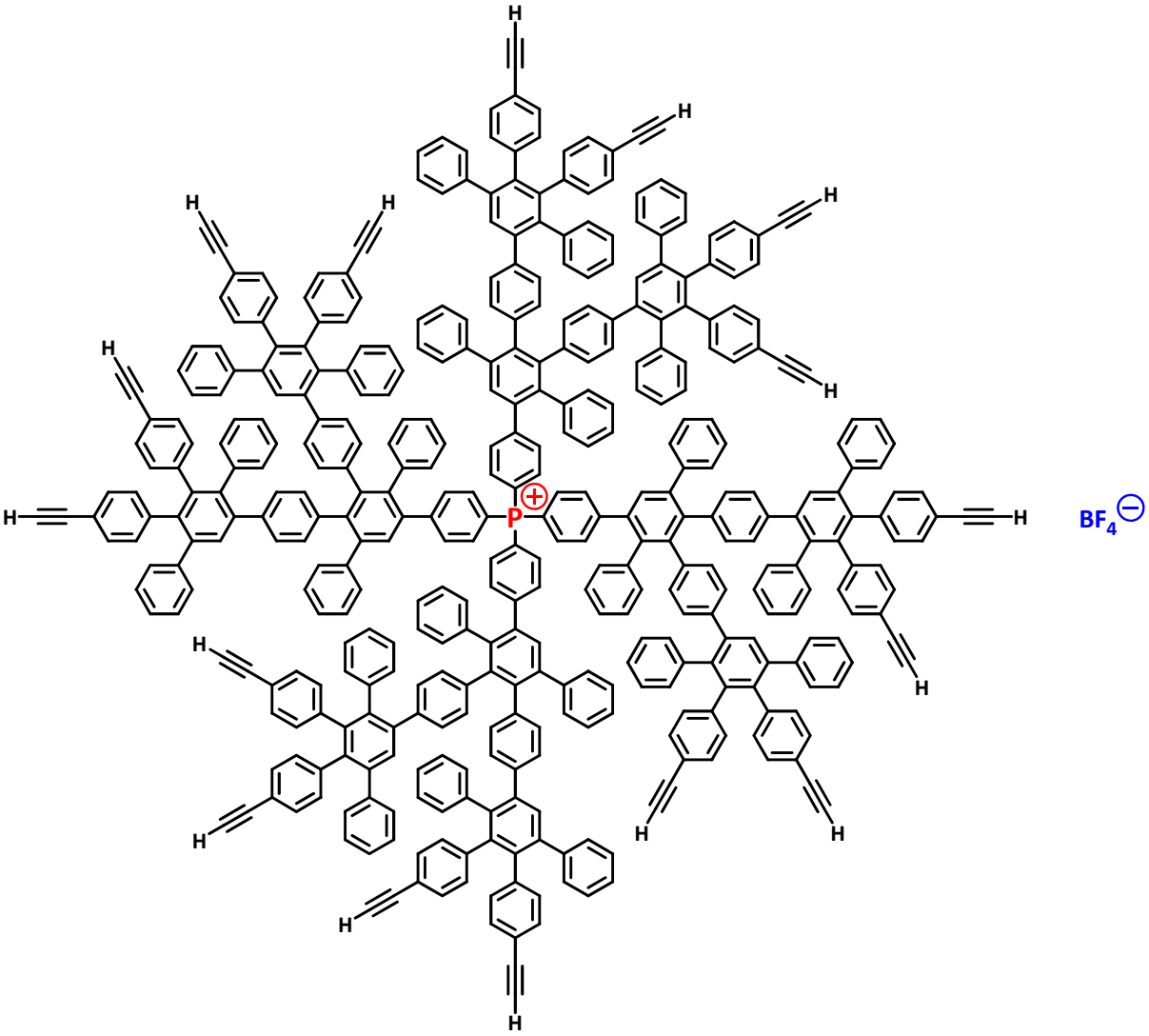

To a solution of 800 mg (0.1 mmol) of phosphonium-((ethinyl-TIPS)$_{16}$)-G2 tetrafluoroborate **(3-11)** in 15 mL dry DCM was added dropwise a solution of tetrabutylammonium fluoride (0.5 mL, 1.0 M in THF, 0.5 mmol) in THF (25 mL). The mixture was stirred for 2 h at -20 °C under argon. After washing 6 times with a concentrated aqueous solution of sodium chloride, the solution was filtered over silica and the solvent removed under vacuum. The remainder was dissolved in methylene chloride, precipitated in hexane, filtered and dried to afford 812 mg (0.38 mmol, 77%) of the product as white powder.

^{1}H-NMR (700 MHz, CD_2Cl_2, 298 K) δ 7.49 – 6.48 (m, 244 H), 4.47 (s, ethynyl, 16 H).

^{31}P-NMR (202 MHz, CD_2Cl_2, 298 K) δ 23.74 ppm.

MALDI-TOF (m/z): calcd. for $C_{416}H_{260}P^+$: 5289.49, found: 5288.85 [M^+].

Phosphonium-G3 tetrafluoroborate (3-13)

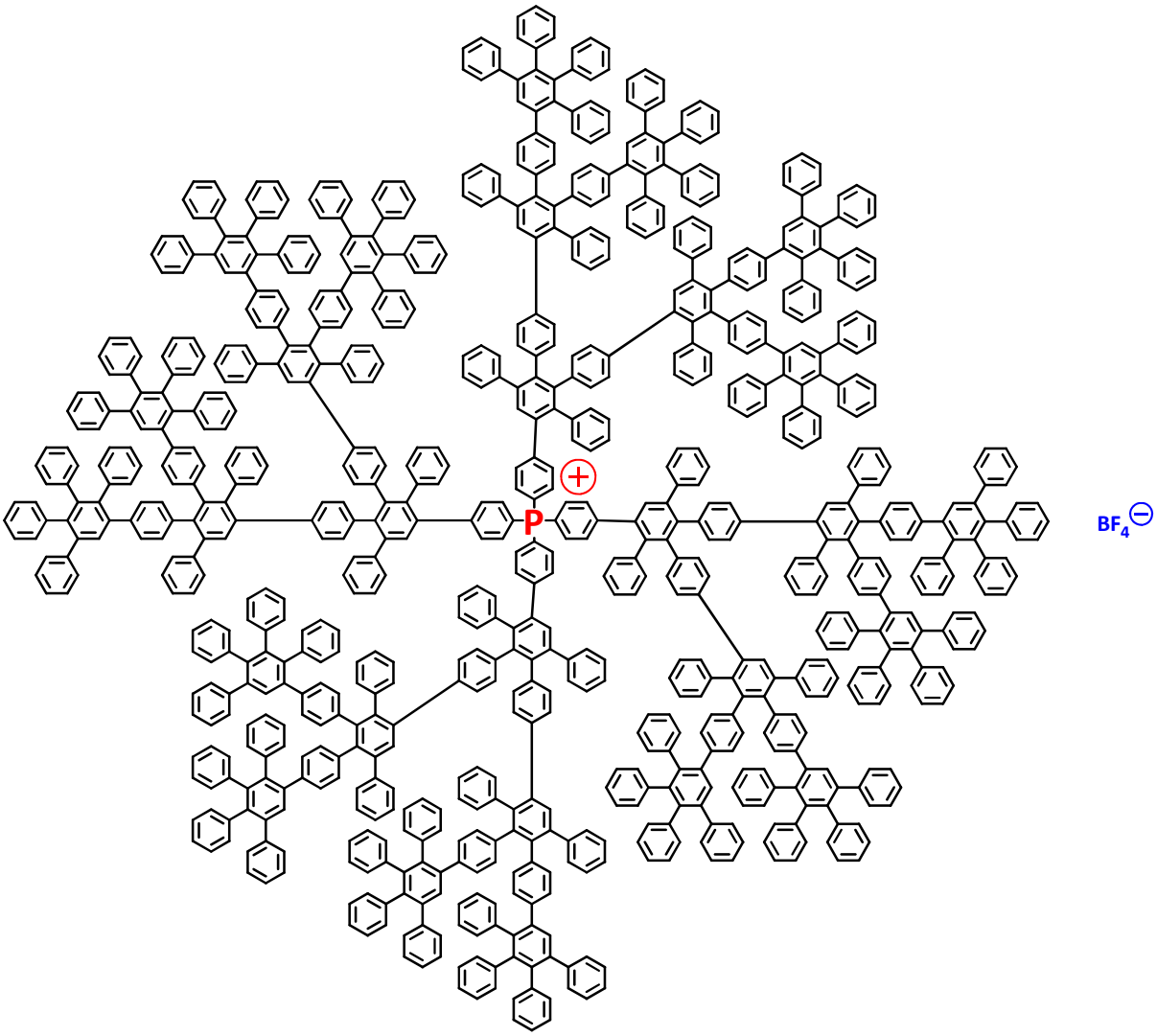

280 mg (0.05 mmol) of phosphonium-(ethinyl)$_{16}$)-G2 tetrafluoroborate **(3-12)** and 338 mg tetraphenylcyclopentadienone (0.88 mmol) were dissolved in o-xylene (3 mL) in a microwave tube. The vial was sealed and degassed by freeze-pump-thaw technique. The mixture was heated to 165 °C in an oil bath and stirred for 36 h. After cooling to room temperature the mixture was purified by column chromatography using a mixture of hexane and ethyl acetate (4:1) and then a mixture of DCM and THF (4:1) as eluent. After removal of the solvent, the crude product was dissolved in methylene chloride, precipitated in Et_2O, filtered and dried in vacuum to afford 370 mg (0.033 mmol, 58 %) pure compound as a beige powder.

^{1}H-NMR (700 MHz, CD_2Cl_2, 298 K) δ 7.53 – 6.42 (m, 580 H).

^{13}C NMR (176 MHz, CD_2Cl_2, 298 K) δ 142.26, 142.11, 141.29, 141.11, 140.98, 140.59, 140.41, 139.85, 139.77, 139.65, 139.52, 139.02, 138.34, 135.78, 131.89, 131.44, 131.04, 130.29, 129.80, 129.65, 129.05, 128.69, 128.51, 128.33, 127.99, 127.89, 127.65, 127.19, 126.85, 126.59, 125.94, 125.63, 124.27.

^{31}P-NMR (202 MHz, CD_2Cl_2, 298 K) δ 21.86 ppm.

MALDI-TOF (m/z): calcd. for $C_{864}H_{580}P^+$: 10983.51, found: 10985.96 [M^+].

Tetraphenylcyclopentadienone-$(CF_3)_8$ (3-22)

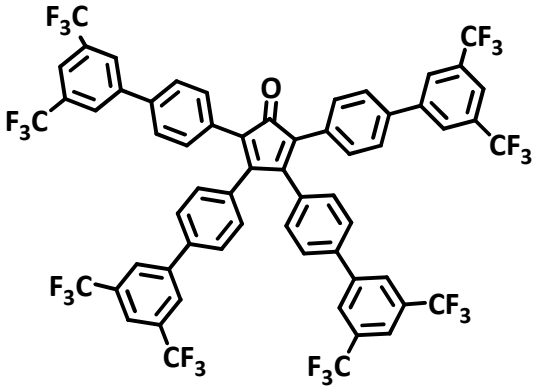

2.1 g (3 mmol) 2,3,4,5-tetrakis(4-bromophenyl)cyclopenta-2,4-dienone and 3.95 g (13.5 mmol) 3,5-bis(trifluoromethyl)phenyl boronic acid were dissolved in 50 mL anhydrous toluene. To this solution were added an aqueous solution of K_2CO_3 (6.62 g in 30 mL, 48 mmol) and 0.5 mL ethanol. After the two-phase system has been degassed and set under argon, 350 mg (0.3 mmol) $Pd(PPh_3)_4$ was added and the mixture was heated to 100 °C for 24 h. The solvent was evaporated afterwards under reduced pressure and the crude product was purified by column chromatography using a mixture of hexane and ethyl acetate (4:1) to afford 3.4 g (92 % yield) of the pure compound as a dark red solid.

^{1}H-NMR (700 MHz, CD_2Cl_2, 298 K) δ 7.92 (s, 8 H, meta-CF_3 aryl), 7.77 (s, 4 H, para-CF_3 aryl), 7.18 – 7.05 (m, 16 H).

^{13}C NMR (176 MHz, CD_2Cl_2, 298 K) δ 155.16 (C quart., C=O), 133.63, 131.39, 130.52, 129.63, 128.81, 128.31, 127.82, 125.85, 124.73, 123.79, 121.59, 121.12.

^{19}F-NMR (470 MHz, CD_2Cl_2, 298 K) δ - 63.71 (s, $^3J_{CF}$ = 278.9 Hz, CF_3).

FDMS (m/z): calcd. for $C_{61}H_{28}F_{24}O$: 1232.84, found: 1232.6 [M^+].

Phosphonium-G1-$(CF_3)_{32}$ tetrafluoroborate (3-23)

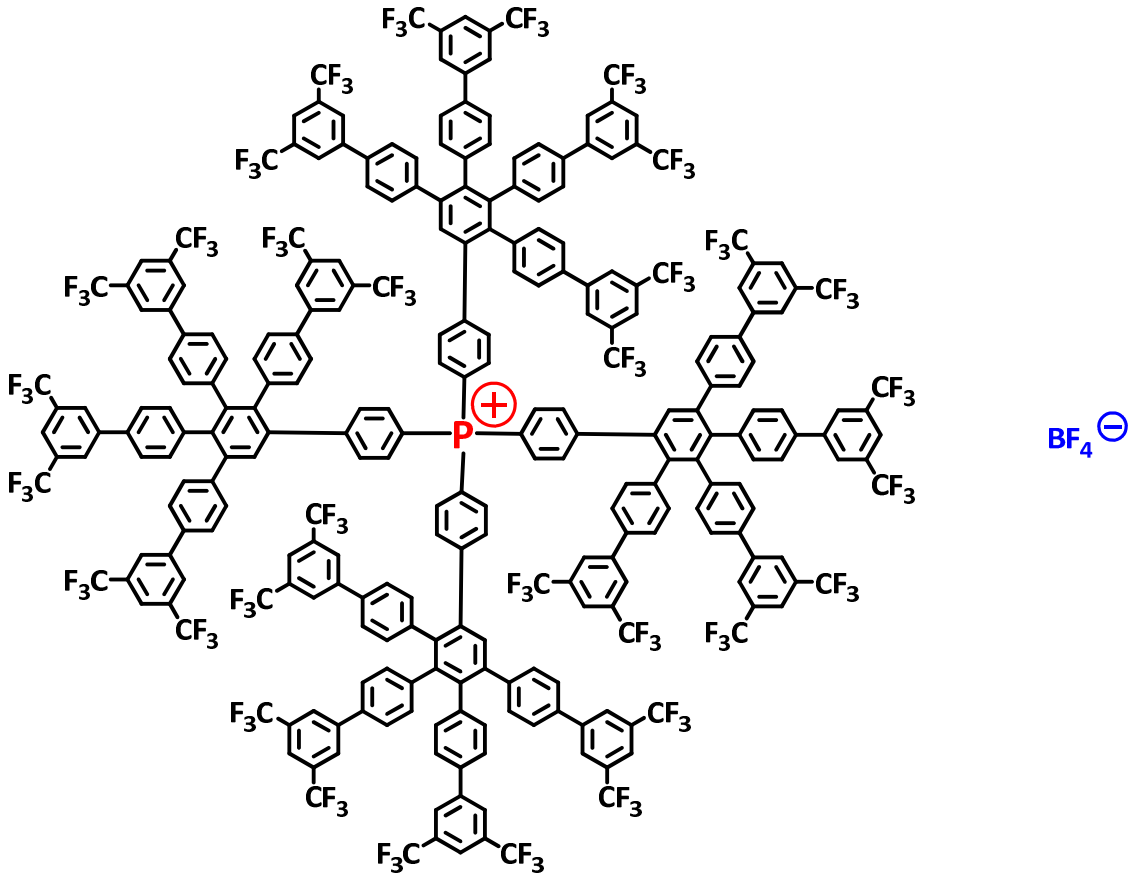

100 mg (0.19 mmol) of tetrakis(4-ethynylphenyl)phosphonium tetrafluoroborate **(3-5)** and 986 mg tetraphenylcyclopentadienone derivative **(3-22)** (0.8 mmol) were dissolved in o-xylene (4 mL) in a microwave tube. The vial was sealed and degassed by freeze-pump-thaw technique. The mixture was heated to 165 °C in an oil bath and stirred for 12 h. After cooling to room temperature the mixture was purified by column chromatography using a mixture of hexane and ethyl acetate (4:1) and then a mixture of DCM and THF (4:1) as eluent. After removal of the solvent, the crude product was dissolved in methylene chloride, precipitated in hexane, filtered and dried in vacuum to afford 702 mg (0.13 mmol, 71 %) pure compound as a beige powder.

^{1}H-NMR (700 MHz, CD_2Cl_2, 298 K) δ 8.01 (s, 32 H, meta CF_3), 7.87 (s, 16 H, para CF_3), 7.78 – 7.64 (m, 32 H), 7.53 (s, 4 H), 7.18 – 6.98 (m, 40 H), 6.77 – 6.69 (dd, $^{3}J_{HH}$ = 8.6 Hz, $^{4}J_{PH}$ = 2.0 Hz, 8 H).

^{13}C-NMR (76 MHz, CD_2Cl_2, 298 K) δ 141.84, 141.66, 141.24, 140.70, 140.04, 139.72, 139.36, 138.19, 136.16, 134.78, 133.45, 132.52, 132.01, 131.77, 130.95, 130.60, 130.29, 130.22, 128.13, 127.96, 127.44, 126.90, 126.77, 126.27, 123.78, 121.63, 120.37, 120.07.

^{31}P-NMR (202 MHz, CD_2Cl_2, 298 K) δ 23.24 ppm.

^{19}F-NMR (470 MHz, CD_2Cl_2, 298 K) δ - 63.43 (s, $^3J_{CF}$ = 278.9 Hz, CF_3).

MALDI-TOF (m/z): calcd. for $C_{272}H_{132}F_{96}P^+$: 5254.8, found: 5255.6 [MH^+].

4-Amino-3',4',5'-triphenyl-1,1':2',1''-terphenyl (3-24), PPD-NH_2

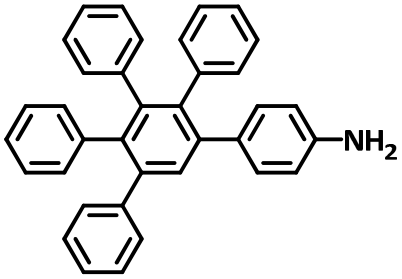

590 mg (5 mmol) of 4-ethynylaniline and 1.96 g (5.1 mmol) of tetraphenylcyclopentadienone were dissolved in 40 mL of o-xylene. The mixture was heated under argon to 155 °C and reacted for 12 h. After that time the solvent was evaporated under reduced pressure and the crude product was adsorbed on silica and purified via column chromatography using a mixture of hexane and ethyl acetate (2:1) as eluent. 2.2 g (94 %) of the pure product were obtained as a beige solid.

^{1}H-NMR (850 MHz, CD_2Cl_2, 298 K) δ 7.50 (s, 1 H), 7.18 – 7.13 (m, 5 H), 6.98 – 6.82 (m, 17 H), 6.48 (d, $^3J_{HH}$ = 8.5 Hz, 2 H, ortho), 3.63 (s, 2 H, NH_2).

^{13}C-NMR (76 MHz, CD_2Cl_2, 298 K) δ 145.55, 142.36, 142.12, 141.08, 140.96, 140.69, 139.55, 139.02, 131.94, 131.84, 131.52, 131.19, 130.31, 127.89, 127.21, 127.16, 126.85, 126.54, 125.86, 125.82, 125.58, 114.44 (CH-aryl, ortho-NH_2).

FDMS (m/z): calcd. for $C_{36}H_{27}N$: 473.61, found: 473.6 [M+].

Melting point: 214.8 °C

Elemental analysis: found: 86.02 % C, 5.03 % H, 7.79 % N (calculated: 86.55 % C, 5.04 % H, 8.41 % N)

4-Azido-3',4',5'-triphenyl-1,1':2',1''-terphenyl (3-25), PPD-N_3

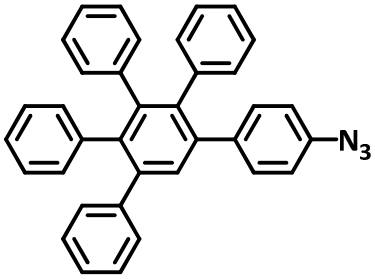

1.42 g (3 mmol) PPD-NH_2 were dissolved in a mixture of acetonitrile and THF (5:1) in a round bottom flask sealed with a rubber septum with a cannula serving as a gas outlet valve. The mixture was cooled to -20 °C. 1.24 g (12 mmol, 4 eq, 1.44 mL) tert-butyl nitrite were added and after 10 minutes stirring at -20 °C, 1.21 g (10.5 mmol, 3.5 eq, 1.39 mL) trimethylsilyl azide were added dropwise. Afterwards the solution was allowed to warm to room temperature and upon that moderate gas evolution was observed indicating the release of N_2. After 2 h no more gas evolved and the solution was adsorbed on silica and purified by column chromatography using a mixture of hexane and ethyl acetate (5:1) as eluent to yield 1.45 g (97 %) of the pure product as a slightly yellow solid.

^{1}H-NMR (850 MHz, CD_2Cl_2, 298 K) δ 7.50 (s, 1 H), 7.17 – 7.15 (m, 8 H), 6.97 – 6.94 (m, 6 H), 6.89 (m, 8 H), 6.84 – 6.82 (m, 4 H).

^{13}C-NMR (76 MHz, CD_2Cl_2, 298 K) δ 142.28, 142.10, 141.25, 140.77, 140.45, 140.38, 140.09, 139.87, 139.68, 138.97, 138.55, 131.85, 131.77, 131.67, 131.41, 130.26, 127.93, 127.35, 127.20, 126.92, 126.67, 126.09, 125.99, 125.71, 118.58 (CH-aryl, ortho-N_3).

FDMS (m/z): calcd. for $C_{36}H_{25}N_3$: 499.6, found: 499.8 [M+].

Elemental analysis: found: 86.77 % C, 6.33 % H, 2.67 % N (calculated: 91.3 % C, 5.75 % H, 2.96 % N; great deviation attributed due to the decomposition of the labile azide group)

Triazole-phosphonium-G1 tetrafluoroborate (3-26)

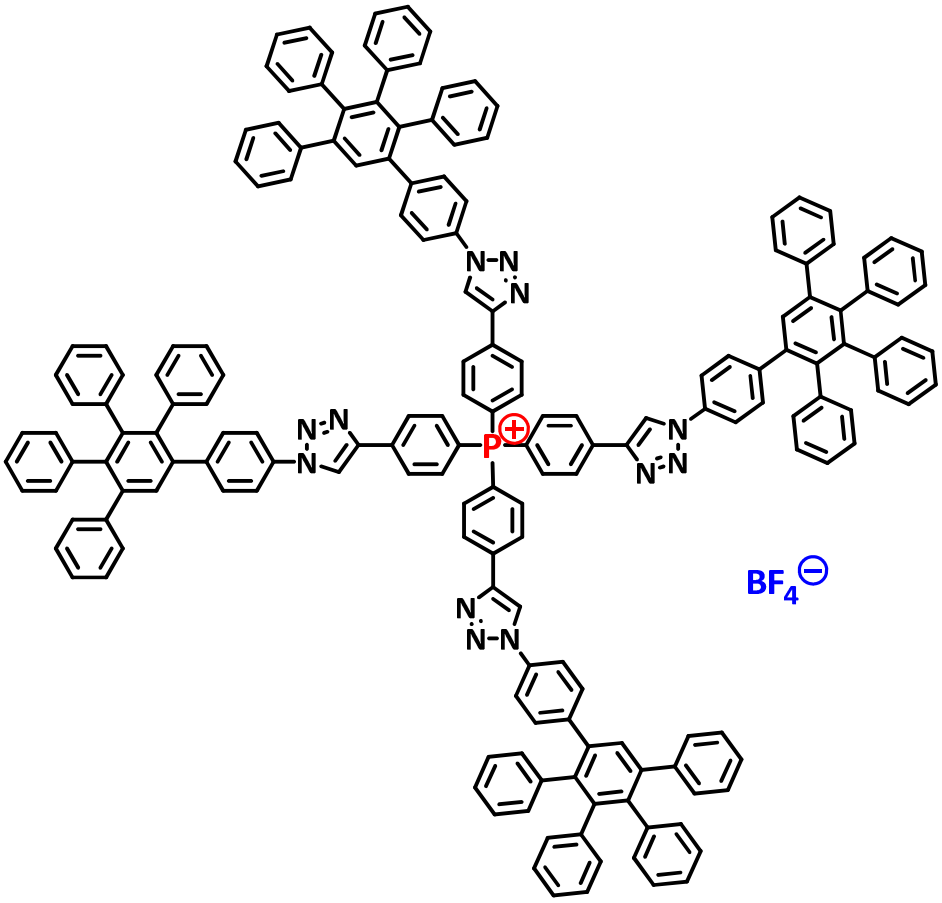

20 mg (0.046 mmol) ethynyl phosphonium core **(3-5)** and 184 mg (0.368 mmol, 8 eq) bulky azide **(3-25)** were dissolved in a mixture of acetonitrile and THF (5:1) in a microwave vial. To the solution were added 10 mg (0.048 mmol) sodium ascorbate, 12 (0.024 mmol) TBTA, 0.5 mL triethylamine and 6 mg (0.024 mmol) $CuSO_4 \cdot 5H_2O$. The suspension was stirred at room temperature for 16 h. Afterwards the mixture was adsorbed on silica and subjected to column chromatography. Initially a mixture of hexane and ethyl acetate (4:1) was used to elute the nonpolar side products as well as excessive azide, then a mixture of DCM and THF (4:1) was used as eluent to yield 96 mg (0.04 mmol, 87 %) of the pure title compound as a yellow solid.

^{1}H-NMR (850 MHz, CD_2Cl_2, 298 K) δ 8.70 + 8.37 (s, 4 H, H_{c1} + H_{c2}), 8.07 – 7.80 (m, $^3J_{HH}$ = 8.2 Hz, 8H, isomer 1 + 2), 7.71 (d, $^3J_{HH}$ = 8.6 Hz, 4 H), 7.66 (d, $^3J_{HH}$ = 8.6 Hz, 4 H), 7.62 (s, generation protons isomer H_{f1} + H_{f2}, 4 H), 7.41 (m, 8 H), 7.24 – 7.21 (m, 20 H), 7.03 – 6.90 (m, 68 H).

^{13}C NMR (126 MHz, CD_2Cl_2, 298 K) δ 146.92, 145.62, 142.89, 142.66, 142.02, 141.59, 141.01, 140.24, 139.95, 139.77, 139.32, 139.17, 137.77, 134.89, 133.98, 132.62, 131.42, 131.37, 131.01, 129.88, 128.18, 127.60, 127.09, 126.86, 126.59, 126.37, 125.87, 125.42, 120.21, 119.52, 118.72, 116.69, 115.96.

^{31}P-NMR (202 MHz, CD_2Cl_2, 298 K) δ 22.29 ppm.

MALDI-TOF (m/z): calcd. for $C_{176}H_{120}N_{12}P^+$: 2433.89, found: 2434.7 [MH^+].

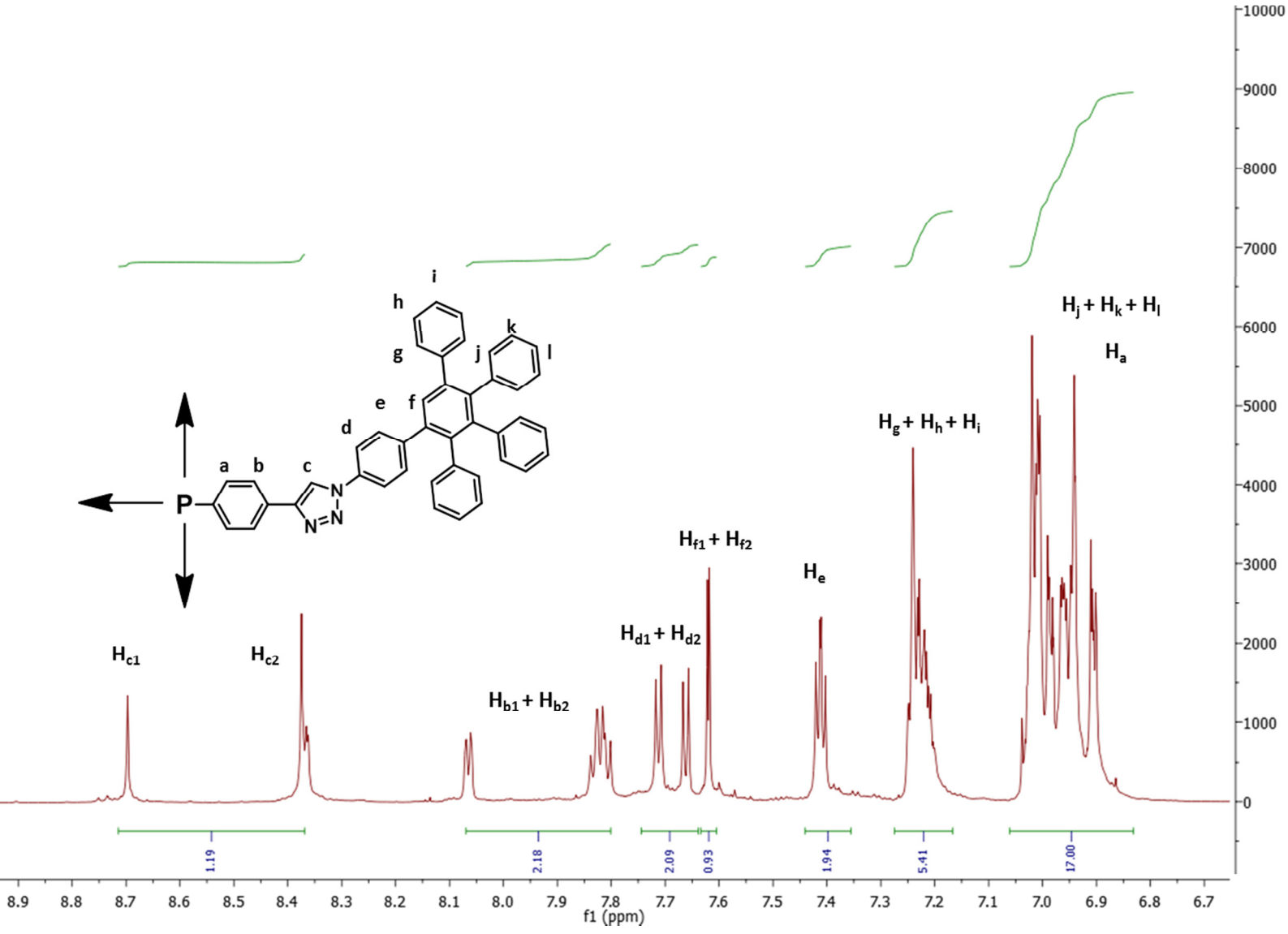

Low-field region of ^{1}H-spectrum (850 MHz, CD_2Cl_2, 298 K) of triazole phosphonium compound **(3-26)**. The complete assignment of the signals was performed with the additional analysis of COSY-, HSQC-, NOESY- and DOSY-NMR spectra. The splitting of the triazole protons and the neighboring ^{1}H cores is attributed to the presence of two atropisomers of compound **(3-26)** in solution, which was most probably the result of blocked rotation in the rigid molecule. This phenomena was also observed for comparable polyphenylene-triazole dendrimers after careful NMR-analysis.

Synthesis protocol of substances from chapter 4

Tetrabutlyammonium tetrakis(2,3,5,6-tetrafluoro-4-(G1)phenyl)borate (4-2), TBA^+ [B^F-G1]-

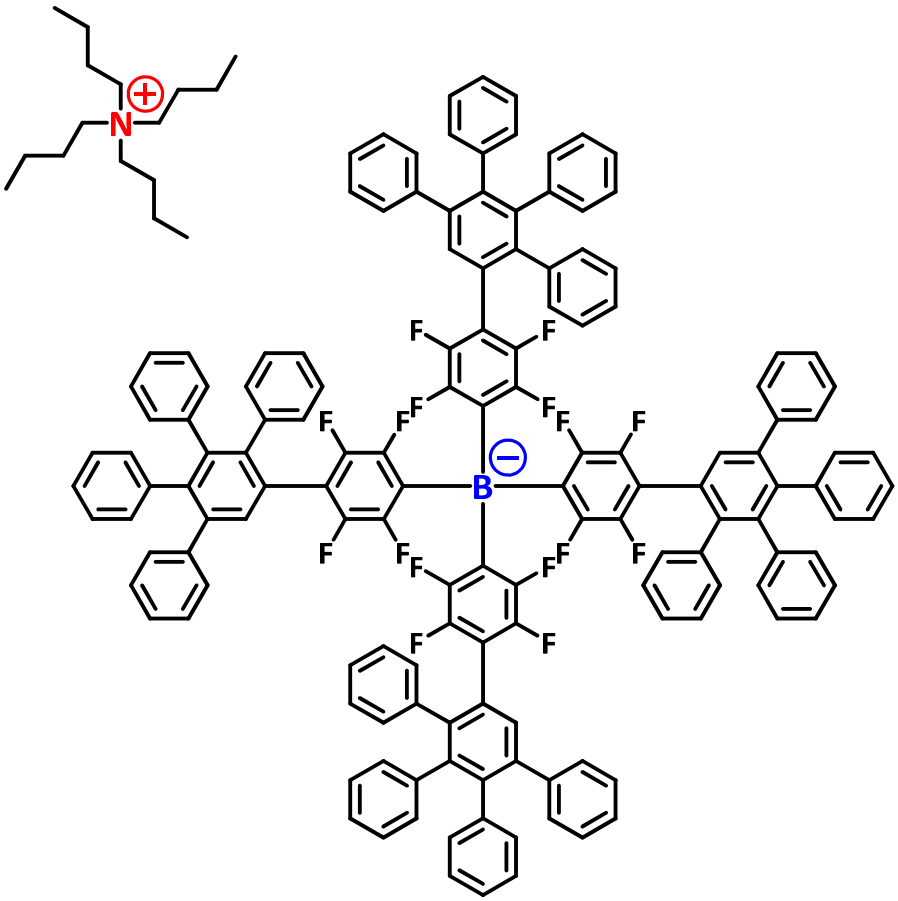

Synthesized according to literature procedure[8]

^{1}H-NMR (500 MHz, THF-d8, 298 K) δ 7.54 – 7.44 (m, 4 H, generation proton), 7.22 – 7.01 (m, 20 H), 6.97 – 6.57 (m, 60 H), 3.19 (m, 8 H, CH_2N), 1.63 (m, 8 H, CH_2), 1.36 (m, 8 H, CH_2), 0.97 (t, $^3J_{HH}$ = 7.4 Hz, 12 H, CH_3).

^{13}C-NMR (176 MHz, THF-d8, 298 K) δ 149.05, 147.71, 143.28, 141.68, 140.57, 140.45, 140.31, 140.08, 139.29, 132.21, 131.83, 130.55, 130.31, 128.78, 127.81, 127.20, 127.01, 126.89, 126.46, 126.12, 125.81, 125.51, 115.84, 59.00, 25.79, 19.82, 13.71.

^{19}F-NMR (471 MHz, THF-d8, 298 K) δ -132.13 – -134.03 (m, 8 F), -146.50 – -147.91 (m, 8 F).

^{11}B-NMR (160 MHz, THF-d8, 298 K) δ - 16.64 ppm.

MALDI-TOF (m/z): calcd. for $C_{144}H_{84}BF_{16}^-$: 2128.6, found: 2128.0 [M^-].

General procedure to synthesize alkali and earth alkali borates (4-4 to 4-9)

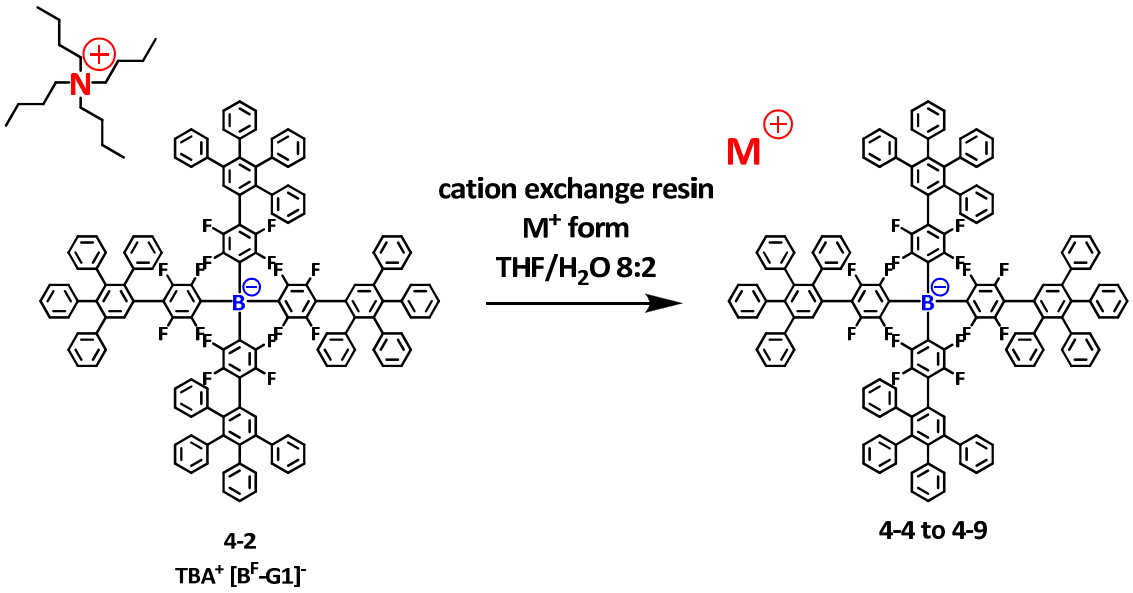

A glass column packed with 50 g of commercially available strongly acidic cation exchange Amberlite IR-120 (H^+ form) was washed with water. Afterwards an aqueous solution of the corresponding metal hydroxide M-$(OH)_n$ (0.5 – 1 mol dissolved in 50 mL H_2O) was passed slowly through the resin until the eluates had the same pH value as the original selected M-$(OH)_n$ solution, and then the resin was washed generously with water until constant neutral pH. The column bed was equilibrated progressively with water-solvent mixtures (THF /H_2O 8:2). A solution of tetrabutylammonium borate salt **(4-2, TBA+ B^F-G1-)** (0.4 – 0.6 mmol) in 30 mL of THF /H_2O (8:2 v/v) was passed slowly through the column and then washed with additional 200 mL of solvent.

The combined eluents were evaporated, and the residue obtained was taken up in a minimum amount of THF, precipitated in hexane, filtered and dried to yield the borate salts as white to yellowish solids. In general it was sufficient to repeat the elution process twice in order to ensure a complete cation exchange.

^{1}H-NMR analysis confirmed the absence of the tetrabutylammonium cation and was used as indication for a complete ion metathesis.

Lithium tetrakis(2,3,5,6-tetrafluoro-4-(G1)phenyl)borate (4-4), Li^+ [B^F-G1]-

^{1}H-NMR (700 MHz, THF-d8, 298 K) δ 7.53 – 7.43 (m, 4 H), 7.22 – 7.10 (m, 20 H), 7.03 – 6.83 (m, 60 H).

^{13}C-NMR (176 MHz, THF-d8, 298 K) δ 147.56, 144.57, 142.04, 138.55, 132.11, 131.94, 131.82, 130.54, 130.45, 129.92, 129.54, 128.87, 128.73, 128.46, 128.41, 128.21, 127.79, 127.56, 127.51, 127.25, 126.87, 126.45, 126.20, 125.81.

^{7}Li-NMR (194 MHz, THF-d8, 298 K) δ 0.12 (s).

^{11}B-NMR (160 MHz, THF-d8, 298 K) δ -16.68.

^{19}F-NMR (471 MHz, THF-d8, 298 K) δ -133.57 – -134.54 (m, 8 F), -146.40 – -147.00 (m, 8 F).

MALDI-TOF (m/z): calculated for $C_{144}H_{84}F_{16}B^-$: 2128.99, found: 2128.71 [M-]; white solid (yield 90 %).

Sodium tetrakis(2,3,5,6-tetrafluoro-4-(G1)phenyl)borate (4-5), Na^+ [B^F-G1]-

^{1}H-NMR (700 MHz, THF-d8, 298 K) δ 7.56 – 7.42 (m, 4 H), 7.20 – 7.08 (m, 20 H), 6.97 – 6.47 (m, 60 H).

^{13}C-NMR (176 MHz, THF-d8, 298 K) δ 147.68, 146.55, 142.17, 138.41, 132.18, 131.86, 131.82, 130.54, 130.45, 129.92, 129.54, 128.92, 128.83, 128.56, 128.31, 128.08, 127.91, 127.76, 127.61, 127.25, 126.87, 126.45, 126.20, 125.42.

^{11}B-NMR (160 MHz, THF-d8, 298 K) δ -17.03.

^{19}F-NMR (471 MHz, THF-d8, 298 K) δ -133.62 – -134.78 (m, 8 F), -146.62 – -147.39 (m, 8 F).

MALDI-TOF (m/z): calculated for $C_{144}H_{84}F_{16}B^-$: 2128.99, found: 2128.71 [M-]; white solid (yield 85 %).

Potassium tetrakis(2,3,5,6-tetrafluoro-4-(G1)phenyl)borate (4-6), K^+ [B^F-G1]-

^{1}H-NMR (700 MHz, THF-d8, 298 K) δ 7.58 – 7.44 (m, 4 H), 7.17 – 7.05 (m, 20 H), 6.95 – 6.42 (m, 60 H).

^{13}C-NMR (176 MHz, THF-d8, 298 K) δ 149.08, 147.55, 147.13, 142.34, 138.59, 132.23, 131.92, 131.87, 130.82, 130.41, 130.07, 129.74, 128.92, 128.87, 128.73, 128.22, 127.99, 127.90, 127.76, 127.61, 127.32, 126.87, 126.45, 126.20, 125.14.

^{11}B-NMR (160 MHz, THF-d8, 298 K) δ -16.88.

^{19}F-NMR (471 MHz, THF-d8, 298 K) δ -132.97 – -133.78 (m, 8 F), -146.12 – -147.53 (m, 8 F).

MALDI-TOF (m/z): calculated for $C_{144}H_{84}F_{16}B^-$: 2128.99, found: 2128.71 [M-]; white solid (yield 82 %).

Caesium tetrakis(2,3,5,6-tetrafluoro-4-(G1)phenyl)borate (4-7), Cs^+ [B^F-G1]-

^{1}H-NMR (700 MHz, THF-d8, 298 K) δ 7.56 – 7.40 (m, 4 H), 7.23 – 7.12 (m, 20 H), 7.01 – 6.49 (m, 60 H).

^{13}C-NMR (176 MHz, THF-d8, 298 K) δ 148.78, 147.35, 147.23, 142.77, 138.21, 132.04, 131.83, 131.71, 130.42, 130.27, 130.09, 129.82, 128.53, 128.48, 128.36, 128.21, 127.96, 127.82, 127.55, 127.43, 127.22, 126.57, 126.35, 126.20, 125.12.

^{11}B-NMR (160 MHz, THF-d8, 298 K) δ -16.53.

^{19}F-NMR (471 MHz, THF-d8, 298 K) δ -132.47 – -133.18 (m, 8 F), -146.73 – -147.94 (m, 8 F).

MALDI-TOF (m/z): calculated for $C_{144}H_{84}F_{16}B^-$: 2128.99, found: 2128.71 [M^-];

white solid (yield 77%).

Calcium tetrakis(2,3,5,6-tetrafluoro-4-(G1)phenyl)borate (4-8), Ca^{2+} [B^F-G1]$^-$ (4-8)

^{1}H-NMR (700 MHz, THF-d8, 298 K) δ 7.51 – 7.39 (m, 4 H), 7.24 – 7.15 (m, 20 H), 6.98 – 6.43 (m, 60 H).

^{13}C-NMR (176 MHz, THF-d8, 298 K) δ 147.76, 144.27, 142.47, 138.95, 132.32, 131.87, 131.80, 130.72, 130.29, 129.89, 129.34, 128.83, 128.71, 128.56, 128.41, 128.21, 127.79, 127.56, 127.51, 127.25, 126.87, 126.45, 126.20, 126.13.

^{11}B-NMR (160 MHz, THF-d8, 298 K) δ - 17.19.

^{19}F-NMR (471 MHz, THF-d8, 298 K) δ -132.67 – -133.31 (m, 8 F), -146.86 – -147.53 (m, 8 F).

MALDI-TOF (m/z): calculated for $C_{144}H_{84}F_{16}B^-$: 2128.99, found: 2128.71 [M-]; white solid (yield 67 %).

Barium tetrakis(2,3,5,6-tetrafluoro-4-(G1)phenyl)borate (4-8), Ba^{2+} [B^F-G1]- (4-9)

^{1}H-NMR (700 MHz, THF-d8, 298 K) δ 7.55 – 7.43 (m, 4 H), 7.21 – 7.08 (m, 20 H), 6.97 – 6.41 (m, 60 H).

^{13}C-NMR (176 MHz, THF-d8, 298 K) δ 147.96, 144.47, 142.69, 138.83, 132.32, 131.87, 131.80, 131.52, 131.19, 129.89, 129.34, 128.83, 128.71, 128.56, 128.41, 128.21, 127.79, 127.46, 127.41, 127.25, 126.87, 126.45, 126.12, 125.67.

^{11}B-NMR (160 MHz, THF-d8, 298 K) δ -16.91.

^{19}F-NMR (471 MHz, THF-d8, 298 K) δ -132.98 – -134.02 (m, 8 F), -146.35 – -147.21 (m, 8 F).

MALDI-TOF (m/z): calculated for $C_{144}H_{84}F_{16}B^-$: 2128.99, found: 2128.71 [M-]; white solid (yield 69 %).

N,N-Dimethylanilinium tetrakis(2,3,5,6-tetrafluoro-4-(G1)phenyl)borate (4-10), $PhNH(CH_3)_2^+$ $[B^F\text{-}G1]^-$

214 mg lithium borate Li^+ $B^F\text{-}G1^-$ **(4-4)** (0.1 mmol) and 17 mg *N*,*N´*-dimethylanilinium hydrochloride (0.105 mmol, 1.05 eq) were placed in a microwave tube and dried in vacuum for 12 h. Then dry toluene (5 mL) was added under inert gas atmosphere and the mixture was stirred at room temperature for 5 h. The solid LiCl formed during the reaction was filtered through a short celite pad and rinsed with DCM. After the solvent was removed under reduced pressure, the product was dissolved in methylene chloride, precipitated in hexane, filtered and dried to afford the pure product as a white powder.

^{1}H-NMR (700 MHz, THF-d8, 298 K) δ 7.45 – 7.42 (m, 4 H), 7.39 – 7.33 (m, 5 H), 7.25 – 7.13 (m, 20 H), 6.99 – 6.86 (m, 60 H), 3.02 (s, 7 H, CH_3).

^{13}C-NMR (76 MHz, THF-d8, 298 K) δ 151.65, 143.99, 142.55, 141.90, 140.98, 139.61, 131.91, 131.75, 131.63, 130.83, 130.31, 129.35, 128.53, 128.01, 127.31, 127.20, 127.05, 126.93, 126.00, 119.43, 46.13 (CH_3).

^{11}B-NMR (160 MHz, THF-d8, 298 K) δ -15.97.

^{19}F-NMR (471 MHz, THF-d8, 298 K) δ -131.93 – -133.51 (m, 8 F), -147.12– -148.37 (m, 8 F). MALDI-TOF (m/z): calculated for $C_{144}H_{84}F_{16}B^-$: 2128.99, found: 2128.71 [M-]; calculated for $C_8H_{12}N^+$: 122.19, found: 122.78 [M^+]; white solid (yield 69 %).

Triphenylcarbenium tetrakis(2,3,5,6-tetrafluoro-4-(G1)phenyl)borate (4-11), Ph_3C^+ $[B^F\text{-}G1]^-$

214 mg lithium borate Li^+ $B^F\text{-}G1^-$ **(4-4)** (0.1 mmol) and 29.3 mg trityl chloride (0.105 mmol, 1.05 eq) were placed in a microwave tube and dried in vacuum for 12 h. Then dry toluene (5 mL) was added under inert gas atmosphere and the mixture was stirred at room temperature for 5 h. The solid LiCl formed during the reaction was filtered through a short celite pad and rinsed with DCM. After the solvent was removed in vacuo, the product was dissolved in tetrahydrofurane, precipitated in hexane, filtered and dried to afford the pure product as a yellow powder.

^{1}H-NMR (700 MHz, THF-d8, 298 K) δ 7.55 – 7.44 (m, 4 H), 7.33 – 7.13 (m, 38 H, polyphenylene + Ph_3C^+), 7.0 – 6.86 (m, 60 H).

^{13}C-NMR (76 MHz, THF-d8, 298 K) δ 146.99, 144.00, 141.47, 137.97, 131.53, 131.37, 131.25, 129.99, 129.35, 128.97, 128.29, 128.16, 127.89, 127.84, 127.64, 127.22, 126.99, 126.67, 126.29, 125.88, 125.62, 125.23.

^{11}B-NMR (160 MHz, THF-d8, 298 K) δ -15.93.

^{19}F-NMR (471 MHz, THF-d8, 298 K) δ -132.65 – -134.32 (m, 8 F), -146.10 – -147.63 (m, 8 F). MALDI-TOF (m/z): calculated for $C_{144}H_{84}F_{16}B^-$: 2128.99, found: 2128.71 [M-]; calculated for $C_{19}H_{15}^+$: 243.32, found: 243.41 [M^+]; yellow solid (yield 78 %).

Tetraphenylphosphonium tetrakis(2,3,5,6-tetrafluoro-4-(G1)phenyl)borate (4-12), Ph_4P^+ [B^F-G1]-

214 mg lithium borate Li^+ B^F-$G1^-$ **(4-4)** (0.1 mmol) and 46 mg tetraphenylphosphonium bromide (0.11 mmol, 1.1 eq) were placed in a microwave tube and dried in vacuum for 12 h. Then dry toluene (5 mL) was added under inert gas atmosphere and the mixture was stirred at room temperature for 5 h. The solid LiBr formed during the reaction gets filtered through a celite pad and rinsed with DCM. After the solvent was removed in under reduced pressure, the product was dissolved in methylene chloride, precipitated in hexane, filtered and dried to afford the pure product as a yellow powder.

^{1}H-NMR (500 MHz, CD_2Cl_2, 298 K) δ 7.51 – 7.41 (m, 4 H), 7.33 – 7.13 (m, 38 H), 7.0 – 6.86 (m, 60 H).

^{13}C-NMR (76 MHz, CD_2Cl_2, 298 K) δ 146.99, 144.00, 141.47, 137.97, 131.53, 131.37, 131.25, 129.99, 129.35, 128.97, 128.29, 128.16, 127.89, 127.84, 127.64, 127.22, 126.99, 126.67, 126.29, 125.88, 125.62, 125.23.

^{11}B-NMR (160 MHz, CD_2Cl_2, 298 K) δ -15.93 ppm.

^{31}P-NMR (202 MHz, CD_2Cl_2, 298 K) δ 23.25 ppm.

^{19}F-NMR (471 MHz, CD_2Cl_2, 298 K) δ -132.65 – -134.32 (m, 8 F), -146.10 – -147.63 (m, 8 F). MALDI-TOF (m/z): calculated for $C_{144}H_{84}F_{16}B^-$: 2128.99, found: 2128.71 [M^-]; calculated for $C_{24}H_{20}P^+$: 326.12, found: 326.32 [M^+]; yellow solid (yield 72 %).

Bis(triphenylphosphine)iminium tetrakis(2,3,5,6-tetrafluoro-4-(G1)phenyl)borate (4-13), $(Ph_3P)_2=N^+$ [B^F-G1]-

214 mg lithium borate Li^+ B^F-$G1^-$ **(4-4)** (0.1 mmol) and 63 mg bis(triphenylphosphine)iminium chloride (0.11 mmol, 1.1 eq) were placed in a microwave tube and vacuum dried for 12h. Then dry toluene (5 mL) was added under inert gas atmosphere and the mixture was stirred at room temperature for 5 h. After filtering off the solid LiCl through a celite pad, the solvent was removed under reduced pressure, the crude product was dissolved in methylene

chloride, precipitated in hexane, filtered and dried to afford the pure product as a yellow powder.

^{1}H-NMR (700 MHz, THF-d8, 298 K) δ 7.57 – 7.46 (m, 4 H), 7.38 – 7.09 (m, 50 H), 7.0 – 6.86 (m, 60 H).

^{13}C-NMR (76 MHz, THF-d8, 298 K) δ 146.99, 144.00, 141.47, 137.97, 131.53, 131.37, 131.25, 129.99, 129.35, 128.97, 128.29, 128.16, 127.89, 127.84, 127.64, 127.22, 126.99, 126.67, 126.29, 125.88, 125.62, 125.23.

^{11}B-NMR (160 MHz, THF-d8, 298 K) δ -16.13.

^{19}F-NMR (471 MHz, THF-d8, 298 K) δ -132.49 – -134.12 (m, 8 F), -146.03 – -147.73 (m, 8 F). MALDI-TOF (m/z): calculated for $C_{144}H_{84}F_{16}B^-$: 2128.99, found: 2128.71 [M-]; calculated for $C_{36}H_{30}NP_2^+$: 538.19, found: 539.04 [M^+]; yellow solid (yield 84 %).

General synthesis of dendronized phosphonium borates [P-G1]$^+$ [B^F-G1]- (4-14), [P-G2]$^+$ [B^F-G1]- (4-15) and [P-G3]$^+$ [B^F-G1]- (4-16)

43 mg lithium borate Li^+ B^F-$G1^-$ **(4-4)** (0.02 mmol) and the corresponding phosphonium tetrafluoroborate (**3-6, 3-10, 3-13**) (0.02 mmol) were placed in a microwave tube and vacuum dried for 12 h. Then dry toluene (3 mL) was added under inert gas atmosphere and the mixture was stirred at room temperature for 5 h. The insoluble solid $LiBF_4$ formed during the reaction was filtered off. After the solvent was removed under reduced pressure, the crude product was dissolved in methylene chloride, precipitated in hexane, filtered and dried to afford the pure phosphonium salts as white powders.

Phosphonium-G1 borate (4-14)

^{1}H-NMR (700 MHz, CD_2Cl_2, 298 K) δ 7.59 – 7.44 (m, 8 H), 7.48 – 7.47 (dd, $^{3}J_{HH}$ = 8.5 Hz, $^{4}J_{PH}$ = 3.2 Hz, 8 H), 7.33 – 7.30 (dd, $^{3}J_{PH}$ = 13.5 Hz, $^{3}J_{HH}$ = 8.1 Hz, 8H), 7.28 – 7.06 (m, 40 H), 7.00 – 6.87 (m, 120 H).

^{31}P-NMR (202 MHz, CD_2Cl_2, 298 K) δ 21.97 ppm.

^{11}B NMR (160 MHz, THF-d8, 298 K) δ -16.61 ppm.

^{19}F NMR (471 MHz, THF-d8, 298 K) δ -131.95 – -133.63 (m, 8 F), -146.90 – -148.06 (m, 8 F)

MALDI-TOF (m/z): calcd. for $C_{144}H_{100}P^+$: 1861.31, found: 1861.01 [M^+]; calcd. for $C_{144}H_{84}F_{16}B^-$: 2128.99, found: 2128.71 [M^-].

Phosphonium-G2 borate (4-15)

^{1}H-NMR (700 MHz, CD_2Cl_2, 298 K) δ 7.61 - 6.49 (m, 344 H).

^{31}P-NMR (202 MHz, CD_2Cl_2, 298 K) δ 22.17 ppm.

^{11}B NMR (160 MHz, THF-d8, 298 K) δ -17.59 ppm.

^{19}F NMR (471 MHz, THF-d8, 298 K) δ -132.55 – -133.89 (m, 8 F), -145.90 – -147.23 (m, 8 F)

MALDI-TOF (m/z): calcd. for $C_{384}H_{260}P^+$: 4905.02, found: 4904.85 [M^+]; calcd. for $C_{144}H_{84}F_{16}B^-$: 2128.99, found: 2128.71 [M^-].

Phosphonium-G3 borate (4-16)

^{1}H-NMR (700 MHz, CD_2Cl_2, 298 K) δ 7.58 - 6.43 (m, 664 H).

^{31}P-NMR (202 MHz, CD_2Cl_2, 298 K) δ 21.93 ppm.

^{11}B NMR (160 MHz, THF-d8, 298 K) δ -16.92 ppm.

^{19}F NMR (471 MHz, THF-d8, 298 K) δ -132.82 – -134.31 (m, 8 F), -144.59 – -146.14 (m, 8 F)

MALDI-TOF (m/z): calcd. for $C_{864}H_{580}P^+$: 10988.53, found: 10987.96 [M^+]; calcd. for $C_{144}H_{84}F_{16}B^-$: 2128.99, found: 2128.71 [M^-].

[1,1'-Biphenyl]-4,4'-diylbis(triphenylphosphonium) tetrakis(2,3,5,6-tetrafluoro-4-(G1)phenyl)borate (4-17), $(Ph_3P)_2Ph\text{-}Ph^+$ [B^F-G1]-

214 mg lithium borate Li^+ B^F-$G1^-$ **(4-4)** (0.1 mmol) and 42 mg [1,1'-biphenyl]-4,4'-diylbis(triphenylphosphonium) dibromide (0.05 mmol, 0.5 eq) were placed in a microwave tube and dried in vacuum for 12 h. Then dry toluene (5 mL) was added under inert gas atmosphere and the mixture was stirred at room temperature for 5 h. After filtering off the solid LiBr through a celite pad, the solvent was removed in vacuo, the residue was dissolved in methylene chloride, precipitated in hexane, filtered and dried to afford the pure title compound as a white powder.

^{1}H-NMR (700 MHz, CD_2Cl_2, 298 K) δ 8.32 (dd, $^{3}J_{HH}$ = 8.5 Hz, $^{4}J_{PH}$ = 3.0 Hz, 4 H), 7.93 (t, $^{3}J_{HH}$ = 7.5 Hz, 6 H), 7.85 (dd, $^{3}J_{PH}$ = 12.7 Hz, $^{3}J_{HH}$ = 8.5 Hz, 4 H), 7.79 (td, $3J_{HH}$ = 7.9 Hz, $^{4}J_{PH}$ = 3.5 Hz, 12 H), 7.69 (dd, $^{3}J_{PH}$ = 13.1 Hz, $^{3}J_{HH}$ = 7.4 Hz, 12 H), 7.55 – 7.42 (m, 4 H), 7.17 – 7.13 (m, 20 H), 7.04 – 6.65 (m, 60 H).

^{13}C-NMR (76 MHz, CD_2Cl_2, 298 K) δ 146.89, 145.89, 144.09, 141.23, 137.18, 136.26, 135.97 (d, $^{3}J_{PC}$ = 10.3 Hz), 135.15 (d, $^{3}J_{PC}$ = 10.6 Hz), 131.67, 131.44, 131.23 (d, $^{2}J_{PC}$ = 13.0 Hz), 130.58 (d, $^{2}J_{PC}$ = 13.3 Hz), 129.90, 129.34, 128.75, 128.70, 128.20, 127.88, 127.61, 126.93, 126.79, 126.39, 125.74, 118.31 (d, $^{1}J_{PC}$ = 90.3 Hz), 118.14 (d, $^{1}J_{PC}$ = 89.6 Hz).

^{31}P-NMR (202 MHz, CD_2Cl_2, 298 K) δ 23.05.

MALDI-TOF (m/z): calculated for $C_{144}H_{84}F_{16}B^-$: 2128.99, found: 2128.71 [M-]; calcd. for $C_{48}H_{38}P_2^{2+}$: 338.1, found: 339.5 [M^{2+}] (+ fragmentation) white solid (yield 74 %).

Synthesis protocol of substances from chapter 5

4-Ethynyl-benzylbromide (5-2)

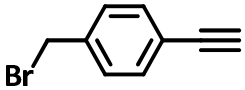

4-ethynyl-benzylalcohol (1.32 g, 10 mmol) was dissolved in 30 mL DCM and cooled to 0 °C. Phosphorus tribromide (2.7 g, 0.93 mL, 10 mmol) was added dropwise. The reaction mixture was allowed to warm to room temperature gradually and stirred under argon overnight. The reaction was quenched by addition of H_2O. After addition of 30 mL DCM and phase separation, the combined organic layers were washed with brine, dried over Na_2SO_4 and concentrated to dryness. The crude material was purified by column chromatography using hexane as eluent to yield the product (1.7 g, 88 % yield) as a colorless liquid.

^{1}H-NMR (300 MHz, CD_2Cl_2, 298 K) δ 7.51 (d, 2 H, $^2J_{HH}$ = 8.3 Hz), 7.40 (d, 2 H, $^2J_{HH}$ = 8.3 Hz), 4.54 (s, 2 H, CH_2Br), 3.21 (s, 1 H, ethynyl-proton).

^{13}C-NMR (76 MHz, CD_2Cl_2, 298 K) δ 139.10, 132.82, 129.45, 122.53, 83.31, 78.28, 33.26.

FDMS (m/z): calcd. for C_9H_7Br: 193.97, found: 194.1 [M+, 100], 196.2 [M+, 100, Br isotope pattern].

4-Ethynylbenzyl-tris-(4-ethynylphenyl)-phosphonium bromide (5-5)

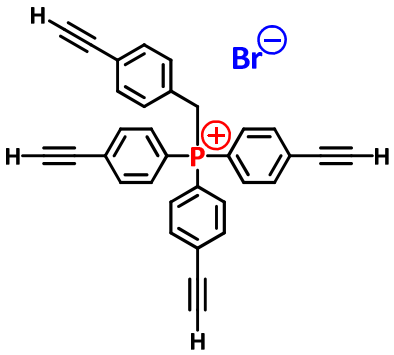

800 mg tris-(4-ethynylphenyl)-phosphine **3-3** (2.4 mmol) was dissolved in dry toluene (5 mL in a microwave vial) and 4-ethynyl-benzylbromide **5-2** (490 mg, 2.5 mmol) was added. The vial was sealed with an aluminum cap and thoroughly degassed by freezing the solvent under vacuum. The reaction mixture was stirred at 40 °C for 12 h under argon atmosphere. After that time the solvent was removed under reduced pressure and the crude product was dissolved in 1 mL DCM and precipitated in cold diethylether. The obtained faintly yellow colored solid was used without further purification (397 mg, 75 % yield).

^{1}H-NMR (300 MHz, CD_2Cl_2, 298 K) δ 7.57 - 7.52 (m, 6 H), 7.42 – 7.13 (m, 8 H), 6.99 (m, 2 H), 4.35 (d, 2 H, CH_2), 3.30 (s, 4 H).

^{31}P-NMR (202 MHz, CD_2Cl_2, 298 K) δ 23.24 ppm.

MALDI-TOF (m/z): calcd. for $C_{33}H_{22}P^+$: 449.15, found: 449.69 [M^+].

G1-Benzyl-phosphonium bromide [P^{CH2}-G1]$^+$ Br^- (5-6)

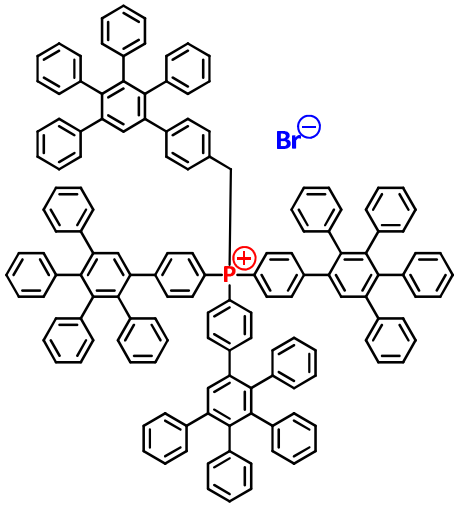

4-ethynylbenzyl-tris-(4-ethynylphenyl)-phosphonium bromide **5-5** (150 mg, 0.28 mmol) was placed in a microwave vial and dissolved in a mixture of diphenylether/DMF (6 mL, 2:1 v/v). Afterwards tetraphenylcyclopentadienone (460 mg, 1.18 mmol, 4.2 eq) was added and the vial was sealed. After thoroughly degassing, the reaction mixture was heated via lab microwave (300 W, 180 °C) for 1 hour. After that time the mixture was poured into 20 mL DCM and the organic phase was washed with H_2O (3 x 10 mL), dried over Na_2SO_4 and the solvent was distilled off under reduced pressure. The residual crude oil was taken up in 3 mL DCM and slowly dropped in hexane to precipitate the target compound. The red supernatant solution was removed and the purification continued with another precipitation step in cold diethylether. For analytical purposes, a small amount of the obtained target molecular salt (white solid, 360 mg, 67 % yield) was subjected to column chromatography (~ 25 g silica gel) using a mixture of DCM/THF (4:1) as eluent. Massive amounts of solvent mixture (~ 500 mL) were required to obtain the final product in analytical purity.

^{1}H-NMR (500 MHz, CD_2Cl_2, 298 K) δ 7.62 (s, 3 H, generation protons), 7.59 (s, 1 H, generation proton), 7.44 – 7.42 (dd, 4 H), 7.24 – 7.19 (m, 28 H,) 7.02 – 6.88 (m, 68 H), 4.97 (d, 2 H, $^2J_{HP}$ = 14.1 Hz, CH_2).

^{13}C NMR (126 MHz, CD_2Cl2) δ 151.48, 149.10, 142.23, 142.13, 141.84, 141.65, 141.35, 141.01, 140.77, 139.90, 139.71, 139.44, 139.28, 139.05, 138.58, 135.90, 133.48, 131.59, 131.36, 130.64, 129.86, 128.57, 127.70, 127.12, 126.97, 126.72, 125.63, 125.42, 30.13 (CH_2).

^{31}P-NMR (202 MHz, CD_2Cl_2, 298 K) δ 21.64 ppm.

MALDI-TOF (m/z): calcd. for $C_{145}H_{102}P^+$: 1874.78, found: 1874.64 [M^+].

5'-(Bromomethyl)-1',2',3',4'-tetraphenylbenzene (5-13, PPD-CH_2Br)

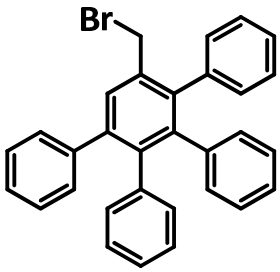

7.68 g (20 mmol) of tetraphenylcyclopentadienone was placed in a 100 mL round bottom flask and dissolved in 40 mL anhydrous o-xylene. Afterwards a solution of propargyl bromide (5.6 mL, 50 mmol, 2.5 molar excess of a 80 wt % solution in toluene) is gradually added and the reaction mixture is degassed and heated to 155 °C for 12 h with an open reflux condenser placed on the flask. The initially deep purple reaction solution has turned to clear colorless during that time, which indicated the completeness of the reaction. After removal of all volatiles under reduced pressure and drying in vacuo, the crude product was obtained as slightly beige powder (9.5 g, 20 mmol, 100%) and used without further purification in the following reaction steps. Fur analytical purposes a small sample of 238 mg (0.5 mmol) was purified by column chromatography using a 5:1 mixture of hexane and EtOAc to yield 200 mg (0.42 mmol, 84 %) of a white solid as pure product.

^{1}H-NMR (300 MHz, CD_2Cl_2, 298 K) δ 7.65 (s, 1 H), 7.23 – 7.18 (m, 10 H), 6.96 – 6.82 (m, 10 H), 4.42 (s, 2 H, CH_2Br). ^{13}C NMR (76 MHz, CD_2Cl_2, 298 K) δ 142.61, 141.81, 141.77, 141.25, 140.93, 140.35, 140.13, 139.03, 135.55, 131.74, 131.72, 131.54, 130.66, 130.20, 128.01, 127.84, 127.25, 127.06, 126.97, 126.82, 126.13, 125.85, 33.09 (CH_2Br).

FDMS (m/z): calcd. for $C_{31}H_{23}Br$: 474.09, found: 474.1 [M^+, 100], 476.1 [M^+, 100, Br isotope pattern].

Melting point: 205.7 °C

Elemental analysis: found: 78.09 % C, 5.39 % H, (calculated: 78.32 % C, 5.23 % H)

Tris-(3',4',5'-triphenyl-[1,1':2',1''-terphenyl]-4-yl)phosphine (5-14, P(Dendr)$_3$)

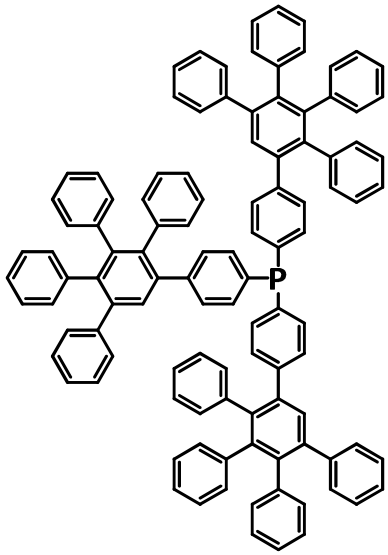

1.0 g (3 mmol) of tris-(4-ethynylphenyl)-phosphine **(2)** were dissolved in 50 mL anhydrous o-xylene and 3.45 g tetraphenylcyclopentadienone (9 mmol) were added. The solution was thoroughly degassed and bubbled with argon before being heated to 150 °C for 12 h. After that time the solvent was removed under reduced pressure and the residue was adsorbed onto silica gel. Purification by column chromatography using a 5:1 mixture of hexane and EtOAc yielded 2.91 g (2.07 mmol, 69 % yield) of the dendronized phosphine as a white solid.

^{1}H-NMR (700 MHz, CD_2Cl_2, 298 K) δ 7.53 (s, 1 H), 7.17 – 7.15 (m, 15 H), 7.09 (dd, 6 H, *J* = 8.16, 1.5 Hz), 6.95 – 6.92 (m, 15 H), 6.89 – 6.83 (m, 36 H).

^{13}C NMR (76 MHz, CD_2Cl_2, 298 K) δ 142.36, 141.72, 140.78, 140.38, 140.07, 139.96, 139.52, 139.39, 134.94, 132.71, 132.60, 131.54, 131.48, 130.87, 129.94, 129.89, 127.55, 126.83, 126.56, 126.28, 125.62, 125.36.

^{31}P-NMR (202 MHz, CD_2Cl_2, 298 K) δ – 8.75 ppm.

FDMS (m/z): calcd. for $C_{108}H_{75}P$: 1402.56, found: 1401.9 [M^+].

Melting point: > 250 °C

Elemental analysis: found: 92.24 % C, 6.16 % H, (calculated: 92.41 % C, 5.39 % H)

General procedure for the preparation of benzylphosphonium bromide salts

The Wittig precursor phosphonium salts (**5-15, 5-16 and 5-17**) bearing the bulky 5'-(3',4'-diphenyl-1,1':2',1''-terphenyl)-substituent (in this work simply denoted as polyphenylene- or PPD-unit) at the phosphorus are synthesized according to the following procedure. The PPD-benzylbromide derivative **5-13** (1.1 eq) is dissolved in anhydrous MeCN (30 – 50 mL) in a 100 mL round bottom flask. To that solution the respective phosphine PL_3 (1.0 eq, PPh_3 → **5-16**; $P(n\text{-}Bu)_3$ → **5-17**; $P(Dendr)_3$ → **5-15**) is added in small portions. The reaction solution is thoroughly degassed and bubbled with argon. Afterwards the mixture is stirred at 60 °C for 18 h under inert gas atmosphere. The solvent is removed under reduced pressure and the residue is dissolved in 4 – 8 mL DCM, precipitated in cold diethylether, filtered and dried in vacuum to afford the pure phosphonium bromide salts as white solids.

First-generation polyphenylene triarylbenzylphosphonium bromide (5-15, $(PPD)_3PCH_2PPD^+$ Br^-)

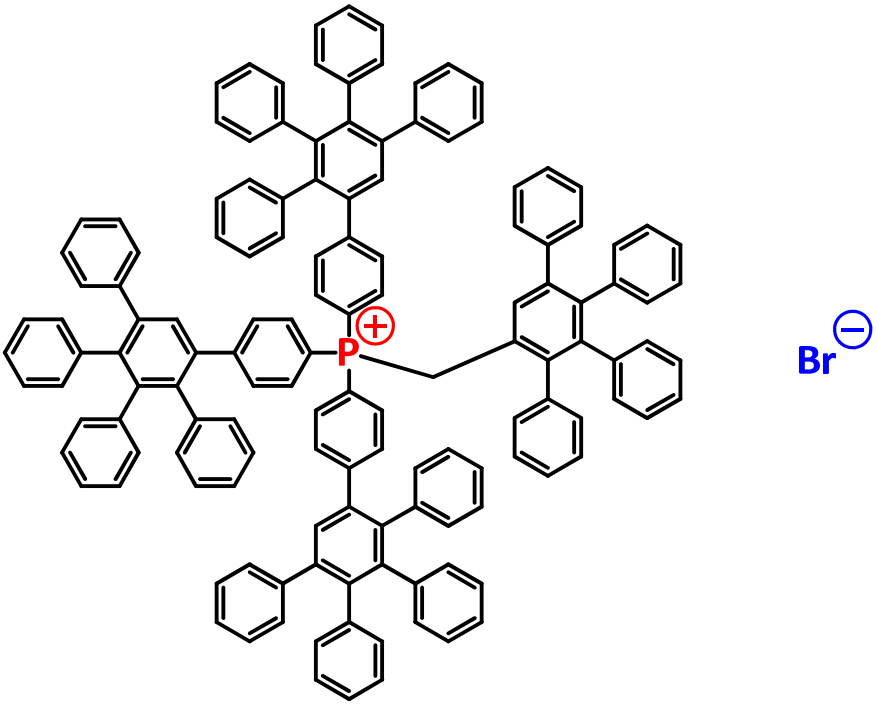

^{1}H-NMR (500 MHz, CD_2Cl_2, 298 K) δ 7.55 (s, 4 H, generation protons), 7.40 (dd, 8 H, *J* = 8.4, 3.3 Hz), 7.23 – 7.11 (m, 28 H), 7.01 – 6.80 (m, 60 H), 4.35 (d, 2 H, $^2J_{HP}$ = 15.3 Hz, CH_2P).

^{31}P-NMR (202 MHz, CD_2Cl_2, 298 K) δ 21.15. White solid (92 % yield).

MALDI-TOF (m/z): calcd. for $C_{139}H_{98}P^+$: 1798.7, found: 1798.5 [M^+].

Elemental analysis: found: 87.05 % C, 6.17 % H (calculated for $C_{139}H_{98}PBr$ * 2 H_2O: 87.17 % C, 6.37 % H)

((3',6'-Diphenyl-[1,1':2',1''-terphenyl]-4'-yl)methyl)triphenylphosphonium bromide (5-16, $Ph_3PCH_2PPD^+ Br^-$)

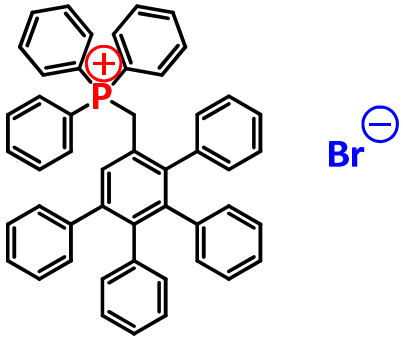

^{1}H-NMR (500 MHz, CD_2Cl_2, 298 K) δ 7.91 (td, 3 H, *J* = 7.38 Hz, 1.67 Hz), 7.70 (td, 6 H, *J* = 7.96 Hz, 3.62 Hz), 7.41 – 7.37 (m, 6 H), 7.33 (s, 1 H, generation proton), 7.18 – 6.98 (m, 9 H), 6.85 (m, 5 H), 6.72 (d, 2 H, *J* = 7.96 Hz), 6.66 (m, 2 H), 6.27 (d, 2 H, *J* = 7.98 Hz), 5.07 (d, 2 H, $^2J_{HP}$ = 14 Hz, CH_2P).

^{13}C NMR (126 MHz, CD_2Cl_2, 298 K) δ 143.13, 143.10, 142.33, 142.28, 141.46, 141.43, 141.17, 141.14, 140.36, 139.38, 139.14, 137.90, 135.39, 135.37, 134.43, 134.35, 131.35 (d, *J* = 4.9 Hz), 131.19, 130.67, 130.33, 130.23, 130.07, 129.53, 128.09, 127.59, 127.03, 126.95, 126.69, 126.03, 125.66, 125.00 (d, *J* = 8.5 Hz), 117.74, 117.06, 29.76 (d, *J* = 47.1 Hz).

^{31}P-NMR (202 MHz, CD_2Cl_2, 298 K) δ 22.87. White solid (95 % yield).

MALDI-TOF (m/z): calcd. for $C_{49}H_{38}P^+$: 657.27, found: 657.27 [M^+].

Elemental analysis: found: 77.43 % C, 5.81 % H, (calculated for $C_{49}H_{38}PBr$ * 1 H_2O : 77.36 % C, 5.86 % H)

((3',6'-Diphenyl-[1,1':2',1''-terphenyl]-4'-yl)methyl)tributylphosphonium bromide (5-17, $Bu_3PCH_2PPD^+ Br^-$)

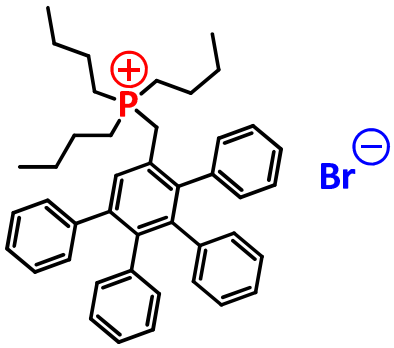

^{1}H-NMR (700 MHz, CD_2Cl_2, 298 K) δ 7.78 (s, 1 H, generation proton), 7.26 – 7.17 (m, 5 H), 7.14 – 7.12 (m, 2 H), 7.08 – 7.07 (m, 2 H), 6.94 (m, 3 H), 6.88 (m, 3 H), 6.82 (m, 2 H), 6.74 (m, 2 H), 4.13 (d, 2 H, $^2J_{HP}$ = 15.3 Hz, CH_2P), 2.27 (ddd, 6 H, *J* = 17.1, 8.4, 4.4 Hz, CH_2P), 1.38 (p, 6 H, *J* = 7.4 Hz, CH_2), 1.20 (h, 6 H, *J* = 7.5, 7.0 Hz, CH_2), 0.90 (t, 9 H, *J* = 7.3 Hz, CH_3).

^{13}C NMR (176 MHz, CD_2Cl_2, 298 K) δ 142.98, 141.90, 140.86, 140.71, 139.70, 139.32, 138.59, 137.94, 131.90, 131.23, 131.03, 129.72, 128.95, 128.42, 128.14, 127.74, 127.26, 126.95, 126.76, 126.35, 125.92, 125.69, 125.22, 65.65, 23.90, 23.32, 19.18, 13.26.

^{31}P-NMR (202 MHz, CD_2Cl_2, 298 K) δ 32.41. White solid (91 % yield).

MALDI-TOF (m/z): calcd. for $C_{43}H_{50}P^+$: 597.37, found: 597.39 [M^+].

Elemental analysis: found: 74.30 % C, 8.51 % H, (calculated for $C_{43}H_{50}PBr$ * 1 H_2O : 74.23 % C, 8.53 % H)

3',4',5'-Triphenyl-[1,1':2',1''-terphenyl]-4-carbaldehyde (5-21, PPD-CHO)

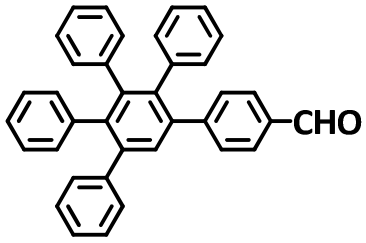

650 mg (5 mmol) of 4-ethynylbenzaldehyde and 1.92 g tetraphenylcyclopentadienone (5 mmol) were dissolved in 20 mL anhydrous o-xylene in a 50 mL Schlenk flask. The solvent was degassed and the reaction mixture was then heated to 150 °C for 12 h under argon. After cooling to room temperature, the solvent was removed under reduced pressure and the crude product was adsorbed onto silica gel. Purification by means of silica gel column chromatography using a 5:1 mixture of hexane and EtOAc yielded 2.19 g of the pure product as a white solid (4.5 mmol, 90 % yield).

^{1}H-NMR (300 MHz, CD_2Cl_2, 298 K) δ 9.93 (s, 1 H, CHO), 7.69 (dd, 2 H, *J* = 8.2 Hz, 1.8 Hz), 7.56 (s, 1 H), 7.36 (dd, 2 H, *J* = 8.2, 1.8 Hz), 7.19 – 7.21 (m, 5 H), 7.02 – 6.84 (m, 15 H).

^{13}C NMR (76 MHz, CD_2Cl_2, 298 K) δ 192.15 (CHO), 148.61, 142.42, 141.95, 141.40, 140.55, 140.31, 140.05, 139.96, 139.68, 138.17, 134.84, 131.84, 131.80, 131.77, 131.29, 130.99, 130.26, 130.17, 129.24, 128.41, 127.99, 127.43, 127.26, 127.00, 126.78, 126.32, 126.30, 126.10, 125.84.

FDMS (m/z): calcd. for $C_{37}H_{26}O$: 486.2, found: 486.2 [M+].

Melting point: 122.9 °C

General procedure for the Wittig reaction

In a dried 10 mL round bottom flask the phosphonium bromide (**5-15 – 5-17**, 0.27 mmol, 1.1 eq) is suspended in dry THF (5 mL) and sealed with a rubber septum. After the reaction mixture is degassed and set under argon, it is cooled down to – 78 °C with an acetone/dry ice bath. At that temperature the base is added gradually (0.25 mmol, 1.0 eq, 0.25 mL, 1 M solution in THF of LiHMDS or KHMDS), whereupon the formation of the strongly yellow colored ylide solution was observed. The mixture was stirred at – 78 °C for 1 h and then the aldehyde (dissolved in THF, 1 M) is added with stirring being continued for 10 minutes. After that time the reaction mixture is allowed to come to room temperature and stirred for additional 6 h to complete the alkene formation. The solvent was removed under reduced pressure and the residue is adsorbed onto silica gel. Purification of the olefins was achieved by column chromatography using a 95:5 mixture of hexane and EtOAc.

Analysis of the olefins

5'-(Styrenyl)-1',2',3',4'-tetraphenylbenzene (5-22):

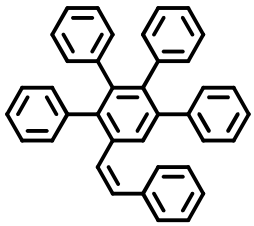

(*Z*)-5-22

^{1}H-NMR (300 MHz, CD_2Cl_2, 298 K) δ 7.89 (s, 1 H, gen.-proton), 7.42 – 7.19 (m, 5 H), 7.13 – 6.87 (m, 20 H), 6.48 (d, 1 H, $^{3}J_{HH}$ (*Z*-alkene) = 12.1 Hz), 6.31 (d, 1 H, $^{3}J_{HH}$ (*Z*-alkene) = 12.1 Hz).

^{13}C NMR (76 MHz, CD_2Cl_2, 298 K, *Z*-isomer) δ 142.44, 142.15, 141.46, 140.75, 140.65, 140.50, 140.39, 140.01, 139.90, 137.90, 137.52, 136.13, 135.65, 131.84, 131.70, 131.38, 130.85, 130.63, 130.44, 130.29, 130.09, 129.95, 129.46, 128.97, 128.56, 127.96, 127.85, 127.72, 127.49, 127.12, 126.92, 126.80, 126.72, 126.67, 126.42, 125.94, 125.72.

FDMS (m/z): calcd. for $C_{38}H_{28}$: 484.2, found: 483.5 [M^+].

Melting point: 95.3 °C (mixture of isomers)

5'-(1-Heptene-1-yl)-1',2',3',4'-tetraphenylbenzene (5-23):

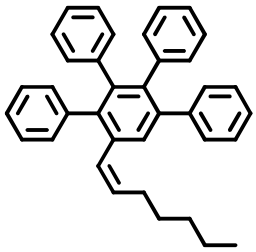

(*Z*)-5-23

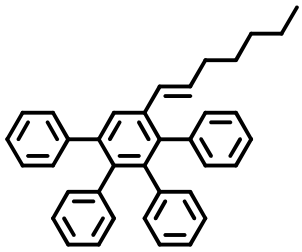

(*E*)-5-23

^{1}H-NMR (300 MHz, CD_2Cl_2, 298 K) δ 7.68 (s, 0.72 H, gen.-proton (*E*-alkene)), 7.47 (s, 0.28 H, gen.-proton (*Z*-alkene)), 7.20 – 7.00 (m, 10 H, phenyl), 6.94 – 6.79 (m, 10 H, phenyl), 6.27 – 6.14 (m, 1.44 H, $^{3}J_{HH}$ (*E*-alkene) = 15.8 Hz, 6.9 Hz), 6.07 (d, 0.28 H, $^{3}J_{HH}$ (*Z*-alkene) = 11.6 Hz), 5.55 (dt, 0.28 H, $^{3}J_{HH}$ (*Z*-alkene) = 11.6 Hz, 7.35 Hz), 2.36 (qd, 0.56 H, *J* = 7.35 Hz, 7.29 Hz, 1.79 Hz, α-CH_2 (*Z*-alkene)), 2.05 (qd, 1.44 H, *J* = 6.9 Hz, 0.8 Hz, α-CH_2 (*E*-alkene)), 1.44 – 1.25 (m, 6 H, CH_2 (*E*+*Z*)), 0.90 – 0.86 (m, 3H, CH_3 (*E*+*Z*)).

^{13}C NMR (76 MHz, CD_2Cl_2, 298 K, *E*+*Z* isomers) δ 143.00, 142.93, 142.89, 142.32, 142.16, 142.08, 141.64, 141.51, 141.46, 141.40, 141.34, 141.31, 141.26, 141.17, 141.06, 140.94, 140.71, 139.84, 139.47, 139.37, 136.76, 136.57, 136.18, 133.57, 133.44, 132.42, 132.34, 132.31, 132.16, 132.12, 132.08, 131.71, 131.64, 131.50, 131.00, 130.96, 130.72, 130.69, 130.67, 129.32, 128.31, 128.29, 128.13, 128.04, 127.98, 127.57, 127.54, 127.30, 127.28, 127.25, 126.96, 126.92, 126.88, 126.85, 126.79, 126.28, 126.25, 126.19, 126.04, 126.01, 125.97, 33.65 (CH_2, *E*), 32.22 (CH_2, *Z*), 31.86 (CH_2, *E*), 30.11 (CH_2, *Z*), 29.53 (CH_2, *E*), 29.18 (CH_2, *Z*), 23.19 (CH_2, *Z*), 23.07 (CH_2, *E*), 14.42 (CH_3, *E*+*Z*).

FDMS (m/z): calcd. for $C_{37}H_{34}$: 478.2, found: 477.8 [M^+].

Melting point: 105.2 °C (mixture of isomers)

5'-(3,3-Dimethyl-1-butene-1-yl)-1',2',3',4'-tetraphenylbenzene (5-24):

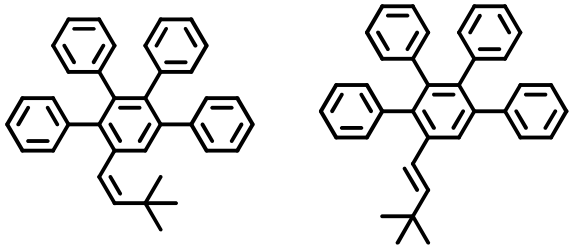

(*Z*)-5-24 **(*E*)-5-24**

^{1}H-NMR (300 MHz, CD_2Cl_2, 298 K) δ 7.65 (s, 0.81 H, gen.-proton (*E*-alkene)), 7.46 (s, 0.19 H, gen.-proton (*Z*-alkene)), 7.19 – 7.01 (m, 10 H, phenyl), 6.92 – 6.79 (m, 10 H, phenyl), 6.20 (d, 0.81 H, $^{3}J_{HH}$ (*E*-alkene) = 16.2 Hz), 6.12 (d, 0.19 H, $^{3}J_{HH}$ (*Z*-alkene) = 11.5 Hz), 6.04 (d, 0.81 H, $^{3}J_{HH}$ (*E*-alkene) = 16.2 Hz), 5.37 (d, 0.19 H, $^{3}J_{HH}$ (*Z*-alkene) = 11.5 Hz), 1.05 (s, 1.7 H, CH_3 (*Z*-alkene)), 0.96 (s, 7.3 H, CH_3 (*E*-alkene)).

^{13}C NMR (76 MHz, CD_2Cl_2, 298 K, *E*+*Z* isomers) δ 143.71, 142.83, 141.96, 141.42, 141.14, 140.85, 140.44, 139.81, 139.22, 136.84, 133.11, 132.10, 131.93, 131.53, 131.28, 131.12, 130.84, 130.47, 129.25, 128.07, 127.73, 127.30, 127.06, 126.73, 126.60, 126.01, 125.80, 124.36, 33.95 (C_{quart}, *E*), 31.40 (C_{quart}, *E*), 31.23 (CH_3, *Z*), 29.74 (CH_3, *E*).

FDMS (m/z): calcd. for $C_{36}H_{32}$: 464.2, found: 463.9 [M^+].

Melting point: 102.4 °C (mixture of isomers)

5'-(1',2',3',4'-Tetraphenylstyrenyl)- 3',4',5'-triphenyl-1,1':2',1''-terphenyl (5-25):

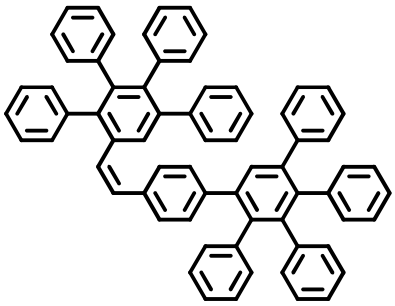

(*Z*)-5-25

^{1}H-NMR (300 MHz, CD_2Cl_2, 298 K) δ 7.85 (s, 1 H), 7.68 (m, 1 H, 7.54 (d, 2 H, *J* = 8.9 Hz), 7.49 (s, 1H), 7.36 (d, 2H, *J* = 7.3 Hz), 7.22 – 7.01 (m, 20 H), 6.98 – 6.82 (m, 20 H), 6.37 (d, 1 H, $^{3}J_{HH}$ (*Z*-alkene) = 12.1 Hz), 6.25 (d, 1 H, $^{3}J_{HH}$ (*Z*-alkene) = 12.1 Hz).

^{13}C NMR (76 MHz, CD_2Cl_2, 298K, *Z* isomer) δ 142.92, 142.69, 142.40, 142.19, 142.13, 141.53, 141.42, 141.18, 140.81, 140.73, 140.62, 140.49, 140.34, 139.97, 139.85, 139.76, 139.56, 136.08, 136.02, 135.84, 135.59, 135.48, 131.87, 131.85, 131.79, 131.73, 131.71, 131.67, 131.57, 131.47, 131.34, 130.84, 130.80, 130.58, 130.30, 130.26, 130.11, 129.86, 129.48, 129.34, 128.74, 128.53, 127.93, 127.91, 127.72, 127.66, 127.65, 127.60, 127.28, 127.25, 127.18, 127.15, 127.09, 126.89, 126.69, 126.65, 126.57, 126.54, 126.45, 126.35, 126.08, 125.95, 125.68.

FDMS (m/z): calcd. for $C_{68}H_{48}$: 864.4, found: 864.4 [M^+].

Melting point: 288 °C (*Z*-isomer).

Tris-(3',4',5'-triphenyl-[1,1':2',1''-terphenyl]-4-yl)-methyl-phosphonium iodide (5-28, $(PPD)_3P\text{-}Me^+ I^-$)

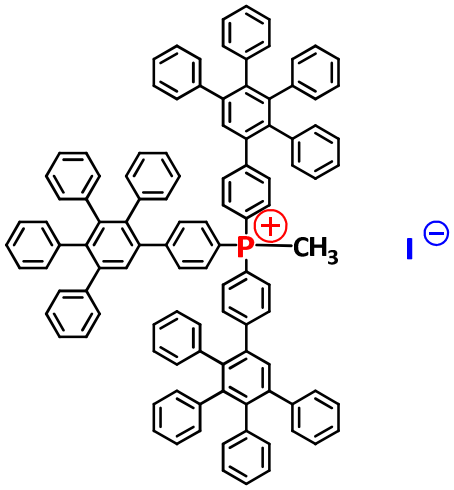

703 mg (0.5 mmol) **tris-(3',4',5'-triphenyl-[1,1':2',1''-terphenyl]-4-yl)phosphine (5-14, $P(Dendr)_3$)** was dissolved in 5 mL dry toluene in a microwave vial. To that solution was added 106 mg (47 µL, 0.75 mmol, 1.5 eq) iodomethane and the reaction vial was sealed with an aluminum cap. The reaction mixture was thoroughly degassed and stirred under argon at 40 °C for 12 hours. After that time the obtained suspension was poured into cold hexane and filtered to get rid of the excess iodomethane. The analytical pure target phosphonium salt was afforded as a white powder (650 mg, 0.42 mmol, 85 % yield) by dissolving the crude product in DCM and precipitate it into cold diethylether.

^{1}H-NMR (300 MHz, CD_2Cl_2, 298 K) δ 7.54 (s, 3 H), 7.44 (dd, 6 H), 7.26 (m, 6 H), 7.24 – 7.18 (m, 18 H), 6.96 – 6.85 (m, 73 H) 2.87 (d, 3 H, $^2J_{PH}$ = 13.2 Hz).

^{31}P-NMR (202 MHz, CD_2Cl_2, 298 K) δ 22.34 ppm.

MALDI-TOF (m/z): calcd. for $C_{109}H_{78}P^+$: 1418.76, found: 1419.13 [M^+].

Elemental analysis: found: 75.60 % C, 5.38 % H (calculated for $C_{109}H_{78}PI$ * 1 H_2O: 75.86 % C, 5.72 % H)

Tris-(3',4',5'-triphenyl-[1,1':2',1''-terphenyl]-4-yl)-(1,3-diphenylpropyl)-phosphonium bromide (5-29, $(PPD)_3P\text{-}CH(CH_2Ph)_2^+\ Br^-$)

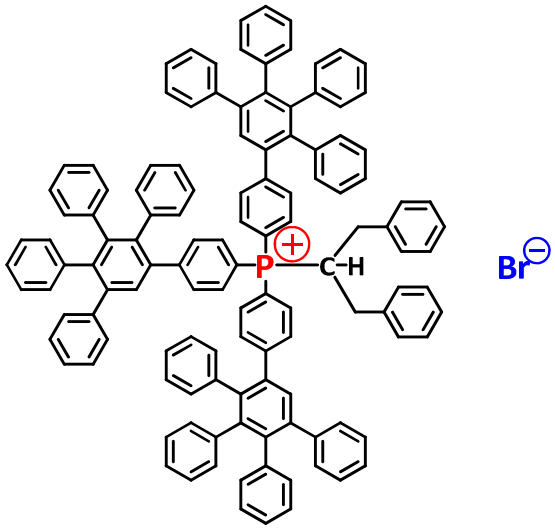

200 mg (0.13 mmol) dendronized methylphosphonium iodide (**5-28**) was dissolved in dry THF (10 mL) and cooled to -78 °C. At that temperature 19.2 mg (187 µL, 0.3 mmol, 1.6 M in hexane, 2.3 eq) n-BuLi was slowly added and the reaction mixture was stirred for 30 minutes. After that time a solution of 52 mg (0.3 mmol, 2.3 eq) benzyl bromide in 2 mL THF was added at -78 °C and the mixture was allowed to warm to room temperature. The reaction was completed after 12 hours, whereupon all volatiles were removed under reduced pressure and the residue was dissolved in DCM and precipitated in cold hexane. The filtered solid was dried in vacuum and thus the title compound was obtained as a white solid (192 mg, 88 % yield).

^{1}H-NMR (300 MHz, CD_2Cl_2, 298 K) δ 7.53 (s, 3 H), 7.41 – 7.30 (m, 4 H, meta benzyl), 7.23 – 7.21 (m, 6 H, ortho and para benzyl), 7.18 – 7.16 (m, 15 H), 6.97 – 6.82 (m, 45 H), 4.52 (s, 1 H, CH), 3.0 (td, 2 H, *J* = 15.4 Hz, 4.8 Hz, CH_2), 2.85 (td, 2 H, *J* = 14.0 Hz, 7.9 Hz, CH_2).

^{31}P-NMR (202 MHz, CD_2Cl_2, 298 K) δ 22.56 ppm.

MALDI-TOF (m/z): calcd. for $C_{117}H_{84}P^+$: 1597.68, found: 1597.13 [M^+].

Tris-(3',4',5'-triphenyl-[1,1':2',1''-terphenyl]-4-yl)-(2,3,4,5,6-pentafluorobenzyl)-phosphonium bromide (5-30, $(PPD)_3P\text{-}CH_2C_6F_5^+$ Br^-)

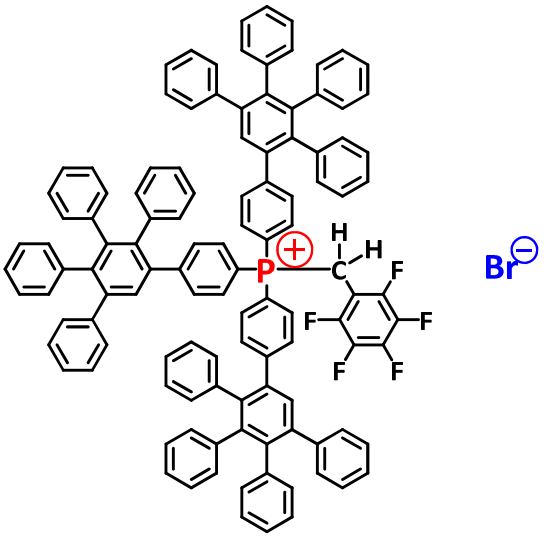

200 mg (0.13 mmol) dendronized methylphosphonium iodide (**5-28**) was dissolved in dry THF (10 mL) and cooled to -78 °C. Then 8.9 mg (81 µL, 0.14 mmol, 1.6 M in hexane, 1.1 eq) n-BuLi was slowly added and the reaction mixture was stirred for 30 minutes. After that time a solution of 37 mg (0.14 mmol, 1.1 eq) 2,3,4,5,6-pentafluoro benzyl bromide in 2 mL THF was added at -78 °C and the mixture was allowed to warm to room temperature. The reaction was completed after 12 hours. Afterwards all volatiles were removed under reduced pressure and the residue was dissolved in DCM and precipitated in cold hexane. The filtered solid was dried in high-vacuum and thus the title compound could be obtained as a white solid (150 mg, 69 % yield).

^{1}H-NMR (300 MHz, CD_2Cl_2, 298 K) δ 7.59 (s, 3 H), 7.46 (dd, 6 H, *J* = 8.4 Hz, 3.5 Hz), 7.37 (dd, 6 H, *J* = 12.4 Hz, 8.4 Hz), 7.27 – 7.20 (m, 15 H), 7.01 – 6.88 (m, 60 H), 5.32 (d, 2 H, $^3J_{PH}$ = 13.9 Hz CH_2).

^{31}P-NMR (202 MHz, CD_2Cl_2, 298 K) δ 20.84 (m) ppm.

MALDI-TOF (m/z): calcd. for $C_{115}H_{77}F_5P^+$: 1583.57, found: 1582.79 [M^+].

Synthesis protocol of substances from chapter 6

Poly-METMA chloride (6-1); poly-[2-(methacryloyloxy)ethyl]trimethylammonium chloride

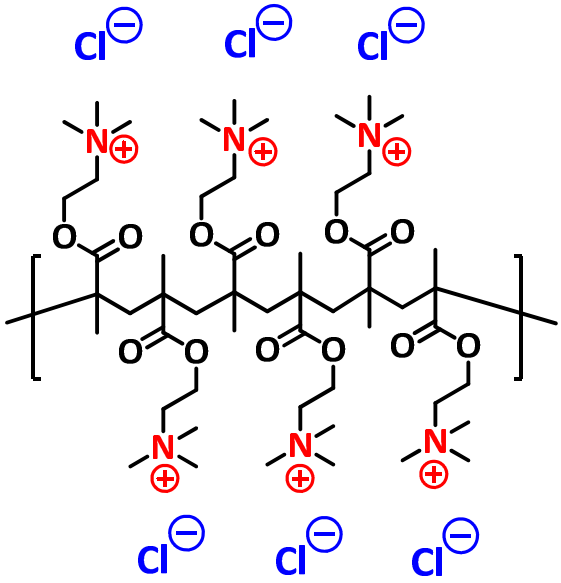

6-1

poly-METMA Cl^-

10 g (48.1 mmol) of [2-(methacryloyloxy)ethyl]trimethylammonium chloride solution (75 wt. % in water, METMA Cl^-), was diluted in 100 ml distilled water. Then, 0.23 g (1 mmol, 2 mol %) of ammonium persulfate was added batch-wise. The solution was then heated under vigorous stirring to 65 °C for 3 h. The product was obtained quantitatively by evaporating the solvent under reduced pressure and drying at high vacuum.

^{1}H-NMR (300 MHz, MeOD, 298 K) δ 4.60 (br, 2 H, CH_2N), 3.93 (br, 2 H, CH_2O), 3.39 (br, 9 H, CH_3N), 2.11 (br, 2 H, CH_2 backbone), 1.19 (br, 3 H, CH_3).

^{13}C NMR (76 MHz, CD_2Cl_2, 298 K) δ 178.0 (quart., COOR), 135.21 (quart.), 64.67 (CH_2N), 58.62 (CH_2O), 53.95 (CH_3), 45.14 (CH_2), 17.27 (CH_3).

General anion exchange procedure to yield hydrophobic poly-METMA borates (6-3, 6-4, 6-5)

poly-[2-(methacryloyloxy)ethyl]trimethylammonium chloride **6-1** (410 mg, 2 mmol) was dissolved in 5 mL distilled water. An aqueous solution of $Na[BPh_4]$ or $Li[B(C_6F_5)_4]$ diethyletherate is added respectively (3 mmol in 5 mL H_2O) at room temperature. After vigorous stirring for 3 h the resulting suspension is filtered and the obtained white solid was washed with distilled water to yield **6-3** and **6-4**.

For the synthesis of **6-5**, the dendronized lithium borate **6-2** (Li^+ $[B^F\text{-}G1]^-$) was dissolved in THF and slowly added to the aqueous poly-METMA chloride solution. The formed precipitate was filtered off and washed with H_2O and dried in vacuum.

Co-polymer of styrene and 4-vinylbenzyl chloride (6-7)

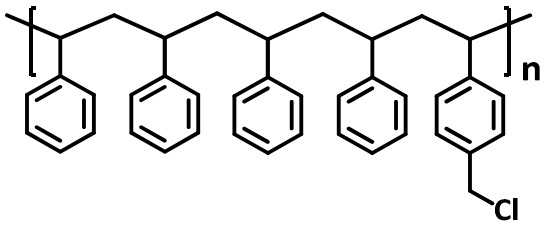

The neat monomers were passed through a short aluminum oxide column prior to use and then 1.08 g (10 mmol) styrene and 0.31 g (2 mmol) of 4-vinylbenzyl chloride were dissolved in 10 mL dry acetonitrile. The reaction mixture was thoroughly degassed and bubbled with argon before 20 mg (0.12 mmol, 1 mol %) of recrystallized AIBN was added. Afterwards the solution was heated to 70 °C for 24 h under inert gas atmosphere. After cooling to room temperature the solvent was removed under reduced pressure and the residue was dissolved in DCM and precipitated in methanol. The obtained solid was filtered and dried.

^{1}H-NMR (300 MHz, MeOD, 298 K) δ 6.99 (br, 3 H, phenyl), 6.51 (br, 2 H, phenyl), 4.45 (br, 0.4 H, CH_2), 1.74 (br, 1 H, CH backbone), 1.43 (br, 2 H, CH_2 backbone).

GPC-data: Mw = 10941.9; Mn = 3742.4; PDI = 2.92

Tris-(3',4',5'-triphenyl-[1,1':2',1''-terphenyl]-4-yl)-(p-vinylbenzyl)-phosphonium chloride (6-12, $(Dendr)_3PCH_2PhCH=CH_2$)

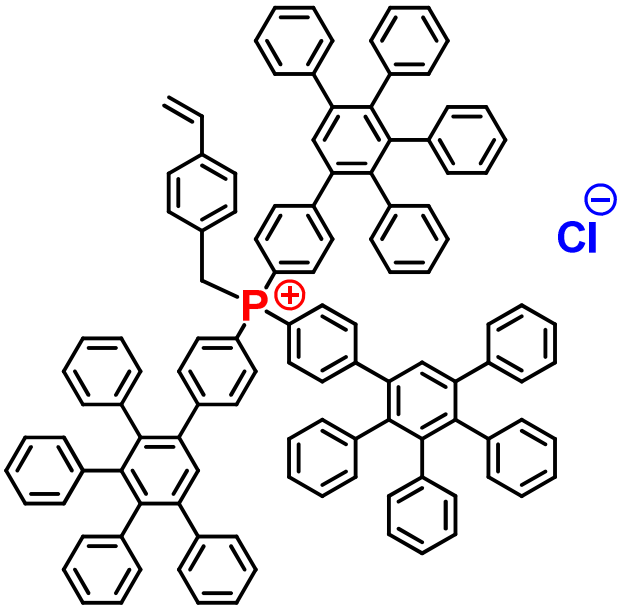

703 mg (0.5 mmol) **tris-(3',4',5'-triphenyl-[1,1':2',1''-terphenyl]-4-yl)phosphine (5-14, $P(Dendr)_3$)** was dissolved in 5 mL dry toluene in a microwave vial. To that solution was added 107 mg (0.7 mmol, 1.4 eq) 4-vinylbenzyl chloride and the reaction vial was sealed with an aluminum cap. The reaction mixture was thoroughly degassed and stirred under argon at 60 °C for 12 hours. After that time the obtained suspension was poured into cold hexane and filtered to get rid of the excess 4-vinylbenzyl chloride. The analytical pure target phosphonium salt was afforded as a white powder (580 mg, 0.38 mmol, 75 % yield) after dissolving the crude product in DCM and precipitate it from cold diethylether.

^{1}H-NMR (300 MHz, CD_2Cl_2, 298 K) δ 7.58 (s, 3 H), 7.41 (dd, 4 H, *J* = 8.5, 3.2 Hz), 7.28 – 7.20 (m, 27 H), 7.03 – 6.88 (m, 45 H), 6.70 (dd, 1 H, $^3J_{HH}$ (trans) = 17.6 Hz, $^3J_{HH}$ (cis) = 9.9 Hz), 5.93 – 5.76 (2 x d, 2 H, $^3J_{HH}$ (trans) = 17.6 Hz, $^3J_{HH}$ (cis) = 9.4 Hz), 5.00 (d, 2 H, $^2J_{HP}$ = 14.5 Hz, CH_2P).

^{13}C NMR (76 MHz, CD_2Cl_2, 298 K) δ 149.62, 142.51, 141.70, 141.64, 141.16, 140.22, 140.03, 139.81, 139.64, 138.89, 133.85, 131.95, 131.70, 130.91, 130.20, 128.04, 127.45, 127.31, 127.07, 126.91, 126.41, 126.23, 125.99, 115.71, 114.55, 34.68.

^{31}P-NMR (202 MHz, CD_2Cl_2, 298 K) δ 21.13 ppm.

MALDI-TOF (m/z): calcd. for $C_{117}H_{84}P^+$: 1520.89, found: 1520.19 [M^+].

8.3 Appendix

Max-Planck-Institut für Polymerforschung
Max Planck Institute for Polymer Research

GPC-Results

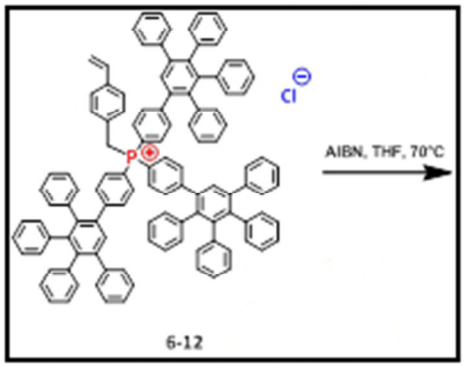

Elugram:

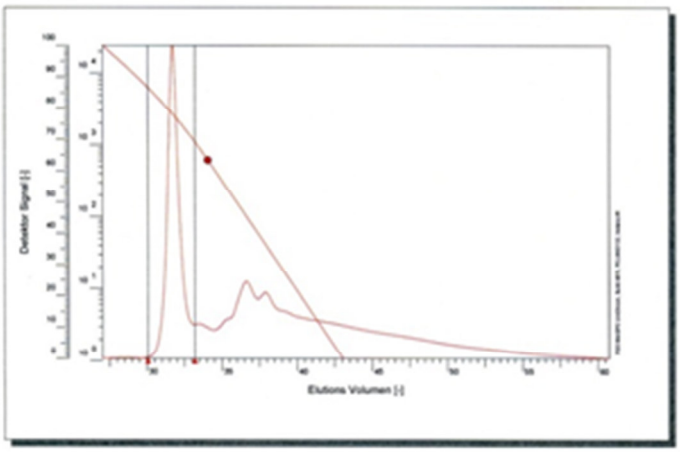

Calibration:	psdmf11.CAL
Eluent:	DMF
Flow rate:	1,0 ml/min
Pump:	PSS SECcurity
Inj.vol.:	100,00
Column1:	GRAM 100
Column2:	GRAM 1000
Column3:	GRAM 1000
Temp.:	60,00 °C
Detector:	SECcurity VWD (270nm)
Detector:	SECcurity RID

Molecular weight distribution:

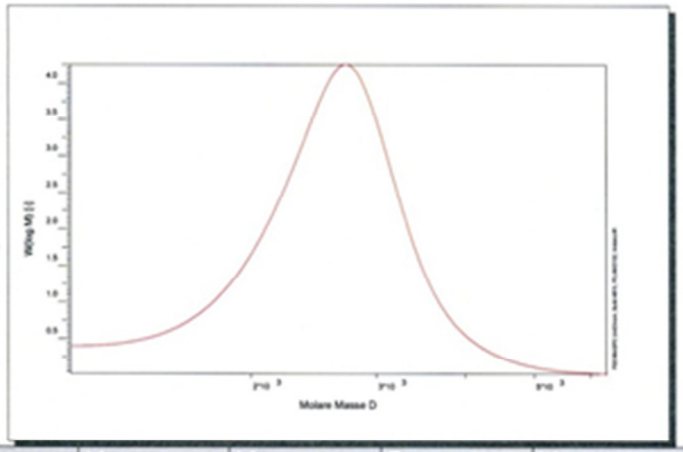

Name	Mn	Mw	D	Vp	Mp	Area
SECcurity VW	2409,72	2603,23	1,08	31,70	2706,24	0,33
SECcurity RID	0,00	0,00	0,00	0,00	0,00	0,00

Figure 8-3: GPC data obtained from the polymerization reaction of compound **6-12** (paragraph 6.3)

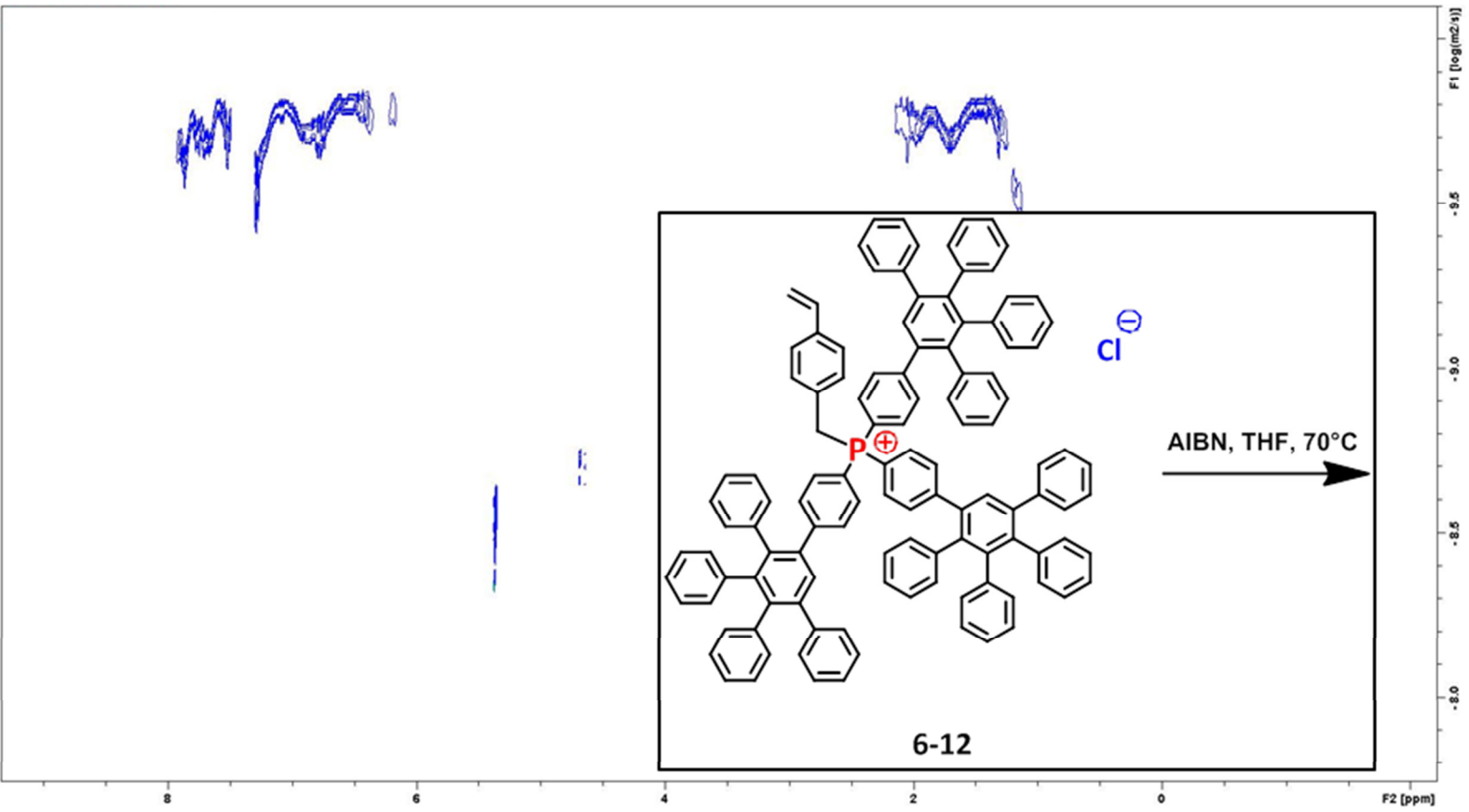

Figure 8-4: ^{1}H-DOSY-NMR spectrum obtained from the polymerization reaction of compound **6-12** (CD_2Cl_2, 500 MHz, 298 K, see paragraph 6.3)

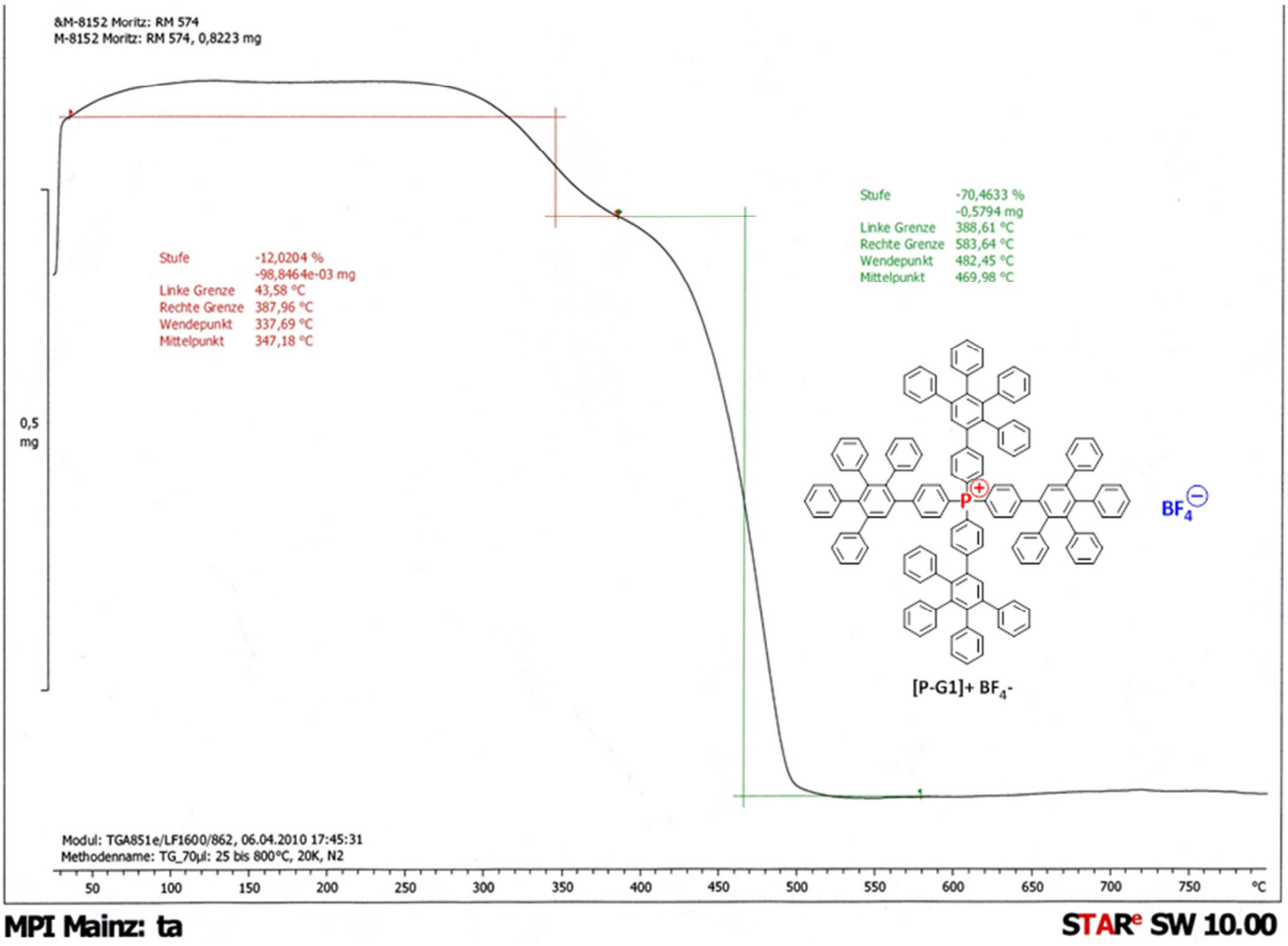

Figure 8-5: TGA spectrum of first-generation phosphonium salt **[P-G1]+ BF4-** under air stream (see stability measurements from section 4.5).

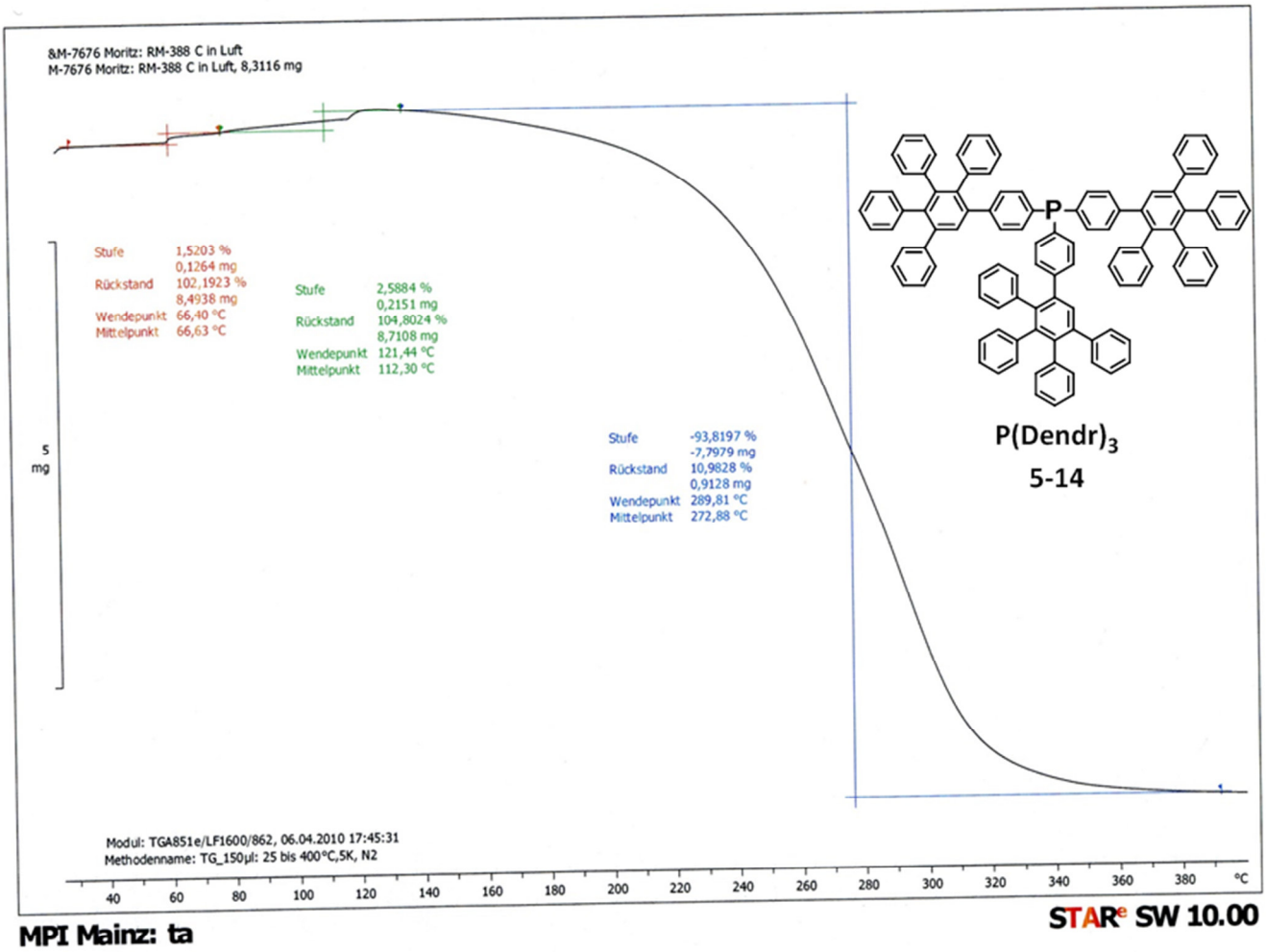

Figure 8-6: TGA spectrum of first-generation phosphine **P(Dendr)$_3$** under air stream.

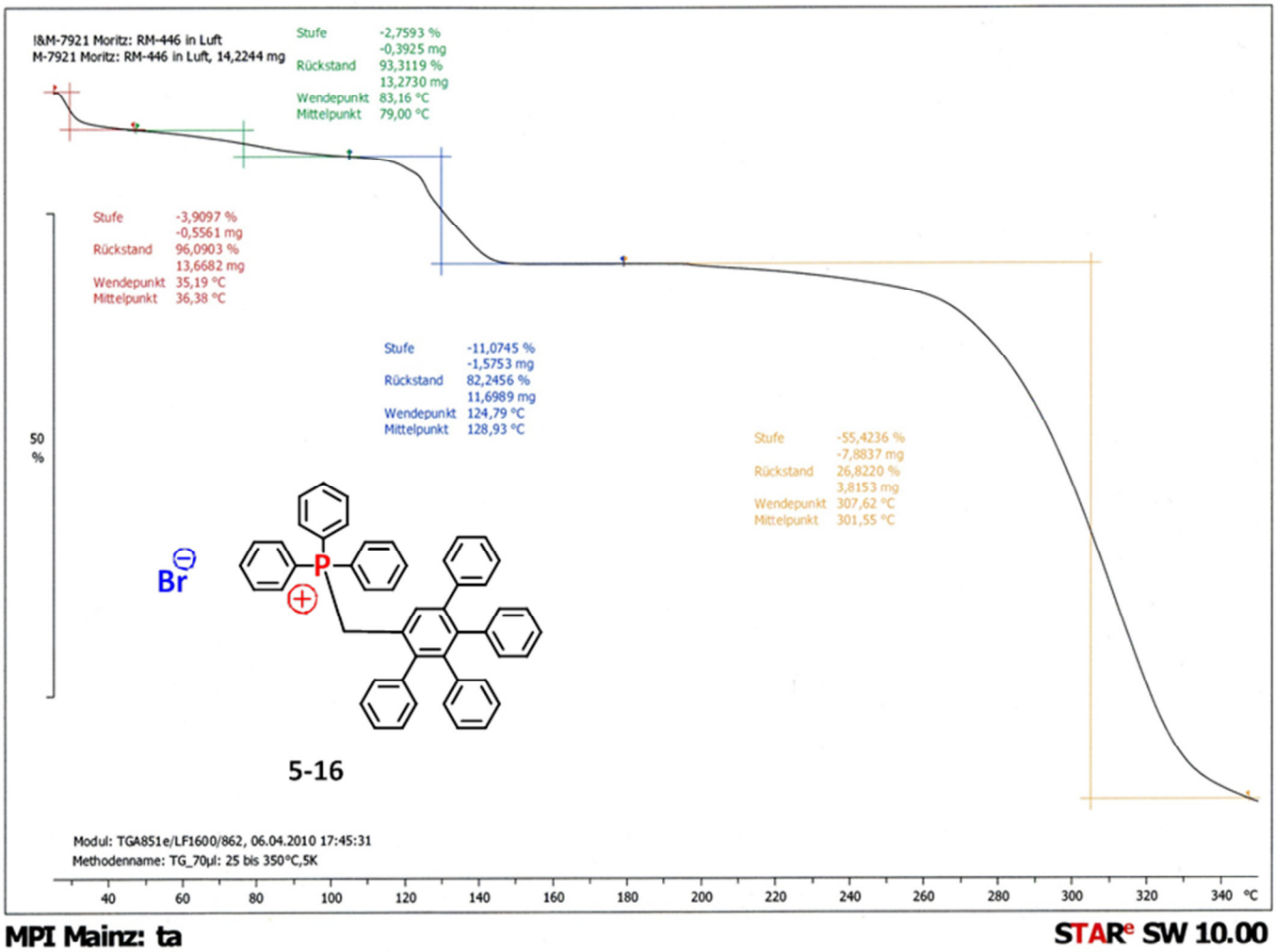

Figure 8-7: TGA spectrum of first-generation phosphonium salt **5-16** under air stream.

Literature

[1] Morgenroth, F.; Reuther, E.; Müllen, K.; *Angew. Chem. Int. Ed. Engl.* **1997**, *36*, 631.
[2] Wiesler, U.-M.; Müllen, K.; *Chemical Communications* **1999**, 2293.
[3] a) Jerschow A., Müller N.; *J. Magn. Reson.* A **1996**, 123, 222-225; b) Jerschow A., Müller N.; *J.Magn. Reson. A* **1997**, 125, 372-375.
[4] Holz et al; *J. Magn. Res.* **1991**, 92, 115-125.
[5] Tanner, J. E.; *J. Chem. Phys.* **1970***, 5*0, 2523-2526.
[6] Einstein, A.; *Annalen der Physik* **1905**, *17*, 549.
[7] Verma,A. K.; Joshi, M; Singh, V. P.; *Org.Lett.* **2011**, Vol. 13, No. 7, 1630 – 1633.

List of Publications

1. Moritz, R.; Zardalidis, G.; Butt, H.-J.; Wagner, M.; Müllen, K.; Floudas, G.: “Ion Size Approaching the Bjerrum Length in Solvents of Low Polarity by Dendritic Encapsulation”, *Macromolecules* **2014**, 47 (1), 191–196. DOI: 10.1021/ma402137x
2. Hammer, B. A.; Moritz, R.; Stangenberg, R.; Baumgarten, M.; Müllen, K.: “The polar side of polyphenylene dendrimers“, *Chem. Soc. Rev.* **2015**, Advance Article. DOI: 10.1039/C4CS00245H
3. Moritz, R.; Wagner, M.; Schollmeyer, D.; Baumgarten, M.; Müllen, K.: “Hydrophobic Encapsulated Phosphonium Salts – Novel Weakly Coordinating Cations”, submitted to

Zusammenfassung

der Dissertation “Synthesis, Properties and Application of Polyphenylene Phosphonium Salts” vorgelegt von Ralf Moritz

Das synthetische Konzept der vorliegenden Arbeit bestand in der Darstellung von Phosphonium-Salzen, deren molekularer Kationenradius durch gezielte chemische Modifikationen signifikant vergrößert werden konnte. Es gelang dabei erstmals monodisperse, hydrophobe Polyphenylen-Phosphoniumelektrolyte präparativ zugänglich zu machen auf Basis einer divergenten Synthesestrategie mittels thermaler, irreversibler [4+2] *Diels-Alder* Cycloaddition. Auch eine gezielte Oberflächenfunktionalisierung des Kations dieser neuartigen Phosphoniumsalze konnte durch den Einsatz von speziellen Wachstumsbausteinen (Derivaten des Tetraphenylcyclopentadienons) erreicht werden. Kristallstrukturanalysen, massenspektrometrische Untersuchungen sowie DOSY-NMR Messungen beweisen die erfolgreiche Umsetzung des synthetischen Konzepts.

Mittels dielektrischer Spektroskopie an einer Serie von Polyphenylen-Boratsalzen (zugänglich durch klassische Ionenmetathesereaktionen) wurde der Zusammenhang zwischen Dissoziationsgrad α und Größe des ladungsneutralisierenden Kations untersucht. Es konnte festgestellt werden, dass die Größe der hier entwickelten Phosphoniumkationen in der Größenordnung der sogenannten Bjerrum-Länge liegt – eine lösungsmittelabhänige, charakteristische Größe für die Beschreibung von Ionendissoziationsgleichgewichten. Die dabei erhaltenen Leitfähigkeitswerte wurden analysiert und enthüllten den Zusammenhang zwischen elektrophoretischer Mobilität und Koordination zum jeweiligen Gegenion.

Außerdem wurden im Rahmen dieser Arbeit neue Benzylphosphoniumsalze mit sterisch außerordentlich anspruchsvollen Polyphenylen-Substituenten in α-Position dargestellt, welche unter Wittig-Bedingungen mit Aldehyden zu den entsprechenden Alkenen umgesetzt wurden. Hierbei konnte ein eindeutiger Zusammenhang zwischen erhöhter (*Z*)-Selektivität der entstandenen Olefine und der Größe des α-Substituenten des Phosphoniumsalzes erforscht werden. Ferner ließen sich sterisch gehinderte (*Z*)-Stilbene in guten Ausbeuten darstellen durch den Einsatz der hier entwickelten Wittig-Vorstufen. Abschließend konnten erste Experimente zur Darstellung hydrophobisierter Polyelektrolyte erfolgreich durchgeführt und ausgewertet werden.

Lebenslauf

Persönliche Angaben

Name:	Ralf Moritz
Geburtsdatum:	19.09.1984
Geburtsort:	Hutthurm
Staatsangehörigkeit:	Deutsch

Bildung und Werdegang

2011 – 2015	Dissertation am Max-Planck-Institut für Polymerforschung, Mainz, im Arbeitskreis von Prof. Dr. Klaus Müllen; Thema: „Synthesis, Properties and Application of Polypenylene Phosphonium Salts“
2008 – 2010	Hauptstudium Organische Chemie (Master) an der Universität Regensburg
2007 – 2008	Auslandssemester an der Universität Leeds (GB)
2005 – 2008	Grundstudium der Chemie (Bachelor) an der Universität Regensburg
1995 – 2004	Johannes-Gutenberg-Gymnasium, Waldkirchen